

Enhancing Scalability in Bayesian Nonparametric Factor Analysis of Spatiotemporal Data

Yifan Cheng ^{*} and Cheng Li [†]

Department of Statistics and Data Science, National University of Singapore

Abstract

This article introduces novel and practicable Bayesian factor analysis frameworks that are computationally feasible for moderate to large spatiotemporal data. Previous Bayesian analysis of spatiotemporal data has utilized a Bayesian factor model with separable temporal latent factors and spatial factor loadings, along with stick-breaking process priors on the loadings to enable clustering of spatial locations. Such a flexible Bayesian model, however, faces a prohibitively high computational cost in posterior sampling when the spatial and temporal dimensions increase to a couple hundred. We address this computational challenge with several speed-up proposals. We integrate a new slice sampling algorithm that permits varying numbers of spatial mixture components across all latent factors and guarantees them to be non-increasing through the posterior sampling iterations, thus effectively reducing the number of mixture parameters. Additionally, we introduce a spatial latent nearest-neighbor Gaussian process prior and new sequential updating algorithms for the spatially varying latent variables in the stick-breaking process prior. Our new models and sampling algorithms exhibit significantly enhanced computational scalability and storage efficiency and possess powerful inferential capabilities for both spatiotemporal prediction and clustering of spatial locations with similar temporal trajectories. The improvement in computational efficiency and inferential performance is substantiated by extensive simulation experiments.

Contents

1	Introduction	3
2	Bayesian Spatiotemporal Gaussian Factor Model and Three Acceleration Techniques	5
3	Slice Sampling for Bayesian Spatial Clustering	9
4	Spatial Scalability via Nearest-Neighbor Gaussian Process and Sequential Updates	12
4.1	Computational Burdens from a Large $F(\rho)_{m \times m}$	12
4.2	Incorporating the Spatial Latent NNGP	13
4.3	Approximating $F(\rho)^{-1}$ and $\det(F(\rho))$	14
4.4	Sequentially Updating α_{jl_j} 's Under Spatial NNGP Prior	15

^{*}y.cheng@u.nus.edu

[†]stalic@nus.edu.sg

5	Spatial Prediction and Temporal Trends Clustering	17
5.1	Predictions at New Spatial Locations	17
5.2	Summarizing Spatial Clusters with Similar Temporal Trends	19
6	Simulation Experiments	19
6.1	Computational Efficiency for Key Gibbs Sampler Steps	19
6.2	Computational Efficiency for Spatial Prediction	22
6.3	Sea Surface Temperature Data	23
7	Discussion	25
A	Gibbs Samplers for Our Spatiotemporal Bayesian Gaussian Factor Models	26
A.1	Full Gibbs Sampling Details for the Basic Model Without Spatial Clustering Capabilities	28
A.2	Full Gibbs Sampling Details for Our Model in Section 2	30
A.3	Full Gibbs Sampling Details for Our Model in Section 3	34
B	Temporal Posterior Sampling and Prediction Acceleration for Evenly Dispersed Time Points	38
B.1	Temporal Part Computational Burdens When T is Large	38
B.2	Some Set-Up and Notations	40
B.3	Simple Sparse Closed-Form Representations for $H(\psi)_{T \times T}^{-1}$ and $\text{Rooti}(H)_{T \times T}$	41
B.3.1	When <code>temporal.structure</code> = ‘ar1’ or ‘exponential’	41
B.3.2	When <code>temporal.structure</code> = ‘sar1’ or ‘sexponential’	42
B.3.3	Attained Acceleration Outcomes Pertaining to Sampling $\Upsilon_{k \times k}$ and ψ & Predicting at Future Time Points	44
B.4	Simple Sparse Closed-Form Representations for the T Vectors H_t^+ ’s of Length $T - 1$ & Repetitive Closed-Form Solutions for the T Scalars H_t^* ’s	44
B.4.1	When <code>temporal.structure</code> = ‘ar1’ or ‘exponential’	44
B.4.2	When <code>temporal.structure</code> = ‘sar1’ or ‘sexponential’	48
B.4.3	Attained Acceleration Outcomes Pertaining to Sampling η_t ’s	48
B.5	Proof of Equation (B.1)	49
C	A VAR(1) Process for the Latent Temporal Factors $\eta_{1:T}$	55
C.1	New Gibbs Sampling Steps for Temporal-Related Parameters	55
C.2	Predictions at Desired Future Time Points	57
D	Facilitating Efficient Computation for Spatial PSBP	58
E	Some Notes on Slice Sampling Adapted in Our Context	60
F	Some Further Comments Regarding the Latent NNGP	60
G	More on Predictions at Future Time Points or New Spatial Locations (Complementary to Section 5.1)	61
G.1	Predicting $\hat{\mathbf{y}}_{(T+1):(T+q)}$ Given $\mathbf{y}_{1:T}$ and $[X_{(T+1):(T+q)}]_{qOm \times p}$ (if $p \geq 1$)	61

G.2	Predicting $\hat{\mathbf{y}}(\mathbf{s}_{(m+1):(m+r)})$ Given $\mathbf{y}(\mathbf{s}_{1:m})$ and $X(\mathbf{s}_{(m+1):(m+r)})_{rTO \times p}$ (if $p \geq 1$) . . .	63
G.2.1	Under the Basic Modeling Framework in Appendix A.1	63
G.2.2	Under Our Modeling Framework in Section 2	64
H	Scalability Improvements Corresponding to Our 3 Novelties – A Summary of Computational Complexity and Memory	66
H.1	Flexibility, Computation, and Storage Improvements Brought About by Our Slice Sampling Approach in Section 3 with Spatial NNGP & Sequential Updates . . .	67
H.2	Posterior Sampling Computational Acceleration & Storage Alleviation and Faster Spatial Prediction Brought About by Our Spatial NNGP Prior in Section 4 with or without Slice Sampling	68
H.3	Posterior Sampling Computational Acceleration Brought About by Our Sequential Updating Methods in Section 4.4 (with spatial NNGP)	70
H.4	An Overall Scalability Improvements Summary for Our Three Novelties	71
I	Complementary Simulation Results and Experiments	71
I.1	Further Details of the Toy Example in Section 2	71
I.2	Additional Tables of Recorded Posterior Sampling Time for Section 6.1	75
I.3	Accuracy for Spatial Clustering of Temporal Trends	78
I.4	VAR(1) for the Latent Temporal Factors $\boldsymbol{\eta}_{1:T}$	79
I.5	Multiple Observation Types	80
I.6	Sensitivity Analysis for the Number of Factors and Hyperparameters	83
J	Extension to Three Non-Gaussian Observed Data Types	83

1 Introduction

One pivotal task frequently occurring in spatiotemporal applications such as infectious disease control and natural disaster prevention involves identifying spatial clusters with similar temporal trajectories and picking out the regions that may require early special attention, which requires modeling the covariance structure with dependence along both the spatial and temporal dimensions. In general, there are several primary goals a spatiotemporal model would want to accomplish. First, the model should effectively characterize the major sources of variation across both dimensions while retaining spatial and temporal dimension reduction properties and hence overall interpretability to a satisfactory extent, given that one typically observes only a single trajectory of data across both space and time with no independent replicates. Second, the model should properly account for spatiotemporal heterogeneity and nonstationarity prevalent in various data types such as imaging data in neurosciences and geosciences, as decently addressing these aspects is crucial for better prediction performances. Third, the model should entail a parsimonious structure that facilitates efficient computation on data with moderate to high spatial and temporal dimensions for practicable implementation, especially when Bayesian inference, which often involves computationally intensive posterior sampling, is concerned.

This article focuses on the Bayesian spatiotemporal latent factor model developed in Berchuck et al. (2022), which achieves the first two goals described above. Factor models can effectively

reduce dimension by producing a handful of informative latent factors from a host of raw variables. Previous works on Bayesian spatial factor analysis often assumed independent replicates (Christensen and Amemiya 2002, Wall and Liu 2009, Ren and Banerjee 2013) and conducted dimension reduction on a large number of observation types at each spatial location, which has been successfully generalized to nonnegative spatial factorization with applications in spatial transcriptomics (Townes and Engelhardt 2022, Ma and Zhou 2022). The separable factor models with temporally dependent latent factors and spatially dependent factor loadings used in recent works such as Bradley, Holan, and Wikle 2015 and Berchuck et al. (2022), in contrast, effectively reduce dimension both spatially and temporally, thus offering convenient interpretability. The general framework in Berchuck et al. (2022) also enables clustering spatial locations into distinct groups, a commonly adopted modeling strategy typically achieved by placing Bayesian mixture priors. Examples of mixture priors employed in recent Bayesian spatiotemporal literature include the mixture of finite mixtures (Hu et al. 2023), the Dirichlet process (Mozdzen et al. 2022), the temporal dependent Dirichlet process (De Iorio et al. 2023), and the Indian buffet process (Yang et al. 2022). More spatially structured priors like the random spanning tree prior (Zhang et al. 2023) may also be considered to enhance the spatial contiguity of clusters. In line with these, the model proposed by Berchuck et al. (2022) incorporates clustering across spatial locations via a probit stick breaking process (PSBP) prior (Rodríguez and Dunson 2011) coupled with a spatial latent neighborhood structure from a Gaussian process, thereby capturing both spatial dependence and heterogeneity.

We make three key contributions to enhance the computational scalability of this baseline Bayesian spatiotemporal factor model. First, we follow Walker (2007) and develop a new slice sampling algorithm specifically tailored to mixture weights determined by the spatially varying latent variables in the PSBP prior, which ensures the correct conditional posterior distributions and differs from the infinite mixture algorithm presented in Berchuck et al. (2022). Under our version of slice sampling, the numbers of spatial mixture components, which do not need to be pre-specified and are permitted to vary across all factors, are ensured non-increasing through the Markov chain Monte Carlo (MCMC) iterations, thus leading to notably accelerated computation for model fitting and spatial prediction as well as significantly alleviated storage requirements for spatial prediction and clustering. Second, we impose the Nearest-Neighbor Gaussian Process (NNGP) prior (Datta et al. 2016) in place of the full GP prior and further propose novel sequential updating algorithms for the spatially varying latent variables. Our approach successfully attains high spatial scalability by reducing the corresponding posterior sampling computational complexity from cubic to linear in the number of locations. Under our spatial NNGP prior, the computational speed for making predictions at new locations is markedly increased as well, and storage with respect to the spatial covariance matrix and its inverse can be reduced from quadratic to linear if needed. Third, we devise and implement two critical inferential procedures—outcome predictions at new spatial locations and spatial clustering of temporal trends. Possibly due to the prohibitive storage requirements that ensue under the baseline model when the numbers of spatial mixture components and location points are large, both inferential procedures are not currently supported by Berchuck et al. (2022)’s R package `spBFA`. Consequently, our improved algorithm manifests considerably superior scalability for MCMC-based posterior sampling as well as subsequent vital inferential tasks on datasets

with a few hundred to a couple thousand spatial locations and time points. Detailed scalability summaries for our novel approaches are presented in Appendix H.

This paper is organized as follows. Section 2 depicts the baseline Bayesian spatiotemporal Gaussian factor model in Berchuck et al. (2022) and illustrates its weaknesses in computational scalability through detailed analysis of a motivating example, demonstrating our techniques' strong acceleration capabilities. Section 3 introduces our novel slice sampling algorithm. Section 4 derives a new spatial latent NNGP prior and sequential updating schemes with theoretical justifications for the improved computational and storage complexity. Section 5 elaborates on spatial prediction and temporal trends clustering. Section 6 presents simulation experiments justifying scalability improvements and a real data example. Section 7 discusses potential future work. Finally, the Supplementary Material details full posterior sampling steps, offers additional acceleration solutions and imposes more complicated temporal structures on equispaced time points, complements Sections 2 to 6, and provides extensions to model non-normal observations.

2 Bayesian Spatiotemporal Gaussian Factor Model and Three Acceleration Techniques

We first describe the baseline latent factor model for spatiotemporal data in Berchuck et al. (2022). For an outcome $y_t^o(\mathbf{s}_i)$ of type o ($o = 1, \dots, O$) observed at time t ($t = 1, \dots, T$) and spatial location \mathbf{s}_i ($i = 1, \dots, m$), we assume the separable latent factor model

$$y_t^o(\mathbf{s}_i) = \mathbf{x}_t^o(\mathbf{s}_i)^\top \boldsymbol{\beta} + \sum_{j=1}^k \lambda_j^o(\mathbf{s}_i) \eta_{tj} + \epsilon_t^o(\mathbf{s}_i), \quad (2.1)$$

where $\mathbf{x}_t^o(\mathbf{s}_i) \in \mathbb{R}^p$ is the spatiotemporal covariate vector, $\boldsymbol{\beta} \in \mathbb{R}^p$ is the vector of coefficients, η_{tj} 's are the latent temporal factors, $\lambda_j^o(\mathbf{s}_i)$'s are the spatial-specific factor loadings, and $\epsilon_t^o(\mathbf{s}_i)$ is the error term. Define the stacked quantities $\mathbf{y}_t = (y_t^1(\mathbf{s}_1), \dots, y_t^1(\mathbf{s}_m), \dots, y_t^O(\mathbf{s}_1), \dots, y_t^O(\mathbf{s}_m))^\top \in \mathbb{R}^{mO \times 1}$, $\mathbf{X}_t = (\mathbf{x}_t^1(\mathbf{s}_1), \dots, \mathbf{x}_t^1(\mathbf{s}_m), \dots, \mathbf{x}_t^O(\mathbf{s}_1), \dots, \mathbf{x}_t^O(\mathbf{s}_m))^\top \in \mathbb{R}^{mO \times p}$, $\Lambda = (\boldsymbol{\lambda}_1, \dots, \boldsymbol{\lambda}_k) \in \mathbb{R}^{mO \times k}$ with $\boldsymbol{\lambda}_j = (\lambda_j^1(\mathbf{s}_1), \dots, \lambda_j^1(\mathbf{s}_m), \dots, \lambda_j^O(\mathbf{s}_1), \dots, \lambda_j^O(\mathbf{s}_m))^\top \in \mathbb{R}^{mO \times 1}$, $\boldsymbol{\eta}_t = (\eta_{t1}, \dots, \eta_{tk})^\top \in \mathbb{R}^{k \times 1}$, and $\boldsymbol{\epsilon}_t = (\epsilon_t^1(\mathbf{s}_1), \dots, \epsilon_t^1(\mathbf{s}_m), \dots, \epsilon_t^O(\mathbf{s}_1), \dots, \epsilon_t^O(\mathbf{s}_m))^\top \in \mathbb{R}^{mO \times 1}$. Then (2.1) is equivalent to the matrix-form $\mathbf{y}_t = \mathbf{X}_t \boldsymbol{\beta} + \Lambda \boldsymbol{\eta}_t + \boldsymbol{\epsilon}_t$, for $t = 1, \dots, T$. We assume that the error vector is distributed as $\boldsymbol{\epsilon}_t \sim N_{mO}(\mathbf{0}, \Xi)$ independently across time $t = 1, \dots, T$, where $\Xi = \text{Diag}((\sigma^2)^1(\mathbf{s}_1), \dots, (\sigma^2)^1(\mathbf{s}_m), \dots, (\sigma^2)^O(\mathbf{s}_1), \dots, (\sigma^2)^O(\mathbf{s}_m))$. Appendix A.1 details prior specification and Gibbs sampler steps for this basic model.

To further integrate spatial clustering capabilities, we opt to fully specify the factor loadings matrix and introduce spatial dependency by adapting the Probit Stick Breaking Process (PSBP, Rodríguez and Dunson 2011), an extension of the stick-breaking construction of the Dirichlet Process (DP, Sethuraman 1994), the workhorse of Bayesian nonparametric clustering. For any given (j, i, o) , we let the latent mixture distribution $G_j^{i,o}$ follow PSBP $((G_j)_0, \boldsymbol{\alpha}_j^{i,o})$ with base measure $(G_j)_0$ and concentration parameter vector $\boldsymbol{\alpha}_j^{i,o}$, whose scalar components are $\alpha_{jl_j}^o(\mathbf{s}_i)$, $l_j \in \mathbb{N}$, $l_j \geq 1$, if

$$G_j^{i,o} = \sum_{l_j=1}^{\infty} w_{jl_j}^o(\mathbf{s}_i) \delta_{\theta_{jl_j}}, \quad \theta_{jl_j} \stackrel{\text{iid}}{\sim} (G_j)_0, \quad w_{jl_j}^o(\mathbf{s}_i) = \Phi(\alpha_{jl_j}^o(\mathbf{s}_i)) \prod_{r_j=1}^{l_j-1} [1 - \Phi(\alpha_{jr_j}^o(\mathbf{s}_i))] \quad (2.2)$$

The above construction is indeed adequate since $\sum_{l_j=1}^{\infty} w_{jl_j}^o(\mathbf{s}_i) = 1$ almost surely for all (j, i, o) (Rodríguez and Dunson 2011). We can often truncate the infinite sequence at a large number of terms to obtain a finite mixture for practical implementation of posterior sampling. Let a pre-specified fixed $L \in \mathbb{N}$, $1 < L < \infty$ be the number of clusters for all factors and let $w_{jL}^o(\mathbf{s}_i) = \prod_{r_j=1}^{L-1} [1 - \Phi(\alpha_{jr_j}^o(\mathbf{s}_i))]$ be the last mixture weight for all (j, i, o) in (2.2). We then impose the PSBP in (2.2) on λ_j 's independently across all (j, i, o) ,

$$\begin{aligned} \lambda_j^o(\mathbf{s}_i) &= \theta_{j\xi_j^o(\mathbf{s}_i)} \mid G_j^{i,o} \sim G_j^{i,o}, \quad \text{where } \xi_j^o(\mathbf{s}_i) \sim \text{Multinomial}(w_{j1}^o(\mathbf{s}_i), \dots, w_{jL}^o(\mathbf{s}_i)) \\ \text{such that } \mathbb{P}(\xi_j^o(\mathbf{s}_i) = l_j) &= w_{jl_j}^o(\mathbf{s}_i), \text{ for any } l_j = 1, \dots, L. \end{aligned} \quad (2.3)$$

With the PSBP model delineated in Equations (2.2) and (2.3), spatial neighborhood proximity can now be incorporated into the columns λ_j , $j \in \{1, \dots, k\}$ of the factor loadings matrix $\Lambda_{mO \times k}$ by jointly modeling the latent variables α_{jl_j} 's that dictate the weights w_{jl_j} 's. Let $\alpha_{jl_j}(\mathbf{s}_i)^T = (\alpha_{jl_j}^1(\mathbf{s}_i), \alpha_{jl_j}^2(\mathbf{s}_i), \dots, \alpha_{jl_j}^O(\mathbf{s}_i))$ for all $i = 1, 2, \dots, m$. We assign the prior

$$\alpha_{jl_j} = (\alpha_{jl_j}(\mathbf{s}_1)^T, \dots, \alpha_{jl_j}(\mathbf{s}_m)^T)^T \sim N_{mO}(\mathbf{0}, F(\rho)_{m \times m} \otimes \kappa_{O \times O}), \quad (2.4)$$

independently across all (j, l_j) for $j = 1, \dots, k$ and $l_j = 1, \dots, L-1$. In (2.4), the covariance structure of α_{jl_j} 's is modeled as the Kronecker product of two matrices. Specifically, the covariance matrix $F(\rho)$ stems from a spatial Gaussian process over the m spatial locations with an exponential covariance function parameterized by ρ , a length-scale parameter specifying the level of spatial correlation. ρ is assigned a uniform prior and requires Metropolis moves in posterior sampling. The other covariance matrix $\kappa_{O \times O}$ depicts the covariance between the O observation types. It is left fully unstructured and imposed a standard conjugate prior $\mathcal{IW}(\nu, \Theta)$. Posterior sampling of α_{jl_j} 's typically relies on introducing latent normal variables $z_{jl_j}^o(\mathbf{s}_i)$'s for probit models to bring about conjugacy for α_{jl_j} 's (see Appendix D). Finally, for the atoms θ_{jl_j} 's in Equation (2.3), we follow Bhattacharya and Dunson (2011) to assign a multiplicative gamma process shrinkage prior

$$\begin{aligned} \theta_{jl_j} &\stackrel{\text{ind}}{\sim} N(0, \tau_j^{-1}), \text{ where} \\ \tau_j &= \prod_{h=1}^j \delta_h \text{ with } \delta_1 \sim \text{Gamma}(a_1, 1) \text{ and } \delta_h \sim \text{Gamma}(a_2, 1), \text{ for all } h \geq 2. \end{aligned} \quad (2.5)$$

Despite its capability and flexibility in model fitting, the standard MCMC algorithm derived in Berchuck et al. (2022) and their R package **spBFA** become prohibitively slow even when m and T increase to a couple hundred. We identify within this algorithm the following principal causes of the computational burdens resulting from a large m .

- (i) Posterior sampling of the spatial covariance parameters ρ and κ requires $F(\rho)^{-1}$ and $\det(F(\rho))$. A computational complexity of $\mathcal{O}(m^3)$ is thus needed.
- (ii) Posterior sampling of the spatially varying latent variables $\alpha_{jl_j}^o(\mathbf{s}_i)$'s in the PSBP prior involves the notorious cubic computational complexity from fitting Gaussian processes.
- (iii) Posterior sampling of the mixture labels $\xi_j^o(\mathbf{s}_i)$'s and introduced latent normal $z_{jl_j}^o(\mathbf{s}_i)$'s across all spatial locations for a moderately large L also incurs computational costs.
- (iv) A major spatial prediction step obtaining predicted spatially varying latent variables $\hat{\alpha}(\mathbf{s}_{(m+1):(m+r)})$ at r new locations requires a computational complexity quadratic in m .

We tackle these challenges by proposing three new techniques detailed in Sections 3 and 4. In particular, slice sampling in Section 3 addresses the issues (iii) and (iv) above; the spatial NNGP prior in Section 4 addresses the issues (i) and (iv) above; the new sequential updating algorithm in Section 4.4 addresses the issue (ii) above.

We first present a small-scale toy example to illustrate posterior sampling time reduction attributable to our three novelties. We consider four methods. `fullGPFixedL` assumes a common number of spatial mixture components L for all k latent factors and imposes the full GP prior on $\alpha_{jl_j}^o(\mathbf{s}_i)$'s; `NNGPblockFixedL` assumes a common fixed L and adopts our spatial NNGP prior with the standard block-wise updating scheme; `NNGPsequenFixedL` assumes a common fixed L and adopts the spatial NNGP prior with our new sequential updating scheme in Section 4.4; `NNGPsequenVaryLj` adopts the spatial NNGP prior, the new sequential updating scheme, and our slice sampling algorithm in Section 3 with varying numbers of spatial mixture components $L_{1:k}$. For comparison, we also ran two variations of algorithms in the R package `spBFA` by Berchuck et al. (2022). `spBFAL10` specifies a fixed $L = 10$ mixture components and `spBFALInf` is under `spBFA`'s infinite mixture implementation. Both adopt the full spatial GP prior.

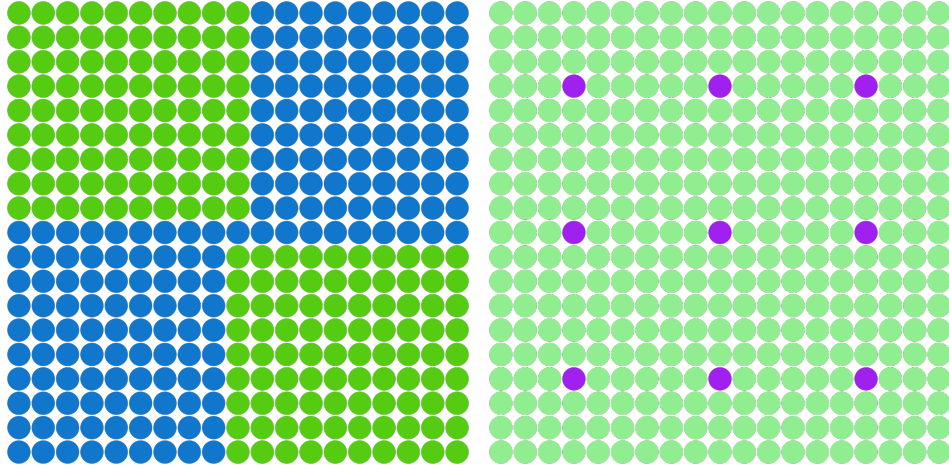


Figure 2.1: The actual spatial grouping (left) for the toy example. The two colors represent the two groups for $m = 19^2 = 361$ spatial locations. In the right panel, the 9 purple locations are testing locations, and the 352 light green locations are training ones.

We generated data following the model (2.1) without the regression term $\mathbf{x}_t^o(\mathbf{s}_i)^T \boldsymbol{\beta}$. The number of factors was set to $k = 2$, and the actual numbers of clusters for both factors were also set to 2. We specified $\theta_{11} = \theta_{12} = 5$, $\theta_{21} = 10$, and $\theta_{22} = -10$ for the atoms θ_{jl_j} 's. We considered $m = 19^2 = 361$ spatial locations $\mathbf{s}_i = (i_1, i_2)$ for $i = 1, 2, \dots, 361$ on an equispaced 2-dimensional grid, where $i_1, i_2 \in \{1, 2, \dots, 19\}$ satisfy $19 \cdot (i_1 - 1) + i_2 = i$ for each i . These 361 locations were assigned to two actual groups as in Figure 2.1A. One group corresponds to $(\theta_{11}, \theta_{21}) = (5, 10)$ and the other corresponds to $(\theta_{12}, \theta_{22}) = (5, -10)$. We set $O = 1$, $\psi = 2.3$, $\sigma^2(\mathbf{s}_i) = 0.01$ for all i and specified $T = 310$ time points. When fitting the models, we utilized a training data set that consists of $y_t(\mathbf{s}_i)$'s at 352 out of the 361 spatial locations (Figure 2.1B) and the first 300 of the 310 time points. We used 10 for both the value of L and an upper bound to $L_{1:k}$. A burn-in length of 80000 and a post-burn-in length of 20000 (thinned to 5000) were used throughout. Simulated $y_t(\mathbf{s}_i)$'s on the remaining 9 testing locations for the first 300 time

points are used to assess spatial prediction performances. Similarly, $y_t(\mathbf{s}_i)$'s on the 352 training locations for the last 10 time points are used to assess temporal prediction performances.

The overall model fitting time for `fullGPfixedL`, `NNGPblockFixedL`, `NNGPsequenFixedL`, `NNGPsequenVaryLj`, `spBFAL10`, and `spBFALInf` are 15.77 hours, 15.46 hours, 15.19 hours, 14.58 hours, 7.24 days, and 3.08 days, respectively. The first four methods based on our implementation are several times faster than the `spBFA` package, as we have optimized several places in `spBFA`. Among the first four methods, `NNGPsequenVaryLj` is the fastest, followed by `NNGPsequenFixedL`, `NNGPblockFixedL`, and finally `fullGPfixedL`, as our three novelties significantly accelerate the posterior sampling of spatial-related parameters. We further provide a

Method Parameter	fullGPfixedL	NNGPblockFixedL	NNGPsequenFixedL	NNGPsequenVaryLj
ρ	11.389	4.961	4.965	4.986
κ	2.006	1.004	1.007	1.001
$\alpha_{jl_j}^o(\mathbf{s}_i)$'s	19.829	17.728	7.14	21.003
$z_{jl_j}^o(\mathbf{s}_i)$'s or $u_j^o(\mathbf{s}_i)$'s	24.408	24.158	24.079	≈ 0
$\xi_j^o(\mathbf{s}_i)$'s	13.164	13.235	13.129	3.279
θ_{jl_j} 's	243.285	242.981	243.138	242.254
$\delta_{1:k}$	0.986	0.977	0.986	0.934

Table 2.1: Average sampling time per MCMC iteration (in milliseconds) corresponding to the spatial-related parameters ρ , κ , $\alpha_{jl_j}^o(\mathbf{s}_i)$'s, $z_{jl_j}^o(\mathbf{s}_i)$'s or $u_j^o(\mathbf{s}_i)$'s, $\xi_j^o(\mathbf{s}_i)$'s, θ_{jl_j} 's, and $\delta_{1:k}$ across 5000 post-burn-in MCMC iterations for our four methods in the toy example.

detailed breakdown of the posterior sampling time for different sets of parameters and report the average time per MCMC iteration in Table 2.1. The NNGP prior has significantly reduced computation time for covariance parameters ρ and κ . On top of that, `NNGPsequenFixedL` using our sequential updating scheme has further reduced sampling time for the spatially varying latent variables $\alpha_{jl_j}^o(\mathbf{s}_i)$'s. `NNGPsequenVaryLj` based on our slice sampling algorithm bypasses sampling latent variables $z_{jl_j}^o(\mathbf{s}_i)$'s and samples instead the auxiliary variables $u_j^o(\mathbf{s}_i)$'s (see Section 3), whose computation is much faster. The Gibbs sampler step for $\xi_j^o(\mathbf{s}_i)$'s has also been significantly accelerated. Overall, the method `NNGPsequenVaryLj`, which utilizes all our three new techniques, exhibits the best computational efficiency. In this toy example, the four methods are still close in overall computation speed, as sampling loadings parameters θ_{jl_j} 's took the most model fitting time. As m increases, however, the acceleration in sampling spatial-related parameters quickly becomes substantial, as we shall see in Section 6.1 and Appendix I.2. $m = 3600$, for instance, leads to an overall computational speed increase of more than 10 times.

Method	fullGPfixedL	NNGPblockFixedL	NNGPsequenFixedL	NNGPsequenVaryLj	spBFAL10	spBFALInf
Spatial Prediction	14.123149	14.003086	14.341286	12.764447	N.A.	N.A.
Temporal Prediction	18.518662	18.754345	18.299211	19.340736	19.409493	164.42639

Table 2.2: Toy example: posterior mean squared errors for spatial and temporal predictions.

Appendix I.1 elaborates on all methods' performances in terms of posterior deviances, diagnostics statistics, temporal prediction metrics, spatial prediction time and metrics, and spatial clustering outcomes, from which we can see that adopting our three novel techniques can indeed

significantly accelerate the default MCMC algorithm for the Bayesian spatiotemporal factor model in Berchuck et al. (2022) without sacrificing inferential performances in model fitting, prediction, and spatial clustering. All four methods' diagnostics, converged posterior deviances, and temporal prediction results are close to their `spBFAL10` counterparts and significantly better than their `spBFALInf` counterparts. Moreover, all four methods deliver close satisfactory spatial prediction performances and achieve 100% accuracy for clustering based on recorded posterior samples the $m_0 = 352$ training locations into the two actual spatial groups. The `spBFA` package currently does not support spatial prediction or clustering. See Table 2.2 and Appendix I.1 for the results we obtained.

3 Slice Sampling for Bayesian Spatial Clustering

We propose a new slice sampling algorithm to address the computational burden incurred by using a common number of mixture components $L \in \mathbb{N}$, $L > 1$ for all latent factors in the PSBP model (2.3). For one thing, pre-specifying a fixed common L is likely restrictive since the numbers of spatial mixtures are unknown and may well differ across the k latent factors. An at least moderately large L would typically be required for fitting many mixture models across m spatial locations, especially when m becomes large. This leads to computational inefficiency since we need to perform more complicated calculations when updating $\xi_j^o(\mathbf{s}_i)$'s, δ_h 's, κ , ρ and sample more spatial clustering parameters θ_{jl_j} 's, $\alpha_{jl_j}^o(\mathbf{s}_i)$'s in each MCMC iteration. Moreover, when both L and the number of spatial locations m are large, storage requirements for either spatial prediction at new locations or clustering of temporal trends can become highly prohibitive, as one needs to store posterior samples of θ_{jl_j} 's, α_{jl_j} 's, and \mathbf{w}_{jl_j} 's from all kept post-burn-in MCMC iterations. Last but not least, posterior sampling of the introduced latent normal variables $z_{jl_j}^o(\mathbf{s}_i)$'s (Appendix D) is required when a common fixed L is assumed and is computationally demanding when L is large.

These concerns can be effectively addressed by assuming a varying number of clusters L_j for the j th latent factor loadings $\boldsymbol{\lambda}_j$ and adapting pertinent slice sampling ideas in Walker (2007). Our novel algorithm follows the original version of slice sampling (Walker 2007) and essentially differs from Berchuck et al. (2022)'s flawed implementation in their supplementary material and R package `spBFA`. Some further notes are in Appendix E.

Let us fix a pair $(i, o) \in \{1, \dots, m\} \times \{1, \dots, O\}$. Consider the spatial PSBP prior under the finite-mixture version of (2.2) with L_j mixture components for the j th latent factor loadings. For $t = 1, \dots, T$, the observation $y_t^o(\mathbf{s}_i)$ has density

$$\begin{aligned} & f(y_t^o(\mathbf{s}_i) \mid \boldsymbol{\beta}, \boldsymbol{\eta}_t, (\sigma^2)^o(\mathbf{s}_i), L_j \text{ for all } j, \boldsymbol{\alpha}^o(\mathbf{s}_i), \boldsymbol{\theta}) \\ &= \sum_{l_1=1}^{L_1} \cdots \sum_{l_k=1}^{L_k} \left\{ \left[\prod_{j=1}^k w_{jl_j}^o(\mathbf{s}_i) \right] \times f(y_t^o(\mathbf{s}_i) \mid \boldsymbol{\beta}, \boldsymbol{\eta}_t, (\sigma^2)^o(\mathbf{s}_i), \theta_{jl_j} \text{ for all } j = 1, \dots, k) \right\}, \end{aligned} \quad (3.1)$$

where $\boldsymbol{\alpha}^o(\mathbf{s}_i) = \{\alpha_{jl_j}^o(\mathbf{s}_i) : j = 1, \dots, k, l_j = 1, \dots, L_j - 1\}$. To incorporate slice sampling (Walker 2007), we further introduce latent variables $u_j^o(\mathbf{s}_i)$, $j \in \{1, \dots, k\}$, such that

$$f(y_t^o(\mathbf{s}_i), u_{1:k}^o(\mathbf{s}_i) \mid \boldsymbol{\beta}, \boldsymbol{\eta}_t, (\sigma^2)^o(\mathbf{s}_i), L_j \text{ for all } j, \boldsymbol{\alpha}^o(\mathbf{s}_i), \boldsymbol{\theta}) \quad (3.2)$$

$$= \sum_{l_1=1}^{L_1} \cdots \sum_{l_k=1}^{L_k} \left\{ \left[\prod_{j=1}^k \mathbb{1}_{\{u_j^o(\mathbf{s}_i) < w_{jl_j}^o(\mathbf{s}_i)\}} \right] \times f(y_t^o(\mathbf{s}_i) \mid \boldsymbol{\beta}, \boldsymbol{\eta}_t, (\sigma^2)^o(\mathbf{s}_i), \theta_{1l_1}, \dots, \theta_{kl_k}) \right\},$$

where $\mathbb{1}_E$ denotes the indicator function of an event E . Since integrating over $u_j^o(\mathbf{s}_i)$'s in (3.2) with respect to the Lebesgue measure on the measurable space $((0, 1]^k, \mathcal{B}((0, 1]^k))$ yields (3.1), the joint density in Equation (3.2) with the corresponding marginal density in Equation (3.1) indeed exists. Hence, the complete data likelihood is

$$\ell_{\text{complete}} = \prod_{o=1}^O \prod_{i=1}^m \prod_{t=1}^T \left[\prod_{j=1}^k \mathbb{1}_{\{u_j^o(\mathbf{s}_i) < w_{j\xi_j^o(\mathbf{s}_i)}^o(\mathbf{s}_i)\}} \right] \times f(y_t^o(\mathbf{s}_i) \mid \boldsymbol{\beta}, \boldsymbol{\eta}_t, (\sigma^2)^o(\mathbf{s}_i), \xi_j^o(\mathbf{s}_i), \theta_{j\xi_j^o(\mathbf{s}_i}) \text{ for all } j = 1, \dots, k), \quad (3.3)$$

where for any $(i, o, j) \in \{1, \dots, m\} \times \{1, \dots, O\} \times \{1, \dots, k\}$ and $l_j \in \{1, \dots, L_j\}$,

$$w_{jl_j}^o(\mathbf{s}_i) = \begin{cases} \Phi(\alpha_{jl_j}^o(\mathbf{s}_i)) \prod_{r_j < l_j} [1 - \Phi(\alpha_{jr_j}^o(\mathbf{s}_i))], & \text{if } l_j \in \{1, \dots, L_j - 1\} \\ \prod_{r_j < L_j} [1 - \Phi(\alpha_{jr_j}^o(\mathbf{s}_i))], & \text{if } l_j = L_j \end{cases}. \quad (3.4)$$

Under this model specification, we no longer need to introduce and sample the latent normal $z_{jl_j}^o(\mathbf{s}_i)$'s (Section 2) from their full conditional distributions (Equation (D.4) in Appendix D) to bring about conjugacy for $\alpha_{jl_j}^o(\mathbf{s}_i)$'s, which requires a total of $\mathcal{O}(kLmO)$ floating point operations (flops) per MCMC iteration and is thus computationally inefficient for a large L . Instead, we only need to sample the latent uniform $u_j^o(\mathbf{s}_i)$'s from their full conditional distributions below.

$$\text{For any } (i, o, j), \quad f(u_j^o(\mathbf{s}_i) \mid \cdot) \propto \mathbb{1}_{\{u_j^o(\mathbf{s}_i) < w_{j\xi_j^o(\mathbf{s}_i)}^o(\mathbf{s}_i)\}} \sim \text{Unif}(0, w_{j\xi_j^o(\mathbf{s}_i)}^o(\mathbf{s}_i)). \quad (3.5)$$

The corresponding computational complexity per MCMC iteration is reduced to $\mathcal{O}(kmO)$.

The pivotal role played by the introduced parameters L_j 's and $u_j^o(\mathbf{s}_i)$'s is reflected in the step updating L_j 's and sampling cluster labels $\xi_j^o(\mathbf{s}_i)$'s from their full conditional distributions. Fix any arbitrary $j \in \{1, \dots, k\}$. For all $l_j \in \{1, \dots, L_j^{\text{old}}\}$ and for any (i, o) ,

$$\begin{aligned} \mathbb{P}(\xi_j^o(\mathbf{s}_i) = l_j \mid \cdot) &\propto \mathbb{1}_{\{w_{jl_j}^o(\mathbf{s}_i) > u_j^o(\mathbf{s}_i)\}} \\ &\times \prod_{t=1}^T f(y_t^o(\mathbf{s}_i) \mid \boldsymbol{\beta}, \boldsymbol{\eta}_t, (\sigma^2)^o(\mathbf{s}_i), \xi_j^o(\mathbf{s}_i) = l_j, \boldsymbol{\xi}_{-j}^o(\mathbf{s}_i), \boldsymbol{\theta}_{\xi^o(\mathbf{s}_i)}), \end{aligned} \quad (3.6)$$

where for any (i, o, j, l_j) such that $w_{jl_j}^o(\mathbf{s}_i) > u_j^o(\mathbf{s}_i)$, for all $t \in \{1, \dots, T\}$,

$$\begin{aligned} &f(y_t^o(\mathbf{s}_i) \mid \boldsymbol{\beta}, \boldsymbol{\eta}_t, (\sigma^2)^o(\mathbf{s}_i), \xi_j^o(\mathbf{s}_i) = l_j, \boldsymbol{\xi}_{-j}^o(\mathbf{s}_i), \boldsymbol{\theta}_{\xi^o(\mathbf{s}_i)}) \\ &= (2\pi)^{-\frac{1}{2}} (\sigma^{-1})^o(\mathbf{s}_i) \exp \left\{ -\frac{1}{2} (\sigma^{-2})^o(\mathbf{s}_i) \left[y_t^o(\mathbf{s}_i) - \mathbf{x}_t^o(\mathbf{s}_i)^\top \boldsymbol{\beta} - \sum_{h \neq j}^{1 \leq h \leq k} \theta_{h\xi_h^o(\mathbf{s}_i)} \eta_{th} - \theta_{jl_j} \eta_{tj} \right]^2 \right\}. \end{aligned}$$

For any $(i, o) \in \{1, \dots, m\} \times \{1, \dots, O\}$, we let

$$\begin{aligned} L_j^{i,o} &= \text{the smallest positive integer such that } \sum_{l_j=1}^{L_j^{i,o}} w_{jl_j}^o(\mathbf{s}_i) > 1 - u_j^o(\mathbf{s}_i) \\ \text{and } L_j^{\text{new}} &= \max \{ L_j^{i,o} : i = 1, \dots, m, o = 1, \dots, O \}. \end{aligned} \quad (3.7)$$

It is clear from Equations (3.6) and (3.7) that for any $l_j > L_j^{\text{new}}$, $\mathbb{P}(\xi_j^o(\mathbf{s}_i) = l_j | \cdot) = 0$ for all (i, o) . Hence, we can update the parameter estimate for $L_j \in \mathbb{N} \setminus \{0\}$ from L_j^{old} to $L_j^{\text{new}} \leq L_j^{\text{old}} < \infty$ in this MCMC iteration and only consider $l_j \in \{1, \dots, L_j^{\text{new}}\}$ to be the possible values for $\xi_j^o(\mathbf{s}_i)$ for all (i, o) . After obtaining $\{L_j^{\text{new}} : j = 1, \dots, k\}$ by Equation (3.7) at the start of this Gibbs sampler step, we immediately update estimates for α_{jl_j} 's by only keeping the $mO \times 1$ vectors corresponding to $l_j \in \{1, 2, \dots, L_j^{\text{new}} - 1\}$ and discarding the ones corresponding to $l_j \in \{L_j^{\text{new}}, L_j^{\text{new}} + 1, \dots, L_j^{\text{old}} - 1\}$. We then formulate our new weights \mathbf{w}_{jl_j} for $l_j = 1, \dots, L_j^{\text{new}}$ (as specified by Equation (3.4)) by discarding the previous \mathbf{w}_{jl_j} estimates with $l_j \in \{L_j^{\text{new}} + 1, \dots, L_j^{\text{old}}\}$ and adjusting the $w_{jL_j^{\text{new}}}^o(\mathbf{s}_i)$ estimates if L_j^{new} is strictly less than L_j^{old} . New cluster labels $\xi_j^o(\mathbf{s}_i)$'s can then be sampled according to Equation (3.6) based on these new weights. Among all kept weights parameters, only the $w_{jL_j^{\text{new}}}^o(\mathbf{s}_i)$ estimates are possibly altered (increased) in this step. Since all updated weights are ensured greater than or equal to their old values, it is indeed guaranteed that $\xi_j^o(\mathbf{s}_i)^{\text{old}} \leq L_j^{i,o} \leq L_j^{\text{new}} \leq L_j^{\text{old}}$ is still in the support for $\xi_j^o(\mathbf{s}_i)^{\text{new}}$ and $u_j^o(\mathbf{s}_i) < w_{j\xi_j^o(\mathbf{s}_i)^{\text{new}}}^o(\mathbf{s}_i)^{\text{new}}$ for each (j, i, o) .

Thanks to this non-increasing property of posterior samples for L_j 's through the MCMC iterations, we can perform simplified calculations when updating $\xi_j^o(\mathbf{s}_i)$'s, δ_h 's, κ , ρ and sample fewer posterior θ_{jl_j} 's and α_{jl_j} 's from their full conditional distributions given in (A.23) and below. In particular, the posterior sampling time of $\xi_j^o(\mathbf{s}_i)$'s is reduced most considerably (Tables 2.1 and 5.1, Section 6.1, Appendix I.2). As each L_j is usually much smaller than its initial upper bound in practice, storage concerns related to θ_{jl_j} 's, α_{jl_j} 's, and \mathbf{w}_{jl_j} 's can be significantly alleviated as well. Spatial prediction can also be considerably accelerated (Sections 5.1 and 6.2, Appendices G.2.2 and I.1). See Appendix H.1 for theoretical analysis of complexities.

We do not need to sample any α_{jl_j} 's for j values with $L_j = 1$, as the corresponding $w_{j1}^o(\mathbf{s}_i)$'s have already been set to 1 in the earlier Gibbs sampling step for $\xi_j^o(\mathbf{s}_i)$'s. Fix any arbitrary (i, o, j) where $L_j > 1$ and fix an $l_j \in \{1, \dots, L_j - 1\}$. The only term in the complete data likelihood (3.3) possibly involving $\alpha_{jl_j}^o(\mathbf{s}_i)$ is $\mathbb{1}_{\{u_j^o(\mathbf{s}_i) < w_{j\xi_j^o(\mathbf{s}_i)}^o(\mathbf{s}_i)\}}$. Hence for any (j, l_j) where $j \in \{1, \dots, k\}$ and $l_j \in \{1, \dots, L_j - 1\}$,

$$\begin{aligned} \alpha_{jl_j} | \cdot &\sim N_{mO}(\mathbf{0}, F(\rho) \otimes \kappa) \times \prod_{i=1}^m \prod_{o=1}^O \mathbb{1}_{\{l_j > \xi_j^o(\mathbf{s}_i) \text{ or } u_j^o(\mathbf{s}_i) < w_{j\xi_j^o(\mathbf{s}_i)}^o(\mathbf{s}_i)\}} \\ &\sim N_{mO}(\mathbf{0}, F(\rho) \otimes \kappa) \times \prod_{i=1}^m \prod_{o=1}^O \begin{cases} 1, & \text{if } l_j > \xi_j^o(\mathbf{s}_i) \\ \mathbb{1}_{\{\alpha_{jl_j}^o(\mathbf{s}_i)^{\text{new}} > \text{lowerBound}_{(j, l_j, i, o)}\}}, & \text{if } l_j = \xi_j^o(\mathbf{s}_i), \\ \mathbb{1}_{\{\alpha_{jl_j}^o(\mathbf{s}_i)^{\text{new}} < \text{upperBound}_{(j, l_j, i, o)}\}}, & \text{if } l_j < \xi_j^o(\mathbf{s}_i) \end{cases} \end{aligned} \quad (3.8)$$

where $\alpha_{jl_j} = (\alpha_{jl_j}(\mathbf{s}_1)^{\text{T}}, \dots, \alpha_{jl_j}(\mathbf{s}_m)^{\text{T}})^{\text{T}}$ with $\alpha_{jl_j}(\mathbf{s}_i)^{\text{T}} = (\alpha_{jl_j}^1(\mathbf{s}_i), \alpha_{jl_j}^2(\mathbf{s}_i), \dots, \alpha_{jl_j}^O(\mathbf{s}_i))$ for all $i = 1, 2, \dots, m$, and for any (j, l_j, i, o) ,

$$\text{lowerBound}_{(j, l_j, i, o)} = \Phi^{-1} \left(\frac{u_j^o(\mathbf{s}_i) \cdot \Phi(\alpha_{jl_j}^o(\mathbf{s}_i)^{\text{old}})}{w_{j\xi_j^o(\mathbf{s}_i)}^o(\mathbf{s}_i)} \right) \text{ and} \quad (3.9)$$

$$\text{upperBound}_{(j, l_j, i, o)} = \Phi^{-1} \left(1 - \frac{u_j^o(\mathbf{s}_i) \cdot [1 - \Phi(\alpha_{jl_j}^o(\mathbf{s}_i)^{\text{old}})]}{w_{j\xi_j^o(\mathbf{s}_i)}^o(\mathbf{s}_i)} \right). \quad (3.10)$$

These truncated multivariate normal posterior distributions of the α_{jl_j} 's can be directly sampled via multivariate rejection sampling, as implemented by for instance the `rtmvnorm()` function in the R package `tmvtnorm`. When m is large, we will further enhance computational efficiency in Section 4.4 by replacing this possibly high-dimensional rejection sampling by a sequential updating algorithm that uses low-dimensional rejection samplings. After obtaining new estimates for $\alpha_{jl_j}^o(\mathbf{s}_i)$'s, we formulate posterior samples of $w_{jl_j}^o(\mathbf{s}_i)$'s via Equation (3.4) correspondingly. The complete Gibbs sampler based on this slice sampling algorithm can be found in Appendix A.3.

We briefly discuss three computational complexity sources of this slice sampling algorithm. One is the posterior sampling of $u_j^o(\mathbf{s}_i)$'s from Equation (3.5), which has a smaller complexity $\mathcal{O}(kmO)$ over the indices j, i, o . The standard Gibbs sampler for PSBP prior, on the other hand, requires sampling the latent normal variables $z_{jl_j}^o(\mathbf{s}_i)$'s from their conditional posteriors that are possibly truncated normal distributions (Equation (A.13)), which has complexity $\mathcal{O}(kLmO)$ over all indices j, l_j, i, o . One concerns the posterior sampling of $\xi_j^o(\mathbf{s}_i)$'s, which has computational complexity $\mathcal{O}\left(\sum_{j=1}^k L_j \cdot mOT(p+k)\right)$. Another stems from the calculation of lower and upper bounds in (3.9) and (3.10) and the cost of rejection sampling from (3.8). We provide a more detailed analysis of and considerably reduce the complexity of this part in Section 4.4. In practice, benefits from replacing the sampling of $z_{jl_j}^o(\mathbf{s}_i)$'s by $u_j^o(\mathbf{s}_i)$'s and accelerating the sampling of $\xi_j^o(\mathbf{s}_i)$'s outweigh the additional cost from rejection sampling of $\alpha_{jl_j}(\mathbf{s}_i)$'s, especially when m and L are large; see our numerical results in Section 6.1 and Appendix I.2.

4 Spatial Scalability via Nearest-Neighbor Gaussian Process and Sequential Updates

4.1 Computational Burdens from a Large $F(\rho)_{m \times m}$

For Berchuck et al. (2022)'s Bayesian spatiotemporal factor model in Section 2, one major source of computational bottleneck is the GP prior in Equation (2.4), where the covariance matrix has a large dimension of $mO \times mO$. For one, sampling ρ and $\kappa_{O \times O}$ from their conditional posterior distributions will inevitably involve computation related to the inversion and determinant of a large matrix $F(\rho)_{m \times m}$. The computational complexity for inversion and determinant calculation are both typically $\mathcal{O}(m^3)$ for $m \times m$ matrices without any special structure, and the storage cost of the entire $F(\rho)$ and $F(\rho)^{-1}$ is $\mathcal{O}(m^2)$, both of which become prohibitive for a large m . For another, the posterior sampling of α_{jl_j} 's is also heavily affected. As deduced in Equation (D.5), for any $(j, l_j) \in \{1, \dots, k\} \times \{1, \dots, L-1\}$, $\alpha_{jl_j} | \cdot \sim N_{mO} \left([I_{mO} + F(\rho)^{-1} \otimes \kappa^{-1}]^{-1} \mathbf{z}_{jl_j}, [I_{mO} + F(\rho)^{-1} \otimes \kappa^{-1}]^{-1} \right)$. We thus need to evaluate $\text{Chol} \left([I_{mO} + F(\rho)^{-1} \otimes \kappa^{-1}]^{-1} \right)$, the Cholesky factor of an $mO \times mO$ matrix, which requires $\mathcal{O}(m^3)$ flops using standard methods. Furthermore, if we adopt the slice sampling algorithm in Section 3, then the full conditional distribution of each α_{jl_j} is likely a truncated mO -variate normal distribution given by (3.8), which often has a very low acceptance rate when m is large. As such, the slow rejection sampling step will likely result in a computational complexity even larger than $\mathcal{O}(m^3)$ for updating all α_{jl_j} 's.

We overcome these computational issues from large-scale GP using two techniques. First, by treating the $\alpha_{jl_j}(\mathbf{s}_i)$'s as the location-specific latent random effects $\mathbf{w}(\mathbf{s}_i)$'s in Datta et al. (2016)

and Finley, Datta, and Banerjee (2022), we can straightforwardly apply the latent Nearest-Neighbor Gaussian Process (NNGP) model framework to significantly reduce the computational and storage complexities related to the inversion and determinant of large $m \times m$ matrices. Second, we propose a sequential updating scheme to bypass the inefficient posterior sampling of α_{jl_j} 's. Computation and storage efficiency can hence be greatly enhanced (Appendices H.2 and H.3). Appendix F gives some further comments.

4.2 Incorporating the Spatial Latent NNGP

We derive an NNGP prior $\tilde{\pi}(\alpha_{jl_j}|\kappa, \rho) = N_{mO}(\mathbf{0}, \tilde{F}(\rho) \otimes \kappa)$ for all (j, l_j) , where $\tilde{F}(\rho)_{m \times m}^{-1}$ is sparse and can be calculated in $\mathcal{O}(m)$ flops together with $\det(\tilde{F}(\rho))$. Fix any arbitrary (j, l_j) and consider the zero-mean O -variate Gaussian process $\alpha_{jl_j}|\kappa, \rho \sim N_{mO}(\mathbf{0}, F(\rho) \otimes \kappa)$ over the spatial domain $\mathcal{D} \subset \mathbb{R}^d, d \in \mathbb{N}$, with $\alpha_{jl_j} = (\alpha_{jl_j}(\mathbf{s}_1)^\top, \dots, \alpha_{jl_j}(\mathbf{s}_m)^\top)^\top$, where each $\alpha_{jl_j}(\mathbf{s}_i), i \in \{1, \dots, m\}$, conceived as a realization of the latent process $\{\alpha_{jl_j}(\mathbf{s})|\mathbf{s} \in \mathcal{D}\}$, is an $O \times 1$ vector corresponding to the observation at location \mathbf{s}_i on the O variables. We take the location reference set to be the same as the set of observed locations $\mathcal{S} = \{\mathbf{s}_1, \dots, \mathbf{s}_m\} \subset \mathcal{D}$, a simple yet effective choice that delivers superb inferences (Datta et al. 2016). Pick a positive integer $h \ll m$ and consider the Euclidean distance (Vecchia 1988). Let $N(\mathbf{s}_1) = \emptyset$ and define for each $i \in \{2, 3, \dots, m\}$ location point \mathbf{s}_i 's neighbor set $N(\mathbf{s}_i)$ as the $\min\{h, i-1\}$ nearest neighbors of \mathbf{s}_i in $\{\mathbf{s}_1, \dots, \mathbf{s}_{i-1}\}$. As shown by Datta et al. (2016), a quite small number of h (between 10 to 15 for instance) can already yield highly competitive performance, and the predictive performance of NNGP is sensitive to neither the choice of reference set nor the ordering of locations.

The GP prior $\alpha_{jl_j}|\kappa, \rho \sim N(\mathbf{0}, F(\rho) \otimes \kappa)$ gives the density

$$\pi(\alpha_{jl_j}|\kappa, \rho) = \pi(\alpha_{jl_j}(\mathbf{s}_1)|\kappa, \rho) \times \prod_{i=2}^m f(\alpha_{jl_j}(\mathbf{s}_i)|\alpha_{jl_j}(\mathbf{s}_{1:(i-1)}), \kappa, \rho),$$

which, under the latent NNGP prior, can be approximated by

$$\tilde{\pi}(\alpha_{jl_j}|\kappa, \rho) = \pi(\alpha_{jl_j}(\mathbf{s}_1)|\kappa, \rho) \times \prod_{i=2}^m f(\alpha_{jl_j}(\mathbf{s}_i)|\alpha_{jl_j, N(\mathbf{s}_i)}, \kappa, \rho), \quad (4.1)$$

where $\alpha_{jl_j, N(\mathbf{s}_i)}$ is at most of length hO for each $i \in \{2, 3, \dots, m\}$. It is clear that $\alpha_{jl_j}(\mathbf{s}_1)|\kappa, \rho \sim N_O(\mathbf{0}, \kappa)$. Since $\alpha_{jl_j}|\kappa, \rho \sim N_{mO}(\mathbf{0}, F(\rho) \otimes \kappa)$, by properties of conditional distributions of jointly multivariate normals, we have

$$\alpha_{jl_j}(\mathbf{s}_i)|\alpha_{jl_j, N(\mathbf{s}_i)}, \kappa, \rho \sim N_O(B_{\mathbf{s}_i} \alpha_{jl_j, N(\mathbf{s}_i)}, F_{\mathbf{s}_i}), \text{ for all } i \in \{2, \dots, m\}, \quad (4.2)$$

where the $O \times (|N(\mathbf{s}_i)| \cdot O)$ matrix $B_{\mathbf{s}_i} = F(\rho)_{\mathbf{s}_i, N(\mathbf{s}_i)} F(\rho)_{N(\mathbf{s}_i)}^{-1} \otimes I_{O \times O}$ and the $O \times O$ matrix $F_{\mathbf{s}_i} = [F(\rho)_{\mathbf{s}_i, \mathbf{s}_i} - F(\rho)_{\mathbf{s}_i, N(\mathbf{s}_i)} F(\rho)_{N(\mathbf{s}_i)}^{-1} F(\rho)_{N(\mathbf{s}_i), \mathbf{s}_i}] \otimes \kappa$ with $F(\rho)_{\mathbf{s}_i, \mathbf{s}_i} = 1$, $F(\rho)_{\mathbf{s}_i, N(\mathbf{s}_i)}$, $F(\rho)_{N(\mathbf{s}_i), \mathbf{s}_i}$, $F(\rho)_{N(\mathbf{s}_i)}$ being the corresponding 1×1 , $1 \times |N(\mathbf{s}_i)|$, $|N(\mathbf{s}_i)| \times 1$, $|N(\mathbf{s}_i)| \times |N(\mathbf{s}_i)|$ sub-matrices of $F(\rho)_{m \times m}$. Hence following Equation (4.1), we have

$$\tilde{\pi}(\alpha_{jl_j}|\kappa, \rho) \sim N_O(\mathbf{0}, \kappa) \times \prod_{i=2}^m N_O(B_{\mathbf{s}_i} \alpha_{jl_j, N(\mathbf{s}_i)}, F_{\mathbf{s}_i}). \quad (4.3)$$

We thus no longer need to store the entire $F(\rho)$ and only need to store the sub-matrices $F(\rho)_{\mathbf{s}_i, N(\mathbf{s}_i)}, F(\rho)_{N(\mathbf{s}_i), \mathbf{s}_i}, F(\rho)_{N(\mathbf{s}_i)}$ for each $i \in \{2, \dots, m\}$. The storage cost of $F(\rho)$ can hence be reduced from $\mathcal{O}(m^2)$ to $\mathcal{O}(m(h+1)^2)$, i.e., quadratic to linear in m since $|N(\mathbf{s}_i)| \leq h \ll m$ for all $i \in \{2, \dots, m\}$. It is known that Equation (4.3) is indeed the joint density from a valid stochastic process (Appendix A in Datta et al. 2016), as its corresponding construction ensures a directed acyclic graph $\mathcal{G} = \{\mathcal{S}, N_{\mathcal{S}}\}$. Also, for any $i \in \{2, \dots, m\}$, $|N(\mathbf{s}_i)| \leq h$ and $B_{\mathbf{s}_i}, F_{\mathbf{s}_i}$ can be calculated by at most $\mathcal{O}(h^3)$ flops, which result from evaluating $F(\rho)_{N(\mathbf{s}_i)}^{-1}$. We thus need $\mathcal{O}(mh^3)$ flops evaluating all $B_{\mathbf{s}_i}$'s and $F_{\mathbf{s}_i}$'s.

4.3 Approximating $F(\rho)^{-1}$ and $\det(F(\rho))$

Let $F_{\mathbf{s}_1} = \kappa_{O \times O}$ and $B_{\mathbf{s}_1}^* = (1, 0, \dots, 0)_{1 \times m} \otimes I_{O \times O}$. Then by Equation (4.3),

$$\begin{aligned} \tilde{\pi}(\alpha_{jl_j} | \kappa, \rho) &\propto \frac{1}{\prod_{i=1}^m \sqrt{\det(F_{\mathbf{s}_i})}} \times \exp \left\{ -\frac{1}{2} \sum_{i=1}^m \alpha_{jl_j}^T (B_{\mathbf{s}_i}^*)^T F_{\mathbf{s}_i}^{-1} B_{\mathbf{s}_i}^* \alpha_{jl_j} \right\} \\ &= \frac{1}{\sqrt{\prod_{i=1}^m \det(F_{\mathbf{s}_i})}} \times \exp \left\{ -\frac{1}{2} \alpha_{jl_j}^T B_S^T F_S^{-1} B_S \alpha_{jl_j} \right\}, \end{aligned} \quad (4.4)$$

where the $mO \times mO$ matrix $F_S = \text{Diag}(F_{\mathbf{s}_1}, \dots, F_{\mathbf{s}_m})$ and $B_S = \left([B_{\mathbf{s}_1}^*]^T, [B_{\mathbf{s}_2}^*]^T, \dots, [B_{\mathbf{s}_m}^*]^T \right)^T$. For each i , the $O \times mO$ matrix $B_{\mathbf{s}_i}^* = (B_{\mathbf{s}_i,1}^*, B_{\mathbf{s}_i,2}^*, \dots, B_{\mathbf{s}_i,m}^*)$ is sparse with at most $h+1$ non-zero $O \times O$ blocks out of the m blocks

$$B_{\mathbf{s}_i,j}^* = \begin{cases} I_{O \times O}, & \text{if } j = i \\ -B_{\mathbf{s}_i}[(l-1)O+1 : lO], & \text{if } \exists l \in \{1, \dots, \min(h, i-1)\} \text{ such that } \mathbf{s}_j = N(\mathbf{s}_i)[l], \\ \mathbf{0}_{O \times O}, & \text{otherwise} \end{cases}$$

for $j \in \{1, \dots, m\}$, where $N(\mathbf{s}_i)[l]$ denotes the l -th point in $N(\mathbf{s}_i)$. Since for any $i \in \{2, 3, \dots, m\}$, $N(\mathbf{s}_i) \subset \{\mathbf{s}_1, \dots, \mathbf{s}_{i-1}\}$, B_S is lower triangular whose main diagonal entries are all 1. This implies that $\det(B_S) = 1$ and that $B_S^T F_S^{-1} B_S$ is invertible. Hence, we can let $\tilde{F}(\rho)^{-1} \otimes \kappa^{-1} = B_S^T F_S^{-1} B_S = \sum_{i=1}^m (B_{\mathbf{s}_i}^*)^T F_{\mathbf{s}_i}^{-1} B_{\mathbf{s}_i}^*$, whose computational complexity given $F_{\mathbf{s}_i}$'s and $B_{\mathbf{s}_i}$'s is $\mathcal{O}(O^3) + \mathcal{O}(m(h+1)^2) = \mathcal{O}(m)$ since $h \ll m$ and $O \in \mathbb{N}$ is also assumed very small. The $\tilde{F}(\rho)_{m \times m}^{-1}$ defined this way simplifies Equation (4.4) to

$$\tilde{\pi}(\alpha_{jl_j} | \kappa, \rho) \propto \left\{ \det \left(\tilde{F}(\rho) \otimes \kappa \right) \right\}^{-1/2} \times \exp \left\{ -\frac{1}{2} \alpha_{jl_j}^T [\tilde{F}(\rho)^{-1} \otimes \kappa^{-1}] \alpha_{jl_j} \right\}. \quad (4.5)$$

Hence $\tilde{\pi}(\alpha_{jl_j} | \kappa, \rho) = N_{mO}(\mathbf{0}, \tilde{F}(\rho) \otimes \kappa)$, which is our NNGP prior. As $\det(B_S) = 1$, we have $\det(\tilde{F}(\rho) \otimes \kappa) = \det([B_S^T F_S^{-1} B_S]^{-1}) = \det(F_S) = \prod_{i=1}^m \det(F_{\mathbf{s}_i})$, which can be calculated in $\mathcal{O}(m) + \mathcal{O}(O^3) = \mathcal{O}(m)$ flops with evaluated $F_{\mathbf{s}_i}$'s. The total computational complexity calculating $\tilde{F}(\rho)^{-1} \otimes \kappa^{-1}$ and $\det(\tilde{F}(\rho) \otimes \kappa)$ is thus linear in m . A full GP with a dense precision matrix $F(\rho) \otimes \kappa$, on the other hand, needs $\mathcal{O}(m^3)$ flops updating the counterpart quantities $F(\rho)^{-1} \otimes \kappa^{-1}$ and $\det(F(\rho) \otimes \kappa)$ in each MCMC iteration.

We now consider elements of the precision matrix $\tilde{F}(\rho)_{m \times m}^{-1}$. For any pair $(i, j) \in \{1, \dots, m\}^2$ and $i < j$, let \tilde{F}_{ij}^{-1} be the (i, j) -th entry of $\tilde{F}(\rho)^{-1}$. Then $\tilde{F}(\rho)^{-1} \otimes \kappa^{-1} = \sum_{l=1}^m (B_{\mathbf{s}_l}^*)^T F_{\mathbf{s}_l}^{-1} B_{\mathbf{s}_l}^*$ implies $\tilde{F}_{ij}^{-1} \otimes \kappa^{-1} = \sum_{l=j}^m (B_{\mathbf{s}_l,i}^*)^T F_{\mathbf{s}_l}^{-1} B_{\mathbf{s}_l,j}^*$. Hence $\tilde{F}_{ij}^{-1} \neq 0$ implies that there exists $l \in$

$\{j, j+1, \dots, m\}$ such that $\mathbf{s}_i \in N(\mathbf{s}_l)$ and $\mathbf{s}_j \in N(\mathbf{s}_l)$ or $\mathbf{s}_j = \mathbf{s}_l$. We can thus obtain an upper bound, $m \cdot \frac{h(h+1)}{2}$, of the maximum number of pairs $(i, j), i < j$ leading to a non-zero \tilde{F}_{ij}^{-1} by looping over $l \in \{1, \dots, m\}$. Further taking the lower triangular and diagonal entries of $\tilde{F}(\rho)^{-1}$ into consideration, we get that $\tilde{F}(\rho)_{m \times m}^{-1}$ is sparse with at most $2 \times m \cdot \frac{h(h+1)}{2} + m = m \cdot [h(h+1) + 1]$ non-zero entries. Hence, the storage complexity for $\tilde{F}(\rho)_{m \times m}^{-1}$ is $\mathcal{O}(mh^2)$, including the nonzero entries and their indices. The spatial NNGP's capability of reducing storage for $F(\rho)^{-1}$ from quadratic to linear in m can be tremendously useful for fitting data with a very large m value.

4.4 Sequentially Updating α_{jl_j} 's Under Spatial NNGP Prior

Although the NNGP prior can reduce sampling costs of ρ and $\kappa_{O \times O}$ (Appendix A.2), the inefficiency in the posterior sampling of α_{jl_j} 's for a large m as described in Section 4.1 cannot be addressed by adopting the spatial NNGP prior alone, as we explain below. Therefore, we further propose a sequential updating scheme to tackle these issues.

Under the model in Section 2, for any arbitrary $(j, l_j) \in \{1, \dots, k\} \times \{1, \dots, L-1\}$, the full conditional posterior of α_{jl_j} under the NNGP prior is

$$\alpha_{jl_j} | \cdot \sim N_{mO} \left(\left[I_{mO} + \tilde{F}(\rho)^{-1} \otimes \kappa^{-1} \right]^{-1} \mathbf{z}_{jl_j}, \left[I_{mO} + \tilde{F}(\rho)^{-1} \otimes \kappa^{-1} \right]^{-1} \right), \quad (4.6)$$

where \mathbf{z}_{jl_j} is the introduced latent normal vector (Appendix D). We thus need to evaluate $\text{Chol}([I_{mO} + \tilde{F}(\rho)^{-1} \otimes \kappa^{-1}]^{-1})$ and $[I_{mO} + \tilde{F}(\rho)^{-1} \otimes \kappa^{-1}]^{-1}$, which requires $\mathcal{O}(m^3)$ flops via standard methods. Hence, directly proceeding with block updating α_{jl_j} 's according to Equation (4.6) for all (j, l_j) still requires $\mathcal{O}(m^3) + \mathcal{O}(k(L-1) \cdot (mO)^2) = \mathcal{O}(m^3)$ flops in each MCMC iteration and thus incurs a high computational cost.

For the slice sampling algorithm in Section 3, for any (j, l_j) where $j \in \{1, \dots, k\}$ and $l_j \in \{1, \dots, L_j - 1\}$, the full conditional posterior of α_{jl_j} under the NNGP prior is

$$\alpha_{jl_j} | \cdot \sim N_{mO} \left(\mathbf{0}, \tilde{F}(\rho) \otimes \kappa \right) \times \prod_{i=1}^m \prod_{o=1}^O \begin{cases} 1, & \text{if } l_j > \xi_j(\mathbf{s}_{i,o}) \\ \mathbb{1}_{\{\alpha_{jl_j}^o(\mathbf{s}_i)^{\text{new}} > \text{lowerBound}_{(j,l_j,i,o)}\}}, & \text{if } l_j = \xi_j^o(\mathbf{s}_i) \\ \mathbb{1}_{\{\alpha_{jl_j}^o(\mathbf{s}_i)^{\text{new}} < \text{upperBound}_{(j,l_j,i,o)}\}}, & \text{if } l_j < \xi_j^o(\mathbf{s}_i) \end{cases}, \quad (4.7)$$

where $\text{lowerBound}_{(j,l_j,i,o)}$'s and $\text{upperBound}_{(j,l_j,i,o)}$'s are given by Equations (3.9) and (3.10). Therefore, we need to evaluate $\text{Chol}(\tilde{F}(\rho) \otimes \kappa)$, which generally still requires $\mathcal{O}(m^3)$ flops. Finding a faster numerical algorithm to evaluate $\text{Chol}(\tilde{F}(\rho) \otimes \kappa)$ is challenging. More seriously, rejection sampling from a high-dimensional truncated mO -variate normal distribution in Equation (4.7) may become extremely slow due to the low acceptance rate.

We propose a novel algorithm to bypass these computational burdens under both models by sequentially updating components of $\alpha_{jl_j} = (\alpha_{jl_j}(\mathbf{s}_1)^T, \dots, \alpha_{jl_j}(\mathbf{s}_m)^T)^T$ for each (j, l_j) instead. Computational complexity orders for updating all α_{jl_j} 's in each MCMC iteration are presented in Table H.3. Let $F_{\mathbf{s}_1} = \kappa_{O \times O}$ and $F_{\mathbf{s}_1}^{-1} B_{\mathbf{s}_1} \alpha_{jl_j, N(\mathbf{s}_1)} = \mathbf{0}_{O \times 1}$ since $N(\mathbf{s}_1) = \emptyset$.

Under the model in Section 2 and the NNGP prior $\tilde{\pi}(\alpha_{jl_j} | \kappa, \rho) = N_{mO}(\mathbf{0}, \tilde{F}(\rho) \otimes \kappa)$ for

all (j, l_j) , for any fixed $(j, l_j, i) \in \{1, \dots, k\} \times \{1, \dots, L-1\} \times \{1, \dots, m\}$,

$$\begin{aligned} f(\alpha_{jl_j}(\mathbf{s}_i)|\cdot) &\propto f(\mathbf{z}_{jl_j}(\mathbf{s}_i)|\alpha_{jl_j}(\mathbf{s}_i)) \times f(\alpha_{jl_j}(\mathbf{s}_i)|\alpha_{jl_j, N(\mathbf{s}_i)}, \kappa, \rho) \times \prod_{r: \mathbf{s}_i \in N(\mathbf{s}_r)} f(\alpha_{jl_j}(\mathbf{s}_r)|\alpha_{jl_j, N(\mathbf{s}_r)}, \kappa, \rho) \\ &\sim N_O(V_{\mathbf{s}_i} \boldsymbol{\mu}_{jl_j, \mathbf{s}_i}, V_{\mathbf{s}_i}), \end{aligned} \quad (4.8)$$

where

$$\begin{aligned} V_{\mathbf{s}_i} &= \left[I_O + F_{\mathbf{s}_i}^{-1} + \sum_{r: \mathbf{s}_i \in N(\mathbf{s}_r)} B_{\mathbf{s}_r, k_r(\mathbf{s}_i)}^T F_{\mathbf{s}_r}^{-1} B_{\mathbf{s}_r, k_r(\mathbf{s}_i)} \right]^{-1} \text{ and} \\ \boldsymbol{\mu}_{jl_j, \mathbf{s}_i} &= \mathbf{z}_{jl_j}(\mathbf{s}_i) + F_{\mathbf{s}_i}^{-1} B_{\mathbf{s}_i} \boldsymbol{\alpha}_{jl_j, N(\mathbf{s}_i)} + \sum_{r: \mathbf{s}_i \in N(\mathbf{s}_r)} B_{\mathbf{s}_r, k_r(\mathbf{s}_i)}^T F_{\mathbf{s}_r}^{-1} \left\{ \boldsymbol{\alpha}_{jl_j}(\mathbf{s}_r) - \sum_{\substack{1 \leq k \leq |N(\mathbf{s}_r)| \\ k \neq k_r(\mathbf{s}_i)}} B_{\mathbf{s}_r, k} \boldsymbol{\alpha}_{jl_j, N(\mathbf{s}_r)}[k] \right\}. \end{aligned}$$

Under the model in Section 3 and the NNGP prior $\tilde{\pi}(\alpha_{jl_j}|\kappa, \rho) = N_{mO}(\mathbf{0}, \tilde{F}(\rho) \otimes \kappa)$ for all (j, l_j) , for any fixed (j, l_j, i) where $j \in \{1, \dots, k\}$, $l_j \in \{1, \dots, L_j - 1\}$, and $i \in \{1, \dots, m\}$,

$$\begin{aligned} f(\alpha_{jl_j}(\mathbf{s}_i)|\cdot) &\propto \prod_{r: r=i \text{ or } \mathbf{s}_i \in N(\mathbf{s}_r)} f(\alpha_{jl_j}(\mathbf{s}_r)|\alpha_{jl_j, N(\mathbf{s}_r)}, \kappa, \rho) \times \prod_{o=1}^O \mathbb{1}_{\left\{ l_j > \xi_j^o(\mathbf{s}_i) \text{ or } u_j^o(\mathbf{s}_i) < w_{j\xi_j^o(\mathbf{s}_i)}^o(\mathbf{s}_i) \right\}} \\ &\sim N_O(V_{\mathbf{s}_i} \boldsymbol{\mu}_{jl_j, \mathbf{s}_i}, V_{\mathbf{s}_i}) \times \prod_{o=1}^O \mathbb{1}_{\left\{ l_j > \xi_j^o(\mathbf{s}_i) \text{ or } u_j^o(\mathbf{s}_i) < w_{j\xi_j^o(\mathbf{s}_i)}^o(\mathbf{s}_i) \right\}}, \end{aligned} \quad (4.9)$$

where

$$\begin{aligned} V_{\mathbf{s}_i} &= \left[F_{\mathbf{s}_i}^{-1} + \sum_{r: \mathbf{s}_i \in N(\mathbf{s}_r)} B_{\mathbf{s}_r, k_r(\mathbf{s}_i)}^T F_{\mathbf{s}_r}^{-1} B_{\mathbf{s}_r, k_r(\mathbf{s}_i)} \right]^{-1} \text{ and} \\ \boldsymbol{\mu}_{jl_j, \mathbf{s}_i} &= F_{\mathbf{s}_i}^{-1} B_{\mathbf{s}_i} \boldsymbol{\alpha}_{jl_j, N(\mathbf{s}_i)} + \sum_{r: \mathbf{s}_i \in N(\mathbf{s}_r)} B_{\mathbf{s}_r, k_r(\mathbf{s}_i)}^T F_{\mathbf{s}_r}^{-1} \left\{ \boldsymbol{\alpha}_{jl_j}(\mathbf{s}_r) - \sum_{\substack{1 \leq k \leq |N(\mathbf{s}_r)| \\ k \neq k_r(\mathbf{s}_i)}} B_{\mathbf{s}_r, k} \boldsymbol{\alpha}_{jl_j, N(\mathbf{s}_r)}[k] \right\}. \end{aligned}$$

Full deduction details pertaining to the above are in Appendices A.2 and A.3. For each r such that $\mathbf{s}_i \in N(\mathbf{s}_r)$, $k_r(\mathbf{s}_i)$ in the expressions above refers to the positive integer less than or equal to $|N(\mathbf{s}_r)|$ such that $\mathbf{s}_i = N(\mathbf{s}_r)[k_r(\mathbf{s}_i)]$. We have written the $O \times (|N(\mathbf{s}_r)| \cdot O)$ matrix $B_{\mathbf{s}_r}$ as $(B_{\mathbf{s}_r, 1}, \dots, B_{\mathbf{s}_r, |N(\mathbf{s}_r)|})$, where each sub-matrix is $O \times O$, and written the $(|N(\mathbf{s}_r)| \cdot O) \times 1$ vector $\boldsymbol{\alpha}_{jl_j, N(\mathbf{s}_r)}$ as $(\boldsymbol{\alpha}_{jl_j, N(\mathbf{s}_r)}^T[1], \dots, \boldsymbol{\alpha}_{jl_j, N(\mathbf{s}_r)}^T[|N(\mathbf{s}_r)|])^T$ so that $B_{\mathbf{s}_r} \boldsymbol{\alpha}_{jl_j, N(\mathbf{s}_r)} = \sum_{k=1}^{|N(\mathbf{s}_r)|} B_{\mathbf{s}_r, k} \boldsymbol{\alpha}_{jl_j, N(\mathbf{s}_r)}[k]$. Note also that we only need to consider $r = i + 1, \dots, m$ for each $i < m$ in order to find out the set $\{r \in \{1, \dots, m\} : \mathbf{s}_i \in N(\mathbf{s}_r)\}$.

Suppose that we have already calculated $B_{\mathbf{s}_i}$'s and $F_{\mathbf{s}_i}$'s in the Gibbs sampler step updating ρ . Then, sequentially sampling the elements $\alpha_{jl_j}(\mathbf{s}_i), i \in \{1, \dots, m\}$, of α_{jl_j} one by one according to Equation (4.8) incurs a computational complexity of $\mathcal{O}(m(O^3 + h)) + \mathcal{O}(k(L-1)mh(hO + O^2)) + \mathcal{O}(mk(L-1)O^2) = \mathcal{O}(m[k(L-1)hO(h+O) + O^3]) = \mathcal{O}(m)$ if $L \ll m$. If we adopt the slice sampling framework in Section 3 and proceed with Equation (4.9) instead, then the corresponding computational complexity for updating all $\alpha_{jl_j}(\mathbf{s}_i)$'s is

$$\mathcal{O}(O^3 + mh) + \mathcal{O}\left(\sum_{j=1}^k (L_j - 1)mh(hO + O^2)\right) + \mathcal{O}\left(\sum_{j=1}^k \left[mO + \sum_{l_j=1}^{L_j-1} \sum_{i=1}^m (k_{jl_j i}^* \cdot O + n_{jl_j i}^* \cdot O^2) \right]\right)$$

$$= \mathcal{O} \left(O \left\{ \sum_{j=1}^k \left[(L_j - 1)mh(h + O) + \sum_{l_j=1}^{L_j-1} \sum_{i=1}^m \left(k_{jl_j i}^* + n_{jl_j i}^* \cdot O \right) \right] + O^2 \right\} \right)$$

where $\mathcal{O} \left(O \cdot \sum_{j=1}^k \left[m + \sum_{l_j=1}^{L_j-1} \sum_{i=1}^m k_{jl_j i}^* \right] \right)$ denote the overall computational complexity required for calculation of the upper and lower bounds, and $n_{jl_j i}^*$'s represent the numbers of draws from $N_O(V_{\mathbf{s}_i} \boldsymbol{\mu}_{jl_j, \mathbf{s}_i}, V_{\mathbf{s}_i})$ required per sample. Sequentially updating $\boldsymbol{\alpha}_{jl_j}$'s as above successfully replaces the inefficient rejection sampling from a high-dimensional truncated mO -variate normal distribution by the more efficient rejection sampling from low-dimensional truncated O -variate normal distributions. As the number of observation types $O \in \mathbb{N}$ is very small and often equals 1, the rejection sampling from truncated O -variate normals (Equation (4.9)) concerned with sequential updating would have adequate acceptance rates with small $n_{jl_j i}^*$'s. If the largest number of mixture components $\max_{j \in \{1, \dots, k\}} L_j$ is of constant order or increases only logarithmically with m as in Dirichlet processes, then given $k, h, O \ll m$ and $\sum_{j=1}^k L_j \leq k \cdot \max_{j \in \{1, \dots, k\}} L_j$, sequential updates in our Gibbs samplers reduce the corresponding computational complexity from likely larger than $\mathcal{O}(m^3)$ to about linear in m in each MCMC iteration (Appendix H.3).

5 Spatial Prediction and Temporal Trends Clustering

5.1 Predictions at New Spatial Locations

Bayesian nonparametric predictions at any arbitrary future time points or new spatial locations under our modeling frameworks in Sections 2 and 3 are straightforward. We can decompose the integral representation of the posterior predictive distribution (PPD) into several known densities and then obtain the PPD via composition sampling. Here in the main text, we elaborate on new-location predictions under our model in Section 3. Details pertaining to the other prediction cases are given in Appendix G.

For Bayesian predictions at r ($r \in \mathbb{N}, r \geq 1$) new locations $\mathbf{s}_{(m+1):(m+r)}$ given their corresponding covariates matrix $X(\mathbf{s}_{(m+1):(m+r)})_{rTO \times p}$, if any, we can write the PPD as

$$\begin{aligned} & f(\mathbf{y}(\mathbf{s}_{(m+1):(m+r)}) | \mathbf{y}(\mathbf{s}_{1:m}), X(\mathbf{s}_{(m+1):(m+r)})) \\ &= \int_{\Theta} f(\mathbf{y}(\mathbf{s}_{(m+1):(m+r)}) | \Theta, \mathbf{y}(\mathbf{s}_{1:m}), X(\mathbf{s}_{(m+1):(m+r)})) \pi(\Theta | \mathbf{y}(\mathbf{s}_{1:m})) d\Theta, \end{aligned}$$

where $\Theta = (\boldsymbol{\eta}, \boldsymbol{\beta}, \boldsymbol{\sigma}^2(\mathbf{s}_{(m+1):(m+r)}), \boldsymbol{\theta}, \boldsymbol{\xi}(\mathbf{s}_{(m+1):(m+r)}), \boldsymbol{\alpha}(\mathbf{s}_{(m+1):(m+r)}), \boldsymbol{\alpha}, \kappa, \rho)$ and $\boldsymbol{\alpha}$ denotes $\boldsymbol{\alpha}(\mathbf{s}_{1:m})$, and then partition the integral into

$$\begin{aligned} & \int_{\Theta} \underbrace{f(\mathbf{y}(\mathbf{s}_{(m+1):(m+r)}) | \boldsymbol{\theta}, \boldsymbol{\xi}(\mathbf{s}_{(m+1):(m+r)}), \boldsymbol{\eta}, \boldsymbol{\beta}, \boldsymbol{\sigma}^2(\mathbf{s}_{(m+1):(m+r)}), X(\mathbf{s}_{(m+1):(m+r)}))}_{T_1} \\ & \quad \times \underbrace{f(\boldsymbol{\xi}(\mathbf{s}_{(m+1):(m+r)}) | \boldsymbol{\alpha}(\mathbf{s}_{(m+1):(m+r)}))}_{T_2} \underbrace{f(\boldsymbol{\alpha}(\mathbf{s}_{(m+1):(m+r)}) | \boldsymbol{\alpha}, \kappa, \rho)}_{T_3} \\ & \quad \times \underbrace{\pi(\boldsymbol{\eta}, \boldsymbol{\beta}, \boldsymbol{\theta}, \boldsymbol{\alpha}, \kappa, \rho | \mathbf{y}(\mathbf{s}_{1:m}))}_{T_4} \underbrace{\pi(\boldsymbol{\sigma}^2(\mathbf{s}_{(m+1):(m+r)}))}_{T_5} d\Theta \end{aligned} \quad (5.1)$$

since the posterior density $\pi(\boldsymbol{\sigma}^2(\mathbf{s}_{(m+1):(m+r)}) | \mathbf{y}(\mathbf{s}_{1:m}))$ equals the prior $\pi(\boldsymbol{\sigma}^2(\mathbf{s}_{(m+1):(m+r)}))$. $\boldsymbol{\alpha}$ and $\boldsymbol{\alpha}(\mathbf{s}_{(m+1):(m+r)})$ already incorporate the cluster number parameters L_j for all j .

In Equation (5.1), T_1 is the likelihood; T_4 is the parameters' posterior distribution obtained from the original model fit's MCMC sampler; T_5 denotes the prior density for $\sigma^2(\mathbf{s}_{(m+1):(m+r)}) = ((\sigma^2)^1(\mathbf{s}_{m+1}), \dots, (\sigma^2)^O(\mathbf{s}_{m+1}), \dots, (\sigma^2)^1(\mathbf{s}_{m+r}), \dots, (\sigma^2)^O(\mathbf{s}_{m+r}))$ with $(\sigma^2)^o(\mathbf{s}_{m+i_r}) \stackrel{\text{ind}}{\sim} \mathcal{IG}(a, b)$, $i_r \in \{1, \dots, r\}$, $o \in \{1, \dots, O\}$; T_2 is the density of the multinomial distribution described in Section 2; and T_3 can be written as

$$f(\boldsymbol{\alpha}(\mathbf{s}_{(m+1):(m+r)}) | \boldsymbol{\alpha}(\mathbf{s}_{1:m}), \kappa, \rho) = \prod_{j=1}^k \prod_{l_j=1}^{L_j-1} f(\boldsymbol{\alpha}_{jl_j}(\mathbf{s}_{(m+1):(m+r)}) | \boldsymbol{\alpha}_{jl_j}(\mathbf{s}_{1:m}), \kappa, \rho). \quad (5.2)$$

From the full spatial GP prior on the combined vector $\boldsymbol{\alpha}_{jl_j}(\mathbf{s}_{1:(m+r)})$, for any (j, l_j) ,

$$\boldsymbol{\alpha}_{jl_j}(\mathbf{s}_{(m+1):(m+r)}) | \boldsymbol{\alpha}_{jl_j}(\mathbf{s}_{1:m}), \kappa, \rho \sim N_{rO} \left(B_{\mathbf{s}_{(m+1):(m+r)}} \boldsymbol{\alpha}_{jl_j}(\mathbf{s}_{1:m}), F_{\mathbf{s}_{(m+1):(m+r)}} \right), \quad (5.3)$$

where $B_{\mathbf{s}_{(m+1):(m+r)}} = \left\{ F(\rho)_{\mathbf{s}_{(m+1):(m+r)}, \mathbf{s}_{1:m}} [F(\rho)_{\mathbf{s}_{1:m}}]^{-1} \right\} \otimes I_{O \times O}$ is $rO \times mO$ and $F_{\mathbf{s}_{(m+1):(m+r)}} = \left\{ F(\rho)_{\mathbf{s}_{(m+1):(m+r)} - F(\rho)_{\mathbf{s}_{(m+1):(m+r)}, \mathbf{s}_{1:m}} [F(\rho)_{\mathbf{s}_{1:m}}]^{-1} F(\rho)_{\mathbf{s}_{1:m}, \mathbf{s}_{(m+1):(m+r)}} \right\} \otimes \kappa_{O \times O}$ is $rO \times rO$ with $F(\rho)_{\mathbf{s}_{1:m}}$, $F(\rho)_{\mathbf{s}_{(m+1):(m+r)}, \mathbf{s}_{1:m}}$, $F(\rho)_{\mathbf{s}_{1:m}, \mathbf{s}_{(m+1):(m+r)}}$, $F(\rho)_{\mathbf{s}_{(m+1):(m+r)}}$ being the corresponding $m \times m$, $r \times m$, $m \times r$, $r \times r$ sub-matrices of the $(m+r) \times (m+r)$ matrix $F(\rho)_{\mathbf{s}_{1:(m+r)}}$.

If we use instead the latent NNGP prior $\tilde{\pi}(\boldsymbol{\alpha}_{jl_j}(\mathbf{s}_{1:(m+r)}) | \kappa, \rho)$, then one primary advantage of NNGP is that it is a valid Gaussian process on the entire spatial domain $\mathcal{D} \subset \mathbb{R}^d$ after extending $\tilde{\pi}(\boldsymbol{\alpha}_{jl_j}(\mathbf{s}_{1:m}) | \kappa, \rho)$ in Equation (4.1). For all $\mathbf{s} \in \mathcal{D} \setminus \mathcal{S}$, we let $N(\mathbf{s})$ consist of the h nearest neighbors of \mathbf{s} in $\mathcal{S} = \{\mathbf{s}_1, \mathbf{s}_2, \dots, \mathbf{s}_m\}$. We then specify the NNGP derived from the parent GP as

$$\begin{aligned} \boldsymbol{\alpha}_{jl_j}(\mathbf{s}_{1:m}) | \kappa, \rho &\sim \pi(\boldsymbol{\alpha}_{jl_j}(\mathbf{s}_1) | \kappa, \rho) \times \prod_{i=2}^m f(\boldsymbol{\alpha}_{jl_j}(\mathbf{s}_i) | \boldsymbol{\alpha}_{jl_j, N(\mathbf{s}_i)}, \kappa, \rho), \\ \boldsymbol{\alpha}_{jl_j}(\mathbf{s}) | \boldsymbol{\alpha}_{jl_j}(\mathbf{s}_{1:m}), \kappa, \rho &\stackrel{\text{ind}}{\sim} f(\boldsymbol{\alpha}_{jl_j}(\mathbf{s}) | \boldsymbol{\alpha}_{jl_j, N(\mathbf{s})}, \kappa, \rho), \text{ for all } \mathbf{s} \in \mathcal{D} \setminus \mathcal{S}. \end{aligned} \quad (5.4)$$

This generalized directed graph on $\mathcal{S} \cup \{\mathbf{s}\}$ is still ensured acyclic with a well-defined NNGP process constructed as above for any parent GP and any fixed reference set \mathcal{S} ; see Section 2.2 and Appendix D & E in Datta et al. (2016). Extension to any location $\mathbf{s} \in \mathcal{D}$ via nearest-neighbor kriging as in Equation (5.4) enables efficient hierarchical predictions (Appendices G.2.2 and H.2). In particular, for any (j, l_j) , at the r new locations $\mathbf{s}_{(m+1):(m+r)}$,

$$\begin{aligned} \tilde{f}(\boldsymbol{\alpha}_{jl_j}(\mathbf{s}_{(m+1):(m+r)}) | \boldsymbol{\alpha}_{jl_j}(\mathbf{s}_{1:m}), \kappa, \rho) &= \prod_{i_r=1}^r \tilde{f}(\boldsymbol{\alpha}_{jl_j}(\mathbf{s}_{(m+i_r)}) | \boldsymbol{\alpha}_{jl_j}(\mathbf{s}_{1:m}), \kappa, \rho) \\ &= \prod_{i_r=1}^r f(\boldsymbol{\alpha}_{jl_j}(\mathbf{s}_{(m+i_r)}) | \boldsymbol{\alpha}_{jl_j, N(\mathbf{s}_{(m+i_r)})}, \kappa, \rho) \sim \prod_{i_r=1}^r N_O \left(B_{\mathbf{s}_{(m+i_r)}} \boldsymbol{\alpha}_{jl_j, N(\mathbf{s}_{(m+i_r)})}, F_{\mathbf{s}_{(m+i_r)}} \right). \end{aligned} \quad (5.5)$$

For each i_r , $B_{\mathbf{s}_{(m+i_r)}} = \left\{ F(\rho)_{\mathbf{s}_{(m+i_r)}, N(\mathbf{s}_{(m+i_r)})} \left[F(\rho)_{N(\mathbf{s}_{(m+i_r)})} \right]^{-1} \right\} \otimes I_{O \times O}$ is $O \times hO$, and $F_{\mathbf{s}_{(m+i_r)}} = \left\{ F(\rho)_{\mathbf{s}_{(m+i_r)} - F(\rho)_{\mathbf{s}_{(m+i_r)}, N(\mathbf{s}_{(m+i_r)})} \left[F(\rho)_{N(\mathbf{s}_{(m+i_r)})} \right]^{-1} F(\rho)_{N(\mathbf{s}_{(m+i_r)})}, \mathbf{s}_{(m+i_r)}} \right\} \otimes \kappa_{O \times O}$ is $O \times O$ with $F(\rho)_{\mathbf{s}_{(m+i_r)}} = 1$, $F(\rho)_{\mathbf{s}_{(m+i_r)}, N(\mathbf{s}_{(m+i_r)})}$, $F(\rho)_{N(\mathbf{s}_{(m+i_r)})}, \mathbf{s}_{(m+i_r)}}$, $F(\rho)_{N(\mathbf{s}_{(m+i_r)})}$ being the corresponding 1×1 , $1 \times h$, $h \times 1$, $h \times h$ sub-matrices of $F(\rho)_{\mathbf{s}_{1:(m+r)}}$.

Table 5.1 summarizes computational complexities associated with the posterior sampling of some key model parameters and a major spatial prediction step. The detailed derivation of these computational complexities can be found in Appendix H.

Method	fullGPFixedL	NNGPblockFixedL	NNGPsequenFixedL	NNGPsequenVaryLj
NNGP Prior	✗	✓	✓	✓
Sequential Updates	✗	✗	✓	✓
Slice Sampling	✗	✗	✗	✓
ρ and $\kappa_{O \times O}$	$\mathcal{O}(m^3)$	$\mathcal{O}(\{k(L-1)O^2[h^2+h+1]+h^3\}m)$		$\mathcal{O}(\{\sum_{j=1}^k (L_j-1) \cdot O^2[h^2+h+1]+h^3\}m)$
$\alpha_{jl_j}^o(\mathbf{s}_i)$'s	$\mathcal{O}(m^3)$		$\mathcal{O}(m[k(L-1)hO(h+O)+O^3])$	$\mathcal{O}(O(\sum_{j=1}^k [(L_j-1)mh(h+O)+\sum_{l_j=1}^{L_j-1} \sum_{i=1}^m (k_{jl_{ji}}^* + n_{jl_{ji}}^* \cdot O)] + O^2))$
$z_{jl_j}^o(\mathbf{s}_i)$'s or $u_j^o(\mathbf{s}_i)$'s	$\mathcal{O}(kLmO)$			$\mathcal{O}(kmO)$
$\delta_{1:k}, \theta_{jl_j}$'s, and $\xi_j^o(\mathbf{s}_i)$'s	$\mathcal{O}(kLmOT(p+k))$			$\mathcal{O}(\sum_{j=1}^k L_j \cdot mOT(p+k))$
Spatial Prediction at r Locations	$\mathcal{O}(r[m^2+r^2+k(L-1)mO])$	$\mathcal{O}(r[h^3+k(L-1)O(h+O)]+O^3)$		$\mathcal{O}(r[h^3+\sum_{j=1}^k (L_j-1) \cdot O(h+O)]+O^3)$

Table 5.1: Summary of computational complexities for the posterior sampling of model parameters and a major step obtaining $\hat{\boldsymbol{\alpha}}(\mathbf{s}_{(m+1):(m+r)})$ for spatial prediction at r new locations in each MCMC iteration, based on our 3 new techniques in Sections 3 and 4.

5.2 Summarizing Spatial Clusters with Similar Temporal Trends

For our spatiotemporal factor models specified in Sections 2 and 3, clustering information for temporal trajectories $\{\mathbf{y}_t : t = 1, \dots, T\}$ is contained in all k columns of the factor loadings matrix Λ . The posterior distribution of the mixture weights $w_{jl_j}^o(\mathbf{s}_i)$'s, which can be readily computed from posterior samples of the spatially varying latent variables $\alpha_{jl_j}^o(\mathbf{s}_i)$'s, contains pertinent spatial clustering information for $\boldsymbol{\lambda}_{1:k}$. Fix an arbitrary $o \in \{1, \dots, O\}$. Let $\mathbf{w}_o(\mathbf{s}_i) = \{w_{jl_j}^o(\mathbf{s}_i) : j = 1, \dots, k, l_j = 1, \dots, L_j\}$ for all i , where L_j can be replaced by a common L under our model in Section 2. Then spatial proximity information has been encoded into $\mathbf{w}_o = [\mathbf{w}_o(\mathbf{s}_1), \dots, \mathbf{w}_o(\mathbf{s}_m)]^T$, which is of dimension $m \times \sum_{j=1}^k L_j$. Any two locations \mathbf{s}_i and $\mathbf{s}_{i'}$ ($i, i' \in \{1, \dots, m\}$) would have similar temporal trajectories for observation type o if the two vectors $\mathbf{w}_o(\mathbf{s}_i)$ and $\mathbf{w}_o(\mathbf{s}_{i'})$ are close to each other. Therefore, we can apply k-means clustering to the $m \times \sum_{i=1}^n \sum_{j=1}^k L_j^{(t_i)}$ matrix $(\hat{\mathbf{w}}_o^{(t_1)}, \hat{\mathbf{w}}_o^{(t_2)}, \dots, \hat{\mathbf{w}}_o^{(t_n)})$, where each $L_j^{(t_i)}$ represents the estimated number of clusters for factor j in the t_i -th MCMC iteration, and $\hat{\mathbf{w}}_o^{(t_1)}, \dots, \hat{\mathbf{w}}_o^{(t_n)}$ denote the corresponding posterior samples of weights parameters for all m locations from $n \in \mathbb{N}$ selected kept post-burn-in MCMC iterations. Under the model in Section 2, the matrix $(\hat{\mathbf{w}}_o^{(t_1)}, \hat{\mathbf{w}}_o^{(t_2)}, \dots, \hat{\mathbf{w}}_o^{(t_n)})$ is of dimension $m \times nkL$ instead.

6 Simulation Experiments

This section concentrates on simulation studies that demonstrate the enhancement in computational scalability and ends with a real data example for sea surface temperature data. Additional numerical results for multiple observation types, more complex temporal structure under the vector autoregressive model, and sensitivity analysis to hyperparameters are presented in Appendix I of the Supplementary Material.

6.1 Computational Efficiency for Key Gibbs Sampler Steps

We first corroborate the computational acceleration capabilities in Bayesian posterior sampling of our three techniques: slice sampling (Section 3), spatial latent NNPG prior (Section 4), and

sequential updating algorithms (Section 4.4). As described in Section 2 and Table 5.1, the four methods we implemented are encoded as `fullGPFixedL`, `NNGPblockFixedL`, `NNGPsequenFixedL`, and `NNGPsequenVaryLj`. We simulated data from the model in Section 2 with no covariate \mathbf{x} , with exponential temporal covariance $[H(\psi)]_{tt'} = \exp\{-\psi|t - t'|\}$ for all $t, t' \in \{1, \dots, T\}$ and spatial dependence under a GP with exponential covariance function, such that $F(\rho) = \exp(-\rho D)$, where $D_{m \times m}$ denotes the Euclidean distance matrix of m locations. The true clustering mechanism was generated from the spatial PSBP prior. A unanimous cluster number upper bound of 10 was set, and the actual numbers of clusters for the k factors were randomly sampled between 1 and 10. We set the number of observation types $O = 1$, the number of latent factors $k = 5$, the temporal tuning parameter $\psi = 2.3$, the spatial tuning parameter $\rho = 0.8$, and $\sigma^2(\mathbf{s}_i) = 0.01$ for all $i \in \{1, \dots, m\}$. We specified T equal-distanced time points $t = 1, \dots, T$ and m spatial locations $\mathbf{s}_i = (i_1, i_2)$ for $i = 1, \dots, m$ on an equispaced 2-dimensional grid, where $(i_1, i_2) \in \{1, \dots, \sqrt{m}\} \times \{1, \dots, \sqrt{m}\}$. We picked 9 different sets of (m, T) pairs: $(m, T) = (400, 30), (400, 50), (900, 30), (900, 50), (1600, 30), (1600, 50), (1600, 100), (3600, 50), (3600, 100)$. m is set large to highlight differences in the computation time of different methods. For the three methods with spatial latent NNGP priors, we set $h = 15$ for the neighborhood size. The fixed number of clusters L is specified to be 50 for the first three methods, and a starting value and hence upper bound of 50 is assigned to all L_j 's for `NNGPsequenVaryLj`. We ran each MCMC chain for 2×10^4 burn-in iterations and 10^4 post-burn-in iterations, which were thinned to 5000 samples for analysis.

Table 6.1 reports the total model fitting time under the 9 (m, T) pairs of our four methods, which are all markedly faster than their `spBFA` counterparts in Table I.4. For most of the 9 cases, the slowest to the fastest are `fullGPFixedL`, `NNGPblockFixedL`, `NNGPsequenFixedL`, and `NNGPsequenVaryLj`. The computational gain from our three new techniques becomes more evident for larger values of m and T . When $m = 3600$ and $T = 100$, `NNGPsequenVaryLj` is more than 10 times faster than the full GP prior based `fullGPFixedL`, demonstrating a substantial enhancement in computational scalability.

Model Setting		<code>fullGPFixedL</code>	<code>NNGPblockFixedL</code>	<code>NNGPsequenFixedL</code>	<code>NNGPsequenVaryLj</code>
$T = 30$	$m = 400$	3.3 hours	2.17 hours	2.41 hours	1.68 hours
	$m = 900$	10.66 hours	7.3 hours	5.42 hours	2.9 hours
	$m = 1600$	1.68 days	1.01 days	10.18 hours	6.51 hours
$T = 50$	$m = 400$	3.68 hours	3.01 hours	3.21 hours	2.17 hours
	$m = 900$	12.56 hours	10.11 hours	7.95 hours	4.52 hours
	$m = 1600$	1.79 days	1.12 days	12.86 hours	9.05 hours
	$m = 3600$	19.41 days	9.42 days	2.03 days	1.39 days
$T = 100$	$m = 1600$	2.3 days	1.5 days	21.24 hours	15.09 hours
	$m = 3600$	20.09 days	9.9 days	2.51 days	1.89 days

Table 6.1: Total model fitting time for the four methods with 2×10^4 burn-in and 10^4 post-burn-in MCMC iterations under 9 different settings of (m, T) values.

Next, we provide a detailed breakdown of the posterior sampling time of different model parameters in each MCMC iteration. Figure 6.1 presents a detailed comparison across all

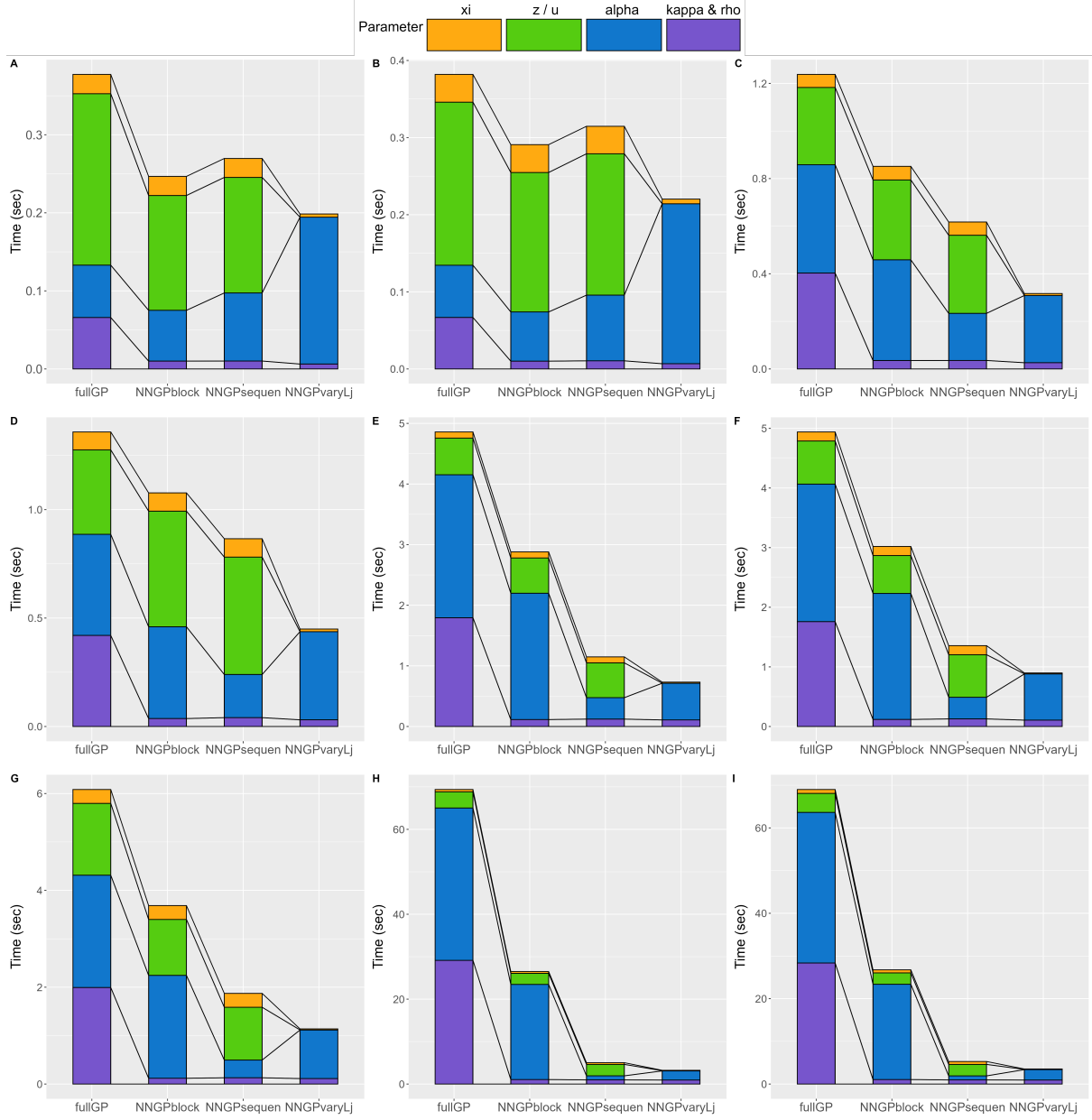


Figure 6.1: Average sampling time per MCMC iteration (in seconds) corresponding to ρ and κ (purple), $\alpha_{jl_j}^o(s_i)$'s (blue), $\xi_j^o(s_i)$'s (orange), and $z_{jl_j}^o(s_i)$'s or $u_j^o(s_i)$'s (green) across all 5000 kept post-burn-in MCMC iterations for the four methods fullGPfixedL (fullGP), NNGPblockFixedL (NNGPblock), NNGPsequenFixedL (NNGPsequen), and NNGPsequenVaryLj (NNGPvaryLj), across 9 different (m, T) settings - (400, 30) (A), (400, 50) (B), (900, 30) (C), (900, 50) (D), (1600, 30) (E), (1600, 50) (F), (1600, 100) (G), (3600, 50) (H), and (3600, 100) (I).

9 pairs of (m, T) values, and Tables I.5 to I.13 reports the average sampling time for all 9 cases. The obtained results for large values of m align with our theoretical computational complexities in Table 5.1. `NNGPblockFixedL` is evidently faster than `fullGPfixedL`, which is mainly attributable to the Gibbs sampler steps for ρ, κ and results from replacing $F(\rho)_{m \times m}$ under the full GP prior by a sparse $\tilde{F}(\rho)_{m \times m}$ under our spatial latent NNGP prior (Section 4.3). The only Gibbs sampler step whose run time significantly differs between `NNGPsequenFixedL` and `NNGPblockFixedL` is the step updating all $\alpha_{jl_j}^o(\mathbf{s}_i)$'s, where `NNGPsequenFixedL` uses the sequential updating algorithm in Section 4.4. As m gets larger, the sequential updates lead to more significant acceleration for sampling $\alpha_{jl_j}^o(\mathbf{s}_i)$'s. When $m = 3600$, for instance, sampling $\alpha_{jl_j}^o(\mathbf{s}_i)$'s in `NNGPsequenFixedL` is more than 20 times faster than that in `NNGPblockFixedL`. `NNGPsequenVaryLj` further accelerates the posterior sampling corresponding to $\xi_j^o(\mathbf{s}_i)$'s and $z_{jl_j}^o(\mathbf{s}_i)$'s (which are replaced by $u_j^o(\mathbf{s}_i)$'s) by using the slice sampling algorithm in Section 3. Consequently, `NNGPsequenVaryLj` stays as the conspicuous fastest algorithm, as it incorporates the non-increasing property for the numbers of spatial clusters L_j 's guaranteed by our slice sampling construction (Section 3), the enhanced spatial scalability from our latent NNGP prior (Section 4.3), and the efficient sequential updates (Equation (4.9) in Section 4.4).

6.2 Computational Efficiency for Spatial Prediction

We validate the significant computational acceleration in spatial prediction attributable to our spatial latent NNGP prior (Section 4) and slice sampling techniques (Section 3). We simulated $N = 3$ datasets from the model in Section 2 with exponential temporal covariance, spatial dependence under a GP with the exponential covariance function, and the PSBP clustering mechanism. We set the number of latent factors $k = 4$, a unanimous upper bound of 10 on the number of clusters for all spatial mixture components, the number of observation types $O = 1$, the spatial tuning parameter $\rho = 0.8$, the temporal tuning parameter $\psi = 2.3$, and $\sigma^2(\mathbf{s}_i) = 0.01$ for all $i \in \{1, \dots, m\}$. We specified $T = 300$ equal-distanced time points $t = 1, 2, \dots, 300$ and $m = 20^2 + 3^2 = 409$ spatial locations $\mathbf{s}_i = (i_1, i_2)$ for $i = 1, 2, \dots, m$ on a 2-dimensional grid, where $(i_1, i_2) \in \{1, 2, \dots, 20\} \times \{1, 2, \dots, 20\} \cup \{9.5, 10.5, 11.5\} \times \{9.5, 10.5, 11.5\}$. Each simulated dataset is divided into a training set and a testing set, where the training set consists of data on $m_0 = 20^2 = 400$ spatial locations $\mathbf{s}_i = (i_1, i_2)$ for $i = 1, 2, \dots, m_0$ with $(i_1, i_2) \in \{1, 2, \dots, 20\} \times \{1, 2, \dots, 20\}$, and the testing set consists of data on the remaining $r = 3^2 = 9$ spatial locations $\mathbf{s}_{i_r} = (i_{r_1}, i_{r_2})$ for $i_r = 1, 2, \dots, r$ with $(i_{r_1}, i_{r_2}) \in \{9.5, 10.5, 11.5\} \times \{9.5, 10.5, 11.5\}$. We set 40 as both the fixed cluster number L in the first three methods and the upper bound for all L_j 's in the last method, and $h = 15$ for the three methods with spatial latent NNGP priors. We run 3×10^4 burn-in iterations and keep $W = 1000$ out of 10^4 post-burn-in iterations' posterior samples for our MCMC chains. From each of our $4 \times N$ fitted results, we obtained $n = 50$ spatial prediction instances using each of our 9 pre-specified random seeds. We thus have four sets of $N \cdot 9 \cdot n$ recorded total (Figure 6.2A) and two-major-step (Figure 6.2B and C) spatial prediction time realizations, which are summarized by the boxplots in Figure 6.2.

We have derived in Appendix H.2 and summarized in Table 5.1 theoretical computational complexities of a major spatial prediction step obtaining $\hat{\alpha}_{jl_j}(\mathbf{s}_{(m+1):(m+r)})$, which indicate that `fullGPfixedL` should take markedly longer time to predict outcomes at new locations

than the other three methods for large m . Since there are no differences between the spatial prediction procedures for `NNGPblockFixedL` and `NNGPsequenFixedL`, these two methods should be comparably fast. Table 5.1 and how we obtain $\hat{\Lambda}(s_{(m+1):(m+r)})$ from $\hat{\alpha}(s_{(m+1):(m+r)})$ suggest that `NNGPsequenVaryLj` should be noticeably faster than the other three methods in spatial prediction, especially when the number of spatial mixture components is moderate to large (Appendix H.1). These theoretical conclusions correspond well to the computation time in Figure 6.2. `NNGPsequenVaryLj` does turn out to be the fastest method in both major steps and thus overall for spatial prediction. `fullGPFixedL` is also the evident slowest, which is caused by the step computing $\hat{\alpha}(s_{(m+1):(m+r)})$ (Figure 6.2B). `NNGPblockFixedL` and `NNGPsequenFixedL` indeed have quite close computation times in spatial prediction both step-wise and overall.

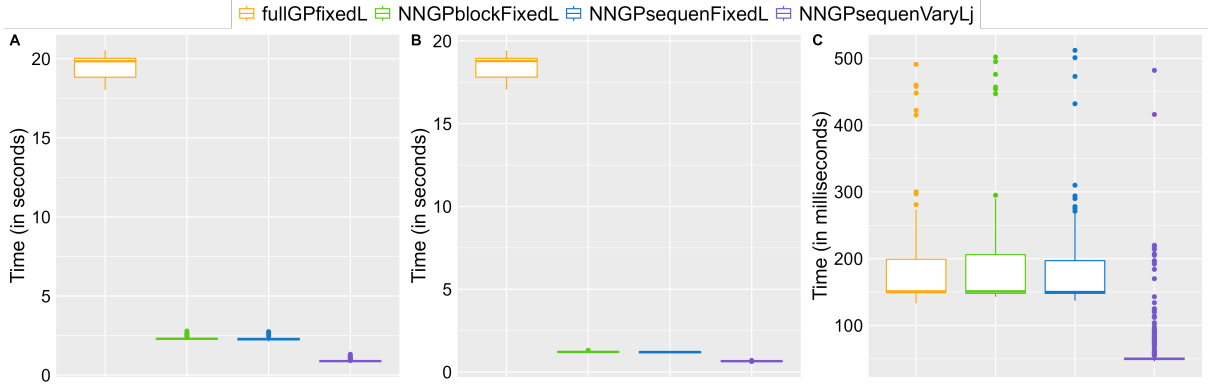


Figure 6.2: Boxplots of the $N \cdot 9 \cdot n$ time realizations for making predictions at the 9 testing locations for our four methods. We have recorded not only the overall spatial prediction time in **A**, but also the time needed for obtaining $\hat{\alpha}(s_{(m+1):(m+r)})$ in **B** and $\hat{w}(s_{(m+1):(m+r)})$, $\hat{\xi}(s_{(m+1):(m+r)})$, and $\hat{\Lambda}(s_{(m+1):(m+r)})$ in **C**, at all kept post-burn-in MCMC iterations.

6.3 Sea Surface Temperature Data

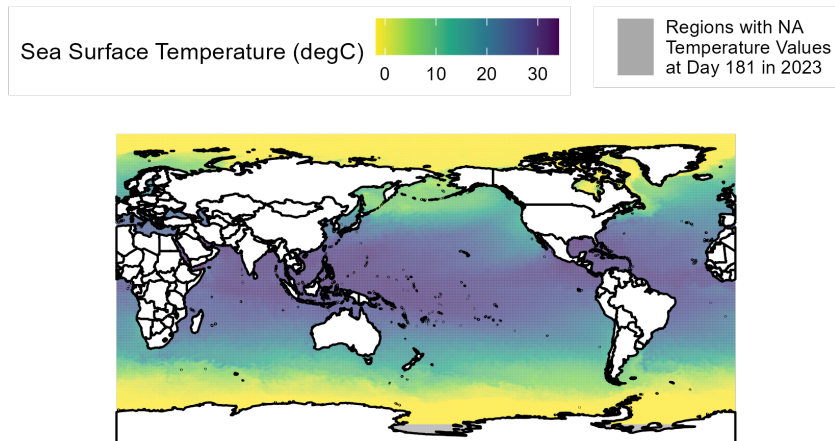


Figure 6.3: Actual Sea Surface Temperature (in degrees Celsius) at all $1440 \times 720 = 1036800$ spatial locations on Day 181 in 2023. World map from Kahle and Wickham (2013).

We downloaded Daily Sea Surface Temperature (SST) data in 2023 from [the NOAA website](https://www.noaa.gov/data/sea-surface-temperature).

The complete data set consists of observations $y_t(\mathbf{s}_i)$'s, which include a large number of NAs, at $1440 \times 720 = 1036800$ spatial locations specified by longitude-latitude pairs for all 365 days in 2023 (Figure 6.3). We only retained locations with no NA observations at all 365 days in the year. Observations at the $m = 1612$ spatial points located between 38° – 50° north latitudes and 135° – 147° east longitudes were used for analysis. We fitted `NNGPsequenFixedL` and `NNGPsequenVaryLj` with a training data set that consists of $y_t(\mathbf{s}_i)$'s at a randomly selected $m_0 = 1577$ out of the 1612 spatial locations and the first 350 days in 2023. We specified the temporal correlation structure and spatial neighborhood structure matrices as $[H(\psi)]_{tt'} = \exp\{-\psi|t - t'|\}$ for all $t, t' \in \{1, \dots, T\}$ and $F(\rho) = \exp\{-\rho D\}$, respectively, where $D_{m_0 \times m_0}$ is a distance matrix for our m_0 spatial locations. We also assumed no additional covariates $\mathbf{x}_t(\mathbf{s}_i)$'s. We set $h = 15$, $L = 50$ for `NNGPsequenFixedL`, and a starting value and hence upper bound of 50 to all L_j 's for `NNGPsequenVaryLj`. We ran each MCMC chain for 10^5 burn-in iterations and 2×10^4 post-burn-in iterations, which were thinned to 1000 samples for analysis. Figures 6.4 and 6.5 demonstrate these two methods' satisfactory temporal prediction and spatial prediction results, respectively.

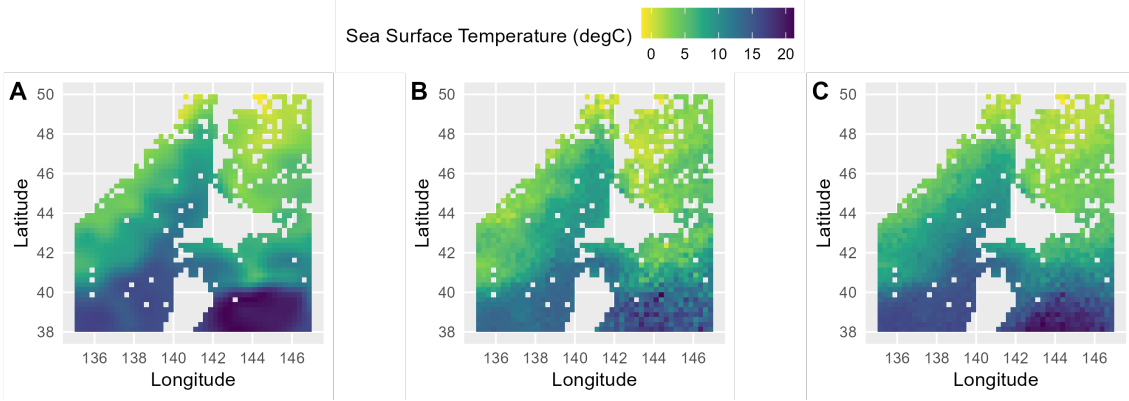


Figure 6.4: Actual (A) and predicted (by `NNGPsequenFixedL` (B) and `NNGPsequenVaryLj` (C)) Sea Surface Temperature (in degrees Celsius) at the 1577 training locations on Day 351 in 2023.

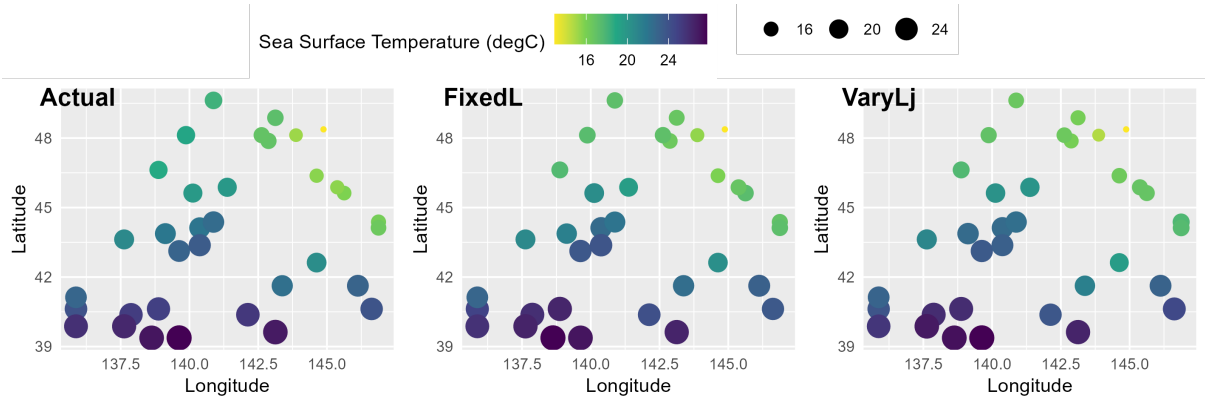


Figure 6.5: Actual and predicted (by `NNGPsequenFixedL` and `NNGPsequenVaryLj`) Sea Surface Temperature (in degrees Celsius) at the 35 testing locations on Day 230 in 2023.

7 Discussion

We discuss several potential extensions for our current work. First, although we have adopted the same PSBP prior as in Berchuck et al. (2022), slice sampling for stick-breaking processes with non-probit links can be similarly derived. Second, we have incorporated the NNGP prior mainly for its computational advantage as a sparse GP approximation. Since NNGP falls in the broader class of Vecchia approximation (Vecchia 1988, Katzfuss and Guinness 2021), one can also integrate other versions of Vecchia approximation that better characterize specific spatial dependencies. Third, our treatment of latent temporal trajectories assumes simple homoscedastic and stationary processes for $\{\boldsymbol{\eta}_t\}_{t=1}^T$, which may be further extended to more complex models for temporal structure, such as Bayesian GARCH (Jensen and Maheu 2013, Virbickaite, Ausín, and Galeano 2015). Finally, the Gaussian response model in the main article is inapplicable to non-normal observed data such as count data. In the Supplementary Material, we have accommodated the binary response model with a logit link by utilizing a Pólya-Gamma data augmentation technique. We can also extend this framework to generalized linear models with non-Gaussian likelihoods such as Poisson regression, which will be particularly useful for modeling spatiotemporal count data.

This Supplementary Material is structured as follows. Appendix A provides full Gibbs sampling details for our spatiotemporal Bayesian Gaussian factor analysis models. Appendix B elaborates on temporal-related computational burdens for a large number of time points $T \in \mathbb{N}$, $T > 1$ and our corresponding powerful acceleration solutions when all time points are equally spaced. Appendix C models the latent temporal process $\{\boldsymbol{\eta}_t\}_{t=1}^T$ using a VAR(1) structure for evenly dispersed time points. Appendices D to I complement Sections 2 to 6. Specifically, Appendix D presents detailed methodology and justification with respect to introducing latent normal variables $z_{jl_j}^o(\mathbf{s}_i) \stackrel{\text{ind}}{\sim} N(\alpha_{jl_j}^o(\mathbf{s}_i), 1)$ to bring about conjugacy for $\boldsymbol{\alpha}_{jl_j}$'s and thus enabling computationally feasible posterior sampling for Section 2's model; Appendix E offers some pivotal notes regarding our novel approach adapting slice sampling (Walker 2007) for computationally and storage-wise efficient Bayesian spatial clustering not mentioned in Section 3; Appendix F gives some general comments on the Nearest-Neighbor Gaussian Process (NNGP); Appendix G discusses detailed procedures for predictions at future time points and cases pertaining to spatial prediction not covered in Section 5.1; Appendix H summarizes the computational complexity and memory improvements (with respect to MCMC-based posterior sampling and subsequent vital inferential tasks including spatial prediction and clustering) corresponding to each of our three novelties, i.e., slice sampling, spatial NNGP prior, and sequential updates; Appendix I displays extensive complementary simulation results with detailed procedures and explanations. Finally, Appendix J extends our models to address three non-normal observation data types that still correspond to Gaussian kernels, possibly after some shrewd transformations.

A Gibbs Samplers for Our Spatiotemporal Bayesian Gaussian Factor Models

We first delineate prior specification regarding $\boldsymbol{\eta}_t$'s, $\Upsilon_{k \times k}$, ψ , $\boldsymbol{\beta}_{p \times 1}$, and $(\sigma^2)^o(\mathbf{s}_i)$'s for the model (2.1). Each error variance $(\sigma^2)^o(\mathbf{s}_i)$ is assigned independent inverse gamma prior $\mathcal{IG}(a, b)$, and the coefficient vector $\boldsymbol{\beta}_{p \times 1}$ is imposed a standard conjugate normal prior $N_p(\boldsymbol{\mu}_{0\beta}, \Sigma_{0\beta})$ in the presence of covariates $\mathbf{x}_i^o(\mathbf{s}_i)$'s. For the temporal latent factors $\boldsymbol{\eta}_t$'s, we consider in the main text a general Kronecker-type covariance structure on the prior $\boldsymbol{\eta} \sim N_{Tk}(\mathbf{0}, H(\psi)_{T \times T} \otimes \Upsilon)$, where $\boldsymbol{\eta} = (\boldsymbol{\eta}_1^T, \dots, \boldsymbol{\eta}_T^T)^T \in \mathbb{R}^{T \times k}$, $H(\psi) \in \mathbb{R}^{T \times T}$ captures the temporal correlation structure on $\boldsymbol{\eta}_1, \dots, \boldsymbol{\eta}_T$ with tuning parameter ψ , and $\Upsilon \in \mathbb{R}^{k \times k}$ describes the covariance between the k latent components. Examples of $H(\psi)$ are the AR(1) process $[H(\psi)]_{tt'} = \psi^{|v_t - v_{t'}|}$ and the Gaussian process with exponential covariance function $[H(\psi)]_{tt'} = \exp\{-\psi|v_t - v_{t'}|\}$ for $t, t' \in \{1, \dots, T\}$, where v_t denotes the time point indexed by t and permits irregularly spaced time points. We also consider the seasonal counterparts of AR(1) and Gaussian processes with an arbitrary temporal seasonal period $d \in \mathbb{N}, d \geq 1$ for modeling the latent process $\{\boldsymbol{\eta}_t\}_{t=1}^T$. The tuning parameter ψ is given a uniform prior on a bounded interval, which lacks conjugacy and requires a Metropolis step in posterior sampling. The covariance matrix $\Upsilon_{k \times k}$ is assumed to be unstructured and assigned a conjugate inverse Wishart prior $\Upsilon \sim \mathcal{IW}(\zeta, \Omega)$. When all time points are equally spaced, a frequently encountered scenario in numerous practical applications, we can considerably accelerate the Gibbs sampling steps for temporal-related parameters $\boldsymbol{\eta}_t$'s, $\Upsilon_{k \times k}$, and ψ (to be elaborated in Appendix B) and adopt a more complicated VAR(1) model for $\{\boldsymbol{\eta}_t\}_{t=1}^T$ (see Appendix C).

Throughout this section, `include.time = TRUE` and `include.space = TRUE` refer to the scenarios when temporal correlation and spatial dependence are taken into consideration, respectively, i.e., when the temporal correlation structure matrix $H(\psi)_{T \times T}$ and spatial neighborhood structure matrix $F(\rho)_{m \times m}$ are not fixed as identity matrices. The four specifications of `temporal.structure` - 'ar1', 'exponential', 'sar1', and 'sexponential', denote AR(1), the exponential process, and their seasonal counterparts, respectively. In almost all circumstances, `spatial.structure = 'continuous'`, i.e., we set $F(\rho) = \exp\{-\rho D\}$, where $D_{m \times m}$ represents the Euclidean distance matrix for our m spatial locations. In the very rare situation when `spatial.structure = 'discrete'`, we consider $F(\rho)^{-1} = D_\omega - \rho W$, which corresponds to a Gaussian Markov random field for discrete spatial data. Finally, `spatApprox` is a logical indicating whether the spatial NNGP prior (Section 4) is adopted in place of the full GP prior. If `spatApprox = TRUE`, then `spatial.structure` must be 'continuous'.

In all our models, the Gibbs sampling steps with respect to $\boldsymbol{\eta}_t$'s, $\Upsilon_{k \times k}$, ψ , $\boldsymbol{\beta}_{p \times 1}$, $(\sigma^2)^o(\mathbf{s}_i)$'s are exactly the same and given as below.

1. Sampling from the full conditional distributions of $\boldsymbol{\eta}_t$'s:

Fix any arbitrary $t \in \{1, \dots, T\}$. Denote $\boldsymbol{\eta}_{-t}$ as the vector $(\boldsymbol{\eta}_1^T, \dots, \boldsymbol{\eta}_{t-1}^T, \boldsymbol{\eta}_{t+1}^T, \dots, \boldsymbol{\eta}_T^T)^T$, which is of length $k(T-1)$. Let $H_{(1:T)_{-t}, (1:T)_{-t}}, H_{(1:T)_{-t}, t}, H_{t, (1:T)_{-t}}, H_{t, t}$ be the corresponding $(T-1) \times (T-1)$, $(T-1) \times 1$, $1 \times (T-1)$, 1×1 sub-matrices of the temporal correlation structure matrix $H(\psi)_{T \times T}$. Then by properties of conditional distributions of jointly multivariate normals, $f(\boldsymbol{\eta}_t | \boldsymbol{\eta}_{-t}, \Upsilon, \psi) \sim N_k(\mathbb{E}_{0\boldsymbol{\eta}_t}, \mathbb{C}_{0\boldsymbol{\eta}_t})$, where $\mathbb{E}_{0\boldsymbol{\eta}_t} = (H_t^+ \otimes I_{k \times k}) \boldsymbol{\eta}_{-t}$ and

$\mathbb{C}_{0\eta_t} = H_t^* \otimes \Upsilon_{k \times k}$ with $H_t^+ = H_{t,(1:T)-t} H_{(1:T)-t,(1:T)-t}^{-1}$ and $H_t^* = H_{t,t} - H_t^+ H_{(1:T)-t,t} = H_{t,t} - H_{t,(1:T)-t} H_{(1:T)-t,(1:T)-t}^{-1} H_{(1:T)-t,t}$. Hence

$$\begin{aligned}
f(\eta_t|\cdot) &\propto f(\mathbf{y}_t|\Lambda, \boldsymbol{\eta}_t, \boldsymbol{\beta}, \Xi) \times f(\boldsymbol{\eta}_{1:T}|\Upsilon, \psi) \\
&= f(\mathbf{y}_t|\Lambda, \boldsymbol{\eta}_t, \boldsymbol{\beta}, \Xi) \times f(\boldsymbol{\eta}_t|\boldsymbol{\eta}_{-t}, \Upsilon, \psi) \times f(\boldsymbol{\eta}_{-t}|\Upsilon, \psi) \\
&\propto f(\mathbf{y}_t|\Lambda, \boldsymbol{\eta}_t, \boldsymbol{\beta}, \Xi) \times f(\boldsymbol{\eta}_t|\boldsymbol{\eta}_{-t}, \Upsilon, \psi) \\
&\propto \exp\left\{-\frac{1}{2}(\mathbf{y}_t - \Lambda\boldsymbol{\eta}_t - X_t\boldsymbol{\beta})^\top \Xi^{-1}(\mathbf{y}_t - \Lambda\boldsymbol{\eta}_t - X_t\boldsymbol{\beta})\right\} \times \\
&\quad \exp\left\{-\frac{1}{2}(\boldsymbol{\eta}_t - \mathbb{E}_{0\eta_t})^\top \mathbb{C}_{0\eta_t}^{-1}(\boldsymbol{\eta}_t - \mathbb{E}_{0\eta_t})\right\} \\
&\propto \exp\left\{-\frac{1}{2}\boldsymbol{\eta}_t^\top \left[\mathbb{C}_{0\eta_t}^{-1} + \Lambda^\top \Xi^{-1} \Lambda\right] \boldsymbol{\eta}_t + \boldsymbol{\eta}_t^\top \left[\mathbb{C}_{0\eta_t}^{-1} \mathbb{E}_{0\eta_t} + \Lambda^\top \Xi^{-1}(\mathbf{y}_t - X_t\boldsymbol{\beta})\right]\right\} \\
&\sim N_k(\mathbb{C}_{\boldsymbol{\eta}_t} \boldsymbol{\mu}_{\boldsymbol{\eta}_t}, \mathbb{C}_{\boldsymbol{\eta}_t}), \text{ where} \\
\mathbb{C}_{\boldsymbol{\eta}_t} &= \left[\mathbb{C}_{0\eta_t}^{-1} + \Lambda^\top \Xi^{-1} \Lambda\right]^{-1} \text{ and } \boldsymbol{\mu}_{\boldsymbol{\eta}_t} = \mathbb{C}_{0\eta_t}^{-1} \mathbb{E}_{0\eta_t} + \Lambda^\top \Xi^{-1}(\mathbf{y}_t - X_t\boldsymbol{\beta}).
\end{aligned} \tag{A.1}$$

2. Sampling from the full conditional distribution of $\Upsilon_{k \times k}$:

$$\begin{aligned}
f(\Upsilon|\cdot) &\propto f(\boldsymbol{\eta}_{1:T}|\Upsilon, \psi) \times f_0(\Upsilon) \sim \mathcal{IW}(T + \zeta, \Phi H(\psi)^{-1} \Phi^\top + \Omega), \\
\text{where } \Phi_{k \times T} &= (\boldsymbol{\eta}_1, \dots, \boldsymbol{\eta}_T).
\end{aligned} \tag{A.2}$$

When the number of factors $k = 1$, the above Inverse-Wishart distribution simplifies to an Inverse-Gamma distribution $\mathcal{IG}\left(\frac{T+\zeta}{2}, \frac{\Phi H(\psi)^{-1} \Phi^\top + \Omega}{2}\right)$.

3. Sampling ψ via a Metropolis step when `include.time = TRUE`:

$$f(\psi|\cdot) \propto f(\boldsymbol{\eta}_{1:T}|\Upsilon, \psi) \times f_0(\psi) \times \left| \frac{\partial}{\partial \Delta} h^{-1}(\Delta) \right| \text{ with } \boldsymbol{\eta}_{1:T}|\Upsilon, \psi \sim N_{Tk}(\mathbf{0}, H(\psi) \otimes \Upsilon). \tag{A.3}$$

In Equation (A.3), $f_0(\psi)$ refers to the uniform prior $\text{Unif}(a_\psi, b_\psi)$ when `temporal.structure = "exponential"` or `"sexponential"` and the transformed Beta prior with p.d.f $f_0(\psi) \propto (1 + \psi)^{\gamma-1} \times (1 - \psi)^{\beta-1}$ when `temporal.structure = "ar1"` or `"sar1"`. Δ is a new parameter defined to be $h(\psi) = \ln\left(\frac{\psi - a_\psi}{b_\psi - \psi}\right)$. Hence $\psi = h^{-1}(\Delta) = \frac{b_\psi \exp(\Delta) + a_\psi}{1 + \exp(\Delta)}$ and $|\frac{\partial}{\partial \Delta} h^{-1}(\Delta)| \propto \frac{\exp(\Delta)}{[1 + \exp(\Delta)]^2}$.

At each MCMC iteration $s \in \mathbb{N}$, let the current parameter estimate for ψ be $\psi^{(s)}$. We propose a new parameter value $\psi^* = h^{-1}(\Delta^*)$ with Δ^* sampled from a symmetric kernel $N(\Delta^{(s)}, \delta)$, where $\Delta^{(s)} = h(\psi^{(s)})$ and $\delta > 0$ is a tuning parameter decided after the burn-in MCMC iterations based on the acceptance rate for ψ^* , and set

$$\psi^{(s+1)} = \begin{cases} \psi^*, & \text{w.p. } \alpha(\psi^{(s)}, \psi^*) = \min\left\{\frac{f(\psi^*|\cdot)}{f(\psi^{(s)}|\cdot)}, 1\right\} \\ \psi^{(s)}, & \text{w.p. } 1 - \alpha(\psi^{(s)}, \psi^*) \end{cases}.$$

4. Sampling from the full conditional distribution of $\boldsymbol{\beta}_{p \times 1}$ when there are additional covariates \mathbf{x} :

$$f(\boldsymbol{\beta}|\cdot) \propto \prod_{t=1}^T f(\mathbf{y}_t|\Lambda, \boldsymbol{\eta}_t, \boldsymbol{\beta}, \Xi) \times f_0(\boldsymbol{\beta}) \tag{A.4}$$

$$\begin{aligned}
& \propto \exp\left\{-\frac{1}{2}(\boldsymbol{\beta} - \boldsymbol{\mu}_{0\boldsymbol{\beta}})^\top \Sigma_{0\boldsymbol{\beta}}^{-1}(\boldsymbol{\beta} - \boldsymbol{\mu}_{0\boldsymbol{\beta}})\right\} \times \\
& \prod_{t=1}^T \exp\left\{-\frac{1}{2}(\mathbf{y}_t - \Lambda \boldsymbol{\eta}_t - X_t \boldsymbol{\beta})^\top \Xi^{-1}(\mathbf{y}_t - \Lambda \boldsymbol{\eta}_t - X_t \boldsymbol{\beta})\right\} \\
& \propto \exp\left\{-\frac{1}{2}\boldsymbol{\beta}^\top \left[\Sigma_{0\boldsymbol{\beta}}^{-1} + \sum_{t=1}^T X_t^\top \Xi^{-1} X_t\right] \boldsymbol{\beta} + \boldsymbol{\beta}^\top \left[\Sigma_{0\boldsymbol{\beta}}^{-1} \boldsymbol{\mu}_{0\boldsymbol{\beta}} + \sum_{t=1}^T X_t^\top \Xi^{-1}(\mathbf{y}_t - \Lambda \boldsymbol{\eta}_t)\right]\right\} \\
& \sim N_p(V_{\boldsymbol{\beta}} \boldsymbol{\mu}_{\boldsymbol{\beta}}, V_{\boldsymbol{\beta}}), \text{ where} \\
& V_{\boldsymbol{\beta}} = \left[\Sigma_{0\boldsymbol{\beta}}^{-1} + \sum_{t=1}^T X_t^\top \Xi^{-1} X_t\right]^{-1} \text{ and } \boldsymbol{\mu}_{\boldsymbol{\beta}} = \Sigma_{0\boldsymbol{\beta}}^{-1} \boldsymbol{\mu}_{0\boldsymbol{\beta}} + \sum_{t=1}^T X_t^\top \Xi^{-1}(\mathbf{y}_t - \Lambda \boldsymbol{\eta}_t).
\end{aligned}$$

5. Sampling from the full conditional distributions of $(\sigma^2)^o(\mathbf{s}_i)$'s when not all observations are from the distribution family 'binomial' (Appendix J):

Fix any arbitrary $(i, o) \in \{1, \dots, m\} \times \{1, \dots, O\}$. Then

$$\begin{aligned}
f((\sigma^2)^o(\mathbf{s}_i) | \cdot) & \propto f_0((\sigma^2)^o(\mathbf{s}_i)) \times \prod_{t=1}^T f(y_t^o(\mathbf{s}_i) | \Lambda^o(\mathbf{s}_i), \boldsymbol{\eta}_t, \boldsymbol{\beta}, (\sigma^2)^o(\mathbf{s}_i)) \quad (\text{A.5}) \\
& \propto [(\sigma^2)^o(\mathbf{s}_i)]^{-a-1} \exp\left\{-\frac{b}{(\sigma^2)^o(\mathbf{s}_i)}\right\} \times \\
& [(\sigma^2)^o(\mathbf{s}_i)]^{-\frac{T}{2}} \exp\left\{-\frac{1}{2(\sigma^2)^o(\mathbf{s}_i)} \sum_{t=1}^T [y_t^o(\mathbf{s}_i) - \mathbf{x}_t^o(\mathbf{s}_i)^\top \boldsymbol{\beta} - \boldsymbol{\lambda}^o(\mathbf{s}_i)^\top \boldsymbol{\eta}_t]^2\right\} \\
& \propto [(\sigma^2)^o(\mathbf{s}_i)]^{-a-\frac{T}{2}-1} \exp\left\{-\frac{1}{(\sigma^2)^o(\mathbf{s}_i)} \left(b + \frac{1}{2} \sum_{t=1}^T [y_t^o(\mathbf{s}_i) - \mathbf{x}_t^o(\mathbf{s}_i)^\top \boldsymbol{\beta} - \boldsymbol{\lambda}^o(\mathbf{s}_i)^\top \boldsymbol{\eta}_t]^2\right)\right\} \\
& \sim \mathcal{IG}\left(a + \frac{T}{2}, b + \frac{1}{2} \sum_{t=1}^T [y_t^o(\mathbf{s}_i) - \mathbf{x}_t^o(\mathbf{s}_i)^\top \boldsymbol{\beta} - \boldsymbol{\lambda}^o(\mathbf{s}_i)^\top \boldsymbol{\eta}_t]^2\right), \text{ where} \\
& \boldsymbol{\lambda}^o(\mathbf{s}_i)_{1 \times k}^\top \text{ denotes the row in } \Lambda_{mO \times k} \text{ corresponding to location } i \text{ and observation type } o.
\end{aligned}$$

A.1 Full Gibbs Sampling Details for the Basic Model Without Spatial Clustering Capabilities

When we do not consider the PSBP clustering mechanism and directly impose spatially correlated Gaussian Processes onto the columns $\{\boldsymbol{\lambda}_j\}_{j=1}^k$ of the factor loadings matrix $\Lambda_{mO \times k}$, i.e., assign a normal prior with Kronecker-type covariance structure $\boldsymbol{\lambda}_j \stackrel{\text{iid}}{\sim} N_{Om}(\mathbf{0}, \kappa_{O \times O} \otimes F(\rho)_{m \times m})$, $j \in \{1, \dots, k\}$, the corresponding Gibbs sampler steps are detailed in the following. The parameters $\boldsymbol{\lambda}_j$'s and $\boldsymbol{\sigma}^2$ (when not all observations are from the 'binomial' family) are all ordered first spatially and then by observation type, i.e., the first m components of each above $Om \times 1$ vector are from observation type 1, the next m components are from observation type 2, and so on. $\kappa \in \mathbb{R}^{O \times O}$ depicts the covariance between the O observation types and is imposed an $\mathcal{IW}(\nu, \Theta)$ prior. For a continuous spatial domain, $F(\rho)$ denotes the covariance matrix from a Gaussian process over the m spatial locations with an exponential covariance function tuning parameter ρ that can be further assigned a uniform prior.

1. Sampling from the full conditional distributions of $\boldsymbol{\lambda}_j$'s:

Fix any arbitrary $j \in \{1, \dots, k\}$. Let $\Xi_{Om \times Om} = \text{Diag}(\sigma_1^2, \dots, \sigma_O^2)$, where $\sigma_o^2 = ((\sigma^2)^o(\mathbf{s}_1), \dots, (\sigma^2)^o(\mathbf{s}_m))^T \forall o \in \{1, \dots, O\}$. Denote Λ_{-j} as $(\lambda_1, \dots, \lambda_{j-1}, \lambda_{j+1}, \dots, \lambda_k)$, the sub-matrix obtained by removing the j^{th} column from $\Lambda_{Om \times k}$. For each t , let $\boldsymbol{\eta}_t^{-j}$ represent the length- $(k-1)$ sub-vector of $\boldsymbol{\eta}_t$ obtained by removing its j^{th} element. Then

$$\begin{aligned}
f(\lambda_j | \cdot) &\propto \prod_{t=1}^T f(\mathbf{y}_t | \Lambda, \boldsymbol{\eta}_t, \boldsymbol{\beta}, \Xi) \times \pi(\lambda_j | \kappa, \rho) \\
&\propto \exp\left\{-\frac{1}{2} \boldsymbol{\lambda}_j^T [\kappa^{-1} \otimes F(\rho)^{-1}] \boldsymbol{\lambda}_j\right\} \times \\
&\quad \prod_{t=1}^T \exp\left\{-\frac{1}{2} \left(\mathbf{y}_t - X_t \boldsymbol{\beta} - \Lambda_{-j} \boldsymbol{\eta}_t^{-j} - \eta_{tj} \lambda_j\right)^T \Xi^{-1} \left(\mathbf{y}_t - X_t \boldsymbol{\beta} - \Lambda_{-j} \boldsymbol{\eta}_t^{-j} - \eta_{tj} \lambda_j\right)\right\} \\
&\propto \exp\left\{-\frac{1}{2} \boldsymbol{\lambda}_j^T \left(\kappa^{-1} \otimes F(\rho)^{-1} + \sum_{t=1}^T \eta_{tj}^2 \Xi^{-1}\right) \boldsymbol{\lambda}_j + \boldsymbol{\lambda}_j^T \Xi^{-1} \left[\sum_{t=1}^T \eta_{tj} \left(\mathbf{y}_t - \Lambda_{-j} \boldsymbol{\eta}_t^{-j} - X_t \boldsymbol{\beta}\right)\right]\right\} \\
&\sim N_{Om}(\mathbf{V}_{\lambda_j} \boldsymbol{\mu}_{\lambda_j}, \mathbf{V}_{\lambda_j}), \text{ where} \\
\mathbf{V}_{\lambda_j} &= \left[\kappa^{-1} \otimes F(\rho)^{-1} + \sum_{t=1}^T \eta_{tj}^2 \Xi^{-1}\right]^{-1} \text{ and } \boldsymbol{\mu}_{\lambda_j} = \Xi^{-1} \left[\sum_{t=1}^T \eta_{tj} \left(\mathbf{y}_t - \Lambda_{-j} \boldsymbol{\eta}_t^{-j} - X_t \boldsymbol{\beta}\right)\right].
\end{aligned} \tag{A.6}$$

When the NNGP instead of the full GP prior is adopted for the λ_j 's, we replace $\pi(\lambda_j | \kappa, \rho)$ and $F(\rho)$ by $\tilde{\pi}(\lambda_j | \kappa, \rho)$ and $\tilde{F}(\rho)$ in the above equations.

2. Sampling from the full conditional distribution of $\kappa_{O \times O}$:

$$\begin{aligned}
f(\kappa | \cdot) &\propto \prod_{j=1}^k \pi(\lambda_j | \kappa, \rho) \times f_0(\kappa) \sim \mathcal{IW}\left(mk + \nu, \sum_{j=1}^k S_{\lambda_j} + \Theta\right), \\
\text{where } S_{\lambda_j} &= A_j^T F(\rho)^{-1} A_j \text{ with } (A_j)_{m \times O} = (\lambda_{j1}, \dots, \lambda_{jO}) \forall j.
\end{aligned} \tag{A.7}$$

In Equation (A.7), we have written the $Om \times 1$ vector λ_j as $(\lambda_{j1}^T, \dots, \lambda_{jO}^T)^T$ for all $j \in \{1, \dots, k\}$.

When $O = 1$, Equation (A.7) reduces to $\mathcal{IG}\left(\frac{mk + \nu}{2}, \frac{\sum_{j=1}^k S_{\lambda_j} + \Theta}{2}\right)$.

When the NNGP prior rather than the full GP prior is adopted for the λ_j 's, we replace $\pi(\lambda_j | \kappa, \rho)$ and $F(\rho)$ in Equation (A.7) by $\tilde{\pi}(\lambda_j | \kappa, \rho)$ and $\tilde{F}(\rho)$ respectively.

3. Sampling ρ via a Metropolis step when `include.space = TRUE`:

$$\begin{aligned}
f(\rho | \cdot) &\propto \prod_{j=1}^k \pi(\lambda_j | \kappa, \rho) \times f_0(\rho) \times \left|\frac{\partial}{\partial \Delta} h^{-1}(\Delta)\right| \\
&\text{with } \lambda_j | \kappa, \rho \sim N_{Om}(\mathbf{0}, \kappa \otimes F(\rho)) \quad \forall j.
\end{aligned} \tag{A.8}$$

When the NNGP prior rather than the full GP prior is adopted for the λ_j 's, we replace $\pi(\lambda_j | \kappa, \rho)$ and $F(\rho)$ in Equation (A.8) by $\tilde{\pi}(\lambda_j | \kappa, \rho)$ and $\tilde{F}(\rho)$ respectively.

In Equation (A.8), $f_0(\rho)$ refers to the uniform prior $\text{Unif}(a_\rho, b_\rho)$, where $a_\rho = 0, b_\rho = 1$ when `spatial.structure = 'discrete'` and $a_\rho, b_\rho \in \mathbb{R}^+$ when `spatial.structure =`

‘continuous’. Δ is a new parameter defined to be $h(\rho) = \ln\left(\frac{\rho - a_\rho}{b_\rho - \rho}\right)$. Hence $\rho = h^{-1}(\Delta) = \frac{b_\rho \exp(\Delta) + a_\rho}{1 + \exp(\Delta)}$ and $|\frac{\partial}{\partial \Delta} h^{-1}(\Delta)| \propto \frac{\exp(\Delta)}{[1 + \exp(\Delta)]^2}$.

At each MCMC iteration $s \in \mathbb{N}$, let the current parameter estimate for ρ be $\rho^{(s)}$. We propose a new parameter value $\rho^* = h^{-1}(\Delta^*)$ with Δ^* sampled from a symmetric kernel $N(\Delta^{(s)}, \delta)$, where $\Delta^{(s)} = h(\rho^{(s)})$ and $\delta > 0$ is a tuning parameter decided after the burn-in MCMC iterations based on the acceptance rate for ρ^* , and set

$$\rho^{(s+1)} = \begin{cases} \rho^*, & \text{w.p. } \alpha(\rho^{(s)}, \rho^*) = \min\left\{\frac{f(\rho^*|\cdot)}{f(\rho^{(s)}|\cdot)}, 1\right\} \\ \rho^{(s)}, & \text{w.p. } 1 - \alpha(\rho^{(s)}, \rho^*) \end{cases}.$$

4. Same as Step 1 given at the start of Appendix A.
5. Same as Step 2 given at the start of Appendix A.
6. Same as Step 3 given at the start of Appendix A.
7. Same as Step 4 given at the start of Appendix A.
8. Same as Step 5 given at the start of Appendix A.

A.2 Full Gibbs Sampling Details for Our Model in Section 2

When we adopt the spatial PSBP clustering mechanism with a pre-determined fixed common $L \in \mathbb{N}, L > 1$ for all factors and assign the prior $\alpha_{jl_j} \stackrel{\text{iid}}{\sim} N_{mO}(\mathbf{0}, F(\rho)_{m \times m} \otimes \kappa_{O \times O})$, $j \in \{1, \dots, k\}$, $l_j \in \{1, \dots, L-1\}$, the corresponding Gibbs sampler steps are detailed in the following. We take note that only \mathbf{z}_{jl_j} ’s and α_{jl_j} ’s are ordered first by observation type and then spatially, i.e., the first O components of each above $mO \times 1$ vector are from location point 1, the next O components are from location point 2, and so on. All other concerned parameters, i.e., \mathbf{w}_{jl_j} ’s, ξ_j ’s, λ_j ’s, and σ^2 when not all observations are from the ‘binomial’ family (Appendix J), are ordered first spatially and then by observation type, i.e., the first m components of each above $Om \times 1$ vector are from observation type 1, the next m components are from observation type 2, and so on.

1. Sampling from the marginal conditional distributions of $\xi_j^o(\mathbf{s}_i)$ ’s with the introduced latent normal $z_{jl_j}^o(\mathbf{s}_i)$ ’s integrated out:

Fix any arbitrary $j \in \{1, \dots, k\}$.

$$\forall (o, i) \in \{1, \dots, O\} \times \{1, \dots, m\}, \forall l_j \in \{1, \dots, L\}, \mathbb{P}(\xi_j^o(\mathbf{s}_i) = l_j | \cdot) \quad (\text{A.9})$$

$$\propto \mathbb{P}(\xi_j^o(\mathbf{s}_i) = l_j | \alpha_{jr_j}^o(\mathbf{s}_i), r_j \leq L-1) \prod_{t=1}^T f(y_t^o(\mathbf{s}_i) | \beta, \eta_t, (\sigma^2)^o(\mathbf{s}_i), \xi_j^o(\mathbf{s}_i) = l_j, \xi_{-j}^o(\mathbf{s}_i), \theta_{\xi^o(\mathbf{s}_i)}) \\ \propto w_{jl_j}^o(\mathbf{s}_i) \times \exp \left\{ -\frac{1}{2} (\sigma^{-2})^o(\mathbf{s}_i) \sum_{t=1}^T \left[y_t^o(\mathbf{s}_i) - \mathbf{x}_t^o(\mathbf{s}_i)^T \beta - \sum_{\substack{1 \leq h \leq k \\ h \neq j}} \theta_{h \xi_h^o(\mathbf{s}_i)} \eta_{th} - \theta_{jl_j} \eta_{tj} \right]^2 \right\}.$$

2. Sampling from the full conditional distributions of θ_{jl_j} ’s for $l_j \leq L$:

Fix any arbitrary $(j, l_j) \in \{1, \dots, k\} \times \{1, \dots, L\}$. Then

$$f(\theta_{jl_j}|\cdot) \propto f_0(\theta_{jl_j}|\tau_j) \times \prod_{(i,o):\xi_j^o(\mathbf{s}_i)=l_j} \prod_{t=1}^T f(y_t^o(\mathbf{s}_i)|\boldsymbol{\beta}, \boldsymbol{\eta}_t, (\sigma^2)^o(\mathbf{s}_i), \boldsymbol{\xi}^o(\mathbf{s}_i), \boldsymbol{\theta}_{\xi^o(\mathbf{s}_i)}). \quad (\text{A.10})$$

If $\nexists (i, o)$ s.t. $\xi_j^o(\mathbf{s}_i) = l_j$, then $f(\theta_{jl_j}|\cdot) = f_0(\theta_{jl_j}|\tau_j) \sim N(0, \tau_j^{-1})$.

If $\exists (i, o)$ s.t. $\xi_j^o(\mathbf{s}_i) = l_j$, then

$$f(\theta_{jl_j}|\cdot) \sim N(V_{\theta_{jl_j}}\mu_{\theta_{jl_j}}, V_{\theta_{jl_j}}), \text{ where } V_{\theta_{jl_j}} = \left[\tau_j + \sum_{(i,o):\xi_j^o(\mathbf{s}_i)=l_j} (\sigma^{-2})^o(\mathbf{s}_i) \sum_{t=1}^T \eta_{tj}^2 \right]^{-1}$$

$$\text{and } \mu_{\theta_{jl_j}} = \sum_{(i,o):\xi_j^o(\mathbf{s}_i)=l_j} (\sigma^{-2})^o(\mathbf{s}_i) \sum_{t=1}^T \eta_{tj} \left[y_t^o(\mathbf{s}_i) - \mathbf{x}_t^o(\mathbf{s}_i)^\top \boldsymbol{\beta} - \sum_{\substack{1 \leq h \leq k \\ h \neq j}} \theta_{h\xi_h^o(\mathbf{s}_i)} \eta_{th} \right].$$

3. Sampling from the full conditional distributions of δ_h 's:

If a multiplicative gamma process shrinkage prior is placed on the atoms so that $\forall (j, l_j)$, $\theta_{jl_j} \stackrel{\text{ind}}{\sim} N(0, \tau_j^{-1})$ with $\tau_j = \prod_{h=1}^j \delta_h$, $\delta_1 \sim \text{Gamma}(a_1, 1)$, $\delta_h \sim \text{Gamma}(a_2, 1) \forall h \geq 2$, then for any arbitrary fixed $h \in \{1, \dots, k\}$,

$$f(\delta_h|\cdot) \propto \prod_{j=h}^k \prod_{l_j=1}^L f(\theta_{jl_j}|\tau_j) \times f_0(\delta_h) \quad (\text{A.11})$$

$$\sim \text{Gamma} \left(a_h + \frac{(k-h+1)L}{2}, 1 + \frac{\sum_{j=h}^k \left[\prod_{x=1, x \neq h}^j \delta_x \right] \sum_{l_j=1}^L \theta_{jl_j}^2}{2} \right).$$

If we consider the non-shrinkage prior $\theta_{jl_j} \stackrel{\text{ind}}{\sim} N(0, \tau_j^{-1} = \delta_j^{-1}) \forall (j, l_j)$ with $\delta_j \stackrel{\text{iid}}{\sim} \text{Gamma}(a_1, a_2) \forall j$, then for any arbitrary fixed $j \in \{1, \dots, k\}$,

$$f(\delta_j|\cdot) \propto \prod_{l_j=1}^L f(\theta_{jl_j}|\delta_j) \times f_0(\delta_j) \sim \text{Gamma} \left(a_1 + \frac{L}{2}, a_2 + \frac{\sum_{l_j=1}^L \theta_{jl_j}^2}{2} \right). \quad (\text{A.12})$$

4. Sampling from the full conditional distributions of $z_{jl_j}^o(\mathbf{s}_i)$'s for $l_j \in \{1, \dots, L-1\}$:

For any arbitrary fixed $(j, i, o, l_j) \in \{1, \dots, k\} \times \{1, \dots, m\} \times \{1, \dots, O\} \times \{1, \dots, L-1\}$,

$$f(z_{jl_j}^o(\mathbf{s}_i)|\cdot) \propto f(\xi_j^o(\mathbf{s}_i)|z_{jl_j}^o(\mathbf{s}_i)) \times f(z_{jl_j}^o(\mathbf{s}_i)|\alpha_{jl_j}^o(\mathbf{s}_i)) \quad (\text{A.13})$$

$$\sim \mathbb{1}_{\{\xi_j^o(\mathbf{s}_i) > l_j\}} N(\alpha_{jl_j}^o(\mathbf{s}_i), 1)_{\mathbb{R}_-} + \mathbb{1}_{\{\xi_j^o(\mathbf{s}_i) = l_j\}} N(\alpha_{jl_j}^o(\mathbf{s}_i), 1)_{\mathbb{R}_+} + \mathbb{1}_{\{\xi_j^o(\mathbf{s}_i) < l_j\}} N(\alpha_{jl_j}^o(\mathbf{s}_i), 1).$$

5. Sampling from the full conditional distributions of α_{jl_j} 's for $l_j \in \{1, \dots, L-1\}$:

For any arbitrary fixed $(j, l_j) \in \{1, \dots, k\} \times \{1, \dots, L-1\}$,

$$f(\alpha_{jl_j}|\cdot) \propto \prod_{(i,o)} f(z_{jl_j}^o(\mathbf{s}_i)|\alpha_{jl_j}^o(\mathbf{s}_i)) \times \pi(\alpha_{jl_j}|\kappa, \rho) = f(\mathbf{z}_{jl_j}|\alpha_{jl_j}) \times \pi(\alpha_{jl_j}|\kappa, \rho)$$

$$\sim N_{mO} \left([I_{mO} + F(\rho)^{-1} \otimes \kappa^{-1}]^{-1} \mathbf{z}_{jl_j}, [I_{mO} + F(\rho)^{-1} \otimes \kappa^{-1}]^{-1} \right). \quad (\text{A.14})$$

When the NNGP prior rather than the full GP prior is adopted for the α_{jl_j} 's, we replace $\pi(\alpha_{jl_j}|\kappa, \rho)$ and $F(\rho)$ in Equation (A.14) by $\tilde{\pi}(\alpha_{jl_j}|\kappa, \rho)$ and $\tilde{F}(\rho)$ respectively.

After obtaining our new estimates for $\alpha_{jl_j}^o(\mathbf{s}_i)$'s ($l_j \in \{1, \dots, L-1\}$), we calculate our new samples for the corresponding weights parameters $w_{jl_j}^o(\mathbf{s}_i)$'s ($l_j \in \{1, \dots, L\}$) via the formula

$$w_{jl_j}^o(\mathbf{s}_i) = \begin{cases} \Phi(\alpha_{jl_j}^o(\mathbf{s}_i)) \prod_{r < l} [1 - \Phi(\alpha_{jr_j}^o(\mathbf{s}_i))] & \text{if } l_j \in \{1, \dots, L-1\} \\ \prod_{r < L} [1 - \Phi(\alpha_{jr_j}^o(\mathbf{s}_i))] & \text{if } l_j = L \end{cases} \quad (\text{A.15})$$

for any arbitrary $(j, o, i) \in \{1, \dots, k\} \times \{1, \dots, O\} \times \{1, \dots, m\}$ and $l_j \in \{1, \dots, L\}$.

Sequentially Updating $\alpha_{jl_j} = (\alpha_{jl_j}(\mathbf{s}_1)^T, \dots, \alpha_{jl_j}(\mathbf{s}_m)^T)^T \forall (j, l_j)$

Under the circumstance when `include.space = TRUE`, `spatial.structure = "continuous"`, and `spatApprox = TRUE`, we can opt to sequentially update the α_{jl_j} 's instead:

Under our NNGP prior $\tilde{\pi}(\alpha_{jl_j}|\kappa, \rho) = N_{mO}(\mathbf{0}, \tilde{F}(\rho) \otimes \kappa)$ for all (j, l_j) , for any arbitrary fixed $(j, l_j, i) \in \{1, \dots, k\} \times \{1, \dots, L-1\} \times \{1, \dots, m\}$,

$$\begin{aligned} f(\alpha_{jl_j}(\mathbf{s}_i)|\cdot) &\propto f(\mathbf{z}_{jl_j}(\mathbf{s}_i)|\alpha_{jl_j}(\mathbf{s}_i)) \times \tilde{f}(\alpha_{jl_j}|\cdot) = f(\mathbf{z}_{jl_j}(\mathbf{s}_i)|\alpha_{jl_j}(\mathbf{s}_i)) \prod_{r=1}^m f(\alpha_{jl_j}(\mathbf{s}_r)|\alpha_{jl_j, N(\mathbf{s}_r)}, \kappa, \rho) \\ &\propto f(\mathbf{z}_{jl_j}(\mathbf{s}_i)|\alpha_{jl_j}(\mathbf{s}_i)) \times f(\alpha_{jl_j}(\mathbf{s}_i)|\alpha_{jl_j, N(\mathbf{s}_i)}, \kappa, \rho) \prod_{r: \mathbf{s}_i \in N(\mathbf{s}_r)} f(\alpha_{jl_j}(\mathbf{s}_r)|\alpha_{jl_j, N(\mathbf{s}_r)}, \kappa, \rho) \\ &\propto \exp \left\{ -\frac{1}{2} (\mathbf{z}_{jl_j}(\mathbf{s}_i) - \alpha_{jl_j}(\mathbf{s}_i))^T I_O (\mathbf{z}_{jl_j}(\mathbf{s}_i) - \alpha_{jl_j}(\mathbf{s}_i)) \right\} \times \quad (\text{A.16}) \\ &\quad \exp \left\{ -\frac{1}{2} (\alpha_{jl_j}(\mathbf{s}_i) - B_{\mathbf{s}_i} \alpha_{jl_j, N(\mathbf{s}_i)})^T F_{\mathbf{s}_i}^{-1} (\alpha_{jl_j}(\mathbf{s}_i) - B_{\mathbf{s}_i} \alpha_{jl_j, N(\mathbf{s}_i)}) \right\} \times \\ &\quad \exp \left\{ -\frac{1}{2} \sum_{r: \mathbf{s}_i \in N(\mathbf{s}_r)} (\alpha_{jl_j}(\mathbf{s}_r) - B_{\mathbf{s}_r} \alpha_{jl_j, N(\mathbf{s}_r)})^T F_{\mathbf{s}_r}^{-1} (\alpha_{jl_j}(\mathbf{s}_r) - B_{\mathbf{s}_r} \alpha_{jl_j, N(\mathbf{s}_r)}) \right\} \\ &\sim N_O(V_{\mathbf{s}_i} \boldsymbol{\mu}_{jl_j, \mathbf{s}_i}, V_{\mathbf{s}_i}), \text{ where } V_{\mathbf{s}_i} = \left[I_O + F_{\mathbf{s}_i}^{-1} + \sum_{r: \mathbf{s}_i \in N(\mathbf{s}_r)} B_{\mathbf{s}_r, k_r(\mathbf{s}_i)}^T F_{\mathbf{s}_r}^{-1} B_{\mathbf{s}_r, k_r(\mathbf{s}_i)} \right]^{-1} \text{ and} \end{aligned} \quad (\text{A.17})$$

$$\boldsymbol{\mu}_{jl_j, \mathbf{s}_i} = \mathbf{z}_{jl_j}(\mathbf{s}_i) + F_{\mathbf{s}_i}^{-1} B_{\mathbf{s}_i} \alpha_{jl_j, N(\mathbf{s}_i)} + \sum_{r: \mathbf{s}_i \in N(\mathbf{s}_r)} B_{\mathbf{s}_r, k_r(\mathbf{s}_i)}^T F_{\mathbf{s}_r}^{-1} \left\{ \alpha_{jl_j}(\mathbf{s}_r) - \sum_{\substack{1 \leq k \leq |N(\mathbf{s}_r)| \\ k \neq k_r(\mathbf{s}_i)}} B_{\mathbf{s}_r, k} \alpha_{jl_j, N(\mathbf{s}_r)[k]} \right\}.$$

For each r such that $\mathbf{s}_i \in N(\mathbf{s}_r)$, $k_r(\mathbf{s}_i)$ in the above refers to the positive integer less than or equal to $|N(\mathbf{s}_r)|$ such that $\mathbf{s}_i = N(\mathbf{s}_r)[k_r(\mathbf{s}_i)]$. We have written the $O \times (|N(\mathbf{s}_r)| \cdot O)$ matrix $B_{\mathbf{s}_r}$ as $(B_{\mathbf{s}_r, 1}, \dots, B_{\mathbf{s}_r, |N(\mathbf{s}_r)|})$, where each sub-matrix is $O \times O$, and written the $(|N(\mathbf{s}_r)| \cdot O) \times 1$ vector $\alpha_{jl_j, N(\mathbf{s}_r)}$ as $(\alpha_{jl_j, N(\mathbf{s}_r)[1]}^T, \dots, \alpha_{jl_j, N(\mathbf{s}_r)[|N(\mathbf{s}_r)|]}^T)^T$ so that $B_{\mathbf{s}_r} \alpha_{jl_j, N(\mathbf{s}_r)} = \sum_{k=1}^{|N(\mathbf{s}_r)|} B_{\mathbf{s}_r, k} \alpha_{jl_j, N(\mathbf{s}_r)[k]}$. Note that we only need to consider $r = i+1, \dots, m$ for each $i < m$ in order to find out the set $\{r \in \{1, \dots, m\} : \mathbf{s}_i \in N(\mathbf{s}_r)\}$. Also note that $F_{\mathbf{s}_1} = \kappa_{O \times O}$, $N(\mathbf{s}_1) = \emptyset \Rightarrow$ we can let $F_{\mathbf{s}_1}^{-1} B_{\mathbf{s}_1} \alpha_{jl_j, N(\mathbf{s}_1)} = \mathbf{0}_{O \times 1}$.

6. Sampling from the full conditional distribution of $\kappa_{O \times O}$:

$$f(\kappa|\cdot) \propto \prod_{j=1}^k \prod_{l_j=1}^{L-1} \pi(\alpha_{jl_j}|\kappa, \rho) \times f_0(\kappa) \sim \mathcal{IW} \left(mk(L-1) + \nu, \sum_{j=1}^k \sum_{l_j=1}^{L-1} S_{\alpha_{\rho}^{jl_j}} + \Theta \right), \quad (\text{A.18})$$

where $S_{\alpha_{\rho}^{jl_j}} = A_{jl_j} F(\rho)^{-1} A_{jl_j}^T$ with $(A_{jl_j})_{O \times m} = (\alpha_{jl_j}(\mathbf{s}_1), \dots, \alpha_{jl_j}(\mathbf{s}_m)) \forall (j, l_j)$.

When $O = 1$, Equation (A.18) reduces to $\mathcal{IG} \left(\frac{mk(L-1)+\nu}{2}, \frac{\sum_{j=1}^k \sum_{l_j=1}^{L-1} S_{\alpha_{\rho}^{jl_j}} + \Theta}{2} \right)$.

When the NNGP prior rather than the full GP prior is adopted for the α_{jl_j} 's, we replace $\pi(\alpha_{jl_j}|\kappa, \rho)$ and $F(\rho)$ in Equation (A.18) by $\tilde{\pi}(\alpha_{jl_j}|\kappa, \rho)$ and $\tilde{F}(\rho)$ respectively.

7. Sampling ρ via a Metropolis step when `include.space = TRUE`:

$$f(\rho|\cdot) \propto \prod_{j=1}^k \prod_{l_j=1}^{L-1} \pi(\alpha_{jl_j}|\kappa, \rho) \times f_0(\rho) \times \left| \frac{\partial}{\partial \Delta} h^{-1}(\Delta) \right| \quad (\text{A.19})$$

with $\alpha_{jl_j}|\kappa, \rho \sim N_{mO}(\mathbf{0}, F(\rho) \otimes \kappa) \quad \forall (j, l_j)$.

When the NNGP prior rather than the full GP prior is adopted for the α_{jl_j} 's, we replace $\pi(\alpha_{jl_j}|\kappa, \rho)$ and $F(\rho)$ in Equation (A.19) by $\tilde{\pi}(\alpha_{jl_j}|\kappa, \rho)$ and $\tilde{F}(\rho)$ respectively.

In Equation (A.19), $f_0(\rho)$ refers to the uniform prior $\text{Unif}(a_{\rho}, b_{\rho})$, where $a_{\rho} = 0, b_{\rho} = 1$ when `spatial.structure = 'discrete'` and $a_{\rho}, b_{\rho} \in \mathbb{R}^+$ when `spatial.structure = 'continuous'`. Δ is a new parameter defined to be $h(\rho) = \ln \left(\frac{\rho - a_{\rho}}{b_{\rho} - \rho} \right)$. Hence $\rho = h^{-1}(\Delta) = \frac{b_{\rho} \exp(\Delta) + a_{\rho}}{1 + \exp(\Delta)}$ and $|\frac{\partial}{\partial \Delta} h^{-1}(\Delta)| \propto \frac{\exp(\Delta)}{[1 + \exp(\Delta)]^2}$.

At each MCMC iteration $s \in \mathbb{N}$, let the current parameter estimate for ρ be $\rho^{(s)}$. We propose a new parameter value $\rho^* = h^{-1}(\Delta^*)$ with Δ^* sampled from a symmetric kernel $N(\Delta^{(s)}, \delta)$, where $\Delta^{(s)} = h(\rho^{(s)})$ and $\delta > 0$ is a tuning parameter decided after the burn-in MCMC iterations based on the acceptance rate for ρ^* , and set

$$\rho^{(s+1)} = \begin{cases} \rho^*, & \text{w.p. } \alpha(\rho^{(s)}, \rho^*) = \min \left\{ \frac{f(\rho^*|\cdot)}{f(\rho^{(s)}|\cdot)}, 1 \right\} \\ \rho^{(s)}, & \text{w.p. } 1 - \alpha(\rho^{(s)}, \rho^*) \end{cases}$$

8. Same as Step 1 given at the start of Appendix A.
9. Same as Step 2 given at the start of Appendix A.
10. Same as Step 3 given at the start of Appendix A.
11. Same as Step 4 given at the start of Appendix A.
12. Same as Step 5 given at the start of Appendix A.

A.3 Full Gibbs Sampling Details for Our Model in Section 3

When we adopt the spatial PSBP clustering mechanism and further integrate pertinent ideas of slice sampling (Walker 2007) by introducing new parameters $L_j \in \mathbb{N} \setminus \{0\}$, $j \in \{1, \dots, k\}$ and $u_j^o(\mathbf{s}_i)$, $(j, i, o) \in \{1, \dots, k\} \times \{1, \dots, m\} \times \{1, \dots, O\}$ so that the spatial prior becomes $\boldsymbol{\alpha}_{jl_j} \stackrel{\text{iid}}{\sim} N_{mO}(\mathbf{0}, F(\rho)_{m \times m} \otimes \kappa_{O \times O})$, $j \in \{1, \dots, k\}$, $l_j \in \{1, \dots, L_j - 1\}$, the corresponding Gibbs sampler steps are detailed in the following. Gibbs sampling steps for θ_{jl_j} ($j \in \{1, \dots, k\}$, $l_j \in \{1, \dots, L_j\}$), δ_h ($h \in \{1, \dots, k\}$), $\kappa_{O \times O}$, and ρ are almost the same as their counterparts in Appendix A.2. We simply sample L_j instead of L many θ_{jl_j} 's for each j and replace L by L_j 's in the three full conditional densities Equations (A.11), (A.18) and (A.19) to obtain Equations (A.24), (A.34) and (A.35). We take note that only $\boldsymbol{\alpha}_{jl_j}$'s are ordered first by observation type and then spatially, i.e., the first O components of each above $mO \times 1$ vector are from location point 1, the next O components are from location point 2, and so on. All other concerned parameters, i.e., \mathbf{u}_j 's, \mathbf{w}_{jl_j} 's, $\boldsymbol{\xi}_j$'s, $\boldsymbol{\lambda}_j$'s, and $\boldsymbol{\sigma}^2$ when not all observations are from the 'binomial' family (Appendix J), are ordered first spatially and then by observation type, i.e., the first m components of each above $Om \times 1$ vector are from observation type 1, the next m components are from observation type 2, and so on.

1. Sampling from the full conditional distributions of $u_j^o(\mathbf{s}_i)$'s:

$$\text{For any arbitrary } (i, o, j), f(u_j^o(\mathbf{s}_i) | \cdot) \propto \mathbb{1}_{\left\{u_j^o(\mathbf{s}_i) < w_{j\xi_j^o(\mathbf{s}_i)}^o(\mathbf{s}_i)\right\}} \sim \text{Unif}\left(0, w_{j\xi_j^o(\mathbf{s}_i)}^o(\mathbf{s}_i)\right).$$

2. Updating the L_j 's and sampling from the full conditional distributions of $\xi_j^o(\mathbf{s}_i)$'s:

Fix any arbitrary $j \in \{1, \dots, k\}$.

$$\begin{aligned} \forall (i, o), \text{ let } L_j^{i,o} = \text{the smallest positive integer s.t. } \sum_{l_j=1}^{L_j^{i,o}} w_{jl_j}^o(\mathbf{s}_i) > 1 - u_j^o(\mathbf{s}_i) \\ \text{and let } L_j^{\text{new}} = \max \left\{ L_j^{i,o} : i = 1, \dots, m, o = 1, \dots, O \right\}. \end{aligned} \quad (\text{A.20})$$

After obtaining $\{L_j^{\text{new}} : j = 1, \dots, k\}$ by Equation (A.20), we immediately update the parameter estimates objects $\boldsymbol{\alpha}_{jl_j}$'s (by only keeping the $mO \times 1$ vectors corresponding to $l_j \in \{1, 2, \dots, L_j^{\text{new}} - 1\}$ and discarding the ones corresponding to $l_j \in \{L_j^{\text{new}}, L_j^{\text{new}} + 1, \dots, L_j^{\text{old}} - 1\}$) and \mathbf{w}_{jl_j} 's correspondingly. Note that

- $\forall l_j \in \{L_j^{\text{new}} + 1, L_j^{\text{new}} + 2, \dots, L_j^{\text{old}}\}$, $w_{jl_j}^o(\mathbf{s}_i)^{\text{old}} < u_j^o(\mathbf{s}_i)$ for all (i, o) . Hence, $\{1, \dots, L_j^{\text{new}}\}$ comprises of all possible choices for $\xi_j^o(\mathbf{s}_i) \forall (i, o)$,
- $\forall j \in \{1, \dots, k\}$, $1 \leq L_j^{\text{new}} \leq L_j^{\text{old}} < \infty$, and
- $\forall (j, i, o) \in \{1, \dots, k\} \times \{1, \dots, m\} \times \{1, \dots, O\}$, $w_{jl_j}^o(\mathbf{s}_i)^{\text{old}} = w_{jl_j}^o(\mathbf{s}_i)^{\text{new}} \forall l_j \in \{1, \dots, L_j^{\text{new}} - 1\}$ and $w_{jL_j^{\text{new}}}^o(\mathbf{s}_i)^{\text{old}} \leq w_{jL_j^{\text{new}}}^o(\mathbf{s}_i)^{\text{new}}$. Hence, $\xi_j^o(\mathbf{s}_i)^{\text{old}}$ is still in the support for $\xi_j^o(\mathbf{s}_i)^{\text{new}}$.

Hence, we can update our parameter estimates for $\xi_j^o(\mathbf{s}_i)$'s via the following:

$$\forall l_j \in \{1, \dots, L_j^{\text{new}}\}, \forall (i, o), \mathbb{P}(\xi_j^o(\mathbf{s}_i) = l_j | \cdot) \propto \mathbb{1}_{\left\{w_{jl_j}^o(\mathbf{s}_i)^{\text{new}} > u_j^o(\mathbf{s}_i)\right\}} \quad (\text{A.21})$$

$$\times \prod_{t=1}^T f(y_t^o(\mathbf{s}_i) | \boldsymbol{\beta}, \boldsymbol{\eta}_t, (\sigma^2)^o(\mathbf{s}_i), \xi_j^o(\mathbf{s}_i) = l_j, \boldsymbol{\xi}_{-j}^o(\mathbf{s}_i), \boldsymbol{\theta}_{\xi^o(\mathbf{s}_i)}) ,$$

where $\forall (i, o, j, l_j)$ s.t. $w_{jl_j}^o(\mathbf{s}_i)^{\text{new}} > u_j^o(\mathbf{s}_i)$, $\forall t \in \{1, \dots, T\}$,

$$\begin{aligned} & f(y_t^o(\mathbf{s}_i) | \boldsymbol{\beta}, \boldsymbol{\eta}_t, (\sigma^2)^o(\mathbf{s}_i), \xi_j^o(\mathbf{s}_i) = l_j, \boldsymbol{\xi}_{-j}^o(\mathbf{s}_i), \boldsymbol{\theta}_{\xi^o(\mathbf{s}_i)}) \\ &= (2\pi)^{-\frac{1}{2}} (\sigma^{-1})^o(\mathbf{s}_i) \exp \left\{ -\frac{1}{2} (\sigma^{-2})^o(\mathbf{s}_i) \left[y_t^o(\mathbf{s}_i) - \mathbf{x}_t^o(\mathbf{s}_i)^T \boldsymbol{\beta} - \sum_{h \neq j}^{1 \leq h \leq k} \theta_{h\xi_h^o(\mathbf{s}_i)} \eta_{th} - \theta_{jl_j} \eta_{tj} \right]^2 \right\}. \end{aligned} \quad (\text{A.22})$$

3. Sampling from the full conditional distributions of θ_{jl_j} 's for $l_j \leq L_j$, as we have assumed a finite mixture model with L_j 's as the spatial cluster numbers in this MCMC iteration :

Fix any arbitrary $j \in \{1, \dots, k\}$ and $l_j \in \{1, \dots, L_j\}$. Then

$$f(\theta_{jl_j} | \cdot) \propto f_0(\theta_{jl_j} | \tau_j) \times \prod_{(i,o): \xi_j^o(\mathbf{s}_i)=l_j} \prod_{t=1}^T f(y_t^o(\mathbf{s}_i) | \boldsymbol{\beta}, \boldsymbol{\eta}_t, (\sigma^2)^o(\mathbf{s}_i), \boldsymbol{\xi}^o(\mathbf{s}_i), \boldsymbol{\theta}_{\xi^o(\mathbf{s}_i)}) . \quad (\text{A.23})$$

If $\nexists (i, o)$ s.t. $\xi_j^o(\mathbf{s}_i) = l_j$, then $f(\theta_{jl_j} | \cdot) = f_0(\theta_{jl_j} | \tau_j) \sim N(0, \tau_j^{-1})$.

If $\exists (i, o)$ s.t. $\xi_j^o(\mathbf{s}_i) = l_j$, then

$$\begin{aligned} & f(\theta_{jl_j} | \cdot) \sim N(V_{\theta_{jl_j}} \mu_{\theta_{jl_j}}, V_{\theta_{jl_j}}), \text{ where } V_{\theta_{jl_j}} = \left[\tau_j + \sum_{(i,o): \xi_j^o(\mathbf{s}_i)=l_j} (\sigma^{-2})^o(\mathbf{s}_i) \sum_{t=1}^T \eta_{tj}^2 \right]^{-1} \\ & \text{and } \mu_{\theta_{jl_j}} = \sum_{(i,o): \xi_j^o(\mathbf{s}_i)=l_j} (\sigma^{-2})^o(\mathbf{s}_i) \sum_{t=1}^T \eta_{tj} \left[y_t^o(\mathbf{s}_i) - \mathbf{x}_t^o(\mathbf{s}_i)^T \boldsymbol{\beta} - \sum_{h \neq j}^{1 \leq h \leq k} \theta_{h\xi_h^o(\mathbf{s}_i)} \eta_{th} \right]. \end{aligned}$$

4. Sampling from the full conditional distributions of δ_h 's:

If a multiplicative gamma process shrinkage prior is placed on the atoms so that $\forall (j, l_j)$, $\theta_{jl_j} \stackrel{\text{ind}}{\sim} N(0, \tau_j^{-1})$ with $\tau_j = \prod_{h=1}^j \delta_h$, $\delta_1 \sim \text{Gamma}(a_1, 1)$, $\delta_h \sim \text{Gamma}(a_2, 1) \forall h \geq 2$, then for any arbitrary fixed $h \in \{1, \dots, k\}$,

$$\begin{aligned} & f(\delta_h | \cdot) \propto \prod_{j=h}^k \prod_{l_j=1}^{L_j} f(\theta_{jl_j} | \tau_j) \times f_0(\delta_h) \\ & \sim \text{Gamma} \left(a_h + \frac{\sum_{j=h}^k L_j}{2}, 1 + \frac{\sum_{j=h}^k \left[\prod_{x=1, x \neq h}^j \delta_x \right] \sum_{l_j=1}^{L_j} \theta_{jl_j}^2}{2} \right). \end{aligned} \quad (\text{A.24})$$

If we consider the non-shrinkage prior $\theta_{jl_j} \stackrel{\text{ind}}{\sim} N(0, \tau_j^{-1} = \delta_j^{-1}) \forall (j, l_j)$ with $\delta_j \stackrel{\text{iid}}{\sim} \text{Gamma}(a_1, a_2) \forall j$, then for any arbitrary fixed $j \in \{1, \dots, k\}$,

$$f(\delta_j | \cdot) \propto \prod_{l_j=1}^{L_j} f(\theta_{jl_j} | \delta_j) \times f_0(\delta_j) \sim \text{Gamma} \left(a_1 + \frac{L_j}{2}, a_2 + \frac{\sum_{l_j=1}^{L_j} \theta_{jl_j}^2}{2} \right). \quad (\text{A.25})$$

5. Sampling from the full conditional distributions of $\boldsymbol{\alpha}_{jl_j}$'s ($l_j \in \{1, \dots, L_j - 1\}$ for each j) and calculating new weights $w_{jl_j}^o(\mathbf{s}_i)$'s ($l_j \in \{1, \dots, L_j\}$ for each j) when $L_j > 1$:

If $L_j = 1$, then we do not need to sample any α_{jl_j} 's for this j . The corresponding $w_{j1}^o(\mathbf{s}_i)$'s have already been set to 1 in the previous Gibbs sampler step for $\xi_j^o(\mathbf{s}_i)$'s in this same MCMC iteration.

For any arbitrary fixed (j, l_j) where $j \in \{1, \dots, k\}$ and $l_j \in \{1, \dots, L_j - 1\}$,

$$f(\alpha_{jl_j}|\cdot) \propto \pi(\alpha_{jl_j}|\kappa, \rho) \times \prod_{i=1}^m \prod_{o=1}^O \mathbb{1}_{\left\{l_j > \xi_j^o(\mathbf{s}_i) \text{ or } u_j^o(\mathbf{s}_i) < w_{j\xi_j^o(\mathbf{s}_i)}^o(\mathbf{s}_i)\right\}} \quad (\text{A.26})$$

$$\begin{aligned} &\sim N_{mO}(\mathbf{0}, F(\rho) \otimes \kappa) \times \prod_{i=1}^m \prod_{o=1}^O \mathbb{1}_{\left\{l_j > \xi_j^o(\mathbf{s}_i) \text{ or } u_j^o(\mathbf{s}_i) < w_{j\xi_j^o(\mathbf{s}_i)}^o(\mathbf{s}_i)\right\}} \\ &\sim N_{mO}(\mathbf{0}, F(\rho) \otimes \kappa) \times \prod_{i=1}^m \prod_{o=1}^O \begin{cases} 1, & \text{if } l_j > \xi_j^o(\mathbf{s}_i) \\ \mathbb{1}_{\left\{\alpha_{jl_j}^o(\mathbf{s}_i)^{\text{new}} > \text{lowerBound}_{(j, l_j, i, o)}\right\}}, & \text{if } l_j = \xi_j^o(\mathbf{s}_i) \\ \mathbb{1}_{\left\{\alpha_{jl_j}^o(\mathbf{s}_i)^{\text{new}} < \text{upperBound}_{(j, l_j, i, o)}\right\}}, & \text{if } l_j < \xi_j^o(\mathbf{s}_i) \end{cases} \end{aligned} \quad (\text{A.27})$$

where $\forall (j, l_j, i, o)$,

$$\text{lowerBound}_{(j, l_j, i, o)} = \Phi^{-1} \left(\frac{u_j^o(\mathbf{s}_i) \cdot \Phi \left(\alpha_{jl_j}^o(\mathbf{s}_i)^{\text{old}} \right)}{w_{j\xi_j^o(\mathbf{s}_i)}^o(\mathbf{s}_i)} \right) \text{ and} \quad (\text{A.28})$$

$$\text{upperBound}_{(j, l_j, i, o)} = \Phi^{-1} \left(1 - \frac{u_j^o(\mathbf{s}_i) \cdot \left[1 - \Phi \left(\alpha_{jl_j}^o(\mathbf{s}_i)^{\text{old}} \right) \right]}{w_{j\xi_j^o(\mathbf{s}_i)}^o(\mathbf{s}_i)} \right). \quad (\text{A.29})$$

When the NNGP instead of the full GP prior is adopted for the α_{jl_j} 's, we replace $\pi(\alpha_{jl_j}|\kappa, \rho)$ and $F(\rho)$ by $\tilde{\pi}(\alpha_{jl_j}|\kappa, \rho)$ and $\tilde{F}(\rho)$ in the above equations.

After obtaining our new estimates for $\alpha_{jl_j}^o(\mathbf{s}_i)$'s ($l_j \in \{1, \dots, L_j - 1\}$), we calculate our new samples for the corresponding weights parameters $w_{jl_j}^o(\mathbf{s}_i)$'s ($l_j \in \{1, \dots, L_j\}$) via

$$w_{jl_j}^o(\mathbf{s}_i) = \begin{cases} \Phi \left(\alpha_{jl_j}^o(\mathbf{s}_i) \right) \prod_{r_j < l_j} \left[1 - \Phi \left(\alpha_{jr_j}^o(\mathbf{s}_i) \right) \right], & \text{if } l_j \in \{1, \dots, L_j - 1\} \\ \prod_{r_j < L_j} \left[1 - \Phi \left(\alpha_{jr_j}^o(\mathbf{s}_i) \right) \right], & \text{if } l_j = L_j \end{cases} \quad (\text{A.30})$$

for any arbitrary $(j, o, i) \in \{1, \dots, k\} \times \{1, \dots, O\} \times \{1, \dots, m\}$ and $l_j \in \{1, \dots, L_j\}$.

The truncated multivariate normal posterior distributions of α_{jl_j} 's (Equation (A.27)) can be directly sampled by multivariate rejection sampling via for instance the `rtmvnorm()` function in the R package `tmvtnorm`. One noteworthy problem with multivariate rejection sampling, in this case, is that it typically gets very inefficient when m is large due to an excessively small acceptance rate associated with sampling from a high-dimensional truncated mO -variate normal distribution. This issue can be successfully addressed by integrating spatial scalability via assuming an NNGP prior and sequentially sampling α_{jl_j} 's instead.

Sequentially Updating $\alpha_{jl_j} = (\alpha_{jl_j}(\mathbf{s}_1)^T, \dots, \alpha_{jl_j}(\mathbf{s}_m)^T)^T \forall (j, l_j)$

Under the circumstance when `include.space = TRUE`, `spatial.structure = "continuous"`, and `spatApprox = TRUE`, we can opt to sequentially update the α_{jl_j} 's instead:

Under our NNGP prior $\tilde{\pi}(\boldsymbol{\alpha}_{jl_j}|\kappa, \rho) = N_{mO}(\mathbf{0}, \tilde{F}(\rho) \otimes \kappa)$ for all (j, l_j) , for any arbitrary fixed (j, l_j, i) where $j \in \{1, \dots, k\}$, $l_j \in \{1, \dots, L_j - 1\}$, and $i \in \{1, \dots, m\}$,

$$f(\boldsymbol{\alpha}_{jl_j}(\mathbf{s}_i)|\cdot) \propto \tilde{f}(\boldsymbol{\alpha}_{jl_j}|\cdot) \times \prod_{o=1}^O \mathbb{1}_{\left\{l_j > \xi_j^o(\mathbf{s}_i) \text{ or } u_j^o(\mathbf{s}_i) < w_{j\xi_j^o(\mathbf{s}_i)}^o(\mathbf{s}_i)\right\}} \quad (\text{A.31})$$

$$\begin{aligned} &= \prod_{r=1}^m f(\boldsymbol{\alpha}_{jl_j}(\mathbf{s}_r)|\boldsymbol{\alpha}_{jl_j, N(\mathbf{s}_r)}, \kappa, \rho) \times \prod_{o=1}^O \mathbb{1}_{\left\{l_j > \xi_j^o(\mathbf{s}_i) \text{ or } u_j^o(\mathbf{s}_i) < w_{j\xi_j^o(\mathbf{s}_i)}^o(\mathbf{s}_i)\right\}} \\ &\propto \prod_{r: r=i \text{ or } \mathbf{s}_i \in N(\mathbf{s}_r)} f(\boldsymbol{\alpha}_{jl_j}(\mathbf{s}_r)|\boldsymbol{\alpha}_{jl_j, N(\mathbf{s}_r)}, \kappa, \rho) \times \prod_{o=1}^O \mathbb{1}_{\left\{l_j > \xi_j^o(\mathbf{s}_i) \text{ or } u_j^o(\mathbf{s}_i) < w_{j\xi_j^o(\mathbf{s}_i)}^o(\mathbf{s}_i)\right\}} \\ &\propto \prod_{o=1}^O \mathbb{1}_{\left\{l_j > \xi_j^o(\mathbf{s}_i) \text{ or } u_j^o(\mathbf{s}_i) < w_{j\xi_j^o(\mathbf{s}_i)}^o(\mathbf{s}_i)\right\}} \times \end{aligned} \quad (\text{A.32})$$

$$\begin{aligned} &\exp\left\{-\frac{1}{2}\left(\boldsymbol{\alpha}_{jl_j}(\mathbf{s}_i) - B_{\mathbf{s}_i}\boldsymbol{\alpha}_{jl_j, N(\mathbf{s}_i)}\right)^T F_{\mathbf{s}_i}^{-1}\left(\boldsymbol{\alpha}_{jl_j}(\mathbf{s}_i) - B_{\mathbf{s}_i}\boldsymbol{\alpha}_{jl_j, N(\mathbf{s}_i)}\right)\right\} \times \\ &\exp\left\{-\frac{1}{2}\sum_{r: \mathbf{s}_i \in N(\mathbf{s}_r)}\left(\boldsymbol{\alpha}_{jl_j}(\mathbf{s}_r) - B_{\mathbf{s}_r}\boldsymbol{\alpha}_{jl_j, N(\mathbf{s}_r)}\right)^T F_{\mathbf{s}_r}^{-1}\left(\boldsymbol{\alpha}_{jl_j}(\mathbf{s}_r) - B_{\mathbf{s}_r}\boldsymbol{\alpha}_{jl_j, N(\mathbf{s}_r)}\right)\right\}. \\ &\sim N_O(V_{\mathbf{s}_i}\boldsymbol{\mu}_{jl_j, \mathbf{s}_i}, V_{\mathbf{s}_i}) \times \prod_{o=1}^O \mathbb{1}_{\left\{l_j > \xi_j^o(\mathbf{s}_i) \text{ or } u_j^o(\mathbf{s}_i) < w_{j\xi_j^o(\mathbf{s}_i)}^o(\mathbf{s}_i)\right\}}, \end{aligned} \quad (\text{A.33})$$

$$\text{where } V_{\mathbf{s}_i} = \left[F_{\mathbf{s}_i}^{-1} + \sum_{r: \mathbf{s}_i \in N(\mathbf{s}_r)} B_{\mathbf{s}_r, k_r(\mathbf{s}_i)}^T F_{\mathbf{s}_r}^{-1} B_{\mathbf{s}_r, k_r(\mathbf{s}_i)}\right]^{-1} \text{ and}$$

$$\boldsymbol{\mu}_{jl_j, \mathbf{s}_i} = F_{\mathbf{s}_i}^{-1} B_{\mathbf{s}_i} \boldsymbol{\alpha}_{jl_j, N(\mathbf{s}_i)} + \sum_{r: \mathbf{s}_i \in N(\mathbf{s}_r)} B_{\mathbf{s}_r, k_r(\mathbf{s}_i)}^T F_{\mathbf{s}_r}^{-1} \left\{ \boldsymbol{\alpha}_{jl_j}(\mathbf{s}_r) - \sum_{\substack{1 \leq k \leq |N(\mathbf{s}_r)| \\ k \neq k_r(\mathbf{s}_i)}} B_{\mathbf{s}_r, k} \boldsymbol{\alpha}_{jl_j, N(\mathbf{s}_r)[k]} \right\}.$$

For each r such that $\mathbf{s}_i \in N(\mathbf{s}_r)$, $k_r(\mathbf{s}_i)$ in the above refers to the positive integer less than or equal to $|N(\mathbf{s}_r)|$ such that $\mathbf{s}_i = N(\mathbf{s}_r)[k_r(\mathbf{s}_i)]$. We have written the $O \times (|N(\mathbf{s}_r)| \cdot O)$ matrix $B_{\mathbf{s}_r}$ as $(B_{\mathbf{s}_r, 1}, \dots, B_{\mathbf{s}_r, |N(\mathbf{s}_r)|})$, where each sub-matrix is $O \times O$, and written the $(|N(\mathbf{s}_r)| \cdot O) \times 1$ vector $\boldsymbol{\alpha}_{jl_j, N(\mathbf{s}_r)}$ as $(\boldsymbol{\alpha}_{jl_j, N(\mathbf{s}_r)[1]}^T, \dots, \boldsymbol{\alpha}_{jl_j, N(\mathbf{s}_r)[|N(\mathbf{s}_r)|]}^T)^T$ so that $B_{\mathbf{s}_r} \boldsymbol{\alpha}_{jl_j, N(\mathbf{s}_r)} = \sum_{k=1}^{|N(\mathbf{s}_r)|} B_{\mathbf{s}_r, k} \boldsymbol{\alpha}_{jl_j, N(\mathbf{s}_r)[k]}$. Note that we only need to consider $r = i + 1, \dots, m$ for each $i < m$ in order to find out the set $\{r \in \{1, \dots, m\} : \mathbf{s}_i \in N(\mathbf{s}_r)\}$. Also note that $F_{\mathbf{s}_1} = \kappa_{O \times O}$, $N(\mathbf{s}_1) = \emptyset \Rightarrow$ we can let $F_{\mathbf{s}_1}^{-1} B_{\mathbf{s}_1} \boldsymbol{\alpha}_{jl_j, N(\mathbf{s}_1)} = \mathbf{0}_{O \times 1}$.

6. Sampling from the full conditional distribution of $\kappa_{O \times O}$:

$$f(\kappa|\cdot) \propto \prod_{j=1}^k \prod_{l_j=1}^{L_j-1} \pi(\boldsymbol{\alpha}_{jl_j}|\kappa, \rho) \times f_0(\kappa) \sim \mathcal{IW}\left(m \sum_{j=1}^k (L_j - 1) + \nu, \sum_{j=1}^k \sum_{l_j=1}^{L_j-1} S_{\alpha_{\rho}^{jl_j}} + \Theta\right), \quad (\text{A.34})$$

where $S_{\alpha_{\rho}^{jl_j}} = A_{jl_j} F(\rho)^{-1} A_{jl_j}^T$ with $(A_{jl_j})_{O \times m} = (\boldsymbol{\alpha}_{jl_j}(\mathbf{s}_1), \dots, \boldsymbol{\alpha}_{jl_j}(\mathbf{s}_m)) \forall (j, l_j)$.

$$\text{When } O = 1, \text{ Equation (A.34) reduces to } \mathcal{IG}\left(\frac{m \sum_{j=1}^k (L_j - 1) + \nu}{2}, \frac{\sum_{j=1}^k \sum_{l_j=1}^{L_j-1} S_{\alpha_{\rho}^{jl_j}} + \Theta}{2}\right).$$

When the NNGP prior rather than the full GP prior is adopted for the $\boldsymbol{\alpha}_{jl_j}$'s, we replace $\pi(\boldsymbol{\alpha}_{jl_j}|\kappa, \rho)$ and $F(\rho)$ in Equation (A.34) by $\tilde{\pi}(\boldsymbol{\alpha}_{jl_j}|\kappa, \rho)$ and $\tilde{F}(\rho)$ respectively.

7. Sampling ρ via a Metropolis step when `include.space = TRUE`:

$$f(\rho|\cdot) \propto \prod_{j=1}^k \prod_{l_j=1}^{L_j-1} \pi(\boldsymbol{\alpha}_{jl_j}|\kappa, \rho) \times f_0(\rho) \times \left| \frac{\partial}{\partial \Delta} h^{-1}(\Delta) \right| \quad (\text{A.35})$$

with $\boldsymbol{\alpha}_{jl_j}|\kappa, \rho \sim N_{mO}(\mathbf{0}, F(\rho) \otimes \kappa) \quad \forall (j, l_j).$

When the NNGP prior rather than the full GP prior is adopted for the $\boldsymbol{\alpha}_{jl_j}$'s, we replace $\pi(\boldsymbol{\alpha}_{jl_j}|\kappa, \rho)$ and $F(\rho)$ in Equation (A.35) by $\tilde{\pi}(\boldsymbol{\alpha}_{jl_j}|\kappa, \rho)$ and $\tilde{F}(\rho)$ respectively.

In Equation (A.35), $f_0(\rho)$ refers to the uniform prior $\text{Unif}(a_\rho, b_\rho)$, where $a_\rho = 0, b_\rho = 1$ when `spatial.structure = 'discrete'` and $a_\rho, b_\rho \in \mathbb{R}^+$ when `spatial.structure = 'continuous'`. Δ is a new parameter defined to be $h(\rho) = \ln\left(\frac{\rho - a_\rho}{b_\rho - \rho}\right)$. Hence $\rho = h^{-1}(\Delta) = \frac{b_\rho \exp(\Delta) + a_\rho}{1 + \exp(\Delta)}$ and $\left| \frac{\partial}{\partial \Delta} h^{-1}(\Delta) \right| \propto \frac{\exp(\Delta)}{[1 + \exp(\Delta)]^2}$.

At each MCMC iteration $s \in \mathbb{N}$, let the current parameter estimate for ρ be $\rho^{(s)}$. We propose a new parameter value $\rho^* = h^{-1}(\Delta^*)$ with Δ^* sampled from a symmetric kernel $N(\Delta^{(s)}, \delta)$, where $\Delta^{(s)} = h(\rho^{(s)})$ and $\delta > 0$ is a tuning parameter decided after the burn-in MCMC iterations based on the acceptance rate for ρ^* , and set

$$\rho^{(s+1)} = \begin{cases} \rho^*, & \text{w.p. } \alpha(\rho^{(s)}, \rho^*) = \min\left\{\frac{f(\rho^*|\cdot)}{f(\rho^{(s)}|\cdot)}, 1\right\} \\ \rho^{(s)}, & \text{w.p. } 1 - \alpha(\rho^{(s)}, \rho^*) \end{cases}.$$

8. Same as Step 1 given at the start of Appendix A.
9. Same as Step 2 given at the start of Appendix A.
10. Same as Step 3 given at the start of Appendix A.
11. Same as Step 4 given at the start of Appendix A.
12. Same as Step 5 given at the start of Appendix A.

B Temporal Posterior Sampling and Prediction Acceleration for Evenly Dispersed Time Points

Throughout this section, we sometimes write $H(\psi)$ as H to simplify notations.

B.1 Temporal Part Computational Burdens When T is Large

Our Gibbs sampling steps with respect to temporal-related parameters $\boldsymbol{\eta}_t$'s, $\Upsilon_{k \times k}$, and ψ given in Appendix A can get very slow when T is large due to the primary reasons listed below, especially the last one. In each MCMC iteration in any of our Gibbs samplers (Appendix A),

- The full conditional distribution of $\Upsilon_{k \times k}$ (Equation (A.2)) concerns $H(\psi)^{-1}$, whose computation requires $\mathcal{O}(T^3)$ flops via standard methods;

- To sample ψ via a Metropolis step, we need to calculate $\log f(\psi|\cdot)$ for both the current parameter estimate and the newly proposed value of ψ . As the full conditional density of ψ is given by Equation (A.3), we have to evaluate $H(\psi)^{-1}$ and $\log [\det (H(\psi))]$,¹ which both require $\mathcal{O}(T^3)$ flops under standard methods. Let $\text{Rooti}(H) = [\text{Chol}(H)]^{-1}$ be the upper triangular matrix with positive diagonal entries such that $H(\psi)^{-1} = \text{Rooti}(H) [\text{Rooti}(H)]^T$. Then $\det (H(\psi))$ can also be conveniently calculated as the inverse of the square of the product of all diagonal entries in $\text{Rooti}(H)$. Adopting $\text{Rooti}(H)$ instead of $H(\psi)^{-1}$ and $\det (H(\psi))$ for this step is usually faster, but $\text{Rooti}(H)$ also has a computational complexity of $\mathcal{O}(T^3)$ for a general $H(\psi)_{T \times T}$ without any special structures.
- When sampling η_t 's from their full conditional distributions (Equation (A.1)), we would need to loop over $t \in \{1, 2, \dots, T\}$ and calculate $H_t^+ = H_{t,(1:T)-t} H_{(1:T)-t,(1:T)-t}^{-1} H_{(1:T)-t,t}^*$, $H_t^* = H_{t,t} - H_{t,(1:T)-t} H_{(1:T)-t,(1:T)-t}^{-1} H_{(1:T)-t,t}$ for each t . This can be computationally intimidating when T is large given that we need to invert T many $(T-1) \times (T-1)$ principal sub-matrices of $H(\psi)_{T \times T}$, which results in an overall computational complexity of $\mathcal{O}(T^4)$. Also, we would have to compute and store the entire $H(\psi)_{T \times T}$ matrix to extract out its aforementioned sub-matrices.

When making predictions at $q \in \mathbb{N}$ future time points $(T+1):(T+q)$, $H(\psi)^{-1}$ is also needed to obtain a predicted $\hat{\eta}_{(T+1):(T+q)}$ given $\eta_{1:T}$, Υ , ψ (Appendix G.1) in each MCMC iteration.

The above points do not exist as problems when temporal independence is assumed, i.e., when the temporal correlation structure matrix $H(\psi)_{T \times T}$ is fixed as the $T \times T$ identity matrix. In that case,

- When sampling $\Upsilon_{k \times k}$ from its full conditional distribution and when obtaining $\hat{\eta}_{(T+1):(T+q)}$ given $\eta_{1:T}$, Υ , ψ , we can directly take $H(\psi)_{T \times T}^{-1}$ as $I_{T \times T}$ throughout;
- We no longer need to sample ψ anymore in any MCMC iteration;
- The step sampling η_t 's can be greatly simplified and accelerated:

$$\begin{aligned}
H &= H(\psi) = I_{T \times T} \\
\Rightarrow H_t^+ &= (0, 0, \dots, 0)_{1 \times (T-1)} I_{(T-1) \times (T-1)} = (0, 0, \dots, 0)_{1 \times (T-1)} \text{ and} \\
H_t^* &= 1 - (0, 0, \dots, 0)_{1 \times (T-1)} (0, 0, \dots, 0)_{(T-1) \times 1}^T = 1 - 0 = 1 \quad \forall t \in \{1, 2, \dots, T\}. \\
\text{Hence } \mathbb{C}_{0\eta_t} &= \Upsilon_{k \times k} \text{ and } \mathbb{E}_{0\eta_t} = (0, 0, \dots, 0)_{k \times 1}^T \quad \forall t \\
\Rightarrow \mathbb{C}_{\eta_t} &= (\Lambda^T \Xi^{-1} \Lambda + \Upsilon^{-1})^{-1} \text{ and } \mu_{\eta_t} = \Lambda^T \Xi^{-1} (\mathbf{y}_t - X_t \boldsymbol{\beta}) \quad \forall t \text{ in Equation (A.1).}
\end{aligned}$$

Under most circumstances, however, temporal correlation should indeed be taken into consideration. Fortunately, under a widely encountered special application scenario when all our time points are equally spaced, substantial computational acceleration is indeed achievable by exploiting the corresponding temporal correlation matrix's special structure.

¹ Note that these two quantities suffice for the ψ part since $[H(\psi) \otimes \Upsilon]^{-1} = H(\psi)^{-1} \otimes \Upsilon^{-1}$ and $\log [\det (H(\psi) \otimes \Upsilon)] = k \cdot \log [\det (H(\psi))] + T \cdot \log [\det (\Upsilon)]$.

B.2 Some Set-Up and Notations

Throughout the rest of this section, we assume the scenario when temporal correlation is included and all time points are equispaced with the adjacent distances normalized to 1. Four temporal structures – `ar1`, `exponential`, `sar1`, `sexponential`, which denote AR(1), the exponential process, and their seasonal counterparts (Appendix A), respectively, are considered.

$$\text{Let } \rho = \begin{cases} \psi \in (0, 1), & \text{if } \text{temporal.structure} = \text{'ar1'} \text{ or 'sar1'} \\ e^{-\psi} \in (0, 1), & \text{if } \text{temporal.structure} = \text{'exponential'} \text{ or 'sexponential'} \end{cases}.$$

Then for $T \geq 3$, the $T \times T$ temporal correlation structure matrix, which is ensured positive definite (Appendix B.3), is

$$H = H(\psi) = \begin{pmatrix} 1 & \rho & \rho^2 & \dots & \rho^{T-1} \\ \rho & 1 & \rho & \dots & \rho^{T-2} \\ \rho^2 & \rho & 1 & \dots & \rho^{T-3} \\ \vdots & \vdots & \vdots & \ddots & \vdots \\ \rho^{T-1} & \rho^{T-2} & \rho^{T-3} & \dots & 1 \end{pmatrix}$$

if `temporal.structure` = "ar1" or "exponential", and $H = H(\psi, d) =$

$$\begin{matrix} & \mathbf{1} & & \mathbf{d+1} & & \mathbf{2d+1} & & \mathbf{kd+1} \\ \mathbf{1} & \left(\begin{array}{cccccc} 1 & & & & & \rho^k \\ & 1 & & \rho & & \rho^2 & \dots & \dots & \rho^k \\ & & \ddots & & \ddots & & \ddots & & \vdots \\ \rho & & & 1 & & \rho & & \rho^2 & \vdots \\ & \rho & & & 1 & \rho & & \rho^2 & \vdots \\ & & \ddots & & \ddots & & \ddots & & \vdots \\ \rho^2 & & & \rho & & 1 & & \rho & \rho^2 \\ & \rho^2 & & & \rho & & 1 & \rho & \rho \\ \vdots & \vdots & \ddots & & \ddots & & \ddots & & \ddots \\ \vdots & \vdots & & \ddots & & \ddots & & \ddots & \rho \\ \rho^k & & \dots & \dots & \rho^2 & & \rho & & 1 \end{array} \right) & \mathbf{T-kd} \\ & & & \rho^k & & \dots & & \rho^2 & & \rho & & 1 \\ & \mathbf{T-kd} & & & \mathbf{T-2d} & & \mathbf{T-d} & & \mathbf{T} \end{matrix}$$

if `temporal.structure` = "sar1" or "sexponential", where $d > 1$, $d \in \mathbb{N}$ is an arbitrary temporal seasonal period and $k = \lfloor \frac{T-1}{d} \rfloor$.

B.3 Simple Sparse Closed-Form Representations for $H(\psi)_{T \times T}^{-1}$ and $\text{Rooti}(H)_{T \times T}$

B.3.1 When temporal.structure = ‘ar1’ or ‘exponential’

Let $D_{T \times T} = \text{Diag}(1, 1 - \rho^2, 1 - \rho^2, \dots, 1 - \rho^2)$ and

$$L_{T \times T} = \begin{pmatrix} 1 & 0 & 0 & \dots & 0 \\ \rho & 1 & 0 & \dots & 0 \\ \rho^2 & \rho & 1 & \dots & 0 \\ \vdots & \vdots & \vdots & \ddots & \vdots \\ \rho^{T-1} & \rho^{T-2} & \rho^{T-3} & \dots & 1 \end{pmatrix}. \text{ Note that } L^{-1} = \begin{pmatrix} 1 & & & & \\ -\rho & 1 & & & \\ & -\rho & 1 & & \\ & & \ddots & \ddots & \\ & & & -\rho & 1 \\ & & & & -\rho & 1 \end{pmatrix}_{T \times T}.$$

Then $H = LDL^T = \text{Chol}(H)^T \text{Chol}(H)$, where

$$\begin{aligned} \text{Chol}(H) = D^{\frac{1}{2}} L^T &= \begin{pmatrix} 1 & 0 & 0 & \dots & 0 \\ 0 & \sqrt{1 - \rho^2} & 0 & \dots & 0 \\ 0 & 0 & \sqrt{1 - \rho^2} & \dots & 0 \\ \vdots & \vdots & \vdots & \ddots & \vdots \\ 0 & 0 & 0 & \dots & \sqrt{1 - \rho^2} \end{pmatrix} \begin{pmatrix} 1 & \rho & \rho^2 & \dots & \rho^{T-1} \\ 0 & 1 & \rho & \dots & \rho^{T-2} \\ 0 & 0 & 1 & \dots & \rho^{T-3} \\ \vdots & \vdots & \vdots & \ddots & \vdots \\ 0 & 0 & 0 & \dots & 1 \end{pmatrix} \\ &= \begin{pmatrix} 1 & \rho & \rho^2 & \dots & \rho^{T-1} \\ 0 & \sqrt{1 - \rho^2} & \rho\sqrt{1 - \rho^2} & \dots & \rho^{T-2}\sqrt{1 - \rho^2} \\ 0 & 0 & \sqrt{1 - \rho^2} & \dots & \rho^{T-3}\sqrt{1 - \rho^2} \\ \vdots & \vdots & \vdots & \ddots & \vdots \\ 0 & 0 & 0 & \dots & \sqrt{1 - \rho^2} \end{pmatrix} \text{ is upper triangular.} \end{aligned}$$

Hence $\text{Rooti}(H) = [\text{Chol}(H)]^{-1} = (L^{-1})^T D^{-\frac{1}{2}}$

$$\begin{aligned} &= \begin{pmatrix} 1 & -\rho & 0 & 0 & \dots & 0 \\ 0 & 1 & -\rho & 0 & \dots & 0 \\ 0 & 0 & 1 & -\rho & \dots & 0 \\ \vdots & \vdots & \vdots & \ddots & \ddots & \vdots \\ 0 & 0 & 0 & \dots & 1 & -\rho \\ 0 & 0 & 0 & \dots & 0 & 1 \end{pmatrix} \begin{pmatrix} 1 & 0 & 0 & \dots & 0 \\ 0 & \frac{1}{\sqrt{1 - \rho^2}} & 0 & \dots & 0 \\ 0 & 0 & \frac{1}{\sqrt{1 - \rho^2}} & \dots & 0 \\ \vdots & \vdots & \vdots & \ddots & \vdots \\ 0 & 0 & 0 & \dots & \frac{1}{\sqrt{1 - \rho^2}} \end{pmatrix} \\ &= \begin{pmatrix} 1 & -\frac{\rho}{\sqrt{1 - \rho^2}} & 0 & 0 & \dots & 0 \\ 0 & \frac{1}{\sqrt{1 - \rho^2}} & -\frac{\rho}{\sqrt{1 - \rho^2}} & 0 & \dots & 0 \\ 0 & 0 & \frac{1}{\sqrt{1 - \rho^2}} & -\frac{\rho}{\sqrt{1 - \rho^2}} & \dots & 0 \\ \vdots & \vdots & \vdots & \ddots & \ddots & \vdots \\ 0 & 0 & 0 & \dots & \frac{1}{\sqrt{1 - \rho^2}} & -\frac{\rho}{\sqrt{1 - \rho^2}} \\ 0 & 0 & 0 & \dots & 0 & \frac{1}{\sqrt{1 - \rho^2}} \end{pmatrix}_{T \times T}, \text{ and} \end{aligned}$$

$$H^{-1} = (L^{-1})^T D^{-1} L^{-1} = \text{Rooti}(H) [\text{Rooti}(H)]^T$$

$$= \frac{1}{1-\rho^2} \begin{pmatrix} 1 & -\rho & & & & \\ -\rho & 1+\rho^2 & -\rho & & & \\ & -\rho & 1+\rho^2 & \ddots & & \\ & & -\rho & \ddots & -\rho & \\ & & & \ddots & 1+\rho^2 & -\rho \\ & & & & -\rho & 1+\rho^2 & -\rho \\ & & & & & -\rho & 1 \end{pmatrix}_{T \times T}.$$

B.3.2 When temporal.structure = ‘sar1’ or ‘sexponential’

Let $L_{T \times T} =$

$$\begin{matrix} & \mathbf{1} & & \mathbf{d+1} & & \mathbf{2d+1} & & \mathbf{kd+1} \\ \mathbf{1} & \left(\begin{array}{cccccccc} 1 & & & & & & & \\ & 1 & & & & & & \\ & & \ddots & & & & & \\ \mathbf{d+1} & \rho & & 1 & & & & \\ & \rho & & & 1 & & & \\ & & \ddots & & & \ddots & & \\ \mathbf{2d+1} & \rho^2 & & \rho & & 1 & & \\ & \rho^2 & & & \rho & & 1 & \\ \vdots & \vdots & \ddots & & & \ddots & & \ddots \\ \vdots & \vdots & & \ddots & & & \ddots & \\ \mathbf{kd+1} & \rho^k & \dots & \dots & \rho^2 & & \rho & 1 \end{array} \right) & & & & & & & \\ & & \ddots & & & \ddots & & \ddots & & & & & & & \\ & & & \rho^k & & \dots & \dots & \rho^2 & & \rho & & & & 1 \\ & & & & \mathbf{T-kd} & & & & \mathbf{T-2d} & & & \mathbf{T-d} & & \mathbf{T} \end{matrix},$$

$$D_{T \times T} = \begin{matrix} & \mathbf{1} & & \mathbf{d} & \mathbf{d+1} & & \mathbf{T} \\ \mathbf{1} & \left(\begin{array}{ccccccc} 1 & & & & & & \\ & 1 & & & & & \\ & & \ddots & & & & \\ \mathbf{d} & & & 1 & & & \\ \mathbf{d+1} & & & & 1-\rho^2 & & \\ & & & & & 1-\rho^2 & \\ & & & & & & \ddots \\ & & & & & & & \ddots \\ \mathbf{T} & & & & & & & & 1-\rho^2 \end{array} \right) & & & & & & \end{matrix}.$$

Then $H = LDL^T = \text{Chol}(H)^T \text{Chol}(H)$, where $\text{Chol}(H) = D^{\frac{1}{2}} L^T$ is upper triangular. Note that

$$L^{-1} = \begin{matrix} & \mathbf{1} & & \mathbf{d+1} & & & & & & \\ & \mathbf{1} & & & & & & & & \\ & & \mathbf{1} & & & & & & & \\ & & & \ddots & & & & & & \\ \mathbf{d+1} & -\rho & & & \mathbf{1} & & & & & \\ & & -\rho & & & \mathbf{1} & & & & \\ & & & \ddots & & & \ddots & & & \\ \mathbf{2d+1} & & & & -\rho & & & & & \\ & & & & & -\rho & & & \mathbf{1} & \\ & & & & & & \ddots & & & \mathbf{1} \\ & & & & & & & \ddots & & \\ & & & & & & & & -\rho & \mathbf{1} \\ & & & & & & & & \mathbf{T-d} & \mathbf{T} \end{matrix} \quad T \times T$$

Hence $\text{Rooti}(H) = [\text{Chol}(H)]^{-1} = (L^{-1})^T D^{-\frac{1}{2}} =$

$$\begin{matrix} & \mathbf{1} & \mathbf{2} & & \mathbf{d} & \mathbf{d+1} & \mathbf{d+2} & & \mathbf{T} \\ \mathbf{1} & \left(\begin{matrix} 1 & & & & \frac{-\rho}{\sqrt{1-\rho^2}} & & & & \\ & 1 & & & & \frac{-\rho}{\sqrt{1-\rho^2}} & & & \\ & & \ddots & & & & \ddots & & \\ & & & 1 & & & & \ddots & \\ \mathbf{d} & & & & \frac{1}{\sqrt{1-\rho^2}} & & & & \\ \mathbf{d+1} & & & & & \ddots & & \frac{-\rho}{\sqrt{1-\rho^2}} & \\ & & & & & & \ddots & & \\ & & & & & & & \frac{1}{\sqrt{1-\rho^2}} \end{matrix} \right) & \mathbf{T-d} \\ & & & & & & & & \mathbf{T} \end{matrix} \quad T \times T$$

and $H^{-1} = (L^{-1})^T D^{-1} L^{-1} = \text{Rooti}(H) [\text{Rooti}(H)]^T = \frac{1}{1-\rho^2} \times$

[illegible]

B.3.3 Attained Acceleration Outcomes Pertaining to Sampling $\Upsilon_{k \times k}$ and ψ & Predicting at Future Time Points

1. We have seen in Appendix B.1 that $H(\psi)^{-1}$ and $\text{Rooti}(H)$ are the only temporal correlation quantities required in each MCMC iteration for the posterior sampling of $\Upsilon_{k \times k}$ and ψ as well as obtaining a predicted $\hat{\boldsymbol{\eta}}_{(T+1):(T+q)}$ given $\boldsymbol{\eta}_{1:T}$, Υ , ψ when making future-time predictions. Since both $T \times T$ matrices have simple sparse closed-form solutions (Appendices B.3.1 and B.3.2), we can now directly specify these two matrices in each MCMC iteration instead of calculating them and thus save the corresponding $\mathcal{O}(T^3)$ flops.
2. We have shown in Appendices B.3.1 and B.3.2 that the symmetric matrix $H = LDL^T = \left[D^{\frac{1}{2}}L^T\right]^T D^{\frac{1}{2}}L^T = \text{Chol}(H)^T \text{Chol}(H)$, where $\text{Chol}(H) = D^{\frac{1}{2}}L^T$ is upper triangular whose diagonal entries are all strictly positive. Hence, the temporal correlation structure matrix $H(\psi)_{T \times T}$ is guaranteed positive definite.

B.4 Simple Sparse Closed-Form Representations for the T Vectors H_t^+ 's of Length $T - 1$ & Repetitive Closed-Form Solutions for the T Scalars H_t^{*} 's

Throughout this subsection, we sometimes write the subscript $(1 : T)_{-t}$ as $-t$ to simplify notations.

B.4.1 When temporal.structure = 'ar1' or 'exponential'

(a) **For** $t \in \{1, T\}$

As deduced in Appendix B.3.1, for $t \in \{1, T\}$,

$$H_{(1:T)_{-t}, (1:T)_{-t}}^{-1} = \frac{1}{1 - \rho^2} \begin{pmatrix} 1 & -\rho & & & & & \\ -\rho & 1 + \rho^2 & -\rho & & & & \\ & -\rho & 1 + \rho^2 & \ddots & & & \\ & & -\rho & \ddots & -\rho & & \\ & & & \ddots & 1 + \rho^2 & -\rho & \\ & & & & -\rho & 1 + \rho^2 & -\rho \\ & & & & & -\rho & 1 \end{pmatrix}_{(T-1) \times (T-1)}.$$

Hence, $H_1^+ = (\rho, \rho^2, \dots, \rho^{T-1}) H_{(2:T), (2:T)}^{-1} = (\rho, 0, 0, \dots, 0, 0)_{1 \times (T-1)}$ and

$$H_1^* = H_{1,1} - H_1^+ H_{(2:T),1} = 1 - (\rho, 0, \dots, 0)_{1 \times (T-1)} \begin{pmatrix} \rho \\ \rho^2 \\ \vdots \\ \rho^{T-1} \end{pmatrix}_{(T-1) \times 1} = 1 - \rho^2.$$

Similarly, $H_T^+ = (\rho^{T-1}, \rho^{T-2}, \dots, \rho) H_{(1:(T-1)), (1:(T-1))}^{-1} = (0, 0, \dots, 0, 0, \rho)_{1 \times (T-1)}$ and

$$H_T^* = H_{T,T} - H_T^+ H_{(1:(T-1)),T} = 1 - (0, \dots, 0, \rho)_{1 \times (T-1)} \begin{pmatrix} \rho^{T-1} \\ \rho^{T-2} \\ \vdots \\ \rho \end{pmatrix}_{(T-1) \times 1} = 1 - \rho^2.$$

(b) **For** $t \in \{2, 3, \dots, T-1\}$

$H_t^* = \frac{1-\rho^2}{1+\rho^2}$ and H_t^+ is the vector of length $(T-1)$ whose $(t-1)^{\text{th}}$, t^{th} positions are $\frac{\rho}{1+\rho^2}$ and all other positions are 0, i.e., $H_t^+ = \left(0, \dots, 0, \frac{\rho}{1+\rho^2}, \frac{\rho}{1+\rho^2}, 0, \dots, 0\right)_{1 \times (T-1)}$.

Proof.

For any arbitrary $t \in (2, 3, \dots, T-1)$,

$$H_{-t, -t} = \begin{matrix} & & & & \mathbf{t-1} & \mathbf{t} & & \\ & & & & & & & \\ & & & & & & & \\ & & & & & & & \\ & & & & & & & \\ \mathbf{t-1} & & & & & & & \\ \mathbf{t} & & & & & & & \end{matrix} \begin{pmatrix} 1 & \rho & \rho^2 & \dots & \rho^{t-2} & \rho^t & \dots & \rho^{T-1} \\ \rho & 1 & \rho & \dots & \rho^{t-3} & \rho^{t-1} & \dots & \rho^{T-2} \\ \rho^2 & \rho & 1 & \dots & \rho^{t-4} & \rho^{t-2} & \dots & \rho^{T-3} \\ \vdots & \vdots & \vdots & \ddots & \vdots & \vdots & & \vdots \\ \rho^{t-2} & \rho^{t-3} & \rho^{t-4} & \dots & 1 & \rho^2 & \dots & \rho^{T-t+1} \\ \rho^t & \rho^{t-1} & \rho^{t-2} & \dots & \rho^2 & 1 & \dots & \rho^{T-t-1} \\ \vdots & \vdots & \vdots & & \vdots & \vdots & \ddots & \vdots \\ \rho^{T-1} & \rho^{T-2} & \rho^{T-3} & \dots & \rho^{T-t+1} & \rho^{T-t-1} & \dots & 1 \end{pmatrix}_{(T-1) \times (T-1)}.$$

$$\text{Let } L_{-t} = \begin{matrix} & & & & \mathbf{t-1} & \mathbf{t} \\ \mathbf{t-1} & \begin{pmatrix} 1 & 0 & 0 & \dots & 0 & 0 & \dots & 0 \\ \rho & 1 & 0 & \dots & 0 & 0 & \dots & 0 \\ \rho^2 & \rho & 1 & \dots & 0 & 0 & \dots & 0 \\ \vdots & \vdots & \vdots & \ddots & \vdots & \vdots & & \vdots \\ \rho^{t-2} & \rho^{t-3} & \rho^{t-4} & \dots & 1 & 0 & \dots & 0 \\ \rho^t & \rho^{t-1} & \rho^{t-2} & \dots & \rho^2 & 1 & \dots & 0 \\ \vdots & \vdots & \vdots & & \vdots & \vdots & \ddots & \vdots \\ \rho^{T-1} & \rho^{T-2} & \rho^{T-3} & \dots & \rho^{T-t+1} & \rho^{T-t-1} & \dots & 1 \end{pmatrix} \\ \mathbf{t} & \end{matrix} \quad (T-1) \times (T-1)$$

$$\text{and } D_{-t} = \begin{matrix} & & & & \mathbf{t-1} & \mathbf{t} & \mathbf{t+1} \\ \mathbf{t-1} & \begin{pmatrix} 1 & 0 & 0 & \dots & 0 & 0 & 0 & \dots & 0 \\ 0 & 1-\rho^2 & 0 & \dots & 0 & 0 & 0 & \dots & 0 \\ 0 & 0 & 1-\rho^2 & \dots & 0 & 0 & 0 & \dots & 0 \\ \vdots & \vdots & \vdots & \ddots & \vdots & \vdots & \vdots & & \vdots \\ 0 & 0 & 0 & \dots & 1-\rho^2 & 0 & 0 & \dots & 0 \\ \mathbf{t} & 0 & 0 & 0 & \dots & 0 & 1-\rho^4 & 0 & \dots & 0 \\ \mathbf{t+1} & 0 & 0 & 0 & \dots & 0 & 0 & 1-\rho^2 & \dots & 0 \\ \vdots & \vdots & \vdots & & \vdots & \vdots & \vdots & \ddots & \vdots \\ 0 & 0 & 0 & \dots & 0 & 0 & 0 & \dots & 1-\rho^2 \end{pmatrix} \\ \end{matrix} \quad (T-1) \times (T-1)$$

Then $H_{-t,-t} = L_{-t} D_{-t} L_{-t}^T$. Note that

$$L_{-t}^{-1} = \begin{matrix} & & \mathbf{t-2} & \mathbf{t-1} & \mathbf{t} \\ \mathbf{t-1} & \begin{pmatrix} 1 & & & & \\ -\rho & 1 & & & \\ & -\rho & \ddots & & \\ & & \ddots & 1 & \\ & & & -\rho & 1 \\ \mathbf{t} & & & & -\rho^2 & 1 \\ & & & & & -\rho & \ddots \\ \mathbf{t+1} & & & & & & \ddots & 1 \\ & & & & & & & -\rho & 1 \end{pmatrix} \\ \end{matrix} \quad (T-1) \times (T-1)$$

Hence, the $(T-1) \times (T-1)$ matrix $H_{-t,-t}^{-1} = (L_{-t}^{-1})^T D_{-t}^{-1} L_{-t}^{-1}$

$$= \begin{matrix} & & & & t-2 & t-1 & t & t+1 \\ \begin{matrix} t-2 \\ t-1 \\ t \\ t+1 \end{matrix} & \begin{pmatrix} \frac{1}{1-\rho^2} & \frac{-\rho}{1-\rho^2} & & & & & & \\ \frac{-\rho}{1-\rho^2} & \frac{1+\rho^2}{1-\rho^2} & \frac{-\rho}{1-\rho^2} & & & & & \\ & \frac{-\rho}{1-\rho^2} & \frac{1+\rho^2}{1-\rho^2} & \ddots & & & & \\ & & \frac{-\rho}{1-\rho^2} & \ddots & \frac{-\rho}{1-\rho^2} & & & \\ & & & \ddots & \frac{1+\rho^2}{1-\rho^2} & \frac{-\rho}{1-\rho^2} & & \\ & & & & \frac{-\rho}{1-\rho^2} & + & \frac{-\rho^2}{1-\rho^4} & \\ & & & & & \frac{-\rho^2}{1-\rho^4} & * & \frac{-\rho}{1-\rho^2} \\ & & & & & & \frac{-\rho}{1-\rho^2} & \frac{1+\rho^2}{1-\rho^2} & \ddots \\ & & & & & & & \frac{-\rho}{1-\rho^2} & \ddots & \frac{-\rho}{1-\rho^2} \\ & & & & & & & & \ddots & \frac{1+\rho^2}{1-\rho^2} & \frac{-\rho}{1-\rho^2} \\ & & & & & & & & & \frac{-\rho}{1-\rho^2} & \frac{1}{1-\rho^2} \end{pmatrix} \end{matrix},$$

$$\text{where } + = \begin{cases} (1, -\rho^2) \begin{pmatrix} 1 & 0 \\ 0 & \frac{1}{1-\rho^4} \end{pmatrix} \begin{pmatrix} 1 \\ -\rho^2 \end{pmatrix} = 1 + \frac{\rho^4}{1-\rho^4} = \frac{1}{1-\rho^4}, & \text{if } t = 2 \\ (1, -\rho^2) \begin{pmatrix} \frac{1}{1-\rho^2} & 0 \\ 0 & \frac{1}{1-\rho^4} \end{pmatrix} \begin{pmatrix} 1 \\ -\rho^2 \end{pmatrix} = \frac{1}{1-\rho^2} + \frac{\rho^4}{1-\rho^4} = \frac{1+\rho^2+\rho^4}{1-\rho^4}, & \text{if } t \in \{3, \dots, T-1\} \end{cases},$$

$$\text{and } * = \begin{cases} (1, -\rho) \begin{pmatrix} \frac{1}{1-\rho^4} & 0 \\ 0 & \frac{1}{1-\rho^2} \end{pmatrix} \begin{pmatrix} 1 \\ -\rho \end{pmatrix} = \frac{1}{1-\rho^4} + \frac{\rho^2}{1-\rho^2} = \frac{1+\rho^2+\rho^4}{1-\rho^4}, & \text{if } t \in \{2, \dots, T-2\} \\ 1 \cdot \frac{1}{1-\rho^4} \cdot 1 = \frac{1}{1-\rho^4}, & \text{if } t = T-1 \end{cases}.$$

Since for $t \in \{2, 3, \dots, T-1\}$, $H_{t, (1:T)_{-t}} = \left(\rho^{t-1}, \dots, \rho^2, \overset{t-1}{\rho}, \overset{t}{\rho}, \rho^2, \dots, \rho^{T-t} \right)_{1 \times (T-1)}$,

we have $H_t^+ = H_{t, (1:T)-t} H_{(1:T)-t, (1:T)-t}^{-1} = \left(0, \dots, 0, \frac{\frac{t-1}{\rho}}{1+\rho^2}, \frac{\frac{t}{\rho}}{1+\rho^2}, 0, \dots, 0 \right)_{1 \times (T-1)}$ and

$$H_t^* = H_{t,t} - H_t^+ H_{(1:T)_{-t},t} = 1 - 2 * \frac{\rho^2}{1 + \rho^2} = \frac{1 - \rho^2}{1 + \rho^2}.$$

Notes: $\forall t \in \{2, 3, \dots, T-1\}, H_t^+[t] = H_t^+[t-1] = \frac{\rho}{1+\rho^2}$ since

- $$\begin{aligned}
\bullet \quad & H_{T-1}^+[T-1] = (\rho, \rho) \cdot \left(\frac{-\rho^2}{1-\rho^4}, \frac{1}{1-\rho^4} \right) = \rho \cdot \frac{1-\rho^2}{1-\rho^4} = \frac{\rho}{1+\rho^2} \text{ for } t = T-1 \text{ and} \\
& H_t^+[t] = (\rho, \rho, \rho^2) \cdot \left(\frac{-\rho^2}{1-\rho^4}, \frac{1}{1-\rho^4} + \frac{\rho^2}{1-\rho^2}, \frac{-\rho^2}{1-\rho^2} \right) = \rho \times \left(\frac{-\rho^2+1}{1-\rho^4} \right) + (\rho, \rho^2) \cdot \left(\frac{\rho^2}{1-\rho^2}, \frac{-\rho^2}{1-\rho^2} \right) = \\
& \frac{\rho}{1+\rho^2} \quad \forall t \in \{2, \dots, T-2\}; \\
\bullet \quad & H_2^+[2-1] = (\rho, \rho) \cdot \left(\frac{1}{1-\rho^4}, \frac{-\rho^2}{1-\rho^4} \right) = \rho \cdot \left(\frac{1-\rho^2}{1-\rho^4} \right) = \frac{\rho}{1+\rho^2} \text{ for } t = 2 \text{ and} \\
& H_t^+[t-1] = (\rho^2, \rho, \rho) \cdot \left(\frac{-\rho^2}{1-\rho^2}, \frac{1}{1-\rho^2} + \frac{\rho^4}{1-\rho^4}, \frac{-\rho^2}{1-\rho^4} \right) = \rho \times \left(\frac{-\rho^2+1}{1-\rho^2} + \frac{\rho^2(\rho^2-1)}{1-\rho^4} \right) = \rho \times \left(1 - \frac{\rho^2}{1+\rho^2} \right) = \\
& \frac{\rho}{1+\rho^2} \quad \forall t \in \{3, \dots, T-1\}.
\end{aligned}$$

B.4.2 When temporal.structure = ‘sar1’ or ‘sexponential’

We have

$$H_t^+ = \begin{cases} \left(0, \dots, 0, \frac{t+d-1}{\rho}, 0, \dots, 0\right), & \text{if } t \in \{1, 2, \dots, d\} \\ \left(0, \dots, 0, \frac{\rho}{1+\rho^2}, 0, \dots, 0, \frac{t+d-1}{1+\rho^2}, 0, \dots, 0\right), & \text{if } t \in \{d+1, d+2, \dots, T-d\} \\ \left(0, \dots, 0, \frac{t-d}{\rho}, 0, \dots, 0\right), & \text{if } t \in \{T-d+1, \dots, T-1, T\} \end{cases} \quad (\text{B.1})$$

\Rightarrow

$$H_t^* = \begin{cases} 1 - \rho^2, & \text{if } t \in \{1, 2, \dots, d, T-d+1, \dots, T-1, T\} \\ 1 - 2 \cdot \rho \cdot \frac{\rho}{1+\rho^2} = \frac{1-\rho^2}{1+\rho^2}, & \text{if } t \in \{d+1, d+2, \dots, T-d\} \end{cases} \quad (\text{B.2})$$

since the t^{th} position in the t^{th} column of $H_{T \times T}$ is 1 and thus

- The $(t+d-1)^{\text{th}}$ position in the $(T-1) \times 1$ vector $H_{(1:T)_{-t},t}$ is ρ for $t \in \{1, 2, \dots, d\}$;
- The $(t-d)^{\text{th}}$ and $(t+d-1)^{\text{th}}$ positions in the $(T-1) \times 1$ vector $H_{(1:T)_{-t},t}$ are both ρ for $t \in \{d+1, d+2, \dots, T-d\}$;
- The $(t-d)^{\text{th}}$ position in the $(T-1) \times 1$ vector $H_{(1:T)_{-t},t}$ is ρ for $t \in \{T-d+1, \dots, T-1, T\}$.

We leave the proof of Equation (B.1) to Appendix B.5.

B.4.3 Attained Acceleration Outcomes Pertaining to Sampling η_t 's

As shown by Appendices B.4.1 and B.4.2, we have simple sparse closed-form representations for the T vectors $H_t^+ = H_{t,-t}H_{-t,-t}^{-1}$ of length $T-1$ and repetitive closed-form solutions for the T scalars $H_t^* = H_{t,t} - H_t^+H_{-t,t} = H_{t,t} - H_{t,-t}H_{-t,-t}^{-1}H_{-t,t}$, $t \in \{1, \dots, T\}$. Hence, in each MCMC iteration,

1. We take $d = 1$ when there is no temporal seasonality. Then

$$H_t^* = \begin{cases} 1 - \rho^2 & \forall t \in \{1, 2, \dots, d, T-d+1, \dots, T-1, T\} \\ \frac{1-\rho^2}{1+\rho^2} & \forall t \in \{d+1, d+2, \dots, T-d\} \end{cases} \quad \text{and thus} \\ \mathbb{C}_{0\eta_t} = H_t^* \otimes \Upsilon_{k \times k} = \begin{cases} (1 - \rho^2) \cdot \Upsilon & \forall t \in \{1, 2, \dots, d, T-d+1, \dots, T-1, T\} \\ \frac{1-\rho^2}{1+\rho^2} \cdot \Upsilon & \forall t \in \{d+1, d+2, \dots, T-d\} \end{cases}.$$

Hence, the values of these quantities can be directly specified rather than calculated. Furthermore, we can opt to first specify $H_t^* = \frac{1-\rho^2}{1+\rho^2}$ and $\mathbb{C}_{0\eta_t} = \frac{1-\rho^2}{1+\rho^2} \cdot \Upsilon \forall t \in \{1, \dots, T\}$ outside of the loop over t and then only modify these two values inside the loop over t for $t \in \{1, 2, \dots, d, T-d+1, \dots, T-1, T\}$.

2. For each $t \in \{1, \dots, T\}$ inside the loop over t , we can specify H_t^+ by modifying one or two entries on the zero vector of length $T-1$ instead of calculating H_t^+ from $H_{(1:T)_{-t},(1:T)_{-t}}^{-1}$.
3. We no longer need to compute and store $H(\psi)_{T \times T}$ itself, since $H(\psi)$ is only used when sampling η_t 's in the entire Gibbs sampler, where we extract out its sub-matrices $H_{-t,-t}$'s, $H_{t,-t}$'s $H_{-t,t}$'s, $H_{t,t}$'s to calculate H_t^+ 's and H_t^* 's.

B.5 Proof of Equation (B.1)

Let $k = \lfloor \frac{T-1}{d} \rfloor$, where $d \in \mathbb{N}$, $d > 1$ is the temporal season period.

(a) **For** $t \in \{1, T\}$

As deduced in Appendix B.3.2, for $t \in \{1, T\}$, the $(T-1) \times (T-1)$ matrix $H_{-t,-t}^{-1} = \frac{1}{1-\rho^2} \times$

$$\begin{matrix} & \begin{matrix} 1 & & d & d+1 & d+2 & & & & T-1 \end{matrix} \\ \begin{matrix} 1 \\ \\ d \\ d+1 \\ d+2 \\ \\ \\ \\ T-1 \end{matrix} & \left(\begin{array}{cccccccccc} 1 & & & & & & & & & \\ & 1 & & & & & & & & \\ & & \ddots & & & & & & & \\ & & & 1 & & & & & & \\ -\rho & & & & 1+\rho^2 & & & & & \\ & -\rho & & & & 1+\rho^2 & & & & \\ & & \ddots & & & & \ddots & & & \\ & & & -\rho & & & & \ddots & & \\ & & & & -\rho & & & & 1+\rho^2 & \\ & & & & & -\rho & & & & 1 \\ & & & & & & \ddots & & & \\ & & & & & & & \ddots & & \\ & & & & & & & & -\rho & \\ & & & & & & & & & 1 \end{array} \right) \end{matrix} \cdot$$

$(T-1) - d \quad T - d$
 $(T-1) - d \quad T - d$
 $T - 1$

$$\begin{aligned} \text{Hence, } H_1^+ &= \left(0, \dots, 0, \rho^1, 0, \dots, 0, \rho^2, 0, \dots, 0, \rho^k, 0, \dots, 0 \right)_{1 \times (T-1)} H_{(2:T), (2:T)}^{-1} \\ &= \left(0, \dots, 0, \rho^d, 0, \dots, 0 \right)_{1 \times (T-1)}. \text{ Similarly,} \\ H_T^+ &= \left(0, \dots, 0, \rho^{T-k \cdot d}, 0, \dots, 0, \rho^{T-2 \cdot d}, 0, \dots, 0, \rho^{T-d}, 0, \dots, 0 \right)_{1 \times (T-1)} H_{(1:(T-1)), (1:(T-1))}^{-1} \\ &= \left(0, \dots, 0, \rho^{T-d}, 0, \dots, 0 \right)_{1 \times (T-1)}. \end{aligned}$$

(b) **For** $t \in \{2, \dots, T-1\}$

Denote L_{-t} as the $(T-1) \times (T-1)$ matrix whose upper-triangular entries are all 0 and lower-triangular (including the main diagonal) entries all equal their counterparts in $H_{-t,-t}$.

(i) **If** $t \in \{2, \dots, d\}$,

then each one of the d sets $\{1, d, 2d, \dots\}$, $\{2, d+1, 2d+1, \dots\}$, \dots , $\{t-1, t+d-2, t+2d-2, \dots\}$, $\{t, t+d, t+2d, \dots\}$, $\{t+1, t+1+d, t+1+2d, \dots\}$, \dots , $\{d-1, 2d-1, 3d-1, \dots\}$ and $\{t+d-1, t+2d-1, t+3d-1, \dots\}$ contains time points **in** $H_{-t,-t}$ (**after deducting the original t^{th} time point**) with a same temporal season period component.

Hence, $L_{-t}^{-1} =$

$$\begin{aligned}
&= \left(0, \dots, 0, \overset{t+d-1}{\rho^1}, 0, \dots, 0, \overset{t+2 \cdot d-1}{\rho^2}, 0, \dots, 0, \overset{t+3 \cdot d-1}{\rho^3}, \dots \right) H_{(1:T)-t, (1:T)-t}^{-1} \\
&= \left(0, \dots, 0, \overset{t+d-1}{\rho}, 0, \dots, 0 \right)_{1 \times (T-1)}.
\end{aligned}$$

(ii) **If** $t \in \{T - d + 1, \dots, T - 1\}$,

then each one of the d sets $\{T-1, T-d, T-2d, \dots\}$, $\{T-2, T-d-1, T-2d-1, \dots\}$, \dots , $\{t, t-d+1, t-2d+1, \dots\}$, $\{t-1, t-1-d, t-1-2d, \dots\}$, $\{t-2, t-2-d, t-2-2d, \dots\}$, \dots , $\{T-d+1, T-2d+1, T-3d+1, \dots\}$ and $\{t-d, t-2d, t-3d, \dots\}$ contains time points, which include exactly one from $\{1, 2, \dots, d\}$, **in $H_{-t, -t}$ (after deducting the original t^{th} time point)** with a same temporal season period component.

Hence, $L_{-t}^{-1} =$

[illegible]

Let D_{-t} be the $(T-1) \times (T-1)$ diagonal matrix

$$\text{Diag} \left(1, 1, \dots, \overset{d}{1}, \overset{d+1}{1 - \rho^2}, 1 - \rho^2, \dots, 1 - \rho^2 \right).$$

Then $H_{-t,-t} = L_{-t}D_{-t}L_{-t}^T$ and hence $H_{-t,-t}^{-1} = (L_{-t}^T)^{-1}D_{-t}^{-1}L_{-t}^{-1} = \frac{1}{1-\rho^2} \times$

[illegible]

$$\begin{aligned} \text{Hence, } H_t^+ &= [H_{t,(1:T)-t}]_{1 \times (T-1)} H_{(1:T)-t, (1:T)-t}^{-1} \\ &= \begin{pmatrix} & t-3 \cdot d & & t-2 \cdot d & & t-d \\ \dots, & \rho^3 & , 0, \dots, 0, & \rho^2 & , 0, \dots, 0, & \rho^1 & , 0, \dots, 0 \end{pmatrix} H_{(1:T)-t, (1:T)-t}^{-1} \\ &= \begin{pmatrix} 0, \dots, 0, & t-d & , 0, \dots, 0 \end{pmatrix}_{1 \times (T-1)}. \end{aligned}$$

(iii) **If** $t \in \{d + 1, \dots, T - d\}$,

then each one of the d sets $\{\dots, t-2d-1, t-d-1, t-1, t+d-2, t+2d-2, \dots\}$, $\{\dots, t-2d, t-d, t+d-1, t+2d-1, \dots\}$, $\{\dots, t-2d+1, t-d+1, t, t+d, t+2d, \dots\}$, $\{\dots, t-2d+2, t-d+2, t+1, t+d+1, t+2d+1, \dots\}$, \dots , $\{\dots, t-2, t+d-3, t+2d-3, \dots\}$ contains time points, which include exactly one from $\{1, 2, \dots, d\}$, **in $H_{-t, -t}$ (after deducting the original t^{th} time point)** with a same temporal season period component.

Hence, $L_{-t}^{-1} =$

and

$$* = \begin{cases} \frac{1^2}{1-\rho^4} + \frac{(-\rho)^2}{1-\rho^2} = \frac{\rho^4+\rho^2+1}{1-\rho^4}, & \text{if } t+d-1 < T-d \iff t \in \{d+1, d+2, \dots, T-2d\} \\ \frac{1^2}{1-\rho^4} = \frac{1}{1-\rho^4}, & \text{if } t+d-1 \geq T-d \iff t \in \{T-2d+1, T-2d+2, \dots, T-d\} \end{cases}. \quad (\text{B.4})$$

$$\begin{aligned} \text{Hence, } H_t^+ &= [H_{t,(1:T)-t}]_{1 \times (T-1)} H_{(1:T)-t, (1:T)-t}^{-1} \\ &= \begin{pmatrix} & t-2d & & t-d & & t+d-1 & & t+2d-1 \\ \dots, & \rho^2 & \dots, 0, & \rho^1 & \dots, 0, & \rho^1 & \dots, & \rho^2 & \dots \end{pmatrix} H_{(1:T)-t, (1:T)-t}^{-1} \\ &= \begin{pmatrix} 0, \dots, 0, \frac{t-d}{1+\rho^2}, 0, \dots, 0, \frac{t+d-1}{1+\rho^2}, 0, \dots, 0 \end{pmatrix} \forall t \in \{d+1, d+2, \dots, T-d\}. \end{aligned}$$

□

Notes: $\forall t \in \{d+1, d+2, \dots, T-d\}$,

- The $(t-d)^{\text{th}}$ entry in the length- $(T-1)$ vector H_t^+ is (by Equation (B.3))

$$\begin{aligned} &\rho \times \left(+ - \frac{\rho^2}{1-\rho^4} \right) + \mathbb{1}_{\{t>2d\}} \times \rho^2 \times \left(- \frac{\rho}{1-\rho^2} \right) \\ &= \begin{cases} \rho \times \left(\frac{\rho^4+\rho^2+1}{1-\rho^4} - \frac{\rho^2}{1-\rho^4} \right) + \rho^2 \times \left(- \frac{\rho}{1-\rho^2} \right) = \rho \times \left(\frac{\rho^4+1}{1-\rho^4} - \frac{\rho^2}{1-\rho^2} \right) = \rho \times \frac{\rho^4+1-\rho^2(1+\rho^2)}{1-\rho^4} \\ \rho \times \frac{1-\rho^2}{1-\rho^4} = \frac{\rho}{1+\rho^2}, & \text{if } t > 2d \iff t \in \{2d+1, \dots, T-d\} \\ \rho \times \left(\frac{1}{1-\rho^4} - \frac{\rho^2}{1-\rho^4} \right) = \rho \times \frac{1}{1+\rho^2} = \frac{\rho}{1+\rho^2}, & \text{if } t \leq 2d \iff t \in \{d+1, \dots, 2d\} \end{cases} \\ &= \frac{\rho}{1+\rho^2} \forall t \in \{d+1, d+2, \dots, T-d\}. \end{aligned}$$

- Similarly, $(t+d-1)^{\text{th}}$ entry in the length- $(T-1)$ vector H_t^+ is (by Equation (B.4))

$$\begin{aligned} &\rho \times \left(* - \frac{\rho^2}{1-\rho^4} \right) + \mathbb{1}_{\{t \leq T-2d\}} \times \rho^2 \times \left(- \frac{\rho}{1-\rho^2} \right) \\ &= \begin{cases} \rho \times \left(\frac{\rho^4+\rho^2+1}{1-\rho^4} - \frac{\rho^2}{1-\rho^4} \right) + \rho^2 \times \left(- \frac{\rho}{1-\rho^2} \right) = \rho \times \left(\frac{\rho^4+1}{1-\rho^4} - \frac{\rho^2}{1-\rho^2} \right) = \rho \times \frac{\rho^4+1-\rho^2(1+\rho^2)}{1-\rho^4} \\ \rho \times \frac{1-\rho^2}{1-\rho^4} = \frac{\rho}{1+\rho^2}, & \text{if } t \leq T-2d \iff t \in \{d+1, \dots, T-2d\} \\ \rho \times \left(\frac{1}{1-\rho^4} - \frac{\rho^2}{1-\rho^4} \right) = \rho \times \frac{1}{1+\rho^2} = \frac{\rho}{1+\rho^2}, & \text{if } t > T-2d \iff t \in \{T-2d+1, \dots, T-d\} \end{cases} \\ &= \frac{\rho}{1+\rho^2} \forall t \in \{d+1, d+2, \dots, T-d\}. \end{aligned}$$

- The $\{(t-d), (t-d)\}^{\text{th}}$ entry in $H_{-t,-t} [H_{-t,-t}]^{-1} = 1$ because

– if $t > 2d$, then this entry equals

$$\begin{aligned} &(\rho, 1, \rho^2) \left(-\frac{\rho}{1-\rho^2}, \frac{1}{1-\rho^2} + \frac{\rho^4}{1-\rho^4}, -\frac{\rho^2}{1-\rho^4} \right)^T \\ &= \frac{1}{1-\rho^2} [\rho \cdot (-\rho) + 1 \cdot 1] + \frac{1}{1-\rho^4} [1 \cdot \rho^4 + \rho^2 \cdot (-\rho^2)] = 1 + 0 = 1; \end{aligned}$$

– if $t \leq 2d$, then this entry equals

$$(1, \rho^2) \left(\frac{1}{1-\rho^4}, -\frac{\rho^2}{1-\rho^4} \right)^T = 1.$$

- Similarly, the $\{(t+d-1), (t+d-1)\}^{\text{th}}$ entry in $H_{-t,-t} [H_{-t,-t}]^{-1} = 1$ because

– if $t \leq T - 2d$, then this entry equals

$$\begin{aligned} & (\rho^2, 1, \rho) \left(-\frac{\rho^2}{1-\rho^4}, \frac{1}{1-\rho^4} + \frac{\rho^2}{1-\rho^2}, -\frac{\rho}{1-\rho^2} \right)^T \\ &= \frac{1}{1-\rho^4} [\rho^2 \cdot (-\rho^2) + 1 \cdot 1] + \frac{1}{1-\rho^2} [1 \cdot \rho^2 - \rho \cdot \rho] = 1 + 0 = 1; \end{aligned}$$

– if $t > T - 2d$, then this entry equals

$$(\rho^2, 1) \left(-\frac{\rho^2}{1-\rho^4}, \frac{1}{1-\rho^4} \right)^T = 1.$$

C A VAR(1) Process for the Latent Temporal Factors $\eta_{1:T}$

Throughout this section, we assume evenly dispersed time points corresponding to our observed data. To model the zero-mean $k \times 1$ latent temporal factors η_t , $t \in \{1, 2, \dots, T\}$, we consider a VAR(1) model in reduced form

$$\eta_t = A\eta_{t-1} + \epsilon_t, \quad \epsilon_t \sim N_k(\mathbf{0}, \Upsilon), \quad t = 1, 2, \dots, T, \quad (\text{C.1})$$

where $\Upsilon_{k \times k}$ is positive definite, $A_{k \times k}$ is invertible, and η_0 is assumed to be $\mathbf{0}_{k \times 1}$. Equation (C.1) simplifies to an AR(1) model if we take $A_{k \times k} = \psi I_{k \times k}$ for some $\psi \in (0, 1)$. We assign priors $A \sim \mathcal{MN}_{k,k}(M, \Upsilon, V)$ and $\Upsilon \sim \mathcal{IW}_k(\zeta, \Omega)$ (the Inverse Wishart distribution with degrees of freedom $\zeta > k-1$ and $k \times k$ positive definite scale matrix Ω) to parameters A and Υ respectively. By modifying the original Gibbs sampling steps for temporal-related parameters, we can form integrated spatiotemporal Bayesian Gaussian factor models that permit convenient adequate predictions at any arbitrary future time points.

C.1 New Gibbs Sampling Steps for Temporal-Related Parameters

The temporal-related parameters in our new holistic modeling frameworks are now $\{\eta_{1:T}, \Upsilon, A\}$ instead of $\{\eta_{1:T}, \Upsilon, \psi\}$. We detail the corresponding new Gibbs sampler steps in what ensues.

Sampling From the Full Conditional Distributions of the $k \times 1$ Vectors η_t 's

Fix any arbitrary $t \in \{1, \dots, T-1\}$. Then

$$\begin{aligned} f(\eta_t | \cdot) &\propto f(\mathbf{y}_t | \beta, \Lambda, \eta_t, \Xi) \times f(\eta_{1:T} | A, \Upsilon) \propto f(\mathbf{y}_t | \beta, \Lambda, \eta_t, \Xi) \times f(\eta_t | \eta_{t-1}, A, \Upsilon) \times f(\eta_{t+1} | \eta_t, A, \Upsilon) \\ &\propto \exp \left\{ -\frac{1}{2} (\mathbf{y}_t - X_t \beta - \Lambda \eta_t)^T \Xi^{-1} (\mathbf{y}_t - X_t \beta - \Lambda \eta_t) \right\} \times \\ &\quad \exp \left\{ -\frac{1}{2} (\eta_t - A \eta_{t-1})^T \Upsilon^{-1} (\eta_t - A \eta_{t-1}) \right\} \times \exp \left\{ -\frac{1}{2} (\eta_{t+1} - A \eta_t)^T \Upsilon^{-1} (\eta_{t+1} - A \eta_t) \right\} \\ &\propto \exp \left\{ -\frac{1}{2} [\eta_t^T V_{\eta_t}^{-1} \eta_t - 2 \cdot \eta_t^T (\Lambda^T \Xi^{-1} (\mathbf{y}_t - X_t \beta) + \Upsilon^{-1} A \eta_{t-1} + A^T \Upsilon^{-1} \eta_{t+1})] \right\} \\ &\Rightarrow \eta_t | \cdot \sim N_k(V_{\eta_t} [\Lambda^T \Xi^{-1} (\mathbf{y}_t - X_t \beta) + \Upsilon^{-1} A \eta_{t-1} + A^T \Upsilon^{-1} \eta_{t+1}], V_{\eta_t}), \\ &\quad \text{where } V_{\eta_t} = [\Lambda^T \Xi^{-1} \Lambda + \Upsilon^{-1} + A^T \Upsilon^{-1} A]^{-1}. \end{aligned} \quad (\text{C.2})$$

For $t = T$,

$$\begin{aligned}
f(\boldsymbol{\eta}_T|\cdot) &\propto f(\mathbf{y}_T|\boldsymbol{\beta}, \Lambda, \boldsymbol{\eta}_T, \Xi) \times f(\boldsymbol{\eta}_{1:T}|A, \Upsilon) \propto f(\mathbf{y}_T|\boldsymbol{\beta}, \Lambda, \boldsymbol{\eta}_T, \Xi) \times f(\boldsymbol{\eta}_T|\boldsymbol{\eta}_{T-1}, A, \Upsilon) \\
&\propto \exp\left\{-\frac{1}{2}(\mathbf{y}_T - X_T\boldsymbol{\beta} - \Lambda\boldsymbol{\eta}_T)^\top \Xi^{-1}(\mathbf{y}_T - X_T\boldsymbol{\beta} - \Lambda\boldsymbol{\eta}_T)\right\} \times \\
&\quad \exp\left\{-\frac{1}{2}(\boldsymbol{\eta}_T - A\boldsymbol{\eta}_{T-1})^\top \Upsilon^{-1}(\boldsymbol{\eta}_T - A\boldsymbol{\eta}_{T-1})\right\} \\
&\propto \exp\left\{-\frac{1}{2}[\boldsymbol{\eta}_T^\top (\Lambda^\top \Xi^{-1}\Lambda + \Upsilon^{-1})\boldsymbol{\eta}_T - 2 \cdot \boldsymbol{\eta}_T^\top (\Lambda^\top \Xi^{-1}(\mathbf{y}_T - X_T\boldsymbol{\beta}) + \Upsilon^{-1}A\boldsymbol{\eta}_{T-1})]\right\} \\
&\Rightarrow \boldsymbol{\eta}_T | \cdot \sim N_k\left([\Lambda^\top \Xi^{-1}\Lambda + \Upsilon^{-1}]^{-1}[\Lambda^\top \Xi^{-1}(\mathbf{y}_T - X_T\boldsymbol{\beta}) + \Upsilon^{-1}A\boldsymbol{\eta}_{T-1}], [\Lambda^\top \Xi^{-1}\Lambda + \Upsilon^{-1}]^{-1}\right).
\end{aligned} \tag{C.3}$$

Sampling From the Full Conditional Distribution of the Positive Definite Matrix

$$\Upsilon_{k \times k}$$

$$\begin{aligned}
f(\Upsilon|\cdot) &\propto f(\boldsymbol{\eta}_{1:T}|A, \Upsilon, \boldsymbol{\eta}_0 = \mathbf{0}_{k \times 1}) \times f_0(\Upsilon), \text{ where } f_0 = \mathcal{IW}_k(\zeta, \Omega) \\
&\propto |\Upsilon|^{-\frac{T}{2}} \prod_{t=1}^T \exp\left\{-\frac{1}{2}(\boldsymbol{\eta}_t - A\boldsymbol{\eta}_{t-1})^\top \Upsilon^{-1}(\boldsymbol{\eta}_t - A\boldsymbol{\eta}_{t-1})\right\} \times |\Upsilon|^{-\frac{\zeta+k+1}{2}} \exp\left\{-\frac{1}{2}\text{tr}(\Omega\Upsilon^{-1})\right\} \\
&= |\Upsilon|^{-\frac{T+\zeta+k+1}{2}} \exp\left\{-\frac{1}{2}\sum_{t=1}^T \text{tr}((\boldsymbol{\eta}_t - A\boldsymbol{\eta}_{t-1})^\top \Upsilon^{-1}(\boldsymbol{\eta}_t - A\boldsymbol{\eta}_{t-1}))\right\} \cdot \exp\left\{-\frac{1}{2}\text{tr}(\Omega\Upsilon^{-1})\right\} \\
&= |\Upsilon|^{-\frac{T+\zeta+k+1}{2}} \exp\left\{-\frac{1}{2}\left[\sum_{t=1}^T \text{tr}((\boldsymbol{\eta}_t - A\boldsymbol{\eta}_{t-1})(\boldsymbol{\eta}_t - A\boldsymbol{\eta}_{t-1})^\top \Upsilon^{-1}) + \text{tr}(\Omega\Upsilon^{-1})\right]\right\} \\
&= |\Upsilon|^{-\frac{T+\zeta+k+1}{2}} \exp\left\{-\frac{1}{2}\text{tr}\left(\left[\sum_{t=1}^T (\boldsymbol{\eta}_t - A\boldsymbol{\eta}_{t-1})(\boldsymbol{\eta}_t - A\boldsymbol{\eta}_{t-1})^\top + \Omega\right]\Upsilon^{-1}\right)\right\} \\
&\Rightarrow \Upsilon | \cdot \sim \mathcal{IW}_k\left(T + \zeta, \sum_{t=1}^T (\boldsymbol{\eta}_t - A\boldsymbol{\eta}_{t-1})(\boldsymbol{\eta}_t - A\boldsymbol{\eta}_{t-1})^\top + \Omega\right).
\end{aligned} \tag{C.4}$$

Sampling From the Full Conditional Distribution of the Invertible Matrix $A_{k \times k}$

Write $A = (\mathbf{a}_1, \mathbf{a}_2, \dots, \mathbf{a}_k)$, where \mathbf{a}_j denotes the j^{th} column of A for $j = 1, 2, \dots, k$, and let $f_0(A) = \mathcal{MN}_{k,k}(M, \Upsilon, V)$, where $\Upsilon_{k \times k}$ and $V_{k \times k}$ are both positive definite scale matrices and $M_{k \times k}$ is a location matrix. Since $A \sim \mathcal{MN}_{k,k}(M, \Upsilon, V) \iff \text{vec}(A) \sim N_{k^2}(\text{vec}(M), V \otimes \Upsilon)$,

$$\begin{aligned}
f(A|\cdot) &\propto f(\boldsymbol{\eta}_{1:T}|A, \Upsilon, \boldsymbol{\eta}_0 = \mathbf{0}_{k \times 1}) \times f_0(A) \\
&\propto \prod_{t=1}^T \exp\left\{-\frac{1}{2}(\boldsymbol{\eta}_t - A\boldsymbol{\eta}_{t-1})^\top \Upsilon^{-1}(\boldsymbol{\eta}_t - A\boldsymbol{\eta}_{t-1})\right\} \times f_0(A) \\
&\propto \exp\left\{-\frac{1}{2}[\text{vec}(A) - \text{vec}(M)]^\top (V^{-1} \otimes \Upsilon^{-1})[\text{vec}(A) - \text{vec}(M)]\right\} \times \\
&\quad \prod_{t=1}^T \exp\left\{-\frac{1}{2}(\eta_{t-1,1}\mathbf{a}_1 + \dots + \eta_{t-1,k}\mathbf{a}_k - \boldsymbol{\eta}_t)^\top \Upsilon^{-1}(\eta_{t-1,1}\mathbf{a}_1 + \dots + \eta_{t-1,k}\mathbf{a}_k - \boldsymbol{\eta}_t)\right\} \\
&= \exp\left\{-\frac{1}{2}[\text{vec}(A) - \text{vec}(M)]^\top (V^{-1} \otimes \Upsilon^{-1})[\text{vec}(A) - \text{vec}(M)]\right\} \times \\
&\quad \prod_{t=1}^T \exp\left[-\frac{1}{2}\text{vec}(A)^\top \{[\boldsymbol{\eta}_{t-1}\boldsymbol{\eta}_{t-1}^\top] \otimes \Upsilon^{-1}\}\text{vec}(A) + \text{vec}(A)^\top (\boldsymbol{\eta}_{t-1} \otimes \Upsilon^{-1})\boldsymbol{\eta}_t\right]
\end{aligned}$$

$$\begin{aligned}
& \propto \exp \left\{ -\frac{1}{2} \text{vec}(A)^T [V_A^{-1} \otimes \Upsilon^{-1}] \text{vec}(A) + \text{vec}(A)^T \left[(V^{-1} \otimes \Upsilon^{-1}) \text{vec}(M) + \sum_{t=1}^T (\boldsymbol{\eta}_{t-1} \otimes \Upsilon^{-1}) \boldsymbol{\eta}_t \right] \right\} \\
& \text{with } V_A = \left(\sum_{t=1}^T [\boldsymbol{\eta}_{t-1} \boldsymbol{\eta}_{t-1}^T] + V^{-1} \right)^{-1} \\
& \Rightarrow \text{vec}(A) \mid \cdot \sim N_{k^2} \left([V_A V^{-1} \otimes I_{k \times k}] \text{vec}(M) + \sum_{t=1}^T [V_A \boldsymbol{\eta}_{t-1} \otimes I_{k \times k}] \boldsymbol{\eta}_t, V_A \otimes \Upsilon \right) \\
& \Longleftrightarrow A \mid \cdot \sim \mathcal{MN}_{k,k} (M_A, \Upsilon, V_A), \tag{C.5}
\end{aligned}$$

where M_A is $k \times k$ with vectorized form $[V_A V^{-1} \otimes I_{k \times k}] \text{vec}(M) + \sum_{t=1}^T [V_A \boldsymbol{\eta}_{t-1} \otimes I_{k \times k}] \boldsymbol{\eta}_t$.

C.2 Predictions at Desired Future Time Points

Suppose we have $q \geq 1$, $q \in \mathbb{N}$ new time points $T+1, \dots, T+q$. Then for predicting $\hat{\mathbf{y}}_{(T+1):(T+q)}$ given $\mathbf{y}_{1:T}$ and covariates matrix $[X_{(T+1):(T+q)}]_{qO_m \times p}$ (if $p \geq 1$) under our integrated frameworks, we can write the posterior predictive distribution (PPD) as

$$\begin{aligned}
& f(\mathbf{y}_{(T+1):(T+q)} | \mathbf{y}_{1:T}, X_{(T+1):(T+q)}) = \int_{\Theta} f(\mathbf{y}_{(T+1):(T+q)} | \Theta, \mathbf{y}_{1:T}, X_{(T+1):(T+q)}) \pi(\Theta | \mathbf{y}_{1:T}) d\Theta, \\
& \text{where } \Theta = \begin{cases} (\Lambda, \beta, \sigma^2, \boldsymbol{\eta}_{(T+1):(T+q)}, \boldsymbol{\eta}, \Upsilon, A), & \text{if clustering} = \text{FALSE} \\ (\boldsymbol{\theta}, \boldsymbol{\xi}, \beta, \sigma^2, \boldsymbol{\eta}_{(T+1):(T+q)}, \boldsymbol{\eta}, \Upsilon, A), & \text{if clustering} = \text{TRUE} \end{cases}. \tag{C.6}
\end{aligned}$$

$\boldsymbol{\eta}$ denotes $\boldsymbol{\eta}_{1:T}$. **clustering** = FALSE refers to the scenario when no spatial clustering mechanism is integrated, and **clustering** = TRUE refers to the case when a spatial PSBP clustering mechanism is incorporated. We can then partition the integral in Equation (C.6) into

$$\begin{aligned}
& \int_{\Theta} \underbrace{f(\mathbf{y}_{(T+1):(T+q)} | \Lambda, \boldsymbol{\eta}_{(T+1):(T+q)}, \beta, \sigma^2, X_{(T+1):(T+q)})}_{T_1} \underbrace{f(\boldsymbol{\eta}_{(T+1):(T+q)} | \boldsymbol{\eta}, \Upsilon, A)}_{T_2} \\
& \quad \times \underbrace{\pi(\Lambda, \beta, \sigma^2, \boldsymbol{\eta}, \Upsilon, A | \mathbf{y}_{1:T})}_{T_3} d\Theta \text{ if clustering} = \text{FALSE, and} \tag{C.7}
\end{aligned}$$

$$\begin{aligned}
& \int_{\Theta} \underbrace{f(\mathbf{y}_{(T+1):(T+q)} | \boldsymbol{\theta}, \boldsymbol{\xi}, \boldsymbol{\eta}_{(T+1):(T+q)}, \beta, \sigma^2, X_{(T+1):(T+q)})}_{T_1} \underbrace{f(\boldsymbol{\eta}_{(T+1):(T+q)} | \boldsymbol{\eta}, \Upsilon, A)}_{T_2} \\
& \quad \times \underbrace{\pi(\boldsymbol{\theta}, \boldsymbol{\xi}, \beta, \sigma^2, \boldsymbol{\eta}, \Upsilon, A | \mathbf{y}_{1:T})}_{T_3} d\Theta \text{ if clustering} = \text{TRUE}. \tag{C.8}
\end{aligned}$$

In Equations (C.7) and (C.8), T_1 is the observed likelihood and T_3 is the parameters' posterior distribution obtained from the original model fit's MCMC sampler. For T_2 ,

$$\begin{aligned}
f(\boldsymbol{\eta}_{(T+1):(T+q)} | \boldsymbol{\eta}_{1:T}, \Upsilon, A) &= \prod_{r=1}^q f(\boldsymbol{\eta}_{T+r} | \boldsymbol{\eta}_{(T+1):(T+r-1)}, \boldsymbol{\eta}_{1:T}, \Upsilon, A) \\
&= \prod_{r=1}^q N_k(\boldsymbol{\eta}_{T+r} | A \boldsymbol{\eta}_{T+r-1}, \Upsilon), \tag{C.9}
\end{aligned}$$

where for each r , $N_k(\boldsymbol{\eta}_{T+r} | A \boldsymbol{\eta}_{T+r-1}, \Upsilon)$ denotes the density of a k -variate normal distribution with mean $A \boldsymbol{\eta}_{T+r-1}$ and covariance matrix Υ evaluated at $\boldsymbol{\eta}_{T+r}$. Hence, we can obtain a

predicted $\hat{\boldsymbol{\eta}}_{(T+1):(T+q)} | \boldsymbol{\eta}_{1:T}, A, \Upsilon$ by first sampling $\hat{\boldsymbol{\eta}}_{T+1}$ from $N_k(A\boldsymbol{\eta}_T, \Upsilon)$ and then sampling $\hat{\boldsymbol{\eta}}_{T+r}$ from $N_k(A\hat{\boldsymbol{\eta}}_{T+r-1}, \Upsilon)$ one by one for $r = 2, 3, \dots, q$.

D Facilitating Efficient Computation for Spatial PSBP

One major computational issue pertaining to our model in Section 2 lies in sampling $\boldsymbol{\alpha}_{jl_j}$'s from their full conditionals $f(\boldsymbol{\alpha}_{jl_j} | \cdot)$'s. We notice that $\{\boldsymbol{\alpha}_{jl_j} : j = 1, \dots, k, l_j = 1, \dots, L-1\}$ affects the fitted response $\hat{\mathbf{y}}$ via $\{\mathbf{w}_{jl_j} : j = 1, \dots, k, l_j = 1, \dots, L\}$, the set of probability parameters for the multinomial distributions of $\xi_j^o(\mathbf{s}_i)$'s, and that

$$\begin{aligned} \forall (i, o, l_j) &\in \{1, \dots, m\} \times \{1, \dots, O\} \times \{1, \dots, L\}, \\ \mathbb{P} \left(\xi_j^o(\mathbf{s}_i) = l_j | \boldsymbol{\alpha}_{jr_j}^o(\mathbf{s}_i), 1 \leq r_j \leq L-1 \right) &= \mathbb{P} \left(\xi_j^o(\mathbf{s}_i) = l_j | \boldsymbol{\alpha}_{jr_j}^o(\mathbf{s}_i), 1 \leq r_j \leq \min\{l_j, L-1\} \right) \\ = w_{jl_j}^o(\mathbf{s}_i) &= \begin{cases} \Phi \left(\boldsymbol{\alpha}_{jl_j}^o(\mathbf{s}_i) \right) \prod_{r_j < l_j} \left[1 - \Phi \left(\boldsymbol{\alpha}_{jr_j}^o(\mathbf{s}_i) \right) \right], & \text{if } l_j \in \{1, \dots, L-1\} \\ \prod_{r_j < L} \left[1 - \Phi \left(\boldsymbol{\alpha}_{jr_j}^o(\mathbf{s}_i) \right) \right], & \text{if } l_j = L \end{cases}. \end{aligned} \quad (\text{D.1})$$

Hence for any arbitrary $(j, l_j) \in \{1, \dots, k\} \times \{1, \dots, L-1\}$, $f(\boldsymbol{\alpha}_{jl_j} | \cdot) \propto f(\boldsymbol{\xi}_j | \boldsymbol{\alpha}_{jr_j}, 1 \leq r_j \leq L-1) \times f_0(\boldsymbol{\alpha}_{jl_j} | \kappa, \rho)$, which is burdensome to sample from due to loss of conjugacy.

This issue can be tackled by adopting ideas put forward by Rodríguez and Dunson (2011). In this context, we introduce a set of latent variables $z_{jl_j}^o(\mathbf{s}_i) \stackrel{\text{ind}}{\sim} N(\boldsymbol{\alpha}_{jl_j}^o(\mathbf{s}_i), 1)$ and define $\xi_j^o(\mathbf{s}_i)$'s values deterministically based on $z_{jl_j}^o(\mathbf{s}_i)$'s as follows:

$$\begin{aligned} \forall (j, i, o) &\in \{1, \dots, k\} \times \{1, \dots, m\} \times \{1, \dots, O\}, \\ \forall l_j \in \{1, \dots, L\}, \xi_j^o(\mathbf{s}_i) = l_j &\iff \begin{cases} z_{jl_j}^o(\mathbf{s}_i) > 0 \text{ and } z_{jr_j}^o(\mathbf{s}_i) < 0 \forall r_j < l_j, & \text{if } l_j < L \\ z_{jr_j}^o(\mathbf{s}_i) < 0 \forall r_j < L, & \text{if } l_j = L \end{cases}. \end{aligned} \quad (\text{D.2})$$

Fix any arbitrary (j, i, o) . With this set of introduced latent variables $\{z_{jl_j}^o(\mathbf{s}_i) : 1 \leq l_j \leq L-1\}$ and value of the clustering label parameter $\xi_j^o(\mathbf{s}_i)$ defined according to Equation (D.2), for any arbitrary $l_j \in \{1, \dots, L\}$,

$$\begin{aligned} \mathbb{P} \left(\xi_j^o(\mathbf{s}_i) = l_j | z_{jr_j}^o(\mathbf{s}_i), \boldsymbol{\alpha}_{jr_j}^o(\mathbf{s}_i), 1 \leq r_j \leq L-1 \right) &= \mathbb{P} \left(\xi_j^o(\mathbf{s}_i) = l_j | z_{jr_j}^o(\mathbf{s}_i), 1 \leq r_j \leq L-1 \right), \\ \text{and the expression } \int \cdots \int \mathbb{P} \left(\xi_j^o(\mathbf{s}_i) = l_j | z_{jr_j}^o(\mathbf{s}_i), \boldsymbol{\alpha}_{jr_j}^o(\mathbf{s}_i), 1 \leq r_j \leq L-1 \right) &\times \\ \mathbb{P} \left(z_{jr_j}^o(\mathbf{s}_i), 1 \leq r_j \leq L-1 | \boldsymbol{\alpha}_{jr_j}^o(\mathbf{s}_i), 1 \leq r_j \leq L-1 \right) dz_{j1}^o(\mathbf{s}_i) \cdots dz_{j(L-1)}^o(\mathbf{s}_i) & \\ = \begin{cases} \mathbb{P} \left(z_{jl_j}^o(\mathbf{s}_i) > 0 \text{ and } z_{jr_j}^o(\mathbf{s}_i) < 0 \forall r_j < l_j | \boldsymbol{\alpha}_{jr_j}^o(\mathbf{s}_i), 1 \leq r_j \leq L-1 \right), & \text{if } l_j < L \\ \mathbb{P} \left(z_{jr_j}^o(\mathbf{s}_i) < 0 \forall r_j < L | \boldsymbol{\alpha}_{jr_j}^o(\mathbf{s}_i), 1 \leq r_j \leq L-1 \right), & \text{if } l_j = L \end{cases} & \\ = \begin{cases} \mathbb{P} \left(z_{jl_j}^o(\mathbf{s}_i) > 0 | \boldsymbol{\alpha}_{jl_j}^o(\mathbf{s}_i) \right) \prod_{r_j=1}^{l_j-1} \mathbb{P} \left(z_{jr_j}^o(\mathbf{s}_i) < 0 | \boldsymbol{\alpha}_{jr_j}^o(\mathbf{s}_i) \right), & \text{if } l_j < L \\ \prod_{r_j=1}^{L-1} \mathbb{P} \left(z_{jr_j}^o(\mathbf{s}_i) < 0 | \boldsymbol{\alpha}_{jr_j}^o(\mathbf{s}_i) \right), & \text{if } l_j = L \end{cases} & \\ = \begin{cases} \Phi \left(\boldsymbol{\alpha}_{jl_j}^o(\mathbf{s}_i) \right) \prod_{r_j < l_j} \left[1 - \Phi \left(\boldsymbol{\alpha}_{jr_j}^o(\mathbf{s}_i) \right) \right], & \text{if } l_j \in \{1, \dots, L-1\} \\ \prod_{r_j < L} \left[1 - \Phi \left(\boldsymbol{\alpha}_{jr_j}^o(\mathbf{s}_i) \right) \right], & \text{if } l_j = L \end{cases} & \end{aligned}$$

does turn out to be the same as $w_{jl_j}^o(\mathbf{s}_i) = \mathbb{P}(\xi_j^o(\mathbf{s}_i) = l_j | \alpha_{jr_j}^o(\mathbf{s}_i), 1 \leq r_j \leq L-1)$, where $\xi_j^o(\mathbf{s}_i)$'s value is obtained probabilistically conditioning on $\alpha_{jr_j}^o(\mathbf{s}_i), 1 \leq r_j \leq L-1$, as in our original model without the introduced latent normal variables $z_{jr_j}^o(\mathbf{s}_i)$'s.

Hence, we can opt to sample $\xi_j^o(\mathbf{s}_i)$'s from their marginal distributions with the latent variables $z_{jl_j}^o(\mathbf{s}_i)$'s integrated out as above. The corresponding Gibbs sampler step for $\xi_j^o(\mathbf{s}_i)$'s is thus unaffected by the introduction of $z_{jl_j}^o(\mathbf{s}_i)$'s:

$$\text{Fix any arbitrary } j \in \{1, \dots, k\}. \quad \forall (o, i) \in \{1, \dots, O\} \times \{1, \dots, m\}, \\ \forall l_j \in \{1, \dots, L\}, \quad \mathbb{P}(\xi_j^o(\mathbf{s}_i) = l_j | \cdot) \quad (\text{D.3})$$

$$\propto \mathbb{P}(\xi_j^o(\mathbf{s}_i) = l_j | \alpha_{jr_j}^o(\mathbf{s}_i), r_j \leq L-1) \prod_{t=1}^T f(y_t^o(\mathbf{s}_i) | \boldsymbol{\beta}, \boldsymbol{\eta}_t, (\sigma^2)^o(\mathbf{s}_i), \xi_j^o(\mathbf{s}_i) = l_j, \boldsymbol{\xi}_{-j}^o(\mathbf{s}_i), \boldsymbol{\theta}_{\xi^o(\mathbf{s}_i)}) \\ \propto w_{jl_j}^o(\mathbf{s}_i) \times \exp \left\{ -\frac{1}{2} (\sigma^{-2})^o(\mathbf{s}_i) \sum_{t=1}^T \left[y_t^o(\mathbf{s}_i) - \mathbf{x}_t^o(\mathbf{s}_i)^\top \boldsymbol{\beta} - \sum_{h \neq j} \theta_{h\xi_h^o(\mathbf{s}_i)} \eta_{th} - \theta_{jl_j} \eta_{tj} \right]^2 \right\}.$$

It is also straightforward to sample from the full conditional distributions of $z_{jl_j}^o(\mathbf{s}_i)$'s:

$$\text{For any arbitrary fixed } (j, i, o, l_j) \in \{1, \dots, k\} \times \{1, \dots, m\} \times \{1, \dots, O\} \times \{1, \dots, L-1\}, \\ f(z_{jl_j}^o(\mathbf{s}_i) | \cdot) \propto f(\xi_j^o(\mathbf{s}_i) | z_{jl_j}^o(\mathbf{s}_i)) \times f(z_{jl_j}^o(\mathbf{s}_i) | \alpha_{jl_j}^o(\mathbf{s}_i)) \quad (\text{D.4}) \\ \sim \mathbb{1}_{\{\xi_j^o(\mathbf{s}_i) > l_j\}} N(\alpha_{jl_j}^o(\mathbf{s}_i), 1)_{\mathbb{R}_-} + \mathbb{1}_{\{\xi_j^o(\mathbf{s}_i) = l_j\}} N(\alpha_{jl_j}^o(\mathbf{s}_i), 1)_{\mathbb{R}_+} + \mathbb{1}_{\{\xi_j^o(\mathbf{s}_i) < l_j\}} N(\alpha_{jl_j}^o(\mathbf{s}_i), 1).$$

The essence of this latent variables introduction approach lies in bringing about conjugacy for $\boldsymbol{\alpha}_{jl_j}$'s. With our introduced $z_{jl_j}^o(\mathbf{s}_i)$'s and $\xi_j^o(\mathbf{s}_i)$'s defined deterministically by Equation (D.2), for any arbitrary fixed $(j, l_j) \in \{1, \dots, k\} \times \{1, \dots, L-1\}$,

$$f(\boldsymbol{\alpha}_{jl_j} | \cdot) \propto f(\boldsymbol{\xi}_j, \mathbf{z}_{jr_j}, 1 \leq r_j \leq L-1 | \boldsymbol{\alpha}_{jr_j}, 1 \leq r_j \leq L-1) \times f_0(\boldsymbol{\alpha}_{jl_j} | \kappa, \rho), \\ \text{where } f(\boldsymbol{\xi}_j, \mathbf{z}_{jr_j}, 1 \leq r_j \leq L-1 | \boldsymbol{\alpha}_{jr_j}, 1 \leq r_j \leq L-1) \\ = f(\boldsymbol{\xi}_j | \mathbf{z}_{jr_j}, \boldsymbol{\alpha}_{jr_j}, 1 \leq r_j \leq L-1) \times f(\mathbf{z}_{jr_j}, 1 \leq r_j \leq L-1 | \boldsymbol{\alpha}_{jr_j}, 1 \leq r_j \leq L-1) \\ = f(\boldsymbol{\xi}_j | \mathbf{z}_{jr_j}, 1 \leq r_j \leq L-1) \times \prod_{(i, o, r_j) \in \{1, \dots, m\} \times \{1, \dots, O\} \times \{1, \dots, L-1\}} f(z_{jr_j}^o(\mathbf{s}_i) | \alpha_{jr_j}^o(\mathbf{s}_i)) \\ = f(\boldsymbol{\xi}_j | \mathbf{z}_{jr_j}, 1 \leq r_j \leq L-1) \times \prod_{1 \leq r_j \leq L-1} f(\mathbf{z}_{jr_j} | \boldsymbol{\alpha}_{jr_j}).$$

$$\text{Hence, } f(\boldsymbol{\alpha}_{jl_j} | \cdot) \propto \prod_{1 \leq r_j \leq L-1} f(\mathbf{z}_{jr_j} | \boldsymbol{\alpha}_{jr_j}) \times f_0(\boldsymbol{\alpha}_{jl_j} | \kappa, \rho) \propto f(\mathbf{z}_{jl_j} | \boldsymbol{\alpha}_{jl_j}) \times f_0(\boldsymbol{\alpha}_{jl_j} | \kappa, \rho) \\ \propto \exp \left\{ (\mathbf{z}_{jl_j} - \boldsymbol{\alpha}_{jl_j})^\top I_{mO} (\mathbf{z}_{jl_j} - \boldsymbol{\alpha}_{jl_j}) + \boldsymbol{\alpha}_{jl_j}^\top [F(\rho)^{-1} \otimes \kappa^{-1}] \boldsymbol{\alpha}_{jl_j} \right\} \\ \propto \exp \left\{ \boldsymbol{\alpha}_{jl_j}^\top [I_{mO} + F(\rho)^{-1} \otimes \kappa^{-1}] \boldsymbol{\alpha}_{jl_j} - 2 \cdot \mathbf{z}_{jl_j}^\top \boldsymbol{\alpha}_{jl_j} \right\} \\ \sim N_{mO} \left([I_{mO} + F(\rho)^{-1} \otimes \kappa^{-1}]^{-1} \mathbf{z}_{jl_j}, [I_{mO} + F(\rho)^{-1} \otimes \kappa^{-1}]^{-1} \right). \quad (\text{D.5})$$

Under our model in Section 2, \mathbf{z}_{jl_j} 's and $\boldsymbol{\alpha}_{jl_j}$'s are ordered first by observation type and then spatially, whereas \mathbf{w}_{jl_j} 's, $\boldsymbol{\xi}_j$'s, $\boldsymbol{\lambda}_j$'s and $\boldsymbol{\sigma}^2$ are ordered first spatially and then by observation type. We also take note that Berchuck et al. (2022)'s finite-mixture-version implementation of Equation (2.2) with a common fixed number of spatial mixture components $L \in \mathbb{N}, L > 1$ for all factors contains some mistakes, in that they omitted the term $\mathbb{1}_{\{\xi_j^o(\mathbf{s}_i) < l_j\}} N(\alpha_{jl_j}^o(\mathbf{s}_i), 1)$ in Equation (D.4) for posterior sampling of $z_{jl_j}^o(\mathbf{s}_i)$'s, calculated the last mixture weights $w_{jL}^o(\mathbf{s}_i) = \prod_{r=1}^{L-1} [1 - \Phi(\alpha_{jr_j}^o(\mathbf{s}_i))] \forall (j, i, o)$ wrongly, and included redundant posterior updating steps for $\alpha_{jL}^o(\mathbf{s}_i)$'s and $z_{jL}^o(\mathbf{s}_i)$'s.

E Some Notes on Slice Sampling Adapted in Our Context

While it might be theoretically more adequate to assume independent infinite mixture models specified by Equation (2.2) $\forall (j, i, o)$ to impose a spatial structure permitting convenient clustering on $\Lambda_{mO \times k}$, we instead opt to introduce new parameters $L_j \in \mathbb{N} \setminus \{0\}, j \in \{1, \dots, k\}$ and proceed with a finite mixture model with the unknown L_j 's as spatial cluster numbers primarily due to the following two reasons:

1. Since we do have a spatial cluster number upper bound mO , it would indeed be reasonable to introduce unknown cluster number parameters $L_j \in \mathbb{N} \setminus \{0\}$ for all latent factors $j = 1, \dots, k$ and proceed with the corresponding finite mixture models.
2. Fix any arbitrary $j \in \{1, \dots, k\}$. Under a baseline infinite mixture model, problems pertaining to the normalizing constants emerge when sampling $\xi_j^o(\mathbf{s}_i)$'s, as the support for any $\xi_j^o(\mathbf{s}_i)$ is the countably infinite set \mathbb{Z}^+ . This issue can be tackled by introducing latent variables $u_j^o(\mathbf{s}_i)$'s with uniform full conditional distributions and thus making the possible values each $\xi_j^o(\mathbf{s}_i)$ can take finite. However, when deciding the new maximum cluster number estimate L_j in the Gibbs sampling step for $\xi_j^o(\mathbf{s}_i)$'s, we may well need more $w_{jl_j}^o(\mathbf{s}_i)$'s for each (i, o) to ensure the criterion in Equation (3.7) due to the slight differences calculating $w_{jl_j}^o(\mathbf{s}_i)$'s between a finite and an infinite mixture model. We can thus end up with an L_j larger than its counterpart in the previous MCMC iteration. Since L_j 's are not ensured non-increasing through the MCMC iterations under an infinite mixture model, we likely need to sample much more α_{jl_j} 's and θ_{jl_j} 's, especially when the cluster number upper bound mO is large. Computational and storage burdens can thus ensue.

Our approach elaborated in Section 3 successfully bypasses the above concerns. We shall also note that Berchuck et al. (2022)'s implementation attempt regarding infinite mixture model via slice sampling in their supplementary material and R package `spBFA` actually does not follow Walker (2007) and is erroneous. One major accomplishment brought about by the introduced latent variables $u_j^o(\mathbf{s}_i)$'s (Section 3) is that we no longer need to enable feasible posterior sampling of $\alpha_{jl_j}^o(\mathbf{s}_i)$'s by introducing latent normal parameters $z_{jl_j}^o(\mathbf{s}_i)$'s (Appendix D). Hence Berchuck et al. (2022)'s Gibbs sampler step for $z_{jl_j}^o(\mathbf{s}_i)$'s is redundant when slice sampling is adopted. Their procedure updating L_j^* 's is also incorrect and placed wrongly.

F Some Further Comments Regarding the Latent NNGP

The NNGP is a highly scalable alternative to the full parent GP while producing comparably good inferences, and has numerous advantages over other approaches for modeling large geostatistical data sets.

In terms of scalability, NNGP typically reduces computational complexity from cubic to linear in m in our context setting $\mathcal{S} = \mathcal{T} = \{\mathbf{s}_1, \dots, \mathbf{s}_m\}$ and significantly outperforms alternative methods like low rank approximation. Low rank models typically require approximately $\mathcal{O}(mr^2)$ flops, where $r \in \mathbb{N}, r \ll m$ is the number of knots that by empirical experiments must

be quite large to approximate the GP well when m is large, thereby making mr^2 computationally prohibitive. NNGP, on the other hand, needs $\mathcal{O}(|\mathcal{S} \cup \mathcal{T}| \cdot h^3)$ flops with $|\mathcal{T}| = m$, where $\mathcal{S} = \mathcal{T}$ and a quite small h , e.g., between 10 to 15, have been shown to perform well. NNGP's capabilities in significantly easing storage (Sections 4.2 and 4.3) may also make it the only feasible candidate under some requirements, e.g., delivering process-based inferences, for certain super large geostatistical data sets (Section 5.2 in Datta et al. 2016).

From the inferential perspective, the NNGP incorporates parameter estimation, outcome prediction, and latent process interpolation into a single fully process-based framework, which had not been explored by any other methods in the literature. A legitimate GP with sparse precision matrices on the entire geographical domain \mathcal{D} , which we shall denote as NNGP $(\mathbf{0}, \tilde{C}(\cdot, \cdot | \boldsymbol{\theta}))$ derived from the parent Gaussian process GP $(\mathbf{0}, C(\cdot, \cdot | \boldsymbol{\theta}))$, the latent NNGP needs not be conceived as an approximation to its parent GP when modeling the latent or observed spatial surface and permits fast and adequate predictions of the latent and outcome variables at arbitrary new locations, a main issue covariance tapering methods are unable to handle. Various simulation experiments (Datta et al. 2016) suggest that NNGP produces estimation & kriging closely resembling those from the parent GP models for diverse covariance functions $C(\cdot, \cdot | \boldsymbol{\theta})$.

Under our spatiotemporal Bayesian Gaussian factor analysis modeling framework, other NNGP methods like Response NNGP and Conjugate NNGP (Finley et al. 2019) are not applicable. A few points to note in our adaptations of the NNGP compared to the framework presented in Datta et al. (2016) not mentioned earlier are as follows:

- The parametric covariance function $C(\cdot, \cdot | \boldsymbol{\theta})$ is over $\mathcal{D} \times \mathcal{D}$, not just over $\mathcal{S} \times \mathcal{S}$. $\forall \mathbf{s}, \mathbf{t} \in \mathcal{D}$, $C(\mathbf{s}, \mathbf{t} | \boldsymbol{\theta})_{q \times q} = \text{Cov}\{\mathbf{w}(\mathbf{s}), \mathbf{w}(\mathbf{t})\}$. q corresponds to O in our model.
- $C_{\mathcal{S}}(\boldsymbol{\theta})$, the covariance function over the reference set \mathcal{S} , corresponds to $F(\rho)_{m \times m} \otimes \kappa_{O \times O}$ in our model.
- We have let $\mathcal{S} = \mathcal{T}$. Thus, $\mathcal{S}^* = \mathcal{T} \cap \mathcal{S} = \mathcal{T}$ and $\mathcal{U} = \mathcal{T} \setminus \mathcal{S}^* = \emptyset$. Hence the likelihood in Equation (10) in Datta et al. (2016) is simplified to only the first portion there, as $k = n = r = m$ in their notations.
- Some software features to further accelerate computation are presented in Section 2.5 of Finley, Datta, and Banerjee (2022).

G More on Predictions at Future Time Points or New Spatial Locations (Complementary to Section 5.1)

G.1 Predicting $\hat{\mathbf{y}}_{(T+1):(T+q)}$ Given $\mathbf{y}_{1:T}$ and $[X_{(T+1):(T+q)}]_{qOm \times p}$ (if $p \geq 1$)

Suppose we have $q \geq 1, q \in \mathbb{N}$ new time points $T+1, \dots, T+q$ with corresponding time $\nu_{T+1}, \dots, \nu_{T+q}$ (distances standardized to 1 if `include.time = equalTimeDist = TRUE`). Then under all our modeling frameworks, for Bayesian predictions at $\nu_{(T+1):(T+q)}$ given their corresponding covariates matrix $[X_{(T+1):(T+q)}]_{qOm \times p}$, if any, we can write the PPD as

$$f(\mathbf{y}_{(T+1):(T+q)} | \mathbf{y}_{1:T}, X_{(T+1):(T+q)}) = \int_{\Theta} f(\mathbf{y}_{(T+1):(T+q)} | \Theta, \mathbf{y}_{1:T}, X_{(T+1):(T+q)}) \pi(\Theta | \mathbf{y}_{1:T}) d\Theta,$$

$$\text{where } \Theta = \begin{cases} (\Lambda, \beta, \sigma^2, \eta_{(T+1):(T+q)}, \boldsymbol{\eta}, \Upsilon, \psi), & \text{if clustering} = \text{FALSE} \\ (\boldsymbol{\theta}, \boldsymbol{\xi}, \beta, \sigma^2, \eta_{(T+1):(T+q)}, \boldsymbol{\eta}, \Upsilon, \psi), & \text{if clustering} = \text{TRUE} \end{cases}. \quad (\text{G.1})$$

$\boldsymbol{\eta}$ denotes $\boldsymbol{\eta}_{1:T}$. `clustering` = FALSE refers to the scenario when no spatial clustering mechanism is integrated, i.e., when our basic model in Appendix A.1 is adopted, and `clustering` = TRUE refers to the case when a spatial PSBP clustering mechanism is incorporated, i.e., when our model in Section 2 or 3 is adopted. We can then partition the integral in Equation (G.1) into

$$\int_{\Theta} \underbrace{f(\mathbf{y}_{(T+1):(T+q)} | \Lambda, \eta_{(T+1):(T+q)}, \beta, \sigma^2, X_{(T+1):(T+q)})}_{T_1} \underbrace{f(\boldsymbol{\eta}_{(T+1):(T+q)} | \boldsymbol{\eta}, \Upsilon, \psi)}_{T_2} \\ \times \underbrace{\pi(\Lambda, \beta, \sigma^2, \boldsymbol{\eta}, \Upsilon, \psi | \mathbf{y}_{1:T})}_{T_3} d\Theta \text{ if clustering} = \text{FALSE, and} \quad (\text{G.2})$$

$$\int_{\Theta} \underbrace{f(\mathbf{y}_{(T+1):(T+q)} | \boldsymbol{\theta}, \boldsymbol{\xi}, \eta_{(T+1):(T+q)}, \beta, \sigma^2, X_{(T+1):(T+q)})}_{T_1} \underbrace{f(\boldsymbol{\eta}_{(T+1):(T+q)} | \boldsymbol{\eta}, \Upsilon, \psi)}_{T_2} \\ \times \underbrace{\pi(\boldsymbol{\theta}, \boldsymbol{\xi}, \beta, \sigma^2, \boldsymbol{\eta}, \Upsilon, \psi | \mathbf{y}_{1:T})}_{T_3} d\Theta \text{ if clustering} = \text{TRUE}. \quad (\text{G.3})$$

In Equations (G.2) and (G.3), T_1 is the likelihood, T_3 is the parameters' posterior distribution obtained from the original model fit's MCMC sampler, and T_2 can be calculated by properties of conditional distributions of jointly multivariate normals as follows. Depending on whether a temporal structure is included and whether the distances between adjacent time points are equal, we can get a predicted value $\hat{\boldsymbol{\eta}}_{(T+1):(T+q)}$ conditioning on $\boldsymbol{\eta}_{1:T}, \Upsilon, \psi$:

- When `include.time` = FALSE, i.e., when temporal independence is assumed and the temporal correlation structure matrix $H(\psi)$ is set to the identity matrix

$$f(\boldsymbol{\eta}_{(T+1):(T+q)} | \boldsymbol{\eta}_{1:T}, \Upsilon, \psi) = \pi(\boldsymbol{\eta}_{(T+1):(T+q)} | \Upsilon, \psi) \sim N_{qk}(\mathbf{0}, I_{q \times q} \otimes \Upsilon). \quad (\text{G.4})$$

- When `include.time` = TRUE, i.e., when temporal correlation is taken into consideration

By properties of conditional distributions of jointly multivariate normals,

$$\boldsymbol{\eta}_{(T+1):(T+q)} | \boldsymbol{\eta}_{1:T}, \Upsilon, \psi \sim N_{qk} \left(\left[H_{(T+1):(T+q)}^+ \otimes I_{k \times k} \right] \boldsymbol{\eta}_{1:T}, \left[H_{(T+1):(T+q)}^* \otimes \Upsilon \right] \right), \quad (\text{G.5})$$

where $H_{(T+1):(T+q)}^+ = H_{(T+1):(T+q), (1:T)} H_{(1:T), (1:T)}^{-1}$ and

$$H_{(T+1):(T+q)}^* = H_{(T+1):(T+q), (T+1):(T+q)} - H_{(T+1):(T+q)}^+ H_{(1:T), (T+1):(T+q)} \\ = H_{(T+1):(T+q), (T+1):(T+q)} - H_{(T+1):(T+q), (1:T)} H_{(1:T), (1:T)}^{-1} H_{(1:T), (T+1):(T+q)}$$

with $H_{(1:T), (1:T)}, H_{(T+1):(T+q), (1:T)}, H_{(1:T), (T+1):(T+q)}, H_{(T+1):(T+q), (T+1):(T+q)}$ being the corresponding $T \times T, q \times T, T \times q, q \times q$ sub-matrices of the $(T+q) \times (T+q)$

temporal correlation structure matrix $H(\psi)_{1:(T+q)}$ for all $(T+q)$ time points.

- When `equalTimeDist` = FALSE, i.e., when the distances between adjacent time points are unequal, we may only get $H_{(1:T), (1:T)}^{-1}$ by straightforwardly inverting $H_{(1:T), (1:T)}$.
- When `equalTimeDist` = TRUE, i.e., when the time $v_1, \dots, v_T, v_{T+1}, \dots, v_{T+q}$ are equispaced with distances normalized to 1, we can bypass this matrix inversion by directly specifying $H_{(1:T), (1:T)}^{-1}$ according to our formula presented in Appendix B.

G.2 Predicting $\hat{\mathbf{y}}(\mathbf{s}_{(m+1):(m+r)})$ Given $\mathbf{y}(\mathbf{s}_{1:m})$ and $X(\mathbf{s}_{(m+1):(m+r)})_{rTO \times p}$ (if $p \geq 1$)

G.2.1 Under the Basic Modeling Framework in Appendix A.1

When spatially correlated Gaussian Processes are directly imposed onto the columns $\{\boldsymbol{\lambda}_j\}_{j=1}^k$ of the factor loadings matrix $\Lambda_{mO \times k}$, for Bayesian predictions at $r \in \mathbb{N}, r \geq 1$ new locations $\mathbf{s}_{(m+1):(m+r)}$ given their covariates matrix $X(\mathbf{s}_{(m+1):(m+r)})_{rTO \times p}$, if any, the PPD becomes

$$\begin{aligned} & f(\mathbf{y}(\mathbf{s}_{(m+1):(m+r)}) | \mathbf{y}(\mathbf{s}_{1:m}), X(\mathbf{s}_{(m+1):(m+r)})) \\ &= \int_{\Theta} f(\mathbf{y}(\mathbf{s}_{(m+1):(m+r)}) | \Theta, \mathbf{y}(\mathbf{s}_{1:m}), X(\mathbf{s}_{(m+1):(m+r)})) \pi(\Theta | \mathbf{y}(\mathbf{s}_{1:m})) d\Theta, \text{ where} \\ & \Theta = (\boldsymbol{\eta}, \boldsymbol{\beta}, \boldsymbol{\sigma}^2(\mathbf{s}_{(m+1):(m+r)}), \Lambda(\mathbf{s}_{(m+1):(m+r)}), \Lambda, \kappa, \rho). \end{aligned} \quad (\text{G.6})$$

In the above, $\Lambda_{mO \times k} = (\boldsymbol{\lambda}_1, \dots, \boldsymbol{\lambda}_k)$ denotes $\Lambda(\mathbf{s}_{1:m})$, with each $mO \times 1$ vector $\boldsymbol{\lambda}_j = \boldsymbol{\lambda}_j(\mathbf{s}_{1:m})$, $j \in \{1, \dots, k\}$ ordered first by observation type and then spatially (different from the ordering of our original factor loadings matrix), i.e., the first O entries correspond to the first location point, the next O entries correspond to the second location point and so on. $\Lambda(\mathbf{s}_{(m+1):(m+r)})_{rO \times k} = (\boldsymbol{\lambda}_1(\mathbf{s}_{(m+1):(m+r)}), \dots, \boldsymbol{\lambda}_k(\mathbf{s}_{(m+1):(m+r)}))$, where for each $j \in \{1, \dots, k\}$, the $rO \times 1$ vector $\boldsymbol{\lambda}_j(\mathbf{s}_{(m+1):(m+r)})$ is ordered first by observation type and then spatially. The integral in Equation (G.6) can then be partitioned into

$$\begin{aligned} & \int_{\Theta} \underbrace{f(\mathbf{y}(\mathbf{s}_{(m+1):(m+r)}) | \Lambda(\mathbf{s}_{(m+1):(m+r)}), \boldsymbol{\eta}, \boldsymbol{\beta}, \boldsymbol{\sigma}^2(\mathbf{s}_{(m+1):(m+r)}), X(\mathbf{s}_{(m+1):(m+r)}))}_{T_1} \\ & \quad \times \underbrace{f(\Lambda(\mathbf{s}_{(m+1):(m+r)}) | \Lambda, \kappa, \rho)}_{T_2} \underbrace{\pi(\boldsymbol{\eta}, \boldsymbol{\beta}, \Lambda, \kappa, \rho | \mathbf{y}(\mathbf{s}_{1:m}))}_{T_3} \underbrace{\pi(\boldsymbol{\sigma}^2(\mathbf{s}_{(m+1):(m+r)}))}_{T_4} d\Theta \end{aligned} \quad (\text{G.7})$$

since the posterior density $\pi(\boldsymbol{\sigma}^2(\mathbf{s}_{(m+1):(m+r)}) | \mathbf{y}(\mathbf{s}_{1:m}))$ equals the prior $\pi(\boldsymbol{\sigma}^2(\mathbf{s}_{(m+1):(m+r)}))$.

In Equation (G.7), T_1 is the likelihood, T_3 is the parameters' posterior distribution obtained from the original model fit's MCMC sampler, T_4 denotes the prior density for $\boldsymbol{\sigma}^2(\mathbf{s}_{(m+1):(m+r)}) = ((\sigma^2)^1(\mathbf{s}_{m+1}), \dots, (\sigma^2)^O(\mathbf{s}_{m+1}), \dots, (\sigma^2)^1(\mathbf{s}_{m+r}), \dots, (\sigma^2)^O(\mathbf{s}_{m+r}))$ with $(\sigma^2)^o(\mathbf{s}_{m+i_r}) \stackrel{\text{iid}}{\sim} \mathcal{IG}(a, b)$, $i_r \in \{1, \dots, r\}$, $o \in \{1, \dots, O\}$, and T_2 can be written as

$$f(\Lambda(\mathbf{s}_{(m+1):(m+r)}) | \Lambda(\mathbf{s}_{1:m}), \kappa, \rho) = \prod_{j=1}^k f(\boldsymbol{\lambda}_j(\mathbf{s}_{(m+1):(m+r)}) | \boldsymbol{\lambda}_j(\mathbf{s}_{1:m}), \kappa, \rho).$$

Hence, we can get a predicted value $\hat{\Lambda}(\mathbf{s}_{(m+1):(m+r)})$ conditioning on $\Lambda(\mathbf{s}_{1:m}), \kappa, \rho$ depending on the following 3 scenarios regarding the spatially extended GP prior on $\boldsymbol{\lambda}_j(\mathbf{s}_{1:(m+r)})$'s (ordered first by observation type and then spatially here):

- When `include.space = FALSE`, i.e., when spatial independence is assumed and the corresponding spatially extended full GP prior $\boldsymbol{\lambda}_j(\mathbf{s}_{1:(m+r)}) \stackrel{\text{iid}}{\sim} N_{(m+r)O}(\mathbf{0}, I_{(m+r) \times (m+r)} \otimes \kappa_{O \times O})$, $j \in \{1, \dots, k\}$ is imposed

$$\begin{aligned} & \text{For any arbitrary } j \in \{1, \dots, k\}, \quad f(\boldsymbol{\lambda}_j(\mathbf{s}_{(m+1):(m+r)}) | \boldsymbol{\lambda}_j(\mathbf{s}_{1:m}), \kappa, \rho) \\ &= \pi(\boldsymbol{\lambda}_j(\mathbf{s}_{(m+1):(m+r)}) | \kappa, \rho) \sim N_{rO}(\mathbf{0}, I_{r \times r} \otimes \kappa). \end{aligned} \quad (\text{G.8})$$

- When `include.space = TRUE` and `spatApprox = FALSE`, i.e., when spatial dependence is taken into consideration and the spatially extended full GP prior $\lambda_j(\mathbf{s}_{1:(m+r)})|\kappa, \rho \stackrel{\text{iid}}{\sim} N_{(m+r)O}(\mathbf{0}, F(\rho)_{(m+r) \times (m+r)} \otimes \kappa_{O \times O})$, $j \in \{1, \dots, k\}$ is placed

By properties of conditional distributions of jointly multivariate normals, \forall arbitrary j ,

$$\lambda_j(\mathbf{s}_{(m+1):(m+r)})|\lambda_j(\mathbf{s}_{1:m}), \kappa, \rho \sim N_{rO} \left(B_{\mathbf{s}_{(m+1):(m+r)}} \lambda_j(\mathbf{s}_{1:m}), F_{\mathbf{s}_{(m+1):(m+r)}} \right), \quad (\text{G.9})$$

where the $rO \times mO$ matrix $B_{\mathbf{s}_{(m+1):(m+r)}} = \left\{ F(\rho)_{\mathbf{s}_{(m+1):(m+r)}, \mathbf{s}_{1:m}} [F(\rho)_{\mathbf{s}_{1:m}}]^{-1} \right\} \otimes I_{O \times O}$

and the $rO \times rO$ matrix $F_{\mathbf{s}_{(m+1):(m+r)}}$

$$= \left\{ F(\rho)_{\mathbf{s}_{(m+1):(m+r)}} - F(\rho)_{\mathbf{s}_{(m+1):(m+r)}, \mathbf{s}_{1:m}} [F(\rho)_{\mathbf{s}_{1:m}}]^{-1} F(\rho)_{\mathbf{s}_{1:m}, \mathbf{s}_{(m+1):(m+r)}} \right\} \otimes \kappa_{O \times O}$$

with $F(\rho)_{\mathbf{s}_{1:m}}, F(\rho)_{\mathbf{s}_{(m+1):(m+r)}, \mathbf{s}_{1:m}}, F(\rho)_{\mathbf{s}_{1:m}, \mathbf{s}_{(m+1):(m+r)}}, F(\rho)_{\mathbf{s}_{(m+1):(m+r)}}$ being the

corresponding $m \times m, r \times m, m \times r, r \times r$ sub-matrices of $\left[F(\rho)_{\mathbf{s}_{1:(m+r)}} \right]_{(m+r) \times (m+r)}$.

- When `include.space = spatApprox = TRUE`, i.e., when spatial dependence is taken into consideration and the spatially extended NNGP prior $\tilde{\pi}(\lambda_j(\mathbf{s}_{1:(m+r)})|\kappa, \rho) \forall j$ is placed

Under the spatially extended NNGP prior applied to λ_j 's instead of α_{jl_j} 's

and by properties of conditional distributions of jointly multivariate normals,

for any arbitrary fixed $j \in \{1, \dots, k\}$, $\tilde{f}(\lambda_j(\mathbf{s}_{(m+1):(m+r)})|\lambda_j(\mathbf{s}_{1:m}), \kappa, \rho)$ (G.10)

$$= \prod_{i_r=1}^r \tilde{f}(\lambda_j(\mathbf{s}_{(m+i_r)}))|\lambda_j(\mathbf{s}_{1:m}), \kappa, \rho = \prod_{i_r=1}^r f(\lambda_j(\mathbf{s}_{(m+i_r)})|\lambda_{j,N(\mathbf{s}_{(m+i_r)})}, \kappa, \rho),$$

where for each $i_r \in \{1, \dots, r\}$,

$$\lambda_j(\mathbf{s}_{(m+i_r)})|\lambda_{j,N(\mathbf{s}_{(m+i_r)})}, \kappa, \rho \sim N_O \left(B_{\mathbf{s}_{(m+i_r)}} \lambda_{j,N(\mathbf{s}_{(m+i_r)})}, F_{\mathbf{s}_{(m+i_r)}} \right) \text{ with}$$

the $O \times hO$ matrix $B_{\mathbf{s}_{(m+i_r)}} = \left\{ F(\rho)_{\mathbf{s}_{(m+i_r)}, N(\mathbf{s}_{(m+i_r)})} \left[F(\rho)_{N(\mathbf{s}_{(m+i_r)})} \right]^{-1} \right\} \otimes I_{O \times O}$

and the $O \times O$ matrix $F_{\mathbf{s}_{(m+i_r)}}$

$$= \left\{ F(\rho)_{\mathbf{s}_{(m+i_r)}} - F(\rho)_{\mathbf{s}_{(m+i_r)}, N(\mathbf{s}_{(m+i_r)})} \left[F(\rho)_{N(\mathbf{s}_{(m+i_r)})} \right]^{-1} F(\rho)_{N(\mathbf{s}_{(m+i_r)}), \mathbf{s}_{(m+i_r)}} \right\} \otimes \kappa_{O \times O}.$$

with $F(\rho)_{\mathbf{s}_{(m+i_r)}} = 1, F(\rho)_{\mathbf{s}_{(m+i_r)}, N(\mathbf{s}_{(m+i_r)})}, F(\rho)_{N(\mathbf{s}_{(m+i_r)}), \mathbf{s}_{(m+i_r)}}, F(\rho)_{N(\mathbf{s}_{(m+i_r)})}$ being the

corresponding $1 \times 1, 1 \times h, h \times 1, h \times h$ sub-matrices of $\left[F(\rho)_{\mathbf{s}_{1:(m+r)}} \right]_{(m+r) \times (m+r)}$.

G.2.2 Under Our Modeling Framework in Section 2

When the prior $\alpha_{jl_j} \stackrel{\text{iid}}{\sim} N_{mO}(\mathbf{0}, F(\rho)_{m \times m} \otimes \kappa_{O \times O})$ for all $(j, l_j) \in \{1, \dots, k\} \times \{1, \dots, L-1\}$ is assigned, for Bayesian predictions at $r \in \mathbb{N}, r \geq 1$ new locations $\mathbf{s}_{(m+1):(m+r)}$ given their corresponding covariates matrix $X(\mathbf{s}_{(m+1):(m+r)})_{rTO \times p}$, if any, we can write the PPD as

$$\begin{aligned} & f(\mathbf{y}(\mathbf{s}_{(m+1):(m+r)})|\mathbf{y}(\mathbf{s}_{1:m}), X(\mathbf{s}_{(m+1):(m+r)})) \\ &= \int_{\Theta} f(\mathbf{y}(\mathbf{s}_{(m+1):(m+r)})|\Theta, \mathbf{y}(\mathbf{s}_{1:m}), X(\mathbf{s}_{(m+1):(m+r)})) \pi(\Theta|\mathbf{y}(\mathbf{s}_{1:m})) d\Theta, \end{aligned}$$

where $\Theta = (\boldsymbol{\eta}, \boldsymbol{\beta}, \boldsymbol{\sigma}^2(\mathbf{s}_{(m+1):(m+r)}), \boldsymbol{\theta}, \boldsymbol{\xi}(\mathbf{s}_{(m+1):(m+r)}), \boldsymbol{\alpha}(\mathbf{s}_{(m+1):(m+r)}), \boldsymbol{\alpha}, \kappa, \rho)$ and $\boldsymbol{\alpha}$ denotes $\boldsymbol{\alpha}(\mathbf{s}_{1:m})$, and then partition the integral into

$$\begin{aligned} & \int_{\Theta} \underbrace{f(\mathbf{y}(\mathbf{s}_{(m+1):(m+r)}) | \boldsymbol{\theta}, \boldsymbol{\xi}(\mathbf{s}_{(m+1):(m+r)}), \boldsymbol{\eta}, \boldsymbol{\beta}, \boldsymbol{\sigma}^2(\mathbf{s}_{(m+1):(m+r)}), X(\mathbf{s}_{(m+1):(m+r)}))}_{T_1} \\ & \quad \times \underbrace{f(\boldsymbol{\xi}(\mathbf{s}_{(m+1):(m+r)}) | \boldsymbol{\alpha}(\mathbf{s}_{(m+1):(m+r)}))}_{T_2} \underbrace{f(\boldsymbol{\alpha}(\mathbf{s}_{(m+1):(m+r)}) | \boldsymbol{\alpha}, \kappa, \rho)}_{T_3} \\ & \quad \times \underbrace{\pi(\boldsymbol{\eta}, \boldsymbol{\beta}, \boldsymbol{\theta}, \boldsymbol{\alpha}, \kappa, \rho | \mathbf{y}(\mathbf{s}_{1:m}))}_{T_4} \underbrace{\pi(\boldsymbol{\sigma}^2(\mathbf{s}_{(m+1):(m+r)}))}_{T_5} d\Theta \end{aligned} \quad (\text{G.11})$$

since the posterior density $\pi(\boldsymbol{\sigma}^2(\mathbf{s}_{(m+1):(m+r)}) | \mathbf{y}(\mathbf{s}_{1:m}))$ equals the prior $\pi(\boldsymbol{\sigma}^2(\mathbf{s}_{(m+1):(m+r)}))$.

In Equation (G.11), T_1 is the likelihood, T_4 is the parameters' posterior distribution obtained from the original model fit's MCMC sampler, T_5 denotes the prior density for $\boldsymbol{\sigma}^2(\mathbf{s}_{(m+1):(m+r)}) = ((\sigma^2)^1(\mathbf{s}_{m+1}), \dots, (\sigma^2)^O(\mathbf{s}_{m+1}), \dots, (\sigma^2)^1(\mathbf{s}_{m+r}), \dots, (\sigma^2)^O(\mathbf{s}_{m+r}))$ with $(\sigma^2)^o(\mathbf{s}_{m+i_r}) \stackrel{\text{iid}}{\sim} \mathcal{IG}(a, b), i_r \in \{1, \dots, r\}, o \in \{1, \dots, O\}$, T_2 is the density of the multinomial distribution described in Section 2, and T_3 can be written as

$$f(\boldsymbol{\alpha}(\mathbf{s}_{(m+1):(m+r)}) | \boldsymbol{\alpha}(\mathbf{s}_{1:m}), \kappa, \rho) = \prod_{j=1}^k \prod_{l_j=1}^{L-1} f(\boldsymbol{\alpha}_{jl_j}(\mathbf{s}_{(m+1):(m+r)}) | \boldsymbol{\alpha}_{jl_j}(\mathbf{s}_{1:m}), \kappa, \rho). \quad (\text{G.12})$$

Hence, we can directly get a predicted value $\hat{\boldsymbol{\alpha}}(\mathbf{s}_{(m+1):(m+r)})$ conditioning on $\boldsymbol{\alpha}(\mathbf{s}_{1:m}), \kappa, \rho$ depending on the following 3 scenarios regarding the spatially extended GP prior on $\boldsymbol{\alpha}_{jl_j}(\mathbf{s}_{1:(m+r)})$'s:

- When `include.space = FALSE`, i.e., when spatial independence is assumed and the spatial neighborhood structure matrix $F(\rho)$ is set to the identity matrix

$$\forall (j, l_j) \in \{1, \dots, k\} \times \{1, \dots, L-1\}, \quad (\text{G.13})$$

$$f(\boldsymbol{\alpha}_{jl_j}(\mathbf{s}_{(m+1):(m+r)}) | \boldsymbol{\alpha}_{jl_j}(\mathbf{s}_{1:m}), \kappa, \rho) = \pi(\boldsymbol{\alpha}_{jl_j}(\mathbf{s}_{(m+1):(m+r)}) | \kappa, \rho) \sim N_{rO}(\mathbf{0}, I_{r \times r} \otimes \kappa).$$

- When `include.space = TRUE` and `spatApprox = FALSE`, i.e., when spatial dependence is taken into consideration and the spatially extended full GP prior $\pi(\boldsymbol{\alpha}_{jl_j}(\mathbf{s}_{1:(m+r)}) | \kappa, \rho) = N_{(m+r)O}(\mathbf{0}, F(\rho)_{(m+r) \times (m+r)} \otimes \kappa_{O \times O}) \forall (j, l_j) \in \{1, \dots, k\} \times \{1, \dots, L-1\}$ is placed

By properties of conditional distributions of jointly multivariate normals, \forall arbitrary (j, l_j) ,

$$\boldsymbol{\alpha}_{jl_j}(\mathbf{s}_{(m+1):(m+r)}) | \boldsymbol{\alpha}_{jl_j}(\mathbf{s}_{1:m}), \kappa, \rho \sim N_{rO} \left(B_{\mathbf{s}_{(m+1):(m+r)}} \boldsymbol{\alpha}_{jl_j}(\mathbf{s}_{1:m}), F_{\mathbf{s}_{(m+1):(m+r)}} \right), \quad (\text{G.14})$$

where the $rO \times mO$ matrix $B_{\mathbf{s}_{(m+1):(m+r)}} = \left\{ F(\rho)_{\mathbf{s}_{(m+1):(m+r)}, \mathbf{s}_{1:m}} [F(\rho)_{\mathbf{s}_{1:m}}]^{-1} \right\} \otimes I_{O \times O}$

and the $rO \times rO$ matrix $F_{\mathbf{s}_{(m+1):(m+r)}}$

$$= \left\{ F(\rho)_{\mathbf{s}_{(m+1):(m+r)}} - F(\rho)_{\mathbf{s}_{(m+1):(m+r)}, \mathbf{s}_{1:m}} [F(\rho)_{\mathbf{s}_{1:m}}]^{-1} F(\rho)_{\mathbf{s}_{1:m}, \mathbf{s}_{(m+1):(m+r)}} \right\} \otimes \kappa_{O \times O}$$

with $F(\rho)_{\mathbf{s}_{1:m}}, F(\rho)_{\mathbf{s}_{(m+1):(m+r)}, \mathbf{s}_{1:m}}, F(\rho)_{\mathbf{s}_{1:m}, \mathbf{s}_{(m+1):(m+r)}}, F(\rho)_{\mathbf{s}_{(m+1):(m+r)}}$ being the corresponding $m \times m, r \times m, m \times r, r \times r$ sub-matrices of $\left[F(\rho)_{\mathbf{s}_{1:(m+r)}} \right]_{(m+r) \times (m+r)}$.

- When `include.space = spatApprox = TRUE`, i.e., when spatial dependence is taken into consideration and the spatially extended NNGP prior $\tilde{\pi}(\boldsymbol{\alpha}_{jl_j}(\mathbf{s}_{1:(m+r)}) | \kappa, \rho) \forall (j, l_j)$ is

placed, under the spatially extended NNGP prior and by properties of conditional distributions of jointly multivariate normals, for any arbitrary fixed (j, l_j) ,

$$\tilde{f}(\alpha_{jl_j}(\mathbf{s}_{(m+1):(m+r)}) | \alpha_{jl_j}(\mathbf{s}_{1:m}), \kappa, \rho) \quad (\text{G.15})$$

$$= \prod_{i_r=1}^r \tilde{f}(\alpha_{jl_j}(\mathbf{s}_{(m+i_r)}) | \alpha_{jl_j}(\mathbf{s}_{1:m}), \kappa, \rho) = \prod_{i_r=1}^r f(\alpha_{jl_j}(\mathbf{s}_{(m+i_r)}) | \alpha_{jl_j, N(\mathbf{s}_{(m+i_r)})}, \kappa, \rho),$$

where for each $i_r \in \{1, \dots, r\}$,

$$\alpha_{jl_j}(\mathbf{s}_{(m+i_r)}) | \alpha_{jl_j, N(\mathbf{s}_{(m+i_r)})}, \kappa, \rho \sim N_O \left(B_{\mathbf{s}_{(m+i_r)}} \alpha_{jl_j, N(\mathbf{s}_{(m+i_r)})}, F_{\mathbf{s}_{(m+i_r)}} \right) \text{ with}$$

$$\text{the } O \times hO \text{ matrix } B_{\mathbf{s}_{(m+i_r)}} = \left\{ F(\rho)_{\mathbf{s}_{(m+i_r)}, N(\mathbf{s}_{(m+i_r)})} \left[F(\rho)_{N(\mathbf{s}_{(m+i_r)})} \right]^{-1} \right\} \otimes I_{O \times O}$$

and the $O \times O$ matrix $F_{\mathbf{s}_{(m+i_r)}}$

$$= \left\{ F(\rho)_{\mathbf{s}_{(m+i_r)}} - F(\rho)_{\mathbf{s}_{(m+i_r)}, N(\mathbf{s}_{(m+i_r)})} \left[F(\rho)_{N(\mathbf{s}_{(m+i_r)})} \right]^{-1} F(\rho)_{N(\mathbf{s}_{(m+i_r)}), \mathbf{s}_{(m+i_r)}} \right\} \otimes \kappa_{O \times O}.$$

$F(\rho)_{\mathbf{s}_{(m+i_r)}} = 1, F(\rho)_{\mathbf{s}_{(m+i_r)}, N(\mathbf{s}_{(m+i_r)})}, F(\rho)_{N(\mathbf{s}_{(m+i_r)}), \mathbf{s}_{(m+i_r)}}, F(\rho)_{N(\mathbf{s}_{(m+i_r)})}$ denote the corresponding $1 \times 1, 1 \times h, h \times 1, h \times h$ sub-matrices of $\left[F(\rho)_{\mathbf{s}_{1:(m+r)}} \right]_{(m+r) \times (m+r)}$.

H Scalability Improvements Corresponding to Our 3 Novelties – A Summary of Computational Complexity and Memory

Our three novelties for enhancing scalability are **slice sampling**, **spatial NNGP prior**, and **sequential updating algorithms**. We first list some important points to note.

- $O \in \mathbb{N}$ is assumed very small; $h, k, p \ll m$; $1 \leq L$ or L_j 's $\leq m$; $T \leq m$.
- Slice sampling is useful when L has to be at least moderately large. Moreover, it resolves intimidating storage concerns regarding θ_{jl_j} 's, α_{jl_j} 's, and \mathbf{w}_{jl_j} 's and thus enables practicable implementation of spatial prediction and clustering when m and L are large.
- Spatial NNGP prior and sequential updates are helpful for a large m . Sequential updating algorithms can only be adopted when our spatial NNGP prior is specified. Hence, when slice sampling is not adopted, we have 3 methods, which we denote as **fullGPFixedL**, **NNGPblockFixedL**, and **NNGPsequenFixedL**.
- When slice sampling is adopted and m is at least moderately large, we may only also specify our spatial NNGP prior with sequential updates for a computationally feasible model, which we shall denote as **NNGPsequenVaryLj**, as multivariate rejection sampling from high-dimensional truncated mO -variate normal distributions of the α_{jl_j} 's (Equations (3.8) and (4.7)) is unbearably slow.

Hence, we only implement the four methods **fullGPFixedL**, **NNGPblockFixedL**, **NNGPsequenFixedL**, and **NNGPsequenVaryLj** for our simulation experiments. To verify what we have obtained theoretically regarding scalability, we may compare

- **fullGPFixedL** and **NNGPblockFixedL** for effects caused by spatial NNGP prior (without slice sampling);
- **NNGPblockFixedL** and **NNGPsequenFixedL** for effects caused by sequential updates (without slice sampling);

- **NNGPsequenFixedL** and **NNGPsequenVaryLj** for effects caused by slice sampling (with our spatial NNGP prior and sequential updating algorithms adopted).

We now elaborate on **theoretical** scalability improvements attributable to each of our three novelties. Computational complexity reduction for certain involved major steps in posterior sampling and spatial prediction, as well as storage requirements alleviation for some concerned key quantities in main model fitting and spatial prediction & clustering, are considered measures of scalability improvements. All computational complexity orders in the subsections below are for only one typical MCMC iteration.

H.1 Flexibility, Computation, and Storage Improvements Brought About by Our Slice Sampling Approach in Section 3 with Spatial NNGP & Sequential Updates

We assume that $\mathcal{O}(T) \leq \mathcal{O}(m)$. Recall that $1 \leq L$ or L_j 's $\leq m$ and that we have assumed $O, h, k, p \ll m$. It is likely restrictive to pre-specify a fixed common $L \in \mathbb{N}$, $L > 1$, as the numbers of spatial mixtures are unknown and may well differ across the k latent factors. Moreover, an at least moderately large L would typically be required to guarantee satisfactory model fitting, resulting in computational burdens and storage issues. Our slice sampling approach (Section 3) not only brings about desired modeling flexibility and adequacy but also decently addresses the involved scalability issues (Table H.1) by ensuring non-increasing L_j estimates through the MCMC iterations.

Let $N \in \mathbb{N}$ be the number of kept post-burn-in MCMC iterations. We denote the corresponding estimated number(s) of spatial mixture components as $L_j^{(t_i)}$'s, $i \in \{1, \dots, N\}$, $j \in \{1, \dots, k\}$. In Table H.1, overall storage orders correspond to all kept MCMC iterations, whereas overall computational complexity orders are only for one typical MCMC iteration.

Domain of Scalability Improvements		Computational Acceleration		Storage Alleviation		
		Posterior Sampling	Spatial Prediction at $r \in \mathbb{N}$ ($r < m$) new locations	Spatial Clustering		
Key Parameters / Quantities Involved		$u_j^o(\mathbf{s}_i)$'s / $z_{jl_j}^o(\mathbf{s}_i)$'s, $\xi_j^o(\mathbf{s}_i)$'s, α_{jl_j} 's, θ_{jl_j} 's, $\delta_{1:k}$, κ , ρ		$\alpha_{jl_j}(\mathbf{s}_{(m+1):(m+r)})$'s	α_{jl_j} 's and θ_{jl_j} 's	w_{jl_j} 's
Overall Standard Computational	Before	$\mathcal{O}(kLmO\{h^2O + T(p+k)\} + mh^3)$		$\mathcal{O}(r[h^3 + k(L-1)O(h+O)] + O^3)$		$\mathcal{O}(NmOkL)$
Complexity or Storage Order	After	$\mathcal{O}\left(mO\sum_{j=1}^k L_j \left\{h^2O + T(p+k)\right\} + mh^3\right)$ $+ \mathcal{O}\left(O^2\sum_{j=1}^k \sum_{l_j=1}^{L_j-1} \sum_{i=1}^m [k_{jl_j i}^*/O + n_{jl_j i}^*]\right)$		$\mathcal{O}\left(r\left[h^3 + \sum_{j=1}^k (L_j - 1) \cdot O(h+O)\right] + O^3\right)$		$\mathcal{O}\left(mO\sum_{i=1}^N \sum_{j=1}^k L_j^{(t_i)}\right)$
References	Section(s)	Section 5.1 and Appendix G.2.2				Section 5.2
	Equations	Equations (5.5) and (G.15)				

Table H.1: A theoretical summary table of posterior sampling & spatial prediction computation acceleration and spatial prediction & clustering storage alleviation brought about by our slice sampling approach in Section 3 with our spatial NNGP prior and sequential updates (Section 4). Our simulation experiments comparing **NNGPsequenFixedL** and **NNGPsequenVaryLj** should lead to results corresponding well to the table in terms of main model fitting time for the involved parameters and spatial prediction time for $\alpha_{jl_j}(s_{(m+1):(m+r)})$'s.

Detailed Posterior Sampling Computational Complexity Order Derivations

(a) Without Slice Sampling (Before)

$$\mathcal{O}(\{k(L-1)O^2[h^2 + h + 1] + h^3\}m) + \mathcal{O}(m[k(L-1)hO(h+O) + O^3]) + \mathcal{O}(kLmOT(p+k))$$

$$= \mathcal{O}(kLmO\{h^2O + T(p+k)\} + mh^3) = \mathcal{O}(mT) \leq \mathcal{O}(m^2) \text{ if } L \ll m \quad (\text{H.1})$$

(b) **With Slice Sampling (After)**

$$\begin{aligned} & \mathcal{O} \left(\left\{ \sum_{j=1}^k (L_j - 1) \cdot O^2[h^2 + h + 1] + h^3 \right\} m \right) + \mathcal{O} \left(\sum_{j=1}^k L_j \cdot mOT(p+k) \right) \\ & + \mathcal{O} \left(O \left\{ \sum_{j=1}^k \left[(L_j - 1)mh(h+O) + \sum_{l_j=1}^{L_j-1} \sum_{i=1}^m (k_{jl_j i}^* + n_{jl_j i}^* \cdot O) \right] + O^2 \right\} \right) \\ & = \mathcal{O} \left(mO \sum_{j=1}^k L_j \{h^2O + T(p+k)\} + mh^3 + O^2 \sum_{j=1}^k \sum_{l_j=1}^{L_j-1} \sum_{i=1}^m \left[\frac{k_{jl_j i}^*}{O} + n_{jl_j i}^* \right] \right) \quad (\text{H.2}) \end{aligned}$$

With our slicing sampling approach (Section 3) adopted on top of our spatial NNGP prior (Section 4) coupled with sequential updates (Section 4.4), rejection sampling from low-dimensional truncated O -variate normal distributions would have adequate acceptance rates and thus small required numbers $n_{jl_j i}^*$'s of draws from $N_O(V_{s_i} \mu_{jl_j, s_i}, V_{s_i})$'s (Equation (4.9) in Section 4.4) per sample of $\alpha_{jl_j}(s_i)$'s. If $\mathcal{O} \left(\max_{(j, l_j, i)} \left[\frac{k_{jl_j i}^*}{O} + n_{jl_j i}^* \right] \right) \leq \mathcal{O}(T)$ and $\max_{j \in \{1, \dots, k\}} L_j \ll m$, then

$$\mathcal{O} \left(mO \sum_{j=1}^k L_j \{h^2O + T(p+k)\} + mh^3 + O^2 \sum_{j=1}^k \sum_{l_j=1}^{L_j-1} \sum_{i=1}^m \left[\frac{k_{jl_j i}^*}{O} + n_{jl_j i}^* \right] \right) = \mathcal{O}(mT) \leq \mathcal{O}(m^2).$$

H.2 Posterior Sampling Computational Acceleration & Storage Alleviation and Faster Spatial Prediction Brought About by Our Spatial NNGP Prior in Section 4 with or without Slice Sampling

Domain of Scalability Improvements		Posterior Sampling		Spatial Prediction
		Acceleration	Storage Alleviation	Acceleration
Parameters Involved		κ and ρ	κ and ρ (and α_{jl_j} 's)	$\alpha_{jl_j}(s_{(m+1):(m+r)}) \alpha_{jl_j}(s_{1:m}), \kappa, \rho$'s for all (j, l_j)
Key Quantities Concerned		$F(\rho)^{-1}$ and $\det(F(\rho))$	$F(\rho)$ and $F(\rho)^{-1}$	conditional normal variances & their Cholesky factors and mean vectors
Standard Computational Complexity or Storage Order for the Key Quantities	Before	$\mathcal{O}(m^3)$	$\mathcal{O}(m^2)$	$\mathcal{O}(rm^2) + \mathcal{O}(r^3) + \mathcal{O}(O^3) + \mathcal{O} \left(\sum_{j=1}^k (L_j - 1) \cdot rmO \right)$
	After	$\mathcal{O}(mh^3)$	$\mathcal{O}(mh^2)$	$\mathcal{O}(rh^3) + \mathcal{O}(r) + \mathcal{O}(O^3) + \mathcal{O} \left(\sum_{j=1}^k (L_j - 1) \cdot r \cdot hO \right)$
Overall Standard Order of Computational Complexity Without Slice Sampling	Before	$\mathcal{O}(m^3)$		$\mathcal{O}(r[m^2 + r^2 + k(L-1)mO])$
	After	$\mathcal{O}(\{k(L-1)O^2[h^2 + h + 1] + h^3\}m)$		$\mathcal{O}(r[h^3 + k(L-1)O(h+O)] + O^3)$
Overall Standard Order of Computational Complexity With Slice Sampling	Before	$\mathcal{O}(m^3)$		$\mathcal{O}(r[m^2 + r^2 + \sum_{j=1}^k (L_j - 1) \cdot mO])$
	After	$\mathcal{O}(\{\sum_{j=1}^k (L_j - 1) \cdot O^2[h^2 + h + 1] + h^3\}m)$		$\mathcal{O}(r[h^3 + \sum_{j=1}^k (L_j - 1) \cdot O(h+O)] + O^3)$
References	Section(s)	Section 4.3	Sections 4.2 and 4.3	Section 5.1 and Appendix G.2.2
	Equations	Equations (A.18), (A.19), (A.34) and (A.35)		Equations (5.3), (5.5), (G.14) and (G.15)

Table H.2: A theoretical summary table of posterior sampling computation acceleration & storage alleviation and spatial prediction acceleration brought about by our spatial NNGP prior in Section 4 with or without slice sampling (Section 3). Our simulation experiments comparing `fullGPfixedL` and `NNGPblockFixedL` should lead to results corresponding well to the table in terms of main model fitting time for κ and ρ and spatial prediction time for $\alpha_{jl_j}(s_{(m+1):(m+r)})$'s.

Suppose we have a large m . Recall that $1 \leq L$ or L_j 's $\leq m$ and that we have assumed $O, h, k \ll m$. We also assume $rO < m$ for spatial prediction at $r \in \mathbb{N}$ new locations $s_{(m+1):(m+r)}$. Note that $[F(\rho) \otimes \kappa]^{-1} = F(\rho)^{-1} \otimes \kappa^{-1}$ and that $\det(F(\rho) \otimes \kappa) = \det(F(\rho))^O \cdot \det(\kappa)^m$.

Detailed Derivations Regarding the Overall Computational Complexity Orders

1. Computational Complexity for the Posterior Sampling Steps of ρ and $\kappa_{O \times O}$

(a) The Full Spatial GP Prior Adopted (Before)

Without Slice Sampling

$$[\mathcal{O}(m^3) + \mathcal{O}(k(L-1)(Om)^2)] + \mathcal{O}(k(L-1) \cdot Om^2) = \mathcal{O}(m^3) \quad (\text{H.3})$$

With Slice Sampling

$$\left[\mathcal{O}(m^3) + \mathcal{O} \left(\sum_{j=1}^k (L_j - 1) \cdot (Om)^2 \right) \right] + \mathcal{O} \left(\sum_{j=1}^k (L_j - 1) \cdot Om^2 \right) = \mathcal{O}(m^3) \quad (\text{H.4})$$

(b) Our Spatial NNGP Prior in Section 4 Adopted (After)

Without Slice Sampling

$$\begin{aligned} & [\{\mathcal{O}(mh^3) + \mathcal{O}(O^3) + \mathcal{O}(m(h+1)^2) + \mathcal{O}(m)\} + \mathcal{O}(k(L-1)m[h^2 + h + 1]O^2)] \\ & + \mathcal{O}(k(L-1) \cdot Om[h^2 + h + 1]) \\ & = \mathcal{O}(\{k(L-1)O^2[h^2 + h + 1] + h^3\}m) = \mathcal{O}(m) \text{ if } L \ll m \end{aligned} \quad (\text{H.5})$$

With Slice Sampling

$$\begin{aligned} & \left[\{\mathcal{O}(mh^3) + \mathcal{O}(O^3) + \mathcal{O}(m(h+1)^2) + \mathcal{O}(m)\} + \mathcal{O} \left(\sum_{j=1}^k (L_j - 1) \cdot m[h^2 + h + 1]O^2 \right) \right] \\ & + \mathcal{O} \left(\sum_{j=1}^k (L_j - 1) \cdot Om[h^2 + h + 1] \right) \\ & = \mathcal{O} \left(\left\{ \sum_{j=1}^k (L_j - 1) \cdot O^2[h^2 + h + 1] + h^3 \right\} m \right) = \mathcal{O}(m) \text{ if } \max_{j \in \{1, \dots, k\}} L_j \ll m \end{aligned} \quad (\text{H.6})$$

2. Computational Complexity for the Spatial Prediction Step Obtaining

$$\hat{\alpha}_{jl_j}(s_{(m+1):(m+r)}) \text{ for all } (j, l_j)$$

(a) The Full Spatial GP Prior Adopted (Before)

Without Slice Sampling

$$\mathcal{O}(rm^2) + \mathcal{O}(r^3) + \mathcal{O}(O^3) + \mathcal{O}(k(L-1) \cdot rmO) + \mathcal{O}(k(L-1) \cdot (rO)^2) = \mathcal{O}(r[m^2 + r^2 + k(L-1)mO]) \quad (\text{H.7})$$

With Slice Sampling

$$\begin{aligned} & \mathcal{O}(rm^2) + \mathcal{O}(r^3) + \mathcal{O}(O^3) + \mathcal{O} \left(\sum_{j=1}^k (L_j - 1) \cdot rmO \right) + \mathcal{O} \left(\sum_{j=1}^k (L_j - 1) \cdot (rO)^2 \right) \\ & = \mathcal{O} \left(r \left[m^2 + r^2 + \sum_{j=1}^k (L_j - 1) \cdot mO \right] \right) \end{aligned} \quad (\text{H.8})$$

(b) **Our Spatial NNGP Prior in Section 4 Adopted (After)**

Without Slice Sampling

$$\mathcal{O}(rh^3) + \mathcal{O}(r) + \mathcal{O}(O^3) + \mathcal{O}(k(L-1) \cdot r \cdot hO) + \mathcal{O}(k(L-1) \cdot r \cdot O^2) = \mathcal{O}(r[h^3 + k(L-1)O(h+O)] + O^3) \quad (\text{H.9})$$

With Slice Sampling

$$\begin{aligned} & \mathcal{O}(rh^3) + \mathcal{O}(r) + \mathcal{O}(O^3) + \mathcal{O}\left(\sum_{j=1}^k (L_j - 1) \cdot r \cdot hO\right) + \mathcal{O}\left(\sum_{j=1}^k (L_j - 1) \cdot r \cdot O^2\right) \\ &= \mathcal{O}\left(r \left[h^3 + \sum_{j=1}^k (L_j - 1) \cdot O(h+O) \right] + O^3\right) \end{aligned} \quad (\text{H.10})$$

H.3 Posterior Sampling Computational Acceleration Brought About by Our Sequential Updating Methods in Section 4.4 (with spatial NNGP)

Place of Scalability Improvements		Computational Acceleration for the Posterior Sampling Step of α_{jl_j} 's for all (j, l_j)	
		Without Slice Sampling	With Slice Sampling
Key Quantities Concerned		$[I_{mO} + \tilde{F}(\rho)^{-1} \otimes \kappa^{-1}]^{-1}$, $\text{Chol}([I_{mO} + \tilde{F}(\rho)^{-1} \otimes \kappa^{-1}]^{-1})$	$\text{Chol}(\tilde{F}(\rho) \otimes \kappa)$ and n_{jl_j} 's for mO -variate rejection sampling
Overall Order of Standard	Before	$\mathcal{O}(m^3) + \mathcal{O}(k(L-1) \cdot (mO)^2) = \mathcal{O}(m^3)$	$\mathcal{O}(m^3) + \mathcal{O}\left(\sum_{j=1}^k \sum_{l_j=1}^{L_j-1} [k_{jl_j} \cdot mO + n_{jl_j} \cdot (mO)^2]\right) > \mathcal{O}(m^3)$
Computational Complexity	After	$\mathcal{O}(m[k(L-1)hO(h+O) + O^3]) = \mathcal{O}(m)$ if $L \ll m$	$\mathcal{O}\left(O \left\{ \sum_{j=1}^k \left[(L_j - 1)mh(h+O) + \sum_{l_j=1}^{L_j-1} \sum_{i=1}^m (k_{jl_j i}^* + n_{jl_j i}^* \cdot O) \right] + O^2 \right\}\right)$
References	Section(s)	Section 4.4	
	Equations	Equations (4.6) and (4.8)	Equations (4.7) and (4.9)

Table H.3: A theoretical summary table of posterior sampling computation acceleration further brought about by our sequential updating methods in Section 4.4 on top of imposing our spatial NNGP prior (Section 4) with or without slice sampling (Section 3). Our simulation experiments comparing NNGPblockFixedL and NNGPsequFixedL should lead to results corresponding well to the table in terms of main model fitting time for α_{jl_j} 's.

Suppose we have a large m . Recall that $1 \leq L$ or L_j 's $\leq m$ and that we have assumed $O, h, k \ll m$. When slice sampling (Section 3) is adopted without our sequential updating method, rejection sampling from a high-dimensional truncated mO -variate normal distribution (Equation (4.7)) gets unbearably slow for feasible computation when m gets large, as a very small acceptance rate leads to a huge number $n_{jl_j} \in \mathbb{N}$ of draws from $N_{mO}(\mathbf{0}, \tilde{F}(\rho) \otimes \kappa)$ required per sample of α_{jl_j} for each (j, l_j) . When m is large, we typically have $n_{jl_j}(m) \gg m$ for any (j, l_j) . With our spatial NNGP prior coupled with sequential updates, rejection sampling from low-dimensional truncated O -variate normal distributions would have adequate acceptance rates and thus small required numbers $n_{jl_j i}^*$'s of draws from $N_O(V_{s_i} \mu_{jl_j, s_i}, V_{s_i})$'s (Equation (4.9) in Section 4.4) per sample of $\alpha_{jl_j}(s_i)$'s. If $\max_{j \in \{1, \dots, k\}} L_j \ll m$, $\max_{(j, l_j, i)} k_{jl_j i}^* \ll m$, and $\max_{(j, l_j, i)} n_{jl_j i}^* \ll m$, then

$$\mathcal{O}\left(O \left\{ \sum_{j=1}^k \left[(L_j - 1)mh(h+O) + \sum_{l_j=1}^{L_j-1} \sum_{i=1}^m (k_{jl_j i}^* + n_{jl_j i}^* \cdot O) \right] + O^2 \right\}\right) = \mathcal{O}(m).$$

H.4 An Overall Scalability Improvements Summary for Our Three Novelties

Suppose we have a large m . Recall that $1 \leq L$ or L_j 's $\leq m$ and that we have assumed $O, h, k, p \ll m$. We also assume $r < m$ for spatial prediction at $r \in \mathbb{N}$ new locations $\mathbf{s}_{(m+1):(m+r)}$. Let $N \in \mathbb{N}$ be the number of kept post-burn-in MCMC iterations. We denote the corresponding estimated number(s) of spatial mixture components as $L_j^{(t_i)}$'s, $j \in \{1, \dots, k\}$, $i \in \{1, \dots, N\}$. In Table H.4, storage requirements for spatial prediction and clustering correspond to all kept MCMC iterations, whereas computational complexity orders are only for one typical MCMC iteration.

Simulation Method		fullGPfixedL	NNGPblockFixedL	NNGPsequenFixedL	NNGPsequenVaryLj
Spatial NNGP Prior		No	Yes	Yes	Yes
Sequential Updating Methods		No	No	Yes	Yes
Slice Sampling Approach		No	No	No	Yes
Spatial Prediction Speed for $\hat{\alpha}_{j t_j}(s_{(m+1):(m+r)}) \alpha_{j t_j}(s_{1:m}), \kappa, \rho^*s$		$\mathcal{O}(r[m^2 + r^2 + k(L-1)mO])$	$\mathcal{O}(r[h^3 + k(L-1)O(h+O)] + O^3)$		$\mathcal{O}\left(r\left[h^3 + \sum_{j=1}^k (L_j - 1) \cdot O(h+O)\right] + O^3\right)$
Posterior Sampling Speed for	ρ and $\kappa_{O \times O}$	$\mathcal{O}(m^3)$	$\mathcal{O}(\{k(L-1)O^2[h^2 + h + 1] + h^3\}m)$		$\mathcal{O}\left(\left\{\sum_{j=1}^k (L_j - 1) \cdot O^2[h^2 + h + 1] + h^3\right\}m\right)$
	$\alpha_{j t_j}^o(s_i)$'s	$\mathcal{O}(m^3)$		$\mathcal{O}(m[k(L-1)hO(h+O) + O^3])$	$\mathcal{O}\left(O\left\{\sum_{j=1}^k (L_j - 1)mh(h+O) + \sum_{t_j=1}^{L_j-1} \sum_{i=1}^m (k_{j t_j}^* + n_{j t_j}^* \cdot O)\right\} + O^2\right)\right)$
	$z_{j t_j}^o(s_i)$'s or $u_{j t_j}^o(s_i)$'s	$\mathcal{O}(kLmO)$		$\mathcal{O}(kmO)$	
	$\delta_{1:k}, \theta_{j t_j}$'s, and $\xi_j^o(s_i)$'s	$\mathcal{O}(kLmOT(p+k))$ (absolute highest order from $\xi_j^o(s_i)$'s)		$\mathcal{O}\left(\sum_{j=1}^k L_j \cdot mOT(p+k)\right)$ (absolute highest order from $\xi_j^o(s_i)$'s)	
Storage Requirements for	$F(\rho)$ and $F(\rho)^{-1}$	$\mathcal{O}(m^2)$	$\mathcal{O}(mh^2)$		
	Spatial Prediction	$\mathcal{O}(NmOkL)$			$\mathcal{O}\left(mO \sum_{i=1}^N \sum_{j=1}^k L_j^{(t_i)}\right)$
Spatial Clustering					

Table H.4: An overall theoretical summary table of scalability improvements brought about by our 3 novelties. For each of the four methods implemented in our simulation experiments, we list its computational complexity orders for involved Gibbs sampler steps in posterior sampling and a major spatial prediction procedure. We also present memory requirements for two key quantities and spatial prediction & clustering under our four methods.

I Complementary Simulation Results and Experiments

I.1 Further Details of the Toy Example in Section 2

We present additional technical details and results for the toy example in Section 2. All our four methods' converged posterior deviances are comparable to that of `spBFAL10` and clearly better than that of `spBFALInf`; see Figure I.1.

To get a more complete picture of all methods' diverse model fitting performances, we further consider some diagnostic statistics below. We first devise some diagnostic metrics based on in-sample prediction. Let $N = m_0 \times O \times T_0$, where $m_0 = 352$, $O = 1$, and $T_0 = 300$, and denote \mathbf{y}_{obs} as our $N \times 1$ observed outcome vector. For each of the kept $W = 5000$ post-burn-in MCMC iterations, we draw a predicted outcome vector $\hat{\mathbf{y}}_{N \times 1}^{(w)}$, $w \in \{1, \dots, W\}$, based on the w^{th} sampled posterior parameters. Let

$$\text{postMeanMSE} = \frac{1}{m_0 O T_0} \sum_{t=1}^{T_0} \sum_{o=1}^O \sum_{i=1}^{m_0} \left(\left[\frac{1}{W} \sum_{w=1}^W \hat{y}^{(w)}(i, o, t) \right] - y_{\text{obs}}(i, o, t) \right)^2,$$

$$\text{postMSE} = \frac{1}{m_0 O T_0} \sum_{t=1}^{T_0} \sum_{o=1}^O \sum_{i=1}^{m_0} \left\{ \frac{1}{W} \sum_{w=1}^W \left[\hat{y}^{(w)}(i, o, t) - y_{\text{obs}}(i, o, t) \right]^2 \right\},$$

$$\text{postVar} = \frac{1}{m_0 O T_0} \sum_{t=1}^{T_0} \sum_{o=1}^O \sum_{i=1}^{m_0} \text{Var} \left(\hat{\mathbf{y}}^{(1:W)}(i, o, t) \right), \text{ and } \text{dinf} = \text{postMeanMSE} + \text{postVar}.$$

Then `postMeanMSE` and `postMSE` adequately assess the model fitting accuracy, and `postVar` is an appropriate precision measure. Small values for the four statistics are desired. We further consider two sets of diagnostic statistics based on the posterior mean estimates and all 5000 kept iterations' posterior parameter estimates, both of which stem from the posterior log-likelihoods and incorporate goodness-of-fit assessments as well as over-complexity penalty terms. The main deviance information criterion DIC statistic `dic` (Spiegelhalter et al. 2002) can be written as the sum of two values, one of which portrays model complexity and is denoted as `pD`. The Watanabe–Akaike information criterion WAIC (Vehtari, Gelman, and Gabry 2017) consists of two over-fit measurements `p_waic_1`, `p_waic_2`, a log predictive density `lppd`, and a main metric `waic = -2lppd + 2p_waic_2`. For all involved metrics except `lppd`, smaller values imply better model fitting.

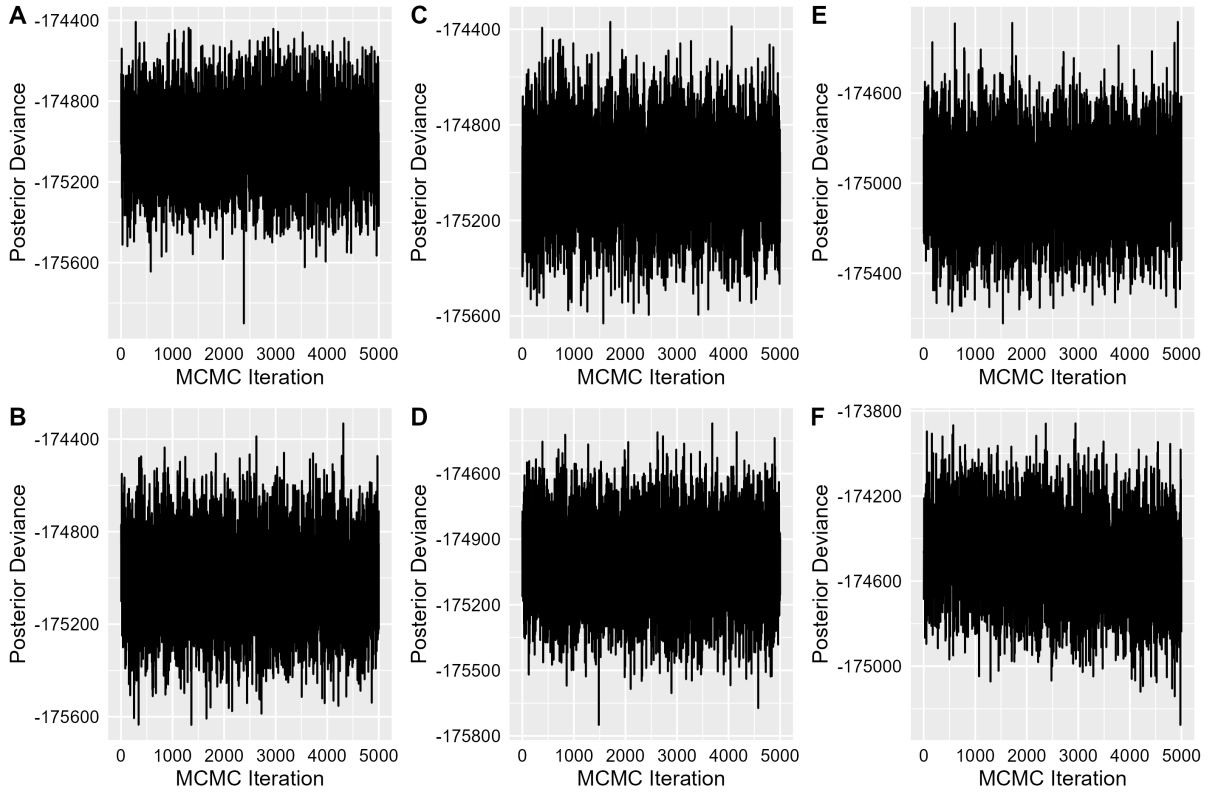


Figure I.1: Posterior deviance plots for `fullGPfixedL` (A), `NNGPblockFixedL` (B), `NNGPsequenFixedL` (C), `NNGPsequenVaryLj` (D), and `spBFAL10` (E), `spBFALInf` (F). For each of the six trace plots, the horizontal axis denotes the kept $20000 \div 4 = 5000$ post-burn-in MCMC iterations, and the vertical axis presents the corresponding posterior deviance values.

Table I.1 reassures us that our four methods deliver comparable satisfactory model fitting performances. `spBFAL10` results in similarly good diagnostic statistics, while `spBFALInf` produces the conspicuous worst metric values.

We construct the following three temporal prediction metrics to assess the performance in predicting at the $q = 10$ future time points $t = 301, 302, \dots, 310$ for all $m_0 = 352$ training

Model	fullGPfixedL	NNGPblockFixedL	NNGPsequenFixedL	NNGPsequenVaryLj	spBFAL10	spBFALInf
postMeanMSE	0.009917465	0.009917465	0.009917531	0.00991737	0.009916747	0.009972942
postMSE	0.02668247	0.02668144	0.02668167	0.02668039	0.02668312	0.02679888
postVar	0.01676836	0.01676733	0.0167675	0.01676638	0.01677255	0.01683156
dinf	0.02668582	0.0266848	0.02668503	0.02668375	0.0266893	0.0268045
pD	621.2673	663.04	646.9392	662.9201	564.7672	557.425
dic	-174384.7	-174345.7	-174361.8	-174348	-174440.4	-173945.4
p.waic.1	878.4693	611.0213	605.4927	721.9712	600.7735	756.1147
p.waic.2	9000.328	8772.018	8705.174	8917.304	9093.332	9281.774
lppd	87942.2	87809.87	87807.12	87866.43	87802.98	87629.49
waic	-157883.7	-158075.7	-158203.9	-157898.2	-157419.3	-156695.4

Table I.1: Values of ten diagnostic statistics in the toy example. Each method uses $W = 20000 \div 4 = 5000$ kept post-burn-in MCMC iterations for analysis.

locations:

$$\begin{aligned}
\text{postMeanMSE} &= \frac{1}{qOm_0} \sum_{t=T_0+1}^{T_0+q} \sum_{i=1}^{m_0} \sum_{o=1}^O \left(\left[\frac{1}{W} \sum_{w=1}^W \hat{y}^{(w)}(t, o, i) \right] - y_{\text{actual}}(t, o, i) \right)^2, \\
\text{postMSE} &= \frac{1}{qOm_0} \sum_{t=T_0+1}^{T_0+q} \sum_{i=1}^{m_0} \sum_{o=1}^O \left\{ \frac{1}{W} \sum_{w=1}^W \left[\hat{y}^{(w)}(t, o, i) - y_{\text{actual}}(t, o, i) \right]^2 \right\}, \text{ and} \\
\text{postVar} &= \frac{1}{qOm_0} \sum_{t=T_0+1}^{T_0+q} \sum_{i=1}^{m_0} \sum_{o=1}^O \text{Var} \left(\hat{\mathbf{y}}^{(1:W)}(t, o, i) \right).
\end{aligned}$$

For each (t, o, i, w) , $\hat{y}^{(w)}(t, o, i)$ represents our out-of-sample predicted outcome for observation type o at location \mathbf{s}_i and time t based on the w^{th} kept post-burn-in MCMC iteration's posterior parameter estimates, and $y_{\text{actual}}(t, o, i)$ is the corresponding actual observed outcome value in the testing data set not utilized when fitting the models. As in Table I.2, spBFALInf produces considerably worse future-time prediction than all other methods. Among our 4 methods and spBFAL10, NNGPsequenFixedL appears to be the best, followed by fullGPfixedL, NNGPblockFixedL, NNGPsequenVaryLj, and finally spBFAL10.

Model	fullGPfixedL	NNGPblockFixedL	NNGPsequenFixedL	NNGPsequenVaryLj	spBFAL10	spBFALInf
postMeanMSE	3.749685	3.753012	3.729849	3.728981	4.009299	11.55326
postMSE	18.518662	18.754345	18.299211	19.340736	19.409493	164.42639
postVar	14.771932	15.004334	14.572277	15.614878	15.403274	152.90371

Table I.2: Temporal prediction metrics in the toy example. Smaller values for the three metrics imply better prediction capability at future time points.

We utilize similar spatial prediction metrics to assess the prediction performance at the $r = 9$ testing spatial locations for all training time points $t = 1, 2, \dots, T_0 = 300$:

$$\begin{aligned}
\text{postMeanMSE} &= \frac{1}{rOT_0} \sum_{i_r=1}^r \sum_{t=1}^{T_0} \sum_{o=1}^O \left(\left[\frac{1}{W} \sum_{w=1}^W \hat{y}^{(w)}(i_r, o, t) \right] - y_{\text{actual}}(i_r, o, t) \right)^2, \\
\text{postMSE} &= \frac{1}{rOT_0} \sum_{i_r=1}^r \sum_{t=1}^{T_0} \sum_{o=1}^O \left\{ \frac{1}{W} \sum_{w=1}^W \left[\hat{y}^{(w)}(i_r, o, t) - y_{\text{actual}}(i_r, o, t) \right]^2 \right\}, \text{ and}
\end{aligned}$$

$$\text{postVar} = \frac{1}{rOT_0} \sum_{i_r=1}^r \sum_{t=1}^{T_0} \sum_{o=1}^O \text{Var} \left(\hat{\mathbf{y}}^{(1:W)}(i_r, o, t) \right).$$

For each (i_r, o, t, w) , $\hat{\mathbf{y}}^{(w)}(i_r, o, t)$ represents our out-of-sample predicted outcome for observation type o at location \mathbf{s}_{i_r} and time t based on the w^{th} kept post-burn-in MCMC iteration's posterior parameter estimates, and $y_{\text{actual}}(i_r, o, t)$ is the corresponding actual observed outcome value in the testing data set not utilized when fitting the models. All spatial prediction metrics are appropriately small (Table I.3). NNGPsequenVaryLj appears to be the best, followed by NNGPblockFixedL, fullGPfixedL, and finally NNGPsequenFixedL.

We also recorded the time required to obtain $\hat{\alpha}(\mathbf{s}_{(m_0+1):m})$ given $\alpha(\mathbf{s}_{1:m_0})$, κ , ρ and to obtain $\hat{\mathbf{w}}(\mathbf{s}_{(m+1):(m+r)})$, $\hat{\xi}(\mathbf{s}_{(m+1):(m+r)})$, and $\hat{\Lambda}(\mathbf{s}_{(m+1):(m+r)})$ from $\hat{\alpha}(\mathbf{s}_{(m_0+1):m})$ and the kept posterior samples of θ_{jl_j} 's (alphaKrigTime and weightsXiLambdaKrigTime). The results (Table I.3) correspond well to what we have derived in Appendix H and obtained in Section 6.2 (Figure 6.2). alphaKrigTime corresponding to NNGPblockFixedL and NNGPsequenFixedL are close and more than 20 times smaller than that of fullGPfixedL. alphaKrigTime corresponding to NNGPsequenVaryLj is even smaller. weightsXiLambdaKrigTime corresponding to NNGPsequenVaryLj is smaller than their counterparts from the other three methods.

Model	fullGPfixedL	NNGPblockFixedL	NNGPsequenFixedL	NNGPsequenVaryLj
postMeanMSE	2.511976	2.478452	2.658194	2.476308
postMSE	14.123149	14.003086	14.341286	12.764447
postVar	11.613496	11.526939	11.685429	10.290197
alphaKrigTime	63.988	2.838	2.888	2.492
weightsXiLambdaKrigTime	0.118	0.129	0.139	0.076

Table I.3: Spatial prediction metrics and time required (in seconds) for the two major spatial prediction steps in the toy example. Smaller values for the three metrics imply better prediction capability at new spatial locations.

For each of our four methods, we performed k-means clustering on three posterior weights matrices formulated from 10, 100, and 1000 selected equally dispersed post-burn-in MCMC iterations' parameter estimates, as described by the last paragraph in Section 5.2. Since we specified only 2 actual spatial groups and k-means clusters, there is no label-switching issue. Reassuringly, all clustering outcomes we obtained from all our four methods agree exactly with the actual spatial groupings and are thus completely accurate.

I.2 Additional Tables of Recorded Posterior Sampling Time for Section 6.1

Model Setting		bfa_sp() from spBFA with a finite $L = 50$	bfa_sp() from spBFA with $L = \text{Inf}$
$T = 30$	$m = 400$	1.41 days	10.21 hours
	$m = 900$	18.5 days	3.83 days
	$m = 1600$	> 3 months	24.34 days
$T = 50$	$m = 400$	1.48 days	11.21 hours
	$m = 900$	18.66 days	4.63 days
	$m = 1600$	> 3 months	25.72 days

Table I.4: Total model fitting time by **spBFA**'s finite mixture and infinite mixture models with 2×10^4 burn-in and 10^4 post-burn-in MCMC iterations under 6 different pairs of (m, T) values.

Model Parameter	fullGPFixedL	NNGPblockFixedL	NNGPsequenFixedL	NNGPsequenVaryLj
ρ	48.8606	7.0378	7.1372	5.28
κ	17.0116	2.9992	3.0006	≈ 1
$\alpha_{jl_j}^o(\mathbf{s}_i)$'s	67.0654	65.0538	87.1808	188.1246
$z_{jl_j}^o(\mathbf{s}_i)$'s or $u_j^o(\mathbf{s}_i)$'s	219.643	147.0992	148.0586	≈ 0
$\xi_j^o(\mathbf{s}_i)$'s	24.7242	24.4538	24.247	4.1488
θ_{jl_j} 's	3.0336	3.1326	3.1088	2.297
$\delta_{1:k}$	4×10^{-4}	≈ 0	6×10^{-4}	≈ 0

Table I.5: Average sampling time per MCMC iteration (in milliseconds) corresponding to the 7 spatial-related parameters ρ , κ , $\alpha_{jl_j}^o(\mathbf{s}_i)$'s, $z_{jl_j}^o(\mathbf{s}_i)$'s or $u_j^o(\mathbf{s}_i)$'s, $\xi_j^o(\mathbf{s}_i)$'s, θ_{jl_j} 's, and $\delta_{1:k}$ across all 5000 post-burn-in MCMC iterations for our four methods with $(m, T) = (400, 30)$.

Model Parameter	fullGPFixedL	NNGPblockFixedL	NNGPsequenFixedL	NNGPsequenVaryLj
ρ	49.7274	7.1076	7.53	5.7782
κ	17.0162	2.9856	3.0002	≈ 1
$\alpha_{jl_j}^o(\mathbf{s}_i)$'s	67.723	63.7966	85.1594	207.3494
$z_{jl_j}^o(\mathbf{s}_i)$'s or $u_j^o(\mathbf{s}_i)$'s	211.5018	180.8608	183.3338	≈ 0
$\xi_j^o(\mathbf{s}_i)$'s	35.9726	36.1242	35.6472	6.1232
θ_{jl_j} 's	18.431	18.7772	18.6408	18.242
$\delta_{1:k}$	6×10^{-4}	2×10^{-4}	≈ 0	≈ 0

Table I.6: Average sampling time per MCMC iteration (in milliseconds) corresponding to the 7 spatial-related parameters ρ , κ , $\alpha_{jl_j}^o(\mathbf{s}_i)$'s, $z_{jl_j}^o(\mathbf{s}_i)$'s or $u_j^o(\mathbf{s}_i)$'s, $\xi_j^o(\mathbf{s}_i)$'s, θ_{jl_j} 's, and $\delta_{1:k}$ across all 5000 post-burn-in MCMC iterations for our four methods with $(m, T) = (400, 50)$.

Model Parameter	fullGPFixedL	NNGPblockFixedL	NNGPsequenFixedL	NNGPsequenVaryLj
ρ	308.928	27.1156	26.7362	22.1778
κ	93.9964	8.1494	8.8828	4.0032
$\alpha_{jl_j}^o(\mathbf{s}_i)$'s	455.3278	423.2304	197.8944	282.4816
$z_{jl_j}^o(\mathbf{s}_i)$'s or $u_j^o(\mathbf{s}_i)$'s	324.7298	335.7746	328.3926	≈ 0
$\xi_j^o(\mathbf{s}_i)$'s	54.7586	57.1688	55.633	8.1984
θ_{jl_j} 's	8.6664	8.8824	8.8414	6.9156
$\delta_{1:k}$	0.9486	0.9938	0.9842	0.0406

Table I.7: Average sampling time per MCMC iteration (in milliseconds) corresponding to the 7 spatial-related parameters ρ , κ , $\alpha_{jl_j}^o(\mathbf{s}_i)$'s, $z_{jl_j}^o(\mathbf{s}_i)$'s or $u_j^o(\mathbf{s}_i)$'s, $\xi_j^o(\mathbf{s}_i)$'s, θ_{jl_j} 's, and $\delta_{1:k}$ across all 5000 post-burn-in MCMC iterations for our four methods with $(m, T) = (900, 30)$.

Model Parameter	fullGPFixedL	NNGPblockFixedL	NNGPsequenFixedL	NNGPsequenVaryLj
ρ	323.9814	28.1102	31.7456	26.6904
κ	95.9408	8.467	9.0628	4.0716
$\alpha_{jl_j}^o(\mathbf{s}_i)$'s	466.1494	423.1224	198.8446	406.3786
$z_{jl_j}^o(\mathbf{s}_i)$'s or $u_j^o(\mathbf{s}_i)$'s	389.276	533.31	541.5196	4×10^{-4}
$\xi_j^o(\mathbf{s}_i)$'s	82.7366	84.2434	84.5774	12.1992
θ_{jl_j} 's	43.8958	44.263	44.3988	42.588
$\delta_{1:k}$	1.008	1.0006	1.0018	0.8306

Table I.8: Average sampling time per MCMC iteration (in milliseconds) corresponding to the 7 spatial-related parameters ρ , κ , $\alpha_{jl_j}^o(\mathbf{s}_i)$'s, $z_{jl_j}^o(\mathbf{s}_i)$'s or $u_j^o(\mathbf{s}_i)$'s, $\xi_j^o(\mathbf{s}_i)$'s, θ_{jl_j} 's, and $\delta_{1:k}$ across all 5000 post-burn-in MCMC iterations for our four methods with $(m, T) = (900, 50)$.

Model Parameter	fullGPFixedL	NNGPblockFixedL	NNGPsequenFixedL	NNGPsequenVaryLj
ρ	1477.033	93.8578	101.1084	95.6168
κ	316.5146	20.362	20.5866	12.4996
$\alpha_{jl_j}^o(\mathbf{s}_i)$'s	2358.661	2083.491	353.8104	604.7246
$z_{jl_j}^o(\mathbf{s}_i)$'s or $u_j^o(\mathbf{s}_i)$'s	604.8164	582.528	574.3044	1.5622
$\xi_j^o(\mathbf{s}_i)$'s	101.5026	100.3484	98.4202	17.5796
θ_{jl_j} 's	26.311	18.127	17.8028	15.6692
$\delta_{1:k}$	3.2974	3.2024	3.0554	2.307

Table I.9: Average sampling time per MCMC iteration (in milliseconds) corresponding to the 7 spatial-related parameters ρ , κ , $\alpha_{jl_j}^o(\mathbf{s}_i)$'s, $z_{jl_j}^o(\mathbf{s}_i)$'s or $u_j^o(\mathbf{s}_i)$'s, $\xi_j^o(\mathbf{s}_i)$'s, θ_{jl_j} 's, and $\delta_{1:k}$ across all 5000 post-burn-in MCMC iterations for our four methods with $(m, T) = (1600, 30)$.

Model Parameter	fullGPFixedL	NNGPblockFixedL	NNGPsequenFixedL	NNGPsequenVaryLj
ρ	1442.891	96.4844	105.1648	93.5652
κ	315.5866	21.5504	21.8626	12.9298
$\alpha_{jl_j}^o(\mathbf{s}_i)$'s	2306.249	2113.644	362.944	774.4342
$z_{jl_j}^o(\mathbf{s}_i)$'s or $u_j^o(\mathbf{s}_i)$'s	723.9746	635.5834	714.0948	2.1136
$\xi_j^o(\mathbf{s}_i)$'s	151.4386	152.5778	152.0324	15.0362
θ_{jl_j} 's	82.9466	83.4584	82.454	77.637
$\delta_{1:k}$	3.869	3.963	3.8754	2.9812

Table I.10: Average sampling time per MCMC iteration (in milliseconds) corresponding to the 7 spatial-related parameters ρ , κ , $\alpha_{jl_j}^o(\mathbf{s}_i)$'s, $z_{jl_j}^o(\mathbf{s}_i)$'s or $u_j^o(\mathbf{s}_i)$'s, $\xi_j^o(\mathbf{s}_i)$'s, θ_{jl_j} 's, and $\delta_{1:k}$ across all 5000 post-burn-in MCMC iterations for our four methods with $(m, T) = (1600, 50)$.

Model Parameter	fullGPFixedL	NNGPblockFixedL	NNGPsequenFixedL	NNGPsequenVaryLj
ρ	1675.367	97.143	106.6914	98.423
κ	317.7624	21.976	22.5796	14.403
$\alpha_{jl_j}^o(\mathbf{s}_i)$'s	2319.485	2124.528	365.9912	1002.139
$z_{jl_j}^o(\mathbf{s}_i)$'s or $u_j^o(\mathbf{s}_i)$'s	1484.252	1155.679	1090.681	3.056
$\xi_j^o(\mathbf{s}_i)$'s	286.3702	286.3756	286.3248	21.3178
θ_{jl_j} 's	317.6382	320.3912	321.6182	320.9168
$\delta_{1:k}$	4.032	4.0894	4.052	3.132

Table I.11: Average sampling time per MCMC iteration (in milliseconds) corresponding to the 7 spatial-related parameters ρ , κ , $\alpha_{jl_j}^o(\mathbf{s}_i)$'s, $z_{jl_j}^o(\mathbf{s}_i)$'s or $u_j^o(\mathbf{s}_i)$'s, $\xi_j^o(\mathbf{s}_i)$'s, θ_{jl_j} 's, and $\delta_{1:k}$ across all 5000 post-burn-in MCMC iterations for our four methods with $(m, T) = (1600, 100)$.

Model Parameter	fullGPFixedL	NNGPblockFixedL	NNGPsequenFixedL	NNGPsequenVaryLj
ρ	25448.17	883.873	814.5748	793.9108
κ	3683.99	170.5392	164.9444	143.551
$\alpha_{jl_j}^o(\mathbf{s}_i)$'s	35893.15	22407.43	953.6206	2154.113
$z_{jl_j}^o(\mathbf{s}_i)$'s or $u_j^o(\mathbf{s}_i)$'s	3819.395	2618.505	2692.092	55.5604
$\xi_j^o(\mathbf{s}_i)$'s	542.3482	425.6026	403.9276	88.806
θ_{jl_j} 's	336.3604	242.8858	241.8212	234.8754
$\delta_{1:k}$	72.5452	58.4904	57.489	55.0086

Table I.12: Average sampling time per MCMC iteration (in milliseconds) corresponding to the 7 spatial-related parameters ρ , κ , $\alpha_{jl_j}^o(\mathbf{s}_i)$'s, $z_{jl_j}^o(\mathbf{s}_i)$'s or $u_j^o(\mathbf{s}_i)$'s, $\xi_j^o(\mathbf{s}_i)$'s, θ_{jl_j} 's, and $\delta_{1:k}$ across all 5000 post-burn-in MCMC iterations for our four methods with $(m, T) = (3600, 50)$.

Model Parameter	fullGPFixedL	NNGPblockFixedL	NNGPsequenFixedL	NNGPsequenVaryLj
ρ	24744.63	879.0884	805.6914	788.5346
κ	3607.779	170.1582	162.2748	142.3264
$\alpha_{jl_j}^o(\mathbf{s}_i)$'s	35275.15	22316.23	941.9378	2442.089
$z_{jl_j}^o(\mathbf{s}_i)$'s or $u_j^o(\mathbf{s}_i)$'s	4460.977	2677.307	2687.017	56.1756
$\xi_j^o(\mathbf{s}_i)$'s	909.047	713.57	681.1242	99.2364
θ_{jl_j} 's	1359.953	779.6124	788.5526	787.6832
$\delta_{1:k}$	73.2364	59.2832	57.5628	55.5148

Table I.13: Average sampling time per MCMC iteration (in milliseconds) corresponding to the 7 spatial-related parameters ρ , κ , $\alpha_{jl_j}^o(\mathbf{s}_i)$'s, $z_{jl_j}^o(\mathbf{s}_i)$'s or $u_j^o(\mathbf{s}_i)$'s, $\xi_j^o(\mathbf{s}_i)$'s, θ_{jl_j} 's, and $\delta_{1:k}$ across all 5000 post-burn-in MCMC iterations for our four methods with $(m, T) = (3600, 100)$.

I.3 Accuracy for Spatial Clustering of Temporal Trends

We design and implement a simulation experiment to demonstrate our four methods' satisfactory performances regarding our prime goal of clustering spatial locations into regions with similar temporal trajectories.

We adopted a data generation mechanism specifically designed to assess clustering accuracy. The number of factors was set to $k = 2$, and the actual numbers of clusters for both factors were also set to 2. We specified $\theta_{11} = \theta_{12} = 5$, $\theta_{21} = 10$, and $\theta_{22} = -10$ for the atoms θ_{jl_j} 's. $m = 10^2 = 100$ spatial points $\mathbf{s}_i = (i_1, i_2)$ for $i = 1, 2, \dots, 100$ on an equispaced 2-dimensional grid, where $i_1, i_2 \in \{1, 2, \dots, 10\}$ satisfy $10 \cdot (i_1 - 1) + i_2 = i$ for each i , were assigned to two actual spatial groups (one corresponding to $(\theta_{11}, \theta_{21}) = (5, 10)$ and the other corresponding to $(\theta_{12}, \theta_{22}) = (5, -10)$) as depicted in Figure I.4. All other settings are almost identical to their counterparts in Section 6.1. We set $O = 1$, $\psi = 2.3$, $\sigma^2(\mathbf{s}_i) = 0.01$ for all i and specified $T = 30$ time points $t = 1, \dots, 30$. When fitting the models, 10 is specified as both L and an upper bound to all L_j 's. A burn-in length of 20000 and a post-burn-in length of 10000 (thinned to 5000) were used throughout.

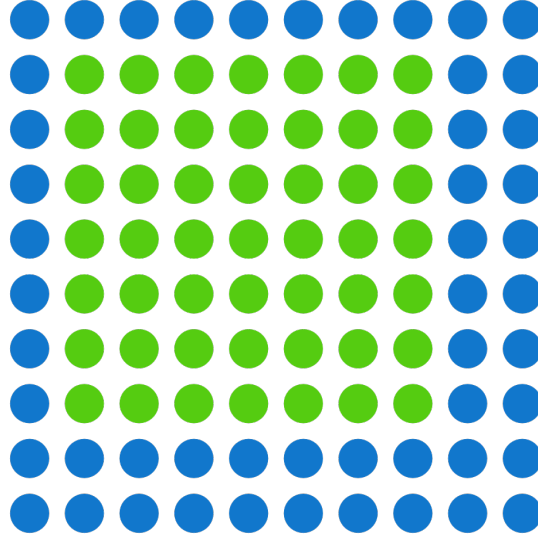


Figure I.2: The actual spatial grouping for Appendix I.3. The two colors represent the two groups for our $m = 10^2 = 100$ spatial locations.

For each of our $N = 100$ simulated data sets and each of the four methods, we performed k-means clustering on three posterior weights matrices formulated from 10, 100, and 1000 selected equally dispersed kept post-burn-in MCMC iterations' parameter estimates, as described by the last paragraph in Section 5.2. Since we specified only 2 actual spatial groups and k-means clusters, there are no label-switching issues. Reassuringly, the $N \times 3 \times 3$ clustering outcomes we obtained from three of our four methods, `fullGPfixedL`, `NNGPblockFixedL`, and `NNGPsequenFixedL`, all agree exactly with Figure I.4 and are thus completely accurate. The fourth method, `NNGPsequenVaryLj`, also produces mean accuracy ratios of 0.9758, 0.9778, 0.9781 and mean rand indices of 0.9604242, 0.9621333, 0.9625717, which all indicate highly accurate clustering results.

I.4 VAR(1) for the Latent Temporal Factors $\eta_{1:T}$

We fitted `fullGPfixedL`, `NNGPblockFixedL`, `NNGPsequenFixedL`, and `NNGPsequenVaryLj` under a VAR(1) structure for the latent temporal factors $\eta_{1:T}$ on two sets of simulated data. The posterior sampling algorithm has been described in Appendix C.

We first adopted the data generation mechanism in Section 6.1 with $(m, T) = (225, 200)$. We ran 80000 burn-in and 20000 post-burn-in (thinned to 10000) MCMC iterations for our four methods, which took 23.99 hours, 1.05 days, 1.05 days, and 18.24 hours, respectively, and resulted in satisfactory diagnostics statistics (Table I.14) and posterior deviances (Figure I.3).

Model	fullGPfixedL	NNGPblockFixedL	NNGPsequenFixedL	NNGPsequenVaryLj
postMeanMSE	0.009766762	0.009880694	0.009925439	0.0165475
postMSE	0.03064002	0.03112684	0.03108509	0.04475963
postVar	0.02087535	0.02124827	0.02116177	0.02821495
dinf	0.03064211	0.03112897	0.0310872	0.04476245
pD	985.3134	1081.714	1042.132	866.5728
dic	-68876.24	-67995.26	-68097.81	-51755.75
p_waic_1	634.8974	646.2995	744.9434	534.5163
p_waic_2	7075.576	7234.089	7385.461	5357.02
lppd	35248.22	34861.64	34942.44	26578.42
waic	-56345.3	-55255.1	-55113.96	-42442.8

Table I.14: VAR(1) temporal factors: Diagnostic statistics for $(m, T) = (225, 200)$, 80000 burn-in MCMC iterations, and 20000 post-burn-in MCMC iterations (thinned to 10000).

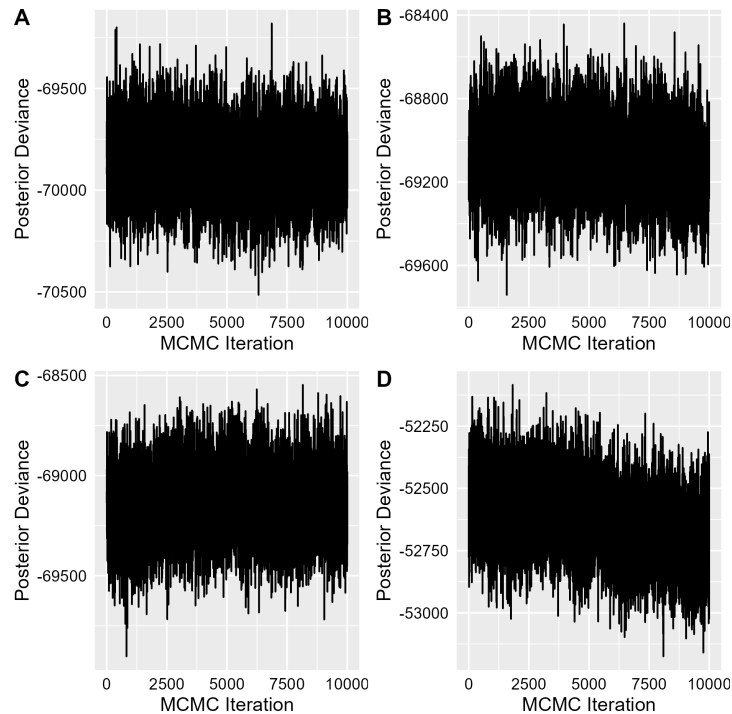


Figure I.3: VAR(1) temporal factors: Posterior deviances for `fullGPfixedL` (A), `NNGPblockFixedL` (B), `NNGPsequenFixedL` (C), and `NNGPsequenVaryLj` (D) under $(m, T) = (225, 200)$, 80000 burn-in MCMC iterations, and 20000 post-burn-in MCMC iterations (thinned to 10000).

We then used a data generation mechanism specifically designed to assess clustering accuracy. The number of factors was set to $k = 2$, and the actual numbers of clusters for both factors were also set to 2. We specified $\theta_{11} = \theta_{12} = 5$, $\theta_{21} = 10$, and $\theta_{22} = -10$ for the atoms θ_{jl_j} 's. $m = 10^2 = 100$ spatial points $\mathbf{s}_i = (i_1, i_2)$ for $i = 1, 2, \dots, 100$ on an equispaced 2-dimensional grid, where $i_1, i_2 \in \{1, 2, \dots, 10\}$ satisfy $10 \cdot (i_1 - 1) + i_2 = i$ for each i , were assigned to two actual spatial groups (one corresponding to $(\theta_{11}, \theta_{21}) = (5, 10)$ and the other corresponding to $(\theta_{12}, \theta_{22}) = (5, -10)$) as depicted in Figure I.4. All other settings are almost identical to their counterparts in Section 6.1. We set $O = 1$, $\psi = 2.3$, $\sigma^2(\mathbf{s}_i) = 0.01$ for all i and specified $T = 30$ time points $t = 1, \dots, 30$. When fitting the models, 10 is specified as both L and an upper bound to all L_j 's. A burn-in length of 20000 and a post-burn-in length of 10000 (thinned to 5000) were used. For each of our $N = 18$ simulated data sets and each of the four methods, we performed k-means clustering on three posterior weights matrices formulated from 10, 100, and 1000 selected equally dispersed kept post-burn-in MCMC iterations' parameter estimates, as described by the last paragraph in Section 5.2. Since we specified only 2 actual spatial groups and k-means clusters, we did not observe the label-switching issue. Reassuringly, the $N \times 3 \times 3$ clustering outcomes we obtained from three of our four methods, `fullGPfixedL`, `NNGPblockFixedL`, and `NNGPsequenFixedL`, all agree exactly with Figure I.4 and are thus completely accurate. The fourth method, `NNGPsequenVaryLj`, also produces mean accuracy ratios of 0.9538889, 0.9511111, 0.9722222 and mean rand indices of 0.9334119, 0.9288215, 0.9523008, which all indicate highly accurate clustering results.

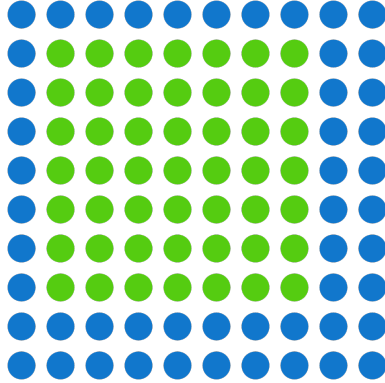


Figure I.4: VAR(1) temporal factors: The actual spatial clusters. The two colors represent the two groups for our $m = 10^2 = 100$ spatial locations.

I.5 Multiple Observation Types

We performed extensive simulation experiments with 2 observation types, i.e., $O = 2$, and the $O \times O$ matrix κ set as 0.7 times the 2×2 identity matrix. We adopted the same data generation mechanism and model fitting specifications as in Section 6.1 with four (m, T) pairs - $(100, 20)$, $(225, 20)$, $(225, 100)$, and $(400, 50)$ and 2×10^4 post-burn-in MCMC iterations (thinned to 10^4). Our four methods `fullGPfixedL`, `NNGPblockFixedL`, `NNGPsequenFixedL`, and `NNGPsequenVaryLj` lead to comparable satisfactory diagnostics statistics and posterior deviances. For the cases $(m, T) = (100, 20)$ and $(m, T) = (400, 50)$, the posterior deviances are plotted in Figures I.5 and I.6, and summaries of diagnostic metrics are in Tables I.15 and I.16.

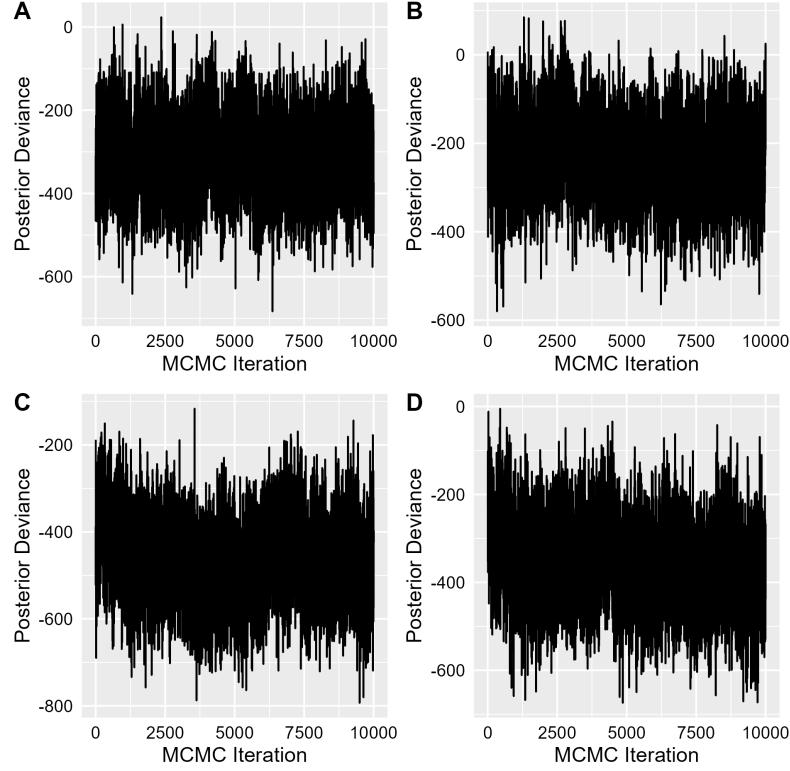


Figure I.5: Simulation for $O = 2$: Posterior deviances for `fullGPfixedL` (A), `NNGPblockFixedL` (B), `NNGPsequenFixedL` (C), and `NNGPsequenVaryLj` (D) under $(m, T) = (100, 20)$, 30000 burn-in MCMC iterations, and 20000 post-burn-in MCMC iterations (thinned to 10000). `NNGPsequenFixedL` appears to be the best, followed by `NNGPsequenVaryLj`, `fullGPfixedL`, and `NNGPblockFixedL`.

Model	<code>fullGPfixedL</code>	<code>NNGPblockFixedL</code>	<code>NNGPsequenFixedL</code>	<code>NNGPsequenVaryLj</code>
<code>postMeanMSE</code>	0.01718825	0.01856277	0.014993	0.01629108
<code>postMSE</code>	0.1533105	0.1553441	0.1478036	0.1514525
<code>postVar</code>	0.1361358	0.136795	0.1328239	0.1351749
<code>dinf</code>	0.1533241	0.1553578	0.1478169	0.151466
<code>pD</code>	-5516.225	-406.5968	-3493.642	-3.422094×10^{36}
<code>dic</code>	-5826.234	-640.621	-3957.715	-3.422094×10^{36}
<code>p_waic_1</code>	354.9216	327.6262	310.7777	299.9709
<code>p_waic_2</code>	1992.049	1910.587	2088.302	2091.322
<code>lppd</code>	332.4655	280.8252	387.425	328.4316
<code>waic</code>	3319.167	3259.524	3401.753	3525.781

Table I.15: Simulation for $O = 2$: Diagnostic statistics for $(m, T) = (100, 20)$, 30000 burn-in MCMC iterations, and 20000 post-burn-in MCMC iterations (thinned to 10000). The fixed number of clusters L is specified to be 30 for the first three methods, and a starting value and hence upper bound of 30 is assigned to all L_j 's for `NNGPsequenVaryLj`. `NNGPsequenFixedL` appears to be the best, followed by `NNGPsequenVaryLj`, `fullGPfixedL`, and `NNGPblockFixedL`.

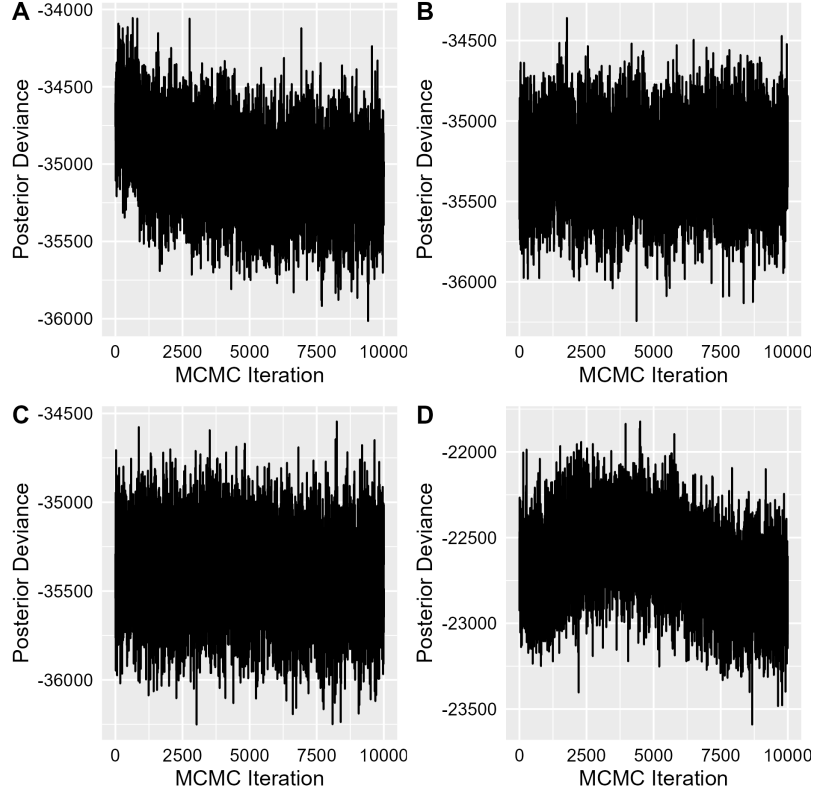


Figure I.6: Simulation for $O = 2$: Posterior deviances for `fullGPfixedL` (A), `NNGPblockFixedL` (B), `NNGPsequenFixedL` (C), and `NNGPsequenVaryLj` (D) under $(m, T) = (400, 50)$, 80000 burn-in MCMC iterations, and 20000 post-burn-in MCMC iterations (thinned to 10000). `NNGPsequenFixedL` appears to be the best, followed by `NNGPblockFixedL`, `fullGPfixedL`, and `NNGPsequenVaryLj`.

Model	<code>fullGPfixedL</code>	<code>NNGPblockFixedL</code>	<code>NNGPsequenFixedL</code>	<code>NNGPsequenVaryLj</code>
<code>postMeanMSE</code>	0.01156502	0.01163034	0.01151077	0.02350727
<code>postMSE</code>	0.06627909	0.0659256	0.06565047	0.0902155
<code>postVar</code>	0.05471954	0.0543007	0.05414511	0.0667149
<code>dinf</code>	0.06628456	0.06593103	0.06565589	0.09022217
<code>pD</code>	-6991868	435.9175	-1115973	-73.88205
<code>dic</code>	-7026893	-34833.96	-1151389	-22724.13
<code>p.waic_1</code>	972.6698	955.6921	818.4227	922.2227
<code>p.waic_2</code>	17411.46	13502.62	13483.7	12435.92
<code>lppd</code>	17998.47	18112.78	18117.06	11786.24
<code>waic</code>	-1174.019	-9220.335	-9266.715	1299.361

Table I.16: Simulation for $O = 2$: Diagnostic statistics for $(m, T) = (400, 50)$, 80000 burn-in MCMC iterations, and 20000 post-burn-in MCMC iterations (thinned to 10000). The fixed number of clusters L is specified to be 50 for the first three methods, and a starting value and hence upper bound of 50 is assigned to all L_j 's for `NNGPsequenVaryLj`. `NNGPsequenFixedL` appears to be the best, followed by `NNGPblockFixedL`, `fullGPfixedL`, and `NNGPsequenVaryLj`.

I.6 Sensitivity Analysis for the Number of Factors and Hyperparameters

We adopted the data generation mechanism and model fitting specifications in Section 6.1 with $O = 1$, $(m, T) = (225, 100)$, 90000 burn-in and 10000 post-burn-in (thinned to 5000) MCMC iterations. We used the same hyper-parameter values as in Section 6.1 (**setting 1**) with $k = 3, 4, 5, 6, 7$. We also specified $k = 5$ with five sets of different hyper-parameter combinations specified below, which we shall denote as **setting 1**, **setting 2**, **setting 3**, **setting 4**, and **setting 5**.

1. $(a, b) = (1, 1)$ for $\sigma^2(\mathbf{s}_i)$'s, $(a_1, a_2) = (1, 1)$ for $\delta_{1:k}$, $(a_\rho, b_\rho) = (0.1, 1)$ for ρ , $(a_\psi, b_\psi) = (0.1, 4.5)$ for ψ , $(\nu, \Theta) = (2, 1)$ for κ , and $(\zeta, \Omega) = (k + 1, I_{k \times k})$ for $\Upsilon_{k \times k}$;
2. $(a, b) = (1, 1)$ for $\sigma^2(\mathbf{s}_i)$'s, $(a_1, a_2) = (1, 1)$ for $\delta_{1:k}$, $(a_\rho, b_\rho) = (1, 2)$ for ρ , $(a_\psi, b_\psi) = (1, 2)$ for ψ , $(\nu, \Theta) = (2, 1)$ for κ , and $(\zeta, \Omega) = (k + 1, I_{k \times k})$ for $\Upsilon_{k \times k}$;
3. $(a, b) = (1, 1)$ for $\sigma^2(\mathbf{s}_i)$'s, $(a_1, a_2) = (1, 1)$ for $\delta_{1:k}$, $(a_\rho, b_\rho) = (0.1, 1)$ for ρ , $(a_\psi, b_\psi) = (0.1, 4.5)$ for ψ , $(\nu, \Theta) = (2, 0.1)$ for κ , and $(\zeta, \Omega) = (k + 1, 0.1 \times I_{k \times k})$ for $\Upsilon_{k \times k}$;
4. $(a, b) = (0.1, 1)$ for $\sigma^2(\mathbf{s}_i)$'s, $(a_1, a_2) = (1, 1)$ for $\delta_{1:k}$, $(a_\rho, b_\rho) = (0.1, 1)$ for ρ , $(a_\psi, b_\psi) = (0.1, 4.5)$ for ψ , $(\nu, \Theta) = (2, 1)$ for κ , and $(\zeta, \Omega) = (k + 1, I_{k \times k})$ for $\Upsilon_{k \times k}$;
5. $(a, b) = (1, 1)$ for $\sigma^2(\mathbf{s}_i)$'s, $(a_1, a_2) = (1, 2)$ for $\delta_{1:k}$, $(a_\rho, b_\rho) = (0.1, 1)$ for ρ , $(a_\psi, b_\psi) = (0.1, 4.5)$ for ψ , $(\nu, \Theta) = (2, 1)$ for κ , and $(\zeta, \Omega) = (k + 1, I_{k \times k})$ for $\Upsilon_{k \times k}$.

Our four methods `fullGPfixedL`, `NNGPblockFixedL`, `NNGPsequenFixedL`, and `NNGPsequenVaryLj` lead to suitable diagnostics statistics and posterior deviances under diverse specifications of k and certain hyper-parameters. Table I.17 suggests that as long as k is not too small (smaller than the true number of spatial clusters), a smaller k summarizes information more efficiently and leads to better model fit compared to overly large k values.

	<code>fullGPfixedL</code>	<code>NNGPblockFixedL</code>	<code>NNGPsequenFixedL</code>	<code>NNGPsequenVaryLj</code>
$k = 3$ and setting 1	0.04249498	0.04132792	0.04131845	0.04130782
$k = 4$ and setting 1	0.04169457	0.0458628	0.04170855	0.04228698
$k = 5$ and setting 1	0.04243256	0.04392605	0.04374525	0.07509951
$k = 6$ and setting 1	0.04654032	0.04463703	0.046456	0.07185972
$k = 7$ and setting 1	0.04590091	0.04622895	0.04577551	0.06927728
$k = 5$ and setting 2	0.05195494	0.05281261	0.05200683	0.08106986
$k = 5$ and setting 3	0.04460182	0.0435225	0.04416449	0.07531454
$k = 5$ and setting 4	0.04448045	0.04291583	0.04338732	0.08113479
$k = 5$ and setting 5	0.04159748	0.04214983	0.04472333	0.07416565

Table I.17: Sensitivity analysis: Posterior mean squared errors for our four methods to the number of latent factors k and different choices of hyperparameters in the prior.

J Extension to Three Non-Gaussian Observed Data Types

Earlier on, we have only considered Gaussian observed data. As we shall see in this section, our models can be conveniently extended to accommodate three non-normal observed data types – ‘**tobit**’, ‘**probit**’, and ‘**binomial**’, which can all still lead to Gaussian kernels. All we need to add is an extra `SampleY()` step sampling transformed normal response variables from our original observed non-normal data and based on our current posterior parameter estimates

at the start of each MCMC iteration in the Gibbs samplers (Appendix A). After obtaining a model fit object, we shall also modify the corresponding portions calculating our diagnostics metrics and making both in-sample and out-of-sample predictions, which all turn out to be quite straightforward.

The first two non-Gaussian observed data types are simply defined based on some original normal distributions. A ‘**tobit**’ variable is obtained from a normally distributed instance that is set to 0 if negative and kept as it is otherwise. A ‘**probit**’ instance is set to 0 if the original normal value is non-positive and set to 1 otherwise. The `SampleY()` steps corresponding to these two data types are hence quite straightforward. For an observed value of 0 corresponding to either data type and for a ‘**probit**’ observed value of 1, we sample a transformed response variable from the truncated normal distribution with our current mean and variance posterior estimates left-censored and right-censored at 0 respectively. When making predictions for a certain outcome variable based on a fitted model, we first obtain a predicted transformed response as in the baseline ‘**normal**’ case and then set the counterpart predicted original response to be 0 or 1 if needed. When calculating log likelihoods for certain diagnostics metrics, we take note that the ‘**tobit**’ distribution is a rectified Gaussian distribution (a half-half mixture of a point mass at 0 and the positive portion of a normal distribution, which is neither discrete nor continuous), and that ‘**probit**’ is a discrete distribution with discontinuity points 0 and 1.

We now consider binomial observed data $y_t^o(\mathbf{s}_i) \sim \text{Binomial}(n_t^o(\mathbf{s}_i), \pi_t^o(\mathbf{s}_i))$, $(i, o, t) \in \{1, \dots, m\} \times \{1, \dots, O\} \times \{1, \dots, T\}$, where $n_t^o(\mathbf{s}_i)$ ’s are the pre-specified numbers of trials. Following Berchuck et al. 2022’s idea, we accommodate the binomial likelihood by extending Equation (2.1) to the general modeling framework²

$$y_t^o(\mathbf{s}_i) | \vartheta_t^o(\mathbf{s}_i), \zeta_t^o(\mathbf{s}_i) \stackrel{\text{ind}}{\sim} f(y_t^o(\mathbf{s}_i); g^{-1}(\vartheta_t^o(\mathbf{s}_i)), \zeta_t^o(\mathbf{s}_i)) \quad (\text{J.1})$$

$$\vartheta_t^o(\mathbf{s}_i) = \mathbf{x}_t^o(\mathbf{s}_i)^\top \boldsymbol{\beta} + \sum_{j=1}^k \lambda_j^o(\mathbf{s}_i) \eta_{tj}$$

$$\forall (i, o, t) \in \{1, \dots, m\} \times \{1, \dots, O\} \times \{1, \dots, T\},$$

where g is the logit link ($\zeta_t^o(\mathbf{s}_i)$ is null) and f is binomial with probability $\pi_t^o(\mathbf{s}_i) = g^{-1}(\vartheta_t^o(\mathbf{s}_i)) = \frac{e^{\vartheta_t^o(\mathbf{s}_i)}}{1 + e^{\vartheta_t^o(\mathbf{s}_i)}} \in (0, 1)$. Our joint data likelihood is hence

$$\begin{aligned} f(\mathbf{y} | \boldsymbol{\vartheta}, \mathbf{n}) &= \prod_{t=1}^T \prod_{o=1}^O \prod_{i=1}^m \left(\frac{e^{\vartheta_t^o(\mathbf{s}_i)}}{1 + e^{\vartheta_t^o(\mathbf{s}_i)}} \right)^{y_t^o(\mathbf{s}_i)} \left(\frac{1}{1 + e^{\vartheta_t^o(\mathbf{s}_i)}} \right)^{n_t^o(\mathbf{s}_i) - y_t^o(\mathbf{s}_i)} \\ &= \prod_{t=1}^T \prod_{o=1}^O \prod_{i=1}^m \frac{\exp\{\vartheta_t^o(\mathbf{s}_i) y_t^o(\mathbf{s}_i)\}}{(1 + \exp\{\vartheta_t^o(\mathbf{s}_i)\})^{n_t^o(\mathbf{s}_i)}}. \end{aligned} \quad (\text{J.2})$$

Directly proceeding with Equation (J.2), however, would be computationally prohibitive due to most parameters’ loss of conjugacy. Hence, Berchuck et al. (2022) introduced Pólya-Gamma (PG) augmented parameters $\omega_t^o(\mathbf{s}_i) \stackrel{\text{ind}}{\sim} \text{PG}(n_t^o(\mathbf{s}_i), 0)$ so that

$$f(\mathbf{y}, \boldsymbol{\omega} | \boldsymbol{\vartheta}, \mathbf{n}) = \prod_{t=1}^T \prod_{o=1}^O \prod_{i=1}^m \left[\frac{\exp\{\vartheta_t^o(\mathbf{s}_i) y_t^o(\mathbf{s}_i)\}}{(1 + \exp\{\vartheta_t^o(\mathbf{s}_i)\})^{n_t^o(\mathbf{s}_i)}} \right] \times f(\boldsymbol{\omega}_t^o(\mathbf{s}_i) | \vartheta_t^o(\mathbf{s}_i), n_t^o(\mathbf{s}_i))$$

² Note that for the Gaussian specification, g is the identity link and f is Gaussian with mean $\mu_t^o(\mathbf{s}_i) = g^{-1}(\vartheta_t^o(\mathbf{s}_i)) = \vartheta_t^o(\mathbf{s}_i)$ and variance (nuisance) $\zeta_t^o(\mathbf{s}_i) = (\sigma^2)^o(\mathbf{s}_i)$.

$$\begin{aligned}
& \propto \prod_{t=1}^T \prod_{o=1}^O \prod_{i=1}^m \left[\frac{\exp\{\vartheta_t^o(\mathbf{s}_i) y_t^o(\mathbf{s}_i)\}}{(1 + \exp\{\vartheta_t^o(\mathbf{s}_i)\})^{n_t^o(\mathbf{s}_i)}} \right] \exp \left\{ -\frac{[\vartheta_t^o(\mathbf{s}_i)]^2 \omega_t^o(\mathbf{s}_i)}{2} \right\} \left(\frac{1 + \exp\{\vartheta_t^o(\mathbf{s}_i)\}}{2 \exp\{\vartheta_t^o(\mathbf{s}_i)/2\}} \right)^{n_t^o(\mathbf{s}_i)} \\
& \propto \prod_{t=1}^T \prod_{o=1}^O \prod_{i=1}^m \exp \left\{ -\frac{\omega_t^o(\mathbf{s}_i)}{2} [y_{t,o}^*(\mathbf{s}_i) - \vartheta_t^o(\mathbf{s}_i)]^2 \right\}, \tag{J.3}
\end{aligned}$$

where $y_{t,o}^*(\mathbf{s}_i) = \frac{\chi_t^o(\mathbf{s}_i)}{\omega_t^o(\mathbf{s}_i)}$ with $\chi_t^o(\mathbf{s}_i) = y_t^o(\mathbf{s}_i) - \frac{n_t^o(\mathbf{s}_i)}{2} \forall (i, o, t)$. This transformed kernel is now Gaussian and conjugacy has thus been introduced.

Equation (J.3) suggests that $(\sigma^2)^o(\mathbf{s}_i)$'s are no longer needed and the corresponding Gibbs sampler step can thus be removed. Instead, we add at the beginning of each MCMC iteration a step sampling the augmented PG parameters $\omega_t^o(\mathbf{s}_i)$'s from their full conditional distributions $\omega_t^o(\mathbf{s}_i) \sim \text{PG} \left(n_t^o(\mathbf{s}_i), \mathbf{x}_t^o(\mathbf{s}_i)^\top \boldsymbol{\beta} + \sum_{j=1}^k \lambda_j^o(\mathbf{s}_i) \eta_{tj} \right) \forall (i, o, t)$. $y_t^o(\mathbf{s}_i)$'s can then be transformed to $y_{t,o}^*(\mathbf{s}_i)$'s accordingly in the `SampleY()` step. We should also replace $(\sigma^2)^o(\mathbf{s}_i)$'s by $\frac{1}{\omega_t^o(\mathbf{s}_i)}$'s in all other concerned Gibbs sampler steps, i.e., the steps sampling $\boldsymbol{\eta}$'s, $\boldsymbol{\beta}$, and $\boldsymbol{\lambda}_j$'s or $\xi_j^o(\mathbf{s}_i)$'s, θ_{jl_j} 's. When calculating a log likelihood for $y_t^o(\mathbf{s}_i)$ or obtaining an in-sample prediction $\hat{y}_t^o(\mathbf{s}_i)$ for any arbitrary $(i, o, t) \in \{1, \dots, m\} \times \{1, \dots, O\} \times \{1, \dots, T\}$ based on a fitted model, we first calculate $\hat{\pi}_t^o(\mathbf{s}_i) = \frac{e^{\hat{\vartheta}_t^o(\mathbf{s}_i)}}{1 + e^{\hat{\vartheta}_t^o(\mathbf{s}_i)}} \in (0, 1)$ from our posterior mean estimate $\hat{\vartheta}_t^o(\mathbf{s}_i)$ and then proceed according to $y_t^o(\mathbf{s}_i)$'s distribution $\text{Binomial}(n_t^o(\mathbf{s}_i), \hat{\pi}_t^o(\mathbf{s}_i))$. Out-of-sample predictions are similar to in-sample predictions in this case.

References

- Berchuck, Samuel I., Mark Janko, Felipe A. Medeiros, William Pan, and Sayan Mukherjee (2022). “Bayesian Non-Parametric Factor Analysis for Longitudinal Spatial Surfaces”. In: *Bayesian Analysis* 17.2, pp. 435–464. DOI: [10.1214/20-BA1253](https://doi.org/10.1214/20-BA1253). arXiv: [1911.04337](https://arxiv.org/abs/1911.04337).
- Bhattacharya, A. and D. B. Dunson (2011). “Sparse Bayesian infinite factor models”. In: *Biometrika* 98.2, pp. 291–306. ISSN: 00063444. DOI: [10.1093/biomet/asr013](https://doi.org/10.1093/biomet/asr013).
- Bradley, Jonathan R., Scott H. Holan, and Christopher K. Wikle (2015). “Multivariate spatio-temporal models for high-dimensional areal data with application to longitudinal employer-household dynamics”. In: *The Annals of Applied Statistics* 9.4, pp. 1761–1791.
- Christensen, W. F. and Y. Amemiya (2002). “Latent variable analysis of multivariate spatial data”. In: *Journal of the American Statistical Association* 97.457, pp. 302–317. ISSN: 01621459. DOI: [10.1198/016214502753479437](https://doi.org/10.1198/016214502753479437).
- Datta, Abhirup, Sudipto Banerjee, Andrew O. Finley, and Alan E. Gelfand (2016). “Hierarchical Nearest-Neighbor Gaussian Process Models for Large Geostatistical Datasets”. In: *Journal of the American Statistical Association* 111.514, pp. 800–812. ISSN: 1537274X. DOI: [10.1080/01621459.2015.1044091](https://doi.org/10.1080/01621459.2015.1044091). arXiv: [1406.7343](https://arxiv.org/abs/1406.7343).
- De Iorio, Maria, Stefano Favaro, Alessandra Guglielmi, and Lifeng Ye (2023). “Bayesian non-parametric mixture modeling for temporal dynamics of gender stereotypes”. In: *Annals of Applied Statistics* 17.3, pp. 2256–2278. ISSN: 19417330. DOI: [10.1214/22-AOAS1717](https://doi.org/10.1214/22-AOAS1717).
- Finley, Andrew O., Abhirup Datta, and Sudipto Banerjee (2022). “spNNGP R Package for Nearest Neighbor Gaussian Process Models”. In: *Journal of Statistical Software* 103.5, pp. 1–40. ISSN: 15487660. DOI: [10.18637/jss.v103.i05](https://doi.org/10.18637/jss.v103.i05). arXiv: [2001.09111](https://arxiv.org/abs/2001.09111).

- Finley, Andrew O., Abhirup Datta, Bruce D. Cook, Douglas C. Morton, Hans E. Andersen, and Sudipto Banerjee (2019). “Efficient Algorithms for Bayesian Nearest Neighbor Gaussian Processes”. In: *Journal of Computational and Graphical Statistics* 28.2, pp. 401–414. ISSN: 15372715. DOI: [10.1080/10618600.2018.1537924](https://doi.org/10.1080/10618600.2018.1537924). arXiv: [1702.00434](https://arxiv.org/abs/1702.00434).
- Hu, Guanyu, Junxian Geng, Yishu Xue, and Huiyan Sang (2023). “Bayesian Spatial Homogeneity Pursuit of Functional Data: An Application to the U.S. Income Distribution”. In: *Bayesian Analysis* 18.2, pp. 579–605. ISSN: 19316690. DOI: [10.1214/22-BA1320](https://doi.org/10.1214/22-BA1320).
- Jensen, Mark J. and John M. Maheu (2013). “Bayesian semiparametric multivariate GARCH modeling”. In: *Journal of Econometrics* 176.1, pp. 3–17. ISSN: 03044076. DOI: [10.1016/j.jeconom.2013.03.009](https://doi.org/10.1016/j.jeconom.2013.03.009).
- Kahle, David and Hadley Wickham (2013). “ggmap: Spatial Visualization with ggplot2”. In: *The R Journal* 5.1, pp. 144–161. URL: <https://journal.r-project.org/archive/2013-1/kahle-wickham.pdf>.
- Katzfuss, Matthias and Joseph Guinness (2021). “A General Framework for Vecchia Approximations of Gaussian Processes”. In: *Statistical Science* 36.1, pp. 124–141. ISSN: 21688745. DOI: [10.1214/19-STS755](https://doi.org/10.1214/19-STS755).
- Ma, Ying and Xiang Zhou (2022). “Spatially informed cell-type deconvolution for spatial transcriptomics”. In: *Nature Biotechnology* 40.9, pp. 1349–1359.
- Mozdzen, Alexander, Andrea Cremaschi, Annalisa Cadonna, Alessandra Guglielmi, and Gregor Kastner (2022). “Bayesian modeling and clustering for spatio-temporal areal data: An application to Italian unemployment”. In: *Spatial Statistics* 52. ISSN: 22116753. DOI: [10.1016/j.spasta.2022.100715](https://doi.org/10.1016/j.spasta.2022.100715).
- Neal, Radford M. (2000). “Markov Chain Sampling Methods for Dirichlet Process Mixture Models”. In: *Journal of Computational and Graphical Statistics* 9.2, pp. 249–265. ISSN: 15372715. DOI: [10.1080/10618600.2000.10474879](https://doi.org/10.1080/10618600.2000.10474879).
- Ren, Qian and Sudipto Banerjee (2013). “Hierarchical Factor Models for Large Spatially Misaligned Data: A Low-Rank Predictive Process Approach”. In: *Biometrics* 69.1, pp. 19–30. ISSN: 0006341X. DOI: [10.1111/j.1541-0420.2012.01832.x](https://doi.org/10.1111/j.1541-0420.2012.01832.x).
- Rodríguez, Abel and David B. Dunson (2011). “Nonparametric Bayesian models through probit stick-breaking processes”. In: *Bayesian Analysis* 6.1, pp. 145–177. ISSN: 19360975. DOI: [10.1214/11-BA605](https://doi.org/10.1214/11-BA605).
- Sethuraman, J. (1994). “A constructive definition of Dirichlet priors”. In: *Statistica Sinica* 4.2, pp. 639–650. URL: <http://www.jstor.org/stable/24305538>.
- Spiegelhalter, David J., Nicola G. Best, Bradley P. Carlin, and Angelika Van Der Linde (2002). “Bayesian measures of model complexity and fit”. In: *Journal of the Royal Statistical Society. Series B: Statistical Methodology* 64.4, pp. 583–639. ISSN: 13697412. DOI: [10.1111/1467-9868.00353](https://doi.org/10.1111/1467-9868.00353).
- Townes, F. Williams and Barbara E. Engelhardt (2022). “Nonnegative spatial factorization applied to spatial genomics”. In: *Nature Methods* 20.2, pp. 229–238.
- Vecchia, A. V. (1988). “Estimation and Model Identification for Continuous Spatial Processes”. In: *Journal of the Royal Statistical Society: Series B (Methodological)* 50.2, pp. 297–312. DOI: [10.1111/j.2517-6161.1988.tb01729.x](https://doi.org/10.1111/j.2517-6161.1988.tb01729.x).

- Vehtari, Aki, Andrew Gelman, and Jonah Gabry (2017). “Practical Bayesian model evaluation using leave-one-out cross-validation and WAIC”. In: *Statistics and Computing* 27.5, pp. 1413–1432. ISSN: 15731375. DOI: [10.1007/s11222-016-9696-4](https://doi.org/10.1007/s11222-016-9696-4).
- Virbickaite, Audrone, M. Concepción Ausín, and Pedro Galeano (2015). “Bayesian inference methods for univariate and multivariate garch models: A survey”. In: *Journal of Economic Surveys* 29.1, pp. 76–96. ISSN: 14676419. DOI: [10.1111/joes.12046](https://doi.org/10.1111/joes.12046). arXiv: [1402.0346](https://arxiv.org/abs/1402.0346).
- Walker, Stephen G. (2007). “Sampling the Dirichlet Mixture Model with Slices”. In: *Communications in Statistics: Simulation and Computation* 36.1, pp. 45–54. DOI: <https://doi.org/10.1080/03610910601096262>.
- Wall, Melanie M. and Xuan Liu (2009). “Spatial latent class analysis model for spatially distributed multivariate binary data”. In: *Computational Statistics and Data Analysis* 53.8, pp. 3057–3069. ISSN: 01679473. DOI: [10.1016/j.csda.2008.07.037](https://doi.org/10.1016/j.csda.2008.07.037).
- Yang, Daewon, Taeryon Choi, Eric Lavigne, and Yeonseung Chung (2022). “Non-parametric Bayesian covariate-dependent multivariate functional clustering: An application to time-series data for multiple air pollutants”. In: *Journal of the Royal Statistical Society. Series C: Applied Statistics* 71.5, pp. 1521–1542. ISSN: 14679876. DOI: [10.1111/rssc.12589](https://doi.org/10.1111/rssc.12589).
- Zhang, Bohai, Huiyan Sang, Zhao Tang Luo, and Hui Huang (2023). “Bayesian clustering of spatial functional data with application to a human mobility study during COVID-19”. In: *Annals of Applied Statistics* 17.1, pp. 583–605. ISSN: 19417330. DOI: [10.1214/22-AOAS1643](https://doi.org/10.1214/22-AOAS1643).